



Norwegian University of  
Science and Technology

# Installation of Subsea Equipment Protection Covers

Establishment of Operation Limits and  
Assessment of Operability and Weather  
Windows

**Ragnhild Brekke**

Marine Technology

Submission date: June 2017

Supervisor: Kjell Larsen, IMT

Norwegian University of Science and Technology  
Department of Marine Technology





## MASTER THESIS SPRING 2017

for

**Stud. tech. Ragnhild Brekke**

### **Installation of Subsea Equipment Protection Covers – Establishment of Operation Limits and Assessment of Operability and Weather Windows**

*Installasjon av beskyttelsesstruktur for undervannsanlegg – vurdering av operasjonsgrenser og operabilitet*

#### Background

Subsea production systems have in most field development scenarios become the most attractive option, both in terms of capital expenditure and technical solution. In order to be able to design, install and operate a subsea oil and gas factory, a cost-effective installation method is crucial. Present capital expenditure of the marine operations for a subsea production system in 300-500m water depth is for some cases in the range 15-30% of the total capital invested. Subsea hardware facilities typically consist of templates, manifolds and wellheads as well as lot of in-field flow-lines and pipeline connections (spool pieces).

A key activity to successful subsea installation operations is the planning process. Lifting of subsea equipment, especially through the wave zone, is a weather critical activity. It is crucial that such operations are planned and understood properly and that effective equipment is used. This thesis shall specifically consider installation of subsea equipment protection covers. Numerical simulations are an important part of the decision basis.

This MSc thesis shall build on the work and report made the project work during autumn 2016. Several numerical simulation suites exist. The thesis shall use the tools available in the SIMA/SIMO program suite.

#### Scope of Work

- 1) Describe briefly state-of-art subsea installation methods by use of crane vessels. For weather restricted operations, an overview of the planning process shall be described; in particular the “alpha factor” concept and how operability and weather windows can be optimized.
- 2) Familiarize with the numerical simulation suite SIMA/SIMO and describe the theory that is relevant for subsea lifting and installation of GRP protection covers for subsea equipment.
- 3) Verify and describe an existing numerical simulation model in SIMA for a GRP protection cover. In particular, describe how important parameters like added mass and drag forces are defined in the numerical simulation model. Propose parameters that may determine the design operational limit and estimate limits based on simulation results. The variability of the design responses shall be assessed.

4) Operability investigation. Operability and times for waiting-on-weather shall be calculated based on given data for North Sea and a location east of Africa. Use results from task 3. The following shall be included: a) safe conditions, b) time consumption and alpha factors, c) required weather windows.

5) Conclusions and recommendations for further work.

#### General information

The start of the thesis shall be the project work carried out during autumn 2016.

In the project report the candidate shall present her personal contribution to the resolution of problems within the scope of the thesis work.

Theories and conclusions should be based on mathematical derivations and/or logic reasoning identifying the various steps in the deduction.

The candidate should utilise the existing possibilities for obtaining relevant literature.

#### Thesis format

The thesis should be organised in a rational manner to give a clear exposition of results, assessments, and conclusions. The text should be brief and to the point, with a clear language. Telegraphic language should be avoided.

The report shall contain the following elements: A text defining the scope, preface, list of contents, summary, main body of thesis, conclusions with recommendations for further work, list of symbols and acronyms, references and (optional) appendices. All figures, tables and equations shall be numerated.

The report shall be submitted in two copies (one hard copy and one electronic copy)

- The hard copy shall be signed by the candidate
- The text defining the scope included

#### Ownership

NTNU has according to the present rules the ownership of the report. Any use of the work has to be approved by NTNU (or external partner when this applies). The department has the right to use the report as if the work was carried out by a NTNU employee, if nothing else has been agreed in advance.

#### Thesis supervisor:

Prof. II Kjell Larsen (Statoil/NTNU)

**Deadline: 9<sup>th</sup> of June 2017**

Trondheim, June, 2017

Kjell Larsen (signature):

Ragnhild Brekke (date and signature):

*Kjell Larsen*  
7/6-17 *Ragnhild Brekke*



---

## Preface

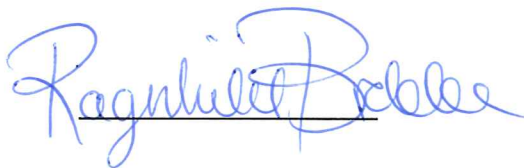
This Master Thesis is the concluding part of my Master of Science degree in Marine Subsea Engineering at the Department of Marine Technology (IMT) at the Norwegian University of Science and Technology (NTNU) in Trondheim, Norway.

The topic is subsea lifting operations, with focus on establishment of manually and simulated operation limits. The work has been carried out at NTNU during the spring semester of 2017, in cooperation with Professor II Kjell Larsen. The workload corresponds to 30 ECTS. The idea of the project was provided by Kjell Larsen, who works both at Statoil and as a professor at NTNU. The simulations have been performed in the simulation software SIMA developed by SINTEF Ocean, former MARINTEK.

The Master Thesis builds on the Project Thesis that was written during the autumn semester of 2016. The Project Thesis corresponded to a workload of 7.5 ECTS and was a scoping study of the planning process of an offshore lifting operation.

The readers of this Master Thesis are assumed to have some prior knowledge about marine lifting operations and hydrodynamics in general.

Trondheim, June 07, 2017



Ragnhild Brekke



---

## Acknowledgements

First, I would like to thank my supervisor Professor II Kjell Larsen. He has been very helpful and taken great interest in my work throughout the whole master period. He has scheduled weekly meetings and his enthusiasm has contributed to high motivation for my thesis work.

I would also like to thank Statoil ASA and SINTEF Ocean, former MARINTEK, for providing all relevant data and developing the simulation model.

The Norwegian Society Of Lifting Technology should be acknowledged for their generosity offering me a place at their Subsea Lifting Operations Seminar in Stavanger December 6<sup>th</sup>-7<sup>th</sup> 2016.

Frøydis Solaas and Pål Levold should also be acknowledged for answering questions regarding the cover installation simulation throughout the whole thesis period.

I would like to thank the teaching assistant in SIMA, Yuna Zhao, for answering questions and assisting with SIMA.

Additionally, I wish to thank Malin Bjørkøy for valuable discussions throughout the thesis period, and my fellow students at office A2.003 for providing a good working environment.

This Master Thesis is dedicated to my very good friend Kristian Vilhelm Sve Mollestad who passed away this May.



---

## Abstract

The oil and gas industry has become more challenging the past years and marine operations must be performed in smarter and more cost-effective ways. Waiting on weather should be minimised and design and planning will be of high importance. A marine operation shall be designed to bring an object from one safe condition to another safe condition. A subsea lift consists of different phases that should be evaluated during the planning process, where the through splash zone phase is usually most critical. In order to account for uncertainty in weather forecast, the operation's design criterion is reduced by an  $\alpha$ -factor.

Installations of protection covers are common offshore operations, but only a few hydrodynamic investigations have been performed on such objects. This Master Thesis describes a study aimed at finding as high operational criterion as possible for an installation of a GRP pipeline protection cover. Further investigations were performed on the differences in use of numerical simulations and DNV GL's Simplified Method. The operation's operability was investigated for the two different operational criteria.

For a light lift operation, the occurrence of slack in slings are critical and does usually determine the maximum operational sea state. Slack arises when the total hydrodynamic force acting on the object exceeds 90% of its submerged weight.

The lift was simulated for the splash zone phase in the non-linear time domain simulation program, SIMA. The minimum tension that arose in the slings for each wave condition with random seed number, were used to develop a Gumbel distribution. The sea state was categorised as operational if the 10% quantile, found by an inversed Gumbel CDF, was above the slack requirement.

The lifting system consisted of the vessel's crane tip, a crane wire, a hook, a hook winch, four slings, a spreader bar and the cover. The cover was implemented as slender elements in SIMA, where each slender element was given depth dependent added mass and drag. The implemented hydrodynamic parameters were estimated by CFD-analyses. The cover was lifted with an angle of  $68^\circ$ , and the short-term environmental conditions were characterised by short-crested JONSWAP wave spectra.

The installation was defined as a weather restricted level B marine operation. The total hydrodynamic force was manually estimated by the Simplified Method. The respective added mass and drag were calculated by use of tabulated coefficients for rectangular flat plates, in two directions; longitudinal and perpendicular to the cover flanges. The total added mass for a rotated cover was found by summing the vertical components of the longitudinal and perpendicular added mass. The largest tension variations occurred right after the cover was fully submerged, hence slamming and varying buoyancy forces could be omitted. The inertia and drag forces were dependent on the most probable largest crane tip motion, found by the crane tip and vessel COG locations. The maximum

sea state was assessed by use of linear scaling. The average manually estimated design criterion was 1.64 m and constant for all peak periods. Hence with an  $\alpha$ -factor of 0.76 the operational criterion was 1.25 m.

For each wave condition, 20-30 lowering simulations were performed with random seed numbers. The average winch speed was 0.2 m/s and the cover was lowered to a depth of approximately 33 m. Both the spreader bar and the cover experienced large motions in air. The motions diminished when the cover entered the water. The tension variation in the lifting system increased when the cover entered the splash zone and calmed down when the cover was lowered to 20 meter depth.

The simulated design criteria were found by investigating the tension in the lifting slings. No large snap forces were observed after a slack condition. The simulated design criteria were dependent on both significant wave heights and peak periods. The average design criterion was independent of peak periods and determined to be 2.5 m. Hence with an  $\alpha$ -factor of 0.81 the operational criterion was 2 m.

The operation can take place if the wave conditions are below the operational criteria over a longer duration than the operation's reference period. The operability was investigated for two fields; Heidrun and Tanzania Block 2. The reference periods were dependent on the water depth, and thus determined to be 2.5 hours and 9.3 hours for the two fields respectively. The operability and actual duration of operation with a random start were heavily season dependent, and were studied for both the manually estimated and simulated operational criteria.

When the operational criterion increased from 1.25 m to 2 m the operability increased with 30-50% at both fields. At the same time the actual duration of operation with a random start decreased with up to 80% at Heidrun. That is, for a given reference period, the waiting on weather decreased with the corresponding. Generally, at both fields the reason of waiting on weather was due to storm periods, where the wave conditions were above the operational criterion.

The operational limit was determined by several factors; the installation method, the environmental conditions, the crane tip motion, the  $\alpha$ -factor and the tension airing in the slings. According to this one can say that an operation should be short in order to be able to take place often. For increased operational criteria the operability increased and waiting on weather decreased.

If the operation should take place at a random time, the risk of waiting on weather will increase. Usually, a marine operation is planned ahead of execution and is based on weather forecasts. Such planning will with a high probability reduce waiting on weather and increase the operation efficiency.

In order to determine the highest operational sea state as possible in such a way that waiting on weather can be reduced, simulations should be performed prior to installations of pipeline protection covers. Hence operational costs, engine idling and pollution can be significantly reduced compared to only relying on the simplified method.



---

## Sammendrag

I løpet av de siste årene har olje- og gass industrien blitt mer utfordrende, og marine operasjoner bør nå bli utført på smartere og mer kostnadseffektive måter. Værventing bør til enhver tid minimeres og design og planlegging utgjør en svært viktig del av dette. En marin operasjon skal være designet til å flytte en gjenstand fra en sikker posisjon til en annen sikker posisjon. Et undervannsløft består av flere faser som bør bli evaluert i planleggingsprosessen, hvor *splash*-sonen vanligvis er mest kritisk. For å kunne ta hensyn til usikkerhet i værmeldingene, vil operasjonens designgrense bli redusert ved hjelp av en  $\alpha$ -faktor.

Beskyttelsesdeksel blir installert ofte, men få hydrodynamiske undersøkelser har blitt utført på slike gjenstander. Denne masteroppgaven beskriver et studie som har hatt som formål å sette høyest mulige operasjonsgrenser for en installasjon av et beskyttelsesdeksel til et undervannsanlegg. Den har videre sett på forskjellene ved bruk av numeriske simuleringer og DNV GL's simplifiserte metode. Operasjonens opererbarhet har også blitt undersøkt for de to ulike operasjonsgrensene.

*Slack* bestemmer vanligvis maksimum operasjonell sjøtilstand for en løfteoperasjon av en lett gjenstand. Slack oppstår når den totale hydrodynamiske kraften som virker på den løftede gjenstanden, overskrider 90% av dens neddykkede vekt.

Løfteoperasjonen ble simulert for *splash*-sonen i tidsplanet til det ikke-lineære simuleringsprogrammet, SIMA. Den minste spenningen som oppstod i løfteslingsene for hver bølgekonisjon, med et tilfeldig frøtall, utviklet Gumbel fordelingen. Sjøtilstanden ble kategorisert som operasjonell dersom 10%-kvantilen, funnet av den inverse kumulative fordelingen til Gumbel, overskred slack-kriteriet.

Løftesystemet bestod av fartøyets kranspiss, en kran-wire, en krok, en vinsj, fire slings, en *spreader bar* og dekselet. Dekselet ble implementert som slanke elementer i SIMA, hvor hvert element ble gitt dybdevarierende hydrodynamisk tilleggs masse (*added mass*) og drag. De implementerte hydrodynamiske parameterne ble estimert ved bruk av CFD-analyser. Dekselet ble løftet med en vinkel på  $68^\circ$ , og de kortsiktige bølgekonisjonene ble beskrevet av JONSWAP bølgespektrere for korte bølgetopper.

Installasjonen var en værbergrenset marin operasjon, kategorisert som nivå B. Den totale hydrodynamiske kraften ble manuelt estimert ved bruk av den simplifiserte metoden til DNV GL. Den hydrodynamiske tilleggs massen og dragkraften ble beregnet for to retninger; langsgående og perpendikulært på dekselets flenser, ved bruk av tabulerte koeffisienter for rektangulære, tynne plater. For et rotert deksel ble den totale hydrodynamiske tilleggs massen funnet ved å summere de vertikale komponentene til både den langsgående og den perpendikulære hydrodynamiske tilleggs massen. De største spenningsvariasjonene i slingsene oppsto rett etter at dekselet var fullt neddykket, og kreftene fra *slamming* og varierende oppdrift kunne derfor bli utelukket. Massekraften og dragkraften var avhengig av den mest sannsynlige største kranspissbevegelsen, og ble beregnet

utifra plasseringen til kranspissen og fartøyets tyngdepunkt. Maks sjøtilstand ble fastsatt ved bruk av lineær skalering. Den gjennomsnittlige designgrensen fra manuell estimering ble satt til 1.64 m, konstant for alle bølgeperioder. Derav ble operasjonsgrensen beregnet til 1.25 m, ved bruk av en  $\alpha$ -faktor på 0.76.

For hver bølgekonisjon ble 20-30 senkninger simulert med tilfeldige frøtall. Gjennomsnittlig vinsj-hastighet var 0.2 m/s og dekselet ble senket til omtrent 33 meters dybde. Både *spreader baren* og dekselet ble utsatt for store bevegelser i luften. Bevegelsene minket når dekselet ble neddykket. Spenningsvariasjonen i løftesystemet økte når dekselet traff vannoverflaten, og avtok først når det var senket ned til 20 meters dybde.

De simulerte designgrensene var basert på spenningen i løfteslingsene. Det ble ikke observert noen store *snap*-krefter etter en *slack*-konisjon. De simulerte designgrensene var avhengig av både bølgehøyde og bølgeperiode. Den gjennomsnittlige designgrensen var beregnet til 2.5 m, og var periodeuavhengig. Derav ble operasjonsgrensen beregnet til 2 m, ved bruk av en  $\alpha$ -faktor på 0.81.

Operasjonen kan finne sted når bølgekonisjonene er under operasjonsgrensen over en lengre periode enn operasjonens referanseperiode. Opererbarheten ble undersøkt på to operasjonsfelt; Heidrun og Tanzania Blokk 2. Referanseperiodene for de to feltene var forskjellige på grunn av dybdeforholdene, og beregnet til å være henholdsvis 2.5 timer og 9.3 timer. Både opererbarheten og den faktiske operasjonstiden, basert på en tilfeldig start, var svært avhengig av årstidene og ble vurdert for operasjonsgrensene fra både manuell estimering og simulering.

Da operasjonsgrensen økte fra 1.25 m til 2 m økte opererbarheten med 30-50% på begge feltene, og den faktiske operasjonstiden for en tilfeldig start ble redusert med nesten 80% på Heidrunfeltet. Det vil si at for en gitt referanseperiode ble værventingsperioden redusert med det tilsvarende. På begge feltene var det som regel stormperioder, hvor bølgekonisjonene overskred operasjonsgrensen, som var grunnen til værventingen.

Operasjonsgrensen ble bestemt av flere faktorer; installasjonsmetoden, bølgekonisjonene, kran-spissbevegelsen,  $\alpha$ -faktoren og spenninger i løfteslingsene. Basert på dette kan man si at en operasjon bør ha en kort referanseperiode for å kunne bli utført ofte. Økt operasjonsgrense førte til økt opererbarhet og redusert værventing.

Dersom operasjonen skal finne sted på et tilfeldig tidspunkt vil risikoen for værventing øke. Vanligvis er en marin operasjon planlagt før utførelse og er da basert på værmeldinger. En slik planlegging vil med stor sannsynlighet redusere værventingen og øke operasjonseffektiviteten.

For å kunne bestemme høyest mulig operasjonsgrense slik at værventing kan reduseres, bør simuleringer bli utført i forkant av beskyttelsesdekselininstallasjoner. Derav kan operasjonskostnader, tomgangskjøring og forurensning kuttes vesentlig i forhold til å kun basere seg på den simplifiserte metoden.

# Contents

<b>1</b>	<b>Introduction</b>	<b>1</b>
1.1	Background . . . . .	1
1.2	Objectives . . . . .	2
1.3	Literature Study . . . . .	2
1.4	Limitations and Assumptions . . . . .	3
1.5	Structure of the Paper . . . . .	4
<b>2</b>	<b>Marine Operations</b>	<b>5</b>
2.1	The $\alpha$ -factor . . . . .	7
2.2	Weather Window . . . . .	8
2.3	Key Challenges . . . . .	10
2.4	The Planning Process . . . . .	10
2.5	Slack and Snap Loads . . . . .	12
<b>3</b>	<b>Lifting Procedures</b>	<b>13</b>
3.1	Lifting Phases . . . . .	13
3.1.1	Lift-off and In-air . . . . .	13
3.1.2	Splash Zone . . . . .	14
3.1.3	Lowering . . . . .	15
3.1.4	Landing on Seabed . . . . .	15
3.2	Heavy- and Light Lifts . . . . .	16
3.3	Heave Compensation . . . . .	16
3.4	Lifting Techniques . . . . .	17
3.4.1	Over Side Crane Operation . . . . .	17
3.4.2	Moonpool . . . . .	18
3.4.3	Special Handling Systems . . . . .	19
<b>4</b>	<b>Hydrodynamic Approach</b>	<b>21</b>
4.1	Linear Wave Theory . . . . .	21
4.2	Irregular Waves . . . . .	22
4.2.1	Wave Spectra . . . . .	23
4.2.2	Swell . . . . .	25
4.2.3	Seed Numbers . . . . .	25
4.3	Time Domain Analysis . . . . .	26
4.3.1	Equation of Motion . . . . .	26
4.3.2	Static and Dynamic Equilibrium . . . . .	27
4.4	Response Amplitude Operator . . . . .	28
4.5	Crane Tip Motion . . . . .	29

4.6	Hydrodynamic Parameters . . . . .	30
4.6.1	Added Mass Value . . . . .	30
4.6.2	Drag Coefficient . . . . .	31
4.7	The Simplified Method . . . . .	32
4.7.1	Wave Kinematics . . . . .	32
4.7.2	Drag Force . . . . .	33
4.7.3	Water Entry (Slamming) Force . . . . .	33
4.7.4	Inertia Force . . . . .	34
4.7.5	Varying Buoyancy Force . . . . .	34
4.7.6	Resulting Force . . . . .	35
<b>5</b>	<b>Statistical Models</b>	<b>37</b>
5.1	Weibull Distribution . . . . .	37
5.2	Extreme Value Distribution . . . . .	39
<b>6</b>	<b>SIMA</b>	<b>45</b>
6.1	Time Domain Simulation . . . . .	46
<b>7</b>	<b>The Simulation Model</b>	<b>49</b>
7.1	Environmental Conditions . . . . .	49
7.1.1	Locations . . . . .	49
7.1.2	Wave Conditions . . . . .	50
7.2	GRP Protection Cover . . . . .	52
7.3	Added Mass and Damping . . . . .	54
7.3.1	From WAMIT- and CFD-analyses . . . . .	54
7.3.2	Implemented in SIMA . . . . .	58
7.4	Lifting Equipment . . . . .	60
7.5	Installation Vessel . . . . .	65
<b>8</b>	<b>Establishment of Hydrodynamic Parameters</b>	<b>71</b>
8.1	Crane Tip Motion . . . . .	71
8.2	The Simplified Method . . . . .	74
8.2.1	Added Mass and Inertia Force . . . . .	74
8.2.2	Drag Force . . . . .	77
8.2.3	Slamming Force . . . . .	78
8.2.4	Varying Buoyancy Force . . . . .	80
8.3	Manually Estimated Design Criteria . . . . .	81
<b>9</b>	<b>Simulation Results</b>	<b>83</b>
9.1	Wave Conditions . . . . .	86
9.1.1	Motions . . . . .	89
9.1.2	Tension in Slings and Wires . . . . .	95

---

9.2	Gumbel Distributions . . . . .	98
9.3	Simulated Design Criteria . . . . .	105
<b>10</b>	<b>Planning</b>	<b>107</b>
10.1	Operability . . . . .	109
10.2	Distribution of Calm Periods . . . . .	115
10.3	Actual Duration of Operation with Random Start . . . . .	118
<b>11</b>	<b>Model Validation</b>	<b>123</b>
11.1	Static Analysis . . . . .	123
11.2	GRP Protection Cover . . . . .	123
11.3	Most Probable Largest Motion . . . . .	124
11.4	Forces Acting on the System . . . . .	124
11.5	Operability . . . . .	127
11.6	Distributions . . . . .	128
<b>12</b>	<b>Discussion</b>	<b>129</b>
12.1	The $\alpha$ -factor . . . . .	129
12.2	Weather Window . . . . .	129
12.3	Lifting Techniques . . . . .	130
12.4	The Simulation Model . . . . .	130
12.4.1	Environmental Conditions . . . . .	130
12.4.2	GRP Protection Cover . . . . .	131
12.4.3	Hydrodynamic Parameters . . . . .	131
12.4.4	Vessel and Crane Tip Motion . . . . .	132
12.5	Manual Estimation with the Simplified Method . . . . .	133
12.5.1	Added Mass . . . . .	133
12.5.2	Manually Estimated Design Criteria . . . . .	134
12.6	Installation Simulation . . . . .	134
12.6.1	Motions . . . . .	135
12.6.2	The Gumbel Distribution . . . . .	136
12.6.3	Slack and Snap Loads . . . . .	137
12.6.4	Simulated Design criteria . . . . .	137
12.7	Planning . . . . .	138
12.7.1	Operability . . . . .	138
12.7.2	Distribution . . . . .	140
12.7.3	Actual Duration of Operation with Random Start . . . . .	141
12.8	Error Sources . . . . .	142
<b>13</b>	<b>Conclusion</b>	<b>143</b>
13.1	Recommendations for Further Work . . . . .	145

<b>Appendices</b>	<b>A</b>
<b>A <math>\alpha</math>-factors for Waves</b>	<b>A</b>
<b>B Input to SIMA</b>	<b>B</b>
<b>C MATLAB codes</b>	<b>C</b>
C.1 Gumbel Plots . . . . .	C
C.2 Season Segregation . . . . .	E
C.3 Season Dependent Duration of Calms . . . . .	F
C.4 Operability . . . . .	H
C.5 Distribution of Length of Calms . . . . .	J
C.6 Actual Duration of Operation with Random Start . . . . .	M



## List of Tables

2.1	Weather forecast levels . . . . .	6
4.1	Overview of significant forces acting during different lifting phases . . . . .	35
7.1	Information about time series at Heidrun and Tanzania . . . . .	50
7.2	Correlation between months and <i>operation seasons</i> in Norway and in Tanzania . . . . .	50
7.3	Cover mass dimensions . . . . .	52
7.4	Cover dimensions . . . . .	53
7.5	Cover COG with respect to origin . . . . .	53
7.6	Added mass values from WAMIT . . . . .	54
7.7	Linear and quadratic damping for fully submerged cover . . . . .	57
7.8	Slender elements' coordinates, volume and mass . . . . .	58
7.9	Slender elements' added mass . . . . .	59
7.10	Slender elements' linear and quadratic damping . . . . .	59
7.11	Total added mass implemented in SIMA . . . . .	60
7.12	Total linear and quadratic damping implemented in SIMA . . . . .	60
7.13	Crane winch properties . . . . .	61
7.14	Structural mass of hook . . . . .	61
7.15	Body points of spreader bar . . . . .	62
7.16	Structural mass of spreader bar . . . . .	62
7.17	Body points of shackle . . . . .	62
7.18	Installation vessel dimensions . . . . .	65
7.19	Structural mass of installation vessel . . . . .	66
8.1	Selected wave conditions . . . . .	71
8.2	Crane tip motion, velocity and acceleration . . . . .	73
8.3	Added mass in longitudinal direction . . . . .	75
8.4	Added mass perpendicular to cover flanges . . . . .	76
8.5	Inertia forces . . . . .	77
8.6	Parameters used to calculate the drag coefficient in vertical direction . . . . .	77
8.7	Drag forces . . . . .	78
8.8	Vertical slamming force for three wave conditions . . . . .	80
8.9	Vertical varying buoyancy force for three wave conditions . . . . .	80
8.10	Total hydrodynamic force and manually estimated design criteria . . . . .	81
9.1	$H_s$ - $T_p$ conditions used in simulations . . . . .	83
9.2	Wave conditions below or above the slack criterion . . . . .	86
9.3	Minimum and maximum tension in slings . . . . .	98
9.4	Amount of seed numbers needed for 7% convergence . . . . .	98
9.5	7% convergence for 10% quantile . . . . .	100
10.1	Planned operation period for different phases . . . . .	107

10.2 $\alpha$ -factor for waves, level B highest forecast . . . . .	108
10.3 Weather categories with appurtenant criteria . . . . .	111
10.4 Average operability at Heidrun, $T_R = 2.5$ hours, $H_{s_{WF}} = 1.25$ m . . . . .	112
10.5 Average downtime at Heidrun, $T_R = 2.5$ hours, $H_{s_{WF}} = 1.25$ m . . . . .	112
10.6 Average operability at Heidrun, $T_R = 2.5$ hours, $H_{s_{WF}} = 2$ m . . . . .	112
10.7 Average downtime at Heidrun, $T_R = 2.5$ hours, $H_{s_{WF}} = 2$ m . . . . .	112
10.8 Average operability at Heidrun, $T_R = 7.25$ hours, $H_{s_{WF}} = 1.25$ m . . . . .	113
10.9 Average downtime at Heidrun, $T_R = 7.25$ hours, $H_{s_{WF}} = 1.25$ m . . . . .	113
10.10 Average operability at Heidrun, $T_R = 7.25$ hours, $H_{s_{WF}} = 2$ m . . . . .	113
10.11 Average downtime at Heidrun, $T_R = 7.25$ hours, $H_{s_{WF}} = 2$ m . . . . .	113
10.12 Operability and downtime for multiple $\alpha$ -factors, $T_R = 2.5$ hours, $H_{s_{LIM}} = 1.64$ m . . . . .	115
10.13 Operability and downtime for multiple $\alpha$ -factors, $T_R = 2.5$ hours, $H_{s_{LIM}} = 2.5$ m . . . . .	115
10.14 Weibull parameters fitting length of calms at Heidrun, $T_R = 2.5$ hours . . . . .	115
10.15 Weibull parameters fitting length of calms at Heidrun $T_R = 7.25$ hours . . . . .	116
10.16 Mean and standard deviation of length of calms and WOW, $T_R = 2.5$ hours . . . . .	116
10.17 Mean and standard deviation of length of calms and WOW, $T_R = 7.25$ hours . . . . .	116
10.18 Weibull parameters for actual duration of operations with random start at Heidrun . . . . .	118
10.19 Actual duration of operation with random start at Heidrun, $T_R = 2.5$ hours . . . . .	118
10.20 Actual duration of operation with random start at Heidrun, $T_R = 7.25$ hours . . . . .	119
11.1 Static analysis positions . . . . .	123
11.2 Linear damping validation . . . . .	124
11.3 Quadratic damping validation . . . . .	124
11.4 Mean and standard deviation of calms . . . . .	128
12.1 Operability at Heidrun for manually estimated and simulated design criteria . . . . .	139
12.2 Operability at Tanzania for manually estimated and simulated design criteria . . . . .	139
A.1 $\alpha$ -factor for waves, level B highest forecast . . . . .	A
A.2 $\alpha$ -factor for waves, level A with meteorologist at site . . . . .	A
A.3 $\alpha$ -factor for waves, monitoring & level A with meteorologist . . . . .	A
B.1 Input variables . . . . .	B

## List of Figures

2.1	Weather window . . . . .	6
2.2	Observed length of calms for different $H_{s_{WF}}$ at Heidrun and Tanzania . . . . .	8
2.3	Significant wave height with examples of work and wait periods . . . . .	9
2.4	Actual duration of operation with random start, $T_R = 12$ hours . . . . .	9
2.5	DNV GL's recommended planning procedure . . . . .	11
2.6	Illustration of slack criterion . . . . .	12
3.1	Lifting phases: 1. <i>In-air</i> , 2. <i>Through splash zone</i> , 3. <i>Fully submerged</i> . . . . .	13
3.2	Example of typical resonance periods . . . . .	15
3.3	Crane operation over side . . . . .	17
3.4	Tower installation over moonpool . . . . .	18
3.5	A test of a Special Handling System on board the North Sea Giant . . . . .	19
4.1	Water particles paths with water depth . . . . .	21
4.2	Wave spectrum, frequency and time Domain . . . . .	22
4.3	Examples of wave spectra . . . . .	24
4.4	Illustration of the seed number concept . . . . .	25
4.5	Table of added mass coefficients for a three-dimensional body . . . . .	31
4.6	Table of drag coefficients for a three-dimensional body . . . . .	31
4.7	An overview of application of the Simplified Method . . . . .	32
4.8	Relation between crane tip- and water particle acceleration . . . . .	34
4.9	Relation between crane tip motion and wave amplitude . . . . .	35
5.1	Distributions of the Gaussian Process, Individual Maxima and Extreme Values . . . . .	39
5.2	Establishment of the Extreme Value Distribution - Maxima . . . . .	40
5.3	Establishment of the Extreme Value Distribution - Minima . . . . .	40
5.4	Gumbel PDF for a) Minima and b) Maxima . . . . .	41
5.5	Gumbel CDF . . . . .	42
5.6	Gumbel Quantile Function . . . . .	42
5.7	Gumbel-plot of cumulative probability with polynomial fitting . . . . .	43
6.1	SIMO model of lifting system . . . . .	46
6.2	Parameters in Morison's equation defined on a cylinder . . . . .	47
7.1	Location of the Tanzania field . . . . .	49
7.2	Location of the Heidrun field . . . . .	49
7.3	$H_s$ - $T_p$ conditions for Heidrun - used in simulations . . . . .	51
7.4	$H_s$ - $T_p$ conditions for Tanzania . . . . .	51
7.5	CAD model of cover . . . . .	52
7.6	Cover dimensions with COG . . . . .	52
7.7	Dimensions of simplified cover . . . . .	53
7.8	Panel models in WAMIT: Simplified model and Complex model . . . . .	54

7.9	Directions of added mass . . . . .	55
7.10	Draught dependent added mass . . . . .	55
7.11	Draught dependent damping . . . . .	55
7.12	Added mass in surge $A_{11}$ from CFD-analyses . . . . .	56
7.13	Added mass in sway $A_{22}$ from CFD-analyses . . . . .	56
7.14	Added mass in heave $A_{33}$ from CFD-analyses . . . . .	57
7.15	Damping for cover calculated by CFD-analyses . . . . .	57
7.16	GRP cover with lifting equipment . . . . .	60
7.17	Vertical dimensions of cover with an angle of $68^\circ$ . . . . .	63
7.18	Upper part of rigging system with global coordinates . . . . .	64
7.19	Lower part of rigging system with global coordinates . . . . .	64
7.20	Vessel used in the simulation model with rigging system . . . . .	65
7.21	Illustration of the simulation model's origin, vessel COG and crane tip . . . . .	66
7.22	Coordinate system and definition of motions . . . . .	67
7.23	Given wave direction and vessel motion . . . . .	67
7.24	RAO for surge motion . . . . .	68
7.25	RAO for sway motion . . . . .	68
7.26	RAO for heave motion . . . . .	69
7.27	RAO for roll motion . . . . .	69
7.28	RAO for pitch motion . . . . .	70
7.29	RAO for yaw motion . . . . .	70
8.1	Vertical motion of the vessel COG and crane tip, $H_s = 3$ m, $T_p = 8$ s . . . . .	72
8.2	Vertical motion of the vessel COG and crane tip, $H_s = 3$ m, $T_p = 12$ s . . . . .	72
8.3	Vertical motion of the vessel COG and crane tip, $H_s = 2$ m, $T_p = 6$ s . . . . .	73
8.4	Decomposing of added mass . . . . .	74
8.5	Dimensions for estimation of longitudinal added mass . . . . .	75
8.6	Dimensions for estimation of perpendicular added mass . . . . .	76
8.7	Illustration of slamming forces and accelerations . . . . .	79
8.8	Linear scaling of hydrodynamic force . . . . .	81
9.1	Surge motion of cover and spreader bar . . . . .	84
9.2	Pitch motion of cover and spreader bar . . . . .	84
9.3	Sway motion of cover and spreader bar . . . . .	84
9.4	Yaw motion of cover and spreader bar . . . . .	84
9.5	Sway and yaw motion of spreader bar . . . . .	84
9.6	Tension in sling 1 and 2 with no environmental loads . . . . .	85
9.7	Tension in sling 3 and 4 with no environmental loads . . . . .	86
9.8	10% quantiles for various $T_p$ compared to slack requirement, $H_s = 2$ m . . . . .	87
9.9	10% quantiles for various $T_p$ compared to slack requirement, $H_s = 3$ m . . . . .	87
9.10	10% quantiles for various $T_p$ compared to slack requirement, $H_s = 4$ m . . . . .	88

9.11 Wave elevation for the three wave conditions . . . . .	88
9.12 Translation of spreader bar and cover, $H_s = 3$ m, $T_p = 8$ s . . . . .	89
9.13 Translation of spreader bar and cover, $H_s = 3$ m, $T_p = 12$ s . . . . .	89
9.14 Translation of spreader bar and cover, $H_s = 2$ m, $T_p = 6$ s . . . . .	90
9.15 Location of cover, $H_s = 3$ m, $T_p = 8$ s . . . . .	90
9.16 Location of cover, $H_s = 3$ m, $T_p = 12$ s . . . . .	91
9.17 Location of cover, $H_s = 2$ m, $T_p = 6$ s . . . . .	91
9.18 Rotation of spreader bar and cover, $H_s = 3$ m, $T_p = 8$ s . . . . .	92
9.19 Rotation of spreader bar and cover, $H_s = 3$ m, $T_p = 12$ s . . . . .	92
9.20 Rotation of spreader bar and cover, $H_s = 2$ m, $T_p = 6$ s . . . . .	93
9.21 Rotation of spreader bar and cover with added stiffness, $H_s = 3$ m, $T_p = 8$ s . . . . .	93
9.22 Rotation of spreader bar and cover with added stiffness, $H_s = 3$ m, $T_p = 12$ s . . . . .	94
9.23 Rotation of spreader bar and cover with added stiffness, $H_s = 2$ m, $T_p = 6$ s . . . . .	94
9.24 Tension in crane wire and force acting on hook, $H_s = 3$ m, $T_p = 8$ s . . . . .	95
9.25 Tension in crane wire and force acting on hook, $H_s = 3$ m, $T_p = 12$ s . . . . .	95
9.26 Tension in crane wire and force acting on hook, $H_s = 2$ m, $T_p = 6$ s . . . . .	96
9.27 Tension arising in slings, $H_s = 3$ m, $T_p = 8$ s . . . . .	96
9.28 Tension arising in slings, $H_s = 3$ m, $T_p = 12$ s . . . . .	97
9.29 Tension arising in slings, $H_s = 2$ m, $T_p = 6$ s . . . . .	97
9.30 Convergence test of Gumbel parameters and 10% quantile, $H_s = 3$ m, $T_p = 8$ s . . . . .	99
9.31 Convergence test of Gumbel parameters and 10% quantile, $H_s = 3$ m, $T_p = 12$ s . . . . .	99
9.32 Convergence test of Gumbel parameters and 10% quantile, $H_s = 2$ m, $T_p = 6$ s . . . . .	100
9.33 Gumbel PDF, $H_s = 3$ m, $T_p = 8$ s . . . . .	101
9.34 Gumbel PDF, $H_s = 3$ m, $T_p = 12$ s . . . . .	101
9.35 Gumbel PDF, $H_s = 2$ m, $T_p = 6$ s . . . . .	102
9.36 Gumbel CDF, $H_s = 3$ m, $T_p = 8$ s . . . . .	102
9.37 Gumbel CDF, $H_s = 3$ m, $T_p = 12$ s . . . . .	103
9.38 Gumbel CDF, $H_s = 2$ m, $T_p = 6$ s . . . . .	103
9.39 Gumbel-plot for tension in sling 1, $H_s = 3$ m, $T_p = 8$ s . . . . .	104
9.40 Gumbel-plot for tension in sling 1, $H_s = 3$ m, $T_p = 12$ s . . . . .	104
9.41 Gumbel-plot for tension in sling 1, $H_s = 2$ m, $T_p = 6$ s . . . . .	105
9.42 Simulated design criteria . . . . .	106
9.43 Manually estimated and simulated design criteria . . . . .	106
10.1 Illustration of safe conditions . . . . .	107
10.2 Vessel lifting cover in vertical direction . . . . .	108
10.3 Wave conditions at Tanzania and Heidrun for two wave criteria . . . . .	109
10.4 Observed duration of calms vs. operational criterion for various seasons at Heidrun . . . . .	110
10.5 Observed duration of calms vs. operational criterion for various seasons at Tanzania . . . . .	110
10.6 Observed duration of calms vs. $H_s$ at Heidrun and Tanzania . . . . .	111

10.7 Operability for each season at Heidrun . . . . .	114
10.8 Operability for each season at Tanzania . . . . .	114
10.9 Weibull distribution of calm periods during spring for $H_{s_{WF}} = 2$ m, $T_R = 2.5$ . . . . .	117
10.10 Weibull distribution of calm periods during spring for $H_{s_{WF}} = 2$ m, $T_R = 7.25$ . . . . .	117
10.11 Actual duration of operation with random start, $T_R = 2.5$ hours, $H_{s_{WF}} = 1.25$ m . . . . .	119
10.12 Actual duration of operation with random start, $T_R = 2.5$ hours, $H_{s_{WF}} = 2$ m . . . . .	120
10.13 Actual duration of operation with random start, $T_R = 7.25$ hours, $H_{s_{WF}} = 1.25$ m . . . . .	120
10.14 Actual duration of operation with random start, $T_R = 7.25$ hours, $H_{s_{WF}} = 2$ m . . . . .	121
10.15 Actual duration of operation with random start, $T_R = 9.3$ hours, $H_{s_{WF}} = 1.25$ m . . . . .	121
10.16 Actual duration of operation with random start, $T_R = 9.3$ hours, $H_{s_{WF}} = 2$ m . . . . .	122
11.1 Forces on lifting equipment . . . . .	125
11.2 Defined forces of lifting equipment . . . . .	125
11.3 Forces acting on hook and tension in crane winch with no environmental loads . . . . .	126
11.4 Tension arising in sling 3 and 4 with no environmental loads . . . . .	126
11.5 Tension arising in sling 1 and 2 with no environmental loads . . . . .	127



# Nomenclature

## Abbreviations

AHC	Active Heave Compensation
CDF	Cumulative Distribution Function
CFD	Computational Fluid Dynamics
COG	Centre Of Gravity
DAF	Dynamic Amplification Factor
DNV GL	Det Norske Veritas Germanischer Lloyd
dof	Degrees of freedom
DP	Dynamic Positioning
FD	Frequency Domain
GRP	Glass Reinforced Plastic
ISSC	International Ship and offshore Structures Congress
ITTC	International Towing Tank Conference
JONSWAP	Joint North Sea Wave Project
LMHS	Light Module Handling System
P-M	Pierson-Moskowitz
PDF	Probability Density Function
PHC	Passive Heave Compensation
RAO	Response Amplitude Operator
ROV	Remotely Operated Vehicle
SHS	Special Handling System
SWL	Safe Working Load
TD	Time Domain
WOW	Waiting On Weather

## Constants

$\gamma$	Euler-Mascheroni	0.5772 [-]
$g$	Gravity	9.81 [ $\frac{m}{s^2}$ ]
$\rho$	Sea Water Density	1 025 [ $\frac{kg}{m^3}$ ]

## Greek Symbols

$\alpha$	$\alpha$ -factor, a correlation factor between forecasted and observed values
$\beta$	Shape Parameter in Weibull distribution

$\beta$	Gumbel Parameter
$\gamma$	Scale Parameter in Weibull distribution
$\gamma$	Peakedness Parameter in JONSWAP spectrum
$\epsilon$	Phase Angle
$\zeta$	Wave Elevation
$\zeta_a$	Wave Amplitude
$\dot{\zeta}$	Wave Velocity
$\eta$	Single Amplitude Motion
$\eta_3$	Translation in Heave
$\dot{\eta}_3$	Velocity in Heave
$\ddot{\eta}_3$	Acceleration in Heave
$\eta_{ct}$	Crane Tip Vertical Motion
$\dot{\eta}_{ct}$	Crane Tip Vertical Velocity
$\eta_{ct}^{max}$	Most probable crane tip motion
$\mu$	Gumbel Parameter
$\xi$	Damping Ratio
$\tau_c$	Calm Period, <i>calms</i>
$\tau_s$	Storm Period, <i>storms</i>
$\phi$	Velocity Potential
$\omega$	Wave Frequency
$\omega_0$	Natural Frequency
$\omega_p$	Peak Frequency

### Roman Symbols

$A_p$	Horizontal Projected Area of Lifted Object
$A_p$	Water plane Area of Lifted Object
$A_{11}$	Perpendicular Added Mass
$A_{22}$	Transverse Added Mass
$A_{33}$	Added Mass in Heave
$A_{33}$	Longitudinal Added Mass
$A_{ij}$	Wave amplitude for wave component <i>ij</i>
$c$	Damping Coefficient
$C_A$	Dimensionless Added Mass Coefficient
$C_D$	Drag Coefficient
$C_S$	Slamming Coefficient

$c_{cr}$	Critical Damping Coefficient
$d$	Distance from sea surface to the centre of gravity of lifted object
$F_3$	Excitation Force in Heave
$F_B$	Varying Buoyancy Force
$F_D$	Drag Force
$F_I$	Inertia Force
$F_S$	Slamming Force
$H_s$	Significant Wave Height, defined as the mean of the one third highest waves
$H_{sLIM}$	Design Criterion for Significant Wave Height
$H_{sWF}$	Operational Criterion for Significant Wave Height
$K$	Stiffness of Hoisting Cable
$k$	Restoring Coefficient
$k$	Wave Number
$L$	Length of Cover
$L$	Wave Length
$m$	Mass of Lifted Object
$m_a$	Added Mass Coefficient
$OP_{LIM}$	Design Criterion
$OP_{WF}$	Operational Criterion
$Re$	Reynolds Number
$T$	Wave Period
$t$	Time
$T_C$	Contingency Time
$T_z$	Zero up-crossing period
$T_{POP}$	Planned Operation Period
$T_R$	Reference Period
$u_{current}$	Average Current Speed
$\delta V$	Varying Volume due to Oscillation
$v_c$	Hoisting Velocity
$V_R$	Reference Volume
$v_r$	Relative Velocity between Lifted Object and Water Particles
$v_w$	Water Particle Velocity
$\dot{v}_w$	Water Particle Acceleration
$z$	Distance from sea surface to lower bound of lifted object



# 1 Introduction

## 1.1 Background

The oil and gas industry has become more challenging the past years and marine operations must be performed in a smarter and more efficient way. An offshore lifting operation is one of the most common marine operation. Subsea production systems have become the most attractive option in most field development scenarios, both in terms of capital expenditure and technical solutions. In order to design, install and operate a subsea oil and gas factory, a cost-effective installation method is crucial. Present capital expenditure of the marine operations for a subsea production system in 300-500 meter water depth is for some cases in the range 15-30% of the total capital invested. Subsea hardware facilities typically consist of templates, manifolds and wellheads as well as lot of in-field flow-lines and pipeline connections.

A key activity to carry out a successful subsea installation operation is the planning process. Lifting of subsea equipment, especially through the wave zone, is a weather critical activity. It is crucial that such operations are planned and understood properly and that effective equipment and lifting methods are used, in order to carry out the operation in a safe, effective and smart way. This thesis shall specifically consider installation of subsea equipment protection covers.

There is an increasing trend to develop processing equipment that can be stationed permanently on the seabed. However, maintenance, repair, inspection and replacement of equipment must be performed regularly. New lifting techniques have been developed lately to increase the limiting sea state and hence increase the operation's operability, decrease waiting on weather and in some cases extend the operational seasons. This may reduce engine idling and unnecessary pollution. Deep water operations will introduce new challenges in terms of operation execution and already existent rules and standards.

This Master Thesis describes a study aimed at finding as high operational design criterion for an installation of a GRP pipeline protection cover as possible, by use of both manual estimation methods and numerical simulations. The advantages of using GRP as a material for protecting subsea equipment in the oil and gas industry, are its high impact absorption capacity, low weight and durability. GRP covers have been installed offshore for many years, and is a part of general installation procedures. However, few analysis and calculations of hydrodynamic forces acting on the cover during a lift have been performed.

## 1.2 Objectives

As stated in the enclosed work description, the objectives of this thesis can be summarised as follows:

1. Describe briefly state of the art subsea installation methods by use of crane vessels. For weather restricted operations, an overview of the planning process shall be described; in particular the  $\alpha$ -factor concept and how operability and weather windows can be optimised.
2. Familiarise with the numerical simulation suite SIMA/SIMO and describe the theory that is relevant for subsea lifting and installation of GRP protection covers for subsea equipment.
3. Verify and describe an existing numerical simulation model in SIMA for a GRP protection cover. In particular, describe how important parameters like added mass and drag forces are defined in the numerical simulation model. Propose parameters that may determine the design operational limit and estimate limits based on simulation results. The variability of the design responses shall be assessed.
4. Operability investigation. Operability and times for waiting on weather shall be calculated based on given data for North Sea and a location east of Africa. Use results from task 3. The following shall be included; a) safe conditions, b) time consumption and alpha factors, c) required weather windows.
5. Conclusions and recommendations for further work.

## 1.3 Literature Study

The general theory behind marine operations is mainly based on DNV GL's *Recommended Practice H103* (2011b) and *Offshore Standard H101* (2011a), in addition to the course material in *TMR4225 - Marine Operations* at NTNU, provided by Kjell Larsen (2017).

Generally, the theory behind the simulation modelling and numerical simulations of the cover installation is based on a paper written by Frøydis Solaas et al. (2016). The theory behind the numerical model suite in SIMA/SIMO has been gained from the SIMA User's Manual.

Several other papers have also been used in order to cover all topics described in this Master Thesis.



## 1.4 Limitations and Assumptions

The cover was implemented as eleven slender elements into the simulation model in SIMA in order to take care of depth dependent hydrodynamic parameters. Amplitude dependent hydrodynamic parameters could not be implemented, hence results from CFD-analysis with an amplitude of 2.5 m were used.

Only the *through splash zone* phase was simulated, and the total hydrodynamic force was manually estimated for only *one* draught.

DNV GL's  $\alpha$ -factors, found in Appendix A, were used for both the Norwegian and Tanzanian fields. The  $\alpha$ -factors were based on the assumptions of no seasonal nor area variations, no differences between the providers and that the forecasts were according to Normal Distribution (Lundby, 2006).

When using DNV GL's Simplified Method for manual estimation it was assumed that the added mass and drag coefficient could be found for a rectangular flat plate with an area equal to the projected area. The Simplified Method is based on following assumptions (DNV GL, 2011b):

- The wave length is large relative to the horizontal length of the lifted object
- The vertical motion of the lifted object follows the crane tip motion
- The vertical motion of the object dominates, and all other motions can be disregarded

For manual estimation it was assumed a horizontal sea bottom and a free-surface of infinite horizontal extent, hence linear wave theory could be used. It was also assumed that the pressure followed Bernoulli's equation for infinite water depth, and that the sea was incompressible, inviscid and the fluid motion was irrotational. In the simulation model the environment was characterised by short-term short-crested irregular waves and directional JONSWAP spectra. For short-term waves it was assumed that the sea surface was stationary for a duration of 3 hours. Simulations were performed for head sea. Current and wind loads were omitted for both manual estimations and simulations.

For simplicity it was assumed that buoyancy did not act on the hook, wire and spreader bar.

Some of the calculations has been performed in MATLAB, but the attached codes do only yield results for sling 1, or operability for *one* wave condition at *one* field. The MATLAB codes for regular plots, as tension in slings etc., have been omitted in the appendices.

## 1.5 Structure of the Paper

The rest of the thesis is organised as follows:

- Section 2 gives general information about marine operations, operational criteria, weather windows, key challenges with marine operations, the planning process in general and the theory behind slack and snap loads.
- Section 3 presents different lifting phases, typical lift categories, heave compensation and state of the art lifting techniques.
- Section 4 focuses on the hydrodynamic approach. Linear wave theory and irregular waves are explained. Time domain analysis are described, where the equation of motion is presented. Crane tip motion and hydrodynamic parameters as added mass and drag are also described here. The last part of the Section presents the Simplified Method in details.
- Section 5 presents the two statistical models used in this thesis; the Weibull distribution and the Gumbel distribution, that is an extreme value distribution,
- Section 6 presents relevant theory about the simulation tool SIMA.
- Section 7 presents the simulation model containing input data and environmental conditions.
- Section 8 presents the manually estimated hydrodynamic force, found by use of the Simplified Method. Calculated added mass, drag, slamming and varying buoyancy forces are described in details. This Section does also present the crane tip motion and the manually estimated design criteria.
- Section 9 contains all the simulation results gathered from three selected wave conditions. The motion of the lifting system is visualised and the tension arising is illustrated graphically. This Section does also present the simulated design criteria and the relevant statistical plots are visualised.
- Section 10 focuses on the installation's operability and actual duration of operation with random start, at both Heidrun and Tanzania, based on both the manually estimated and simulated design criteria. A distribution of the length of calms is also presented.
- Section 11 presents the model validation and verification.
- Section 12 provides the discussion of this Master Thesis where the aforementioned material has been synthesised. This Section does also contain error sources.
- Section 13 presents the conclusions of this Master Thesis in addition to recommendations for further work.

## 2 Marine Operations

A marine operation is a non-routine operation of a limited defined duration related to handling objects and/or vessels in the marine environment. A marine operation shall be designed to bring an object from *one* defined safe condition to another safe condition. A safe condition is where the object is considered exposed to *normal* risk for damage or loss, where *normal* refers to a risk similar to the risk expected during *in-place* condition (Larsen, 2016). A marine operation consists of *two* phases; the design and planning phase *and* the execution of the operation phase (DNV GL, 2011b). The marine operation shall always be planned and performed with adequate consideration for environmental conditions in addition to the vessel motions' and structural loads' operational limits (Natskår et al., 2015). A marine operation shall also be planned according to defined codes and standards to ensure high safety. The operations should be designed based on the assumption that it may be needed to interrupt by either reversing the operation or bring it back to a safe condition. They shall be performed within defined safety levels, and the design acceptance criterion is to ensure a probability for structural failure less than  $10^{-4}$  per operation (DNV GL, 2011a). The given probability might increase when operational errors, human errors and other factors that affect the probability are taken into account.

Marine operations are divided into two categories; *weather restricted* and *weather unrestricted* operations. A weather restricted operation shall be of a limited duration, and the planned operation time is usually less than 72 hours. The operation can take place safely within the limits of a given weather forecast. A weather unrestricted operation can take place safely in any weather condition and is usually longer than 72 hours. The weather window for an unrestricted operation is based on long term statistics with seasonal and statistical extremes for the operation area. The weather window for a restricted operation is given by forecasts at the specific operation location, independently of statistical data. Thus the operation can be designed and planned for a significantly lower environmental condition than an unrestricted operation. A consequence of planning a weather restricted operation is that an  $\alpha$ -factor has to be considered. The  $\alpha$ -factor takes uncertainties in the weather forecast into account and is further described in *section 2.1 The  $\alpha$ -factor*.

A marine operation's reference period  $T_R$  is given by equation (2.1) and is the total operation period.  $T_{POP}$  is the planned operation period and starts simultaneously when the first weather forecast is given.  $T_C$  is the estimated maximum contingency period.

$$T_R = T_{POP} + T_C \quad (2.1)$$

$T_{POP}$  should be based on a detailed, planned schedule for the operation and is the basis for selecting the  $\alpha$ -factor, while  $T_C$  shall consider uncertainties in the planned operation period. For a weather restricted operation  $T_C$  shall cover possible unforeseen situations and delays due to weather. If uncertainties in the planned operation period and required time for contingency situations are not assessed in detail,  $T_C$  should be similar to  $T_{POP}$ . An applied contingency time less than 6 hours

is normally not acceptable (DNV GL, 2011a). The relation between  $T_{POP}$ ,  $T_C$  and  $T_R$  is shown in figure 2.1.

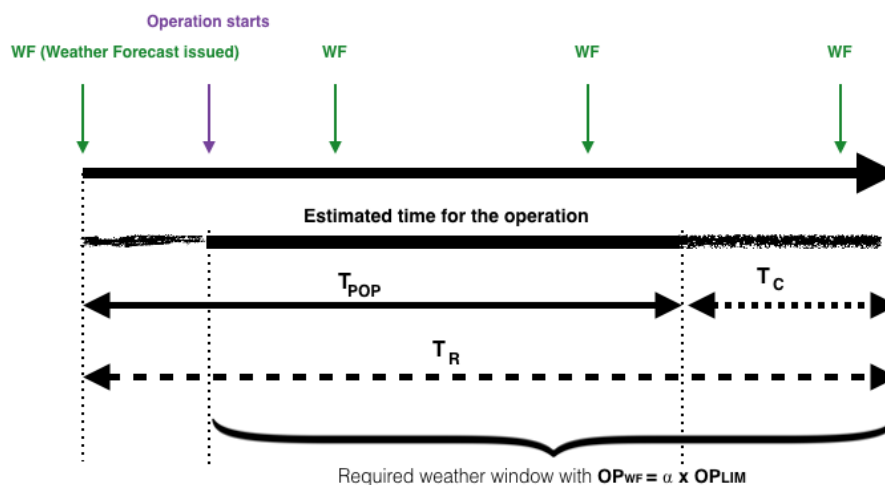


Figure 2.1: Weather window

Weather restricted marine operations are divided into *three* categories; *level A, B* and *C*. Every category has their own requirements that have to be fulfilled before the operation can take place. These requirements are listed in Table 2.1. Level A marine operations are major operations sensitive to weather, such as; mating operations, offshore float over and offshore installation operations among others. Level B marine operations are of significant importance with regard to value and consequences and are sensitive to weather conditions, e.g. offshore lifting and subsea installation. Level C marine operations are more ordinary operations less sensitive to environmental conditions, and are typically onshore and inshore lifting (DNV GL, 2011a).

Table 2.1: Weather forecast levels (DNV GL, 2011a, H101, section 4)

Weather Forecast Level	Meteorologist required on site?	Independent WF WF sources	Maximum WF interval
A	Yes <sup>1</sup>	2 <sup>2</sup>	12 hours <sup>3</sup>
B	No <sup>4</sup>	2 <sup>5</sup>	12 hours
C	No	1	12 hours

<sup>1</sup> There should be a dedicated meteorologist, but it may be acceptable that he/she is not physically present at site. The meteorologist opinion regarding his/her preferable location should be duly considered. It is anyhow mandatory that the dedicated meteorologist has continuous access to weather information from the site and that he/she is familiar with any local phenomenon that may influence the weather conditions. Note also that the meteorologist shall be on site in order to use alpha factors from Table A.2 and A.3 in Appendix A.

<sup>2</sup> It is assumed that the dedicated meteorologist (and other involved key personnel) will consider weather information/forecasts from several (all available) sources.

<sup>3</sup> Based on sensitivity with regards to weather conditions smaller intervals may be required.

<sup>4</sup> Meteorologist shall be conferred if the weather situation is unstable and/or close to the defined limit.

<sup>5</sup> The most severe weather forecast to be used.

## 2.1 The $\alpha$ -factor

In order to account for uncertainties in weather forecasts, the weather limit for performing a marine operation has to be reduced compared to the design weather conditions. This is done by introducing an  $\alpha$ -factor. The  $\alpha$ -factor is based on  $T_{POP}$  and  $H_s$  and is the relation between the design criterion and the operational criterion, given by equation (2.2). The design criterion  $OP_{LIM}$  is the weather condition used for calculation of design load effects.  $OP_{LIM}$  should never be greater than; maximum environmental criteria, the conditions for safe working of personnel, the equipment restrictions or limiting conditions for diving systems and position keeping (Alv er, 2008). The operational criterion  $OP_{WF}$  is the maximum weather condition for carrying out the marine operation, and is determined during the planning process and controlled by the weather forecast (Larsen, 2016).

$$OP_{WF} = \alpha \cdot OP_{LIM} \quad (2.2)$$

The  $\alpha$ -factor was introduced in 1995 as an allowance for uncertainties in forecasted versus actual weather. It was based on forecasted and observed values over a period of two years at two locations in the North Sea, in addition to *one* provider. When introduced it was considered a more accurate and documented approach than all previous practice. The  $\alpha$ -factor found in 1995 did not consider short-term operations with real time monitoring of environmental conditions. One of the main challenges in 1995 was a limited amount of data available (DNV, 2007). The  $\alpha$ -factor was improved in 2006 due to increased quality of forecasting services and more advanced monitoring techniques. The update was based on more locations and *three* providers (Alv er, 2008). Some consistent improvements of the results from 1995 were found, but these were less than initially expected (DNV, 2007).

The  $\alpha$ -factor is an important parameter for safety and cost for offshore operations and should be as reliable as possible in order to maintain high operation operability.  $\alpha$ -factors for different levels of marine operations can be found in *Appendix A*. The  $\alpha$ -factors given by DNV GL are reliable within Europe (Lundby, 2006).

The  $\alpha$ -factor should be calibrated to ensure that the probability of exceeding the design criterion with more than 50% is less than  $10^{-4}$  (DNV GL, 2011a). The  $\alpha$ -factor should be estimated based on the weather uncertainty for the actual site and the planned period of the operation. It includes the fact that it is harder to estimate the wave height for small sea conditions than for larger seas. The  $\alpha$ -factor does always have a magnitude less than one and will increase with increased quality of weather forecasts and the use of on-site monitoring systems. It decreases with the length of the planned operation, hence the difference between  $OP_{LIM}$  and  $OP_{WF}$  increases with increased  $T_{POP}$ .  $H_s$  is a preferred assessment parameter because waves are considered as the most influencing parameter with respect to performance for the majority of marine operations. The amount, availability and quality of the data records for  $H_s$  are usually satisfactory (DNV, 2007).

## 2.2 Weather Window

A weather window is a period of time that is sufficient in length to safely carry out a marine operation. Weather forecasted environmental conditions shall remain below the operational criterion for the whole length of the operation's reference period (Larsen, 2016). Calm periods, also called *calms* ( $\tau_c$ ), are periods where  $H_s$  is lower than the operational criterion. Storm period, also called *storms* ( $\tau_s$ ), are periods where  $H_s$  is higher than the operational criterion. An operation can only take place when the weather forecast predicts a calm period that is of *longer* duration than the determined reference period  $T_R$ .

Figure 2.2 shows an example of observed length of calms at Heidrun (blue) and at Tanzania (black) for multiple operational significant wave heights  $H_{s_{WF}}$ .  $H_{s_{WF}}$  and  $T_R$  were determined to be 3 m and 72 hours respectively, and the two criteria segregate the observed length of calms into *work* and *wait* categories. A *work period* is defined as a calm period of longer duration than the reference period. *Wait periods* are storm periods and calm period of shorter duration than  $T_R$ , also referred to as *calm-wait* periods.

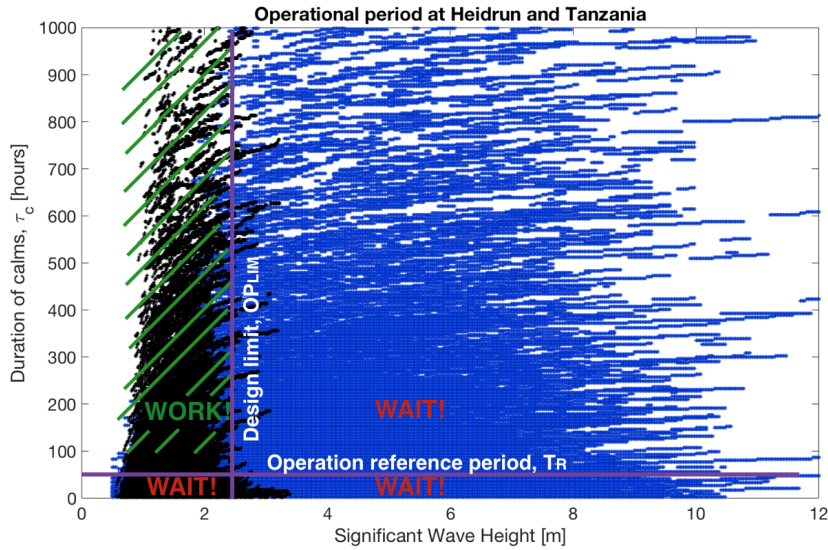


Figure 2.2: Observed length of calms for different  $H_{s_{WF}}$  at Heidrun (blue) and Tanzania (black)

Figure 2.3 shows a time series of wave elevation with examples of work periods and wait periods for a given operational criterion  $H_{s_{WF}}$ . The wait period does include calms of shorter duration than  $T_R$ . The likelihood that the planned operation can take place and carried through safely is equal to the probability that  $H_s$  is lower than  $OP_{WF}$  for a longer duration than  $T_R$ . The likelihood can be calculated by equation (2.3) and determines the operation's operability (Larsen, 2017).

$$P_{work} = P((H_s \leq OP_{WF}) \cap (\tau_c \geq T_R)) = P[(\tau_c \geq T_R) | (H_s \leq OP_{WF})] \cdot P(H_s \leq OP_{WF}) \quad (2.3)$$

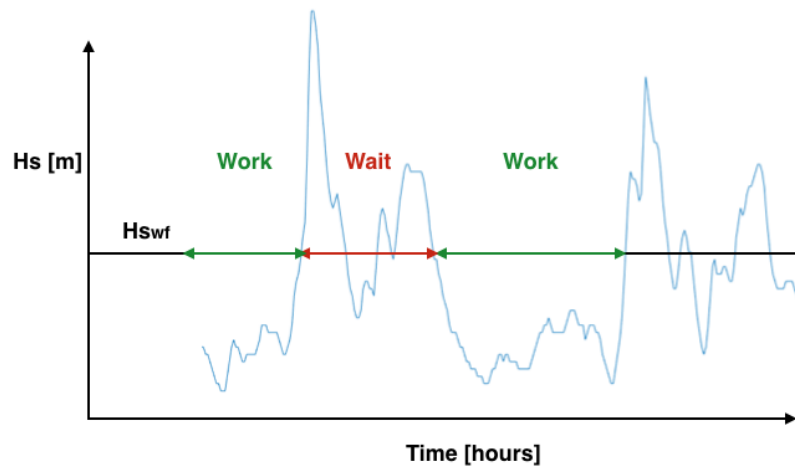


Figure 2.3: Significant wave height with examples of work and wait periods

In most cases it will be interesting to predict the total duration of the operation, including Waiting on Weather (WOW), if the operation starts at a random time, i.e. without checking the weather forecast in advance. This is called the actual duration of operation  $T_{op}$  and can be found by the average length of several work-periods starting at a random time for a given time series.  $T_{op}$  will be season dependent, thus season variation should be considered. It is preferred to have the actual duration of operation close to  $T_R$  in order to avoid waiting. An example of a time series with a given  $H_{sWF}$  and  $T_R$  of 12 hours is shown in Figure 2.4, where the actual duration of the operation is illustrated for seven random starts, where only  $T_7$  includes zero waiting. The other six periods contain 12 hours work (green line) in addition to some waiting (red line). In these cases, the average duration of operation for a random start will be of longer duration than the reference period.

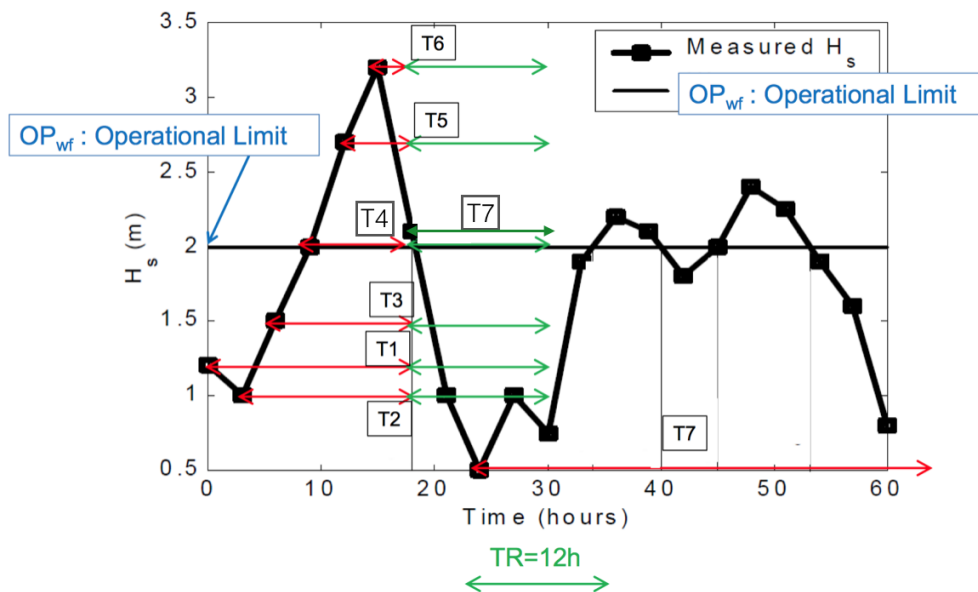


Figure 2.4: Actual duration of operation with random start,  $T_R = 12$  hours (Larsen, 2017)

## 2.3 Key Challenges

The environment has become more challenging the past years and exploration of new frontiers and areas is more common. Some challenges are deep water oil and gas operations in up to 3000 meter depth, operations in arctic areas and operations related to renewable energy such as offshore wind. The aquaculture is becoming more competence driven and stricter regulations have been developed also within this area. The combination of environmental conditions as wind, waves and current is hard to simulate and adequate results can be difficult to achieve. During a deep water lift the static weight acting on the crane tip will increase due to a longer hoisting wire. This might lead to larger oscillation periods in heave, decreased cable stiffness and resonance might occur. The drag forces in horizontal direction may increase due to the cable's large projected area, which can result in large offset. It is also difficult to manoeuvre and relocate an object in deep water, hence operation delays can be provided (Larsen, 2016).

To increase the lifetime of already existing structures and equipment, complex maintenance and reparations have to be performed. Removal of marine structures might be challenging and involve new vessel types. More complex operations and larger modules may introduce difficulties in simulations. There are strict requirements to cost, efficiency and safety, and in order to optimise the operation based on these three requirements, detailed planning and design become highly important. Increased weather windows will optimise operation cost and efficiency. To ensure safety it is important to understand and manage exposed risk and system behaviour. Typical marine operation risks are position loss, collisions and grounding during transport, icing, dropped objects and structural failures. Also lack of competence of personal and insufficient operational procedures are of potential high risk (Larsen, 2016).

Planning and performing marine operations more cost effectively while the safety and accuracy are maintained will always be a challenge. Smarter and faster solutions are required, and increased use of autonomy is probably necessary. Political requirements, e.g. emission regulations, introduce new challenges in terms of cost, efficiency and safety and can result in development of new technology.

## 2.4 The Planning Process

Planning of a marine operation shall be according to *fail safe*-principles. An operation is safe if it fails to a safe state (Gjersvik, 2015). Planning is important in order to ensure safety and reduce cost. The operation's classification in terms of weather restrictions might have a great impact on the safety and the cost of the operation, and should therefore be defined as early as possible in the planning process. The planning should as far as it is attainable be based on well proven principles, techniques, systems and equipment. Operations within an unknown environment or with new technology shall be documented through acceptable qualification processes. During the



planning process any unforeseen situations shall be identified, and plans shall be made to prevent those kinds of situations.

A complex marine operation should be divided into sub-operations where each sub-operation can be either weather restricted or unrestricted, and different  $\alpha$ -factors can be determined. This determination may have a great impact on the weather windows, the safety and cost of the operation (Larsen, 2017). When a marine operation shall be planned and designed, DNV GL (2011a) recommends to follow the iterative procedure shown in Figure 2.5.

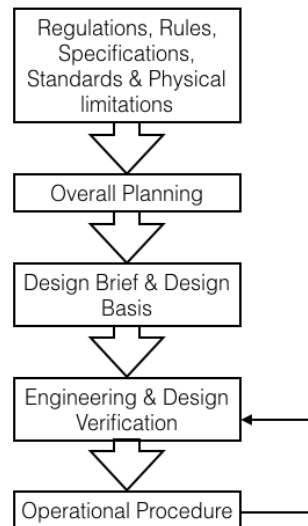


Figure 2.5: DNV GL's recommended planning procedure (DNV GL, 2011a)

The following sequence includes more details for each step in Figure 2.5 (DNV GL, 2011a, H101).

1. Identify rules, company specifications and standards and physical limitations as surveys of structures and local environmental conditions.
2. Overall planning; operational concepts, available vessels and equipment, cost and schedule and risk assessment.
3. Establish design basis and briefs; describing environmental conditions and physical limitations, and specify applicable codes and acceptance criteria.
4. Perform design; estimate load effects and decide required structural resistance.
5. Develop operation procedures.

To ensure planning with appropriate safety margins and weather forecast, all marine operations shall be documented. The documentation shall be checked by an external part before the operation takes place. The documentation shall include environmental conditions, operational criteria and weather forecasts (Larsen, 2016).

## 2.5 Slack and Snap Loads

A marine lifting operation is usually performed with a crane wire and lifting slings. Slings do not compress loads and do only have capacity in tension. Hence they can be exposed to *slack* during the lift, which is when there is no tension in the lifting wire or sling. Slack is usually due to the combination of the vessel and crane tip motion and vertical velocity, and will occur when the hydrodynamic forces exceed the submerged static weight of the lifted object. This occurrence does usually take place during the *splash zone* phase or when the cover is fully submerged, particularly for a wave environment.

Snap loads are impact loads caused by abrupt retention of the wire or sling, and do usually occur if the cable system is exposed to motions with large amplitudes and/or high frequency (NTIS, 1973). The snap loads can have a magnitude many times greater than the dynamic equilibrium forces that occur in a steady state response (Thurston et al., 2011). Slack is therefore critical because the snap load can exceed the sling's or wire's yield strength and break the material. Another critical aspect with slack is that the sling can be deformed and bent during the slack condition. This can damage the fibres and defect the sling. Pursuant to DNV GL's Recommended Practice of Modelling and Analysis of Marine Operations (DNV GL, 2011b) all snap forces shall as far as possible be avoided and the weather criteria should be adjusted to ensure this. The required minimum margin against slack is 10% of the submerged weight in each sling, and is illustrated in Figure 2.6. The hydrodynamic force shall therefore never exceed 90% of the submerged weight of the lifted object. In addition to the slack criterion, the lifting equipment needs to go through a capacity check, according to *DNV-OS-H205*, before the operation can be executed.

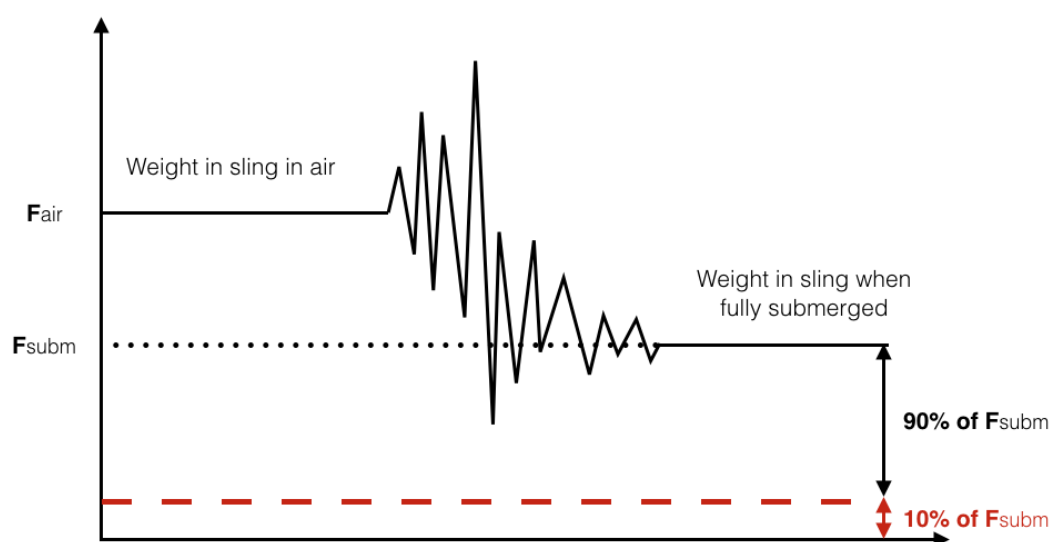


Figure 2.6: Illustration of slack criterion

## 3 Lifting Procedures

Launch and recovery of objects should always be performed in a safe way. Waiting on weather is a costly stop of a marine operation and should be reduced to its minimum, without impairing the safety of personnel or equipment. There are several ways to perform an offshore lift and the selected method and used equipment are usually dependent on the dimensions of the lifted object. The following subsections will describe the different lifting phases and their respective challenges in addition to the difference between heavy and light lifts and three state of the art lifting techniques.

### 3.1 Lifting Phases

A lifting operation does usually involve a vessel, a crane and the lifted object. A subsea lift consists of different phases; lift-off and in-air, lowering through splash zone, further lowering to seabed and positioning and landing. All the phases shall be evaluated during the planning process. In the following subsection the different phases will be described in detail and the challenges that one can be exposed to during each phase will be highlighted. Figure 3.1 shows the lifting phases *In-air*, *Through Splash Zone* and *Fully Submerged*.

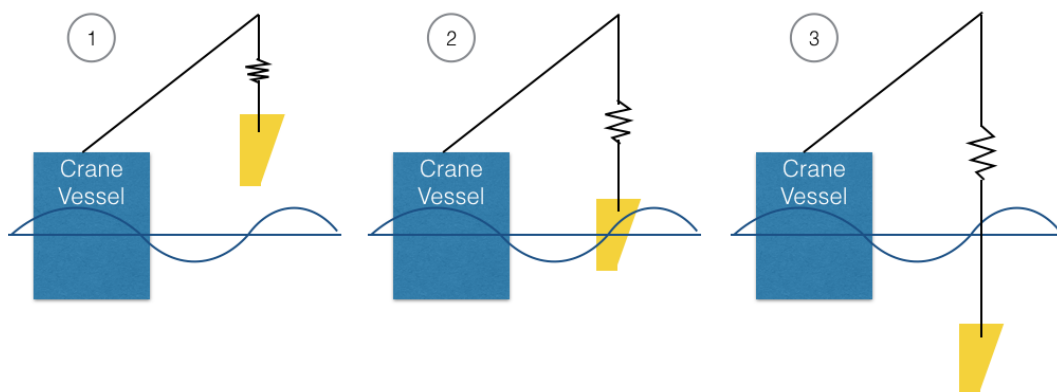


Figure 3.1: Lifting phases: 1. In-air, 2. Through splash zone, 3. Fully submerged

#### 3.1.1 Lift-off and In-air

A lift-off operation includes lift from other vessel, from deck or from shore. In this paper a lift-off is referred to as a lift from a deck of a crane vessel. Before the lifting can take place, the sea fastening has to be unfastened. If the weather restrictions allow it, this process can start prior to the given planned operation period, while waiting on operational weather window. The duration of this process is highly dependent on how it is sea fastened, e.g. if it is strapped or welded.

Vertical and horizontal motions of the crane tip will occur when the crane starts to lift, and it is

important to be aware of any snap loads that can arise due to start. Dynamic coupling between the object and the vessel can occur. Ballasting operations might be performed to compensate for such motions, either by active ballasting or anti-heeling systems. It is important to be aware of the crane radius and its reach capacity. For safety reasons one should ensure clearance to other structures and people, and have clear communication between deck crew, crane operator and the bridge.

Identified hazards during lift-off can be unacceptable tension in the lifting wire and slings, as either snap or slack loads, and horizontal motion or re-hit of the object after lift-off. It is important to be aware of the criteria related to these hazards, and determine the hoisting speed based on the wire stiffness, the total mass of the lifted object with rigging equipment, in addition to other forces acting on the lifting system.

In air, when the crane rotates and lift the object over the vessel side, wind and other weather conditions and limitations are of great importance. Manoeuvring the object may be difficult, so tugger lines can be used in order to guide the object through the splash zone. One must be aware of the limitations of all equipment used in the lift-off and in-air phase, in addition to hydrostatic stability of the vessel and weather conditions and limitations. Snap loads should be avoided (Larsen, 2016).

### **3.1.2 Splash Zone**

The splash zone is the part of the installation where the structure is intermittently exposed to air and immersed in the sea (DNV GL, 2008). During this phase following forces will act on the lifted object; tension in lifting wire and slings, weight of object in air, buoyancy, current, inertia, wave damping, drag, wave excitation, slamming and water exit forces. Hence this phase is usually the most critical one. All the forces have to be taken into consideration when the total response should be determined. Some of these forces are difficult to predict and calculate, hence a simplified method for estimating the hydrodynamic forces will be introduced (DNV GL, 2011a). This method is further described in *section 4.7 Simplified Method*.

Lifting through the splash zone might introduce snap loads due to slack in lifting lines. In order to prevent snap loads and to be able to manoeuvre the object easily through the splash zone, module handling systems can be used.

The lifted object might be exposed to instability due to unsymmetrical submergence or filling. Unsymmetrical forces in the lifting wires may arise and in worst case the design criteria may be exceeded. Rotation of the object might also occur and without awareness this can lead to complications in subsequent phases.

### 3.1.3 Lowering

During further lowering of the object the water depth and the cable length will increase. A complex structure might have air trapped inside it that has to be released, thus a defined wait period has to be included in the plan. Light structures usually have a slow sinking speed that also has to be considered (Brandsvoll, 2016).

Cable stretch can occur due to the cable weight and the weight of the lifted object. Ocean current can be time-dependent and vary with depth. Strong currents can lead to horizontal offset of the lifted object. Increased horizontal drag forces can be observed due to larger projected area with increased cable length. Wave induced motion of the vessel crane tip can lead to vertical oscillations of the lifted object, which in some cases can result in dynamic resonance. This does usually occur for heavier lifts with a long lifting wire, as illustrated in Figure 3.2. Heave compensation, which is a system that can compensate for an object's heave motion, can be used to control the vertical motion during a light lift operation (Larsen, 2016).

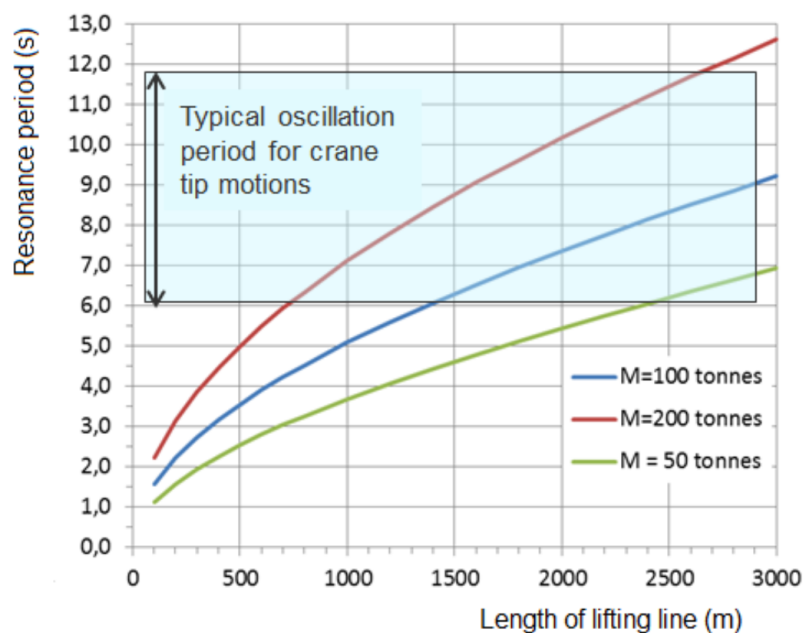


Figure 3.2: Example of typical resonance periods

### 3.1.4 Landing on Seabed

Landing of the lifted object must take place in exact location and in designated rotation. Offset may occur due to current acting on the lifting wire. Offset is highly dependent on current speed and cable length. Hence a deep water lift will most likely experience offset. Reposition of the object can be performed by an ROV, by positioning the vessel or by use of clump weights and a distance wire (Brandsvoll, 2016). The ROV is able to relocate the object in an accurate and efficient way.

Repositioning of the vessel is a time consuming process, especially for deep water lifts, and it is not given that the object actually moves to desired location. Positioning by use of distance wires and clump weights are known and reliable processes, but are also time consuming. The efficiency of this phase can be increased by introducing new technologies, e.g. thrusters can be attached to the object and steered from the vessel.

The landing speed of the lifted object is important. Constant tension in the wire is desired and as for lift-off, one has to be careful with possible re-hits. Slight differences in seabed characteristics will induce tilt on the object and cause unsymmetrical tension in lifting slings (Brandsvoll, 2016).

## 3.2 Heavy- and Light Lifts

It is important to be aware of the object's weight while planning a lifting operation. The ratio between the weight of the lifted object and the vessel classifies the lift. If the object's weight is less than 1-2% of the vessel's weight it is classified as a *light lift*. If the object's weight is above 1-2% of the vessel's weight it is classified as a *heavy lift*. During a light lift operation, the lift will not affect the vessel's motion. Heave compensation can be used during a light lift operation. During a heavy lift operation, there will be dynamic coupling between the lifted object and the vessel, in addition to hydrodynamic coupling from the environment. This leads to a more complex operation and heave compensation cannot be used. A heavy lift is usually above a thousand tonnes (Nielsen, 2007).

## 3.3 Heave Compensation

During a light lift operation, heave compensation is the most commonly used device of controlling the vertical motion of a lifted object and the tension in the lifting wire. Using heave compensation can increase the weather window, the safety and efficiency of the operation. The vertical motion of the crane tip is a combination of the vessel's heave motion, rolling and pitch moment. There are three main heave compensator groups; Passive Heave Compensation (PHC), Active Heave Compensation (AHC) and combined PHC and AHC. A passive heave compensator is a spring/damper system that does not consume external power. PHC is effective for shock absorption through the splash zone phase, and can also be effective in eliminating any resonance that may occur. An active heave compensator does utilise external power. AHC may use winches and hydraulic pistons to compensate for vertical motions, where the winch length is used actively. It is an accurate, but time consuming technique, and is effective during landing on seabed (Larsen, 2016). A light lift in approximately 350 meter depth will most likely not need a heave compensator, thus more detailed explanation of such systems will not be further described.

## 3.4 Lifting Techniques

There are several ways to do offshore lifting operations, and *three* state of the art lifting techniques will be further described; over side crane operations, moonpool operations and installation with special handling systems.

Generally, the critical phase of a lift is the splash zone where the object enters the water and gets hit by waves, and slamming forces arise. Large impulsive hydrodynamic slamming loads can damage the object. The tension in the lifting slings or wire should be carefully controlled during the lift, in order to avoid snap loads.

It is of interest to be able to operate in harsh sea conditions in order to increase the operational seasons and thus reduce operational costs. But one should remember that offshore lifts will always be a risk to people and assets, and the risk does usually increase with harsher environmental conditions. The following three lifting techniques will focus on the maximum sea limit and the dynamic forces acting on the systems will not be described in detail.

### 3.4.1 Over Side Crane Operation

Today, transitional over side crane operations are the most commonly used lifting technique. Such operations are among others used to launch and recover objects, used during vessel mobilisation and demobilisation or to lift an object to another vessel. Figure 3.3 shows an offshore over side crane lift, where a container is moved from one vessel to another one.

The crane tip is located far away from the vessel's centre of gravity (COG), hence unideal large crane tip motions can be expected. The crane tip motion is described in detail in *section 4.5*. Traditional crane lifts of large, heavy complex structures will usually have sea state limitations of 1-2.5 m (Dahle et al., 2016).

Usually, traditional crane operations do not involve much extra equipment. Hence planning and operational costs will stay at its minimum. Tugger wires can be used in order to control the object's motions in air.



Figure 3.3: Crane operation over side



### 3.4.2 Moonpool

A typical solution to operate in harsher sea conditions is to lower the object through a "moonpool". A moonpool is a vertical opening through the deck and the hull of the ship where a water plug arises. Moonpool operations are often preferred because the dynamic forces acting on the system are reduced, and the limiting sea state can therefore be increased. The aim is to have an object moving with constant vertical velocity in order to reduce large tension variations in the lifting slings or wires. Hence the lifting operation is controlled by an actively controlled crane and the object is usually connected to a module handling system and a cursor frame (Messineo et al., 2007).

Moonpools are implemented into several types of vessels. The size of the lifted object is limited by the moonpool dimensions, hence launch and recovery through a moonpool is preferred for small modules. The moonpool is usually located close to the intersection between the vessel's roll and pitch axis in order to minimise angular motions. The lifting equipment is connected to a tower located above the moonpool. This is attached to a skidding system that transports the object on deck. Thus there is no need for a regular crane lift during the operation, except during mobilisation and demobilisation. Figure 3.4 shows a moonpool during a moonpool tower mobilisation.

During a moonpool operation the vertical oscillation of the water plug and the appurtenant damping are important hydrodynamic parameters. The water motion amplitude inside the moonpool is dependent on the level of damping, that is mainly provided by viscous drag (Larsen, 2017). The vessel motion and forward speed can increase the oscillations of the water plug, and in case of resonance the oscillation can reach three to four times the outer wave height. Such cases can be observed during transit if the moonpool bottom is left open. Large water plug oscillations can lead to water on deck, damage of equipment and increase the vessel motions in surge and heave. There have been developed solutions to reduce such kind of oscillations, but they often reduce the moonpool area and are only effective for some forward speed (MARIN, 2017).



Figure 3.4: Tower installation over moonpool

DNV GL has made a Simplified Method for moonpool operations where the important hydrodynamic parameters can be easily calculated. Today the behaviour of the water inside a moonpool is an important research area.



### 3.4.3 Special Handling Systems

Special Handling System (SHS) is a brand new launch and recovery system that has been developed to ensure that lifts of heavy subsea modules can be performed under extreme environmental conditions. The lifting system is permanently stationed mid ship on the vessel, close to the vessel COG. This is important in order to minimise motions acting on the lifted object (Dahle et al., 2016). The whole lifting cycle is conducted over the side of the vessel and the module is guided during all of the lifting phases in a safe, accurate and reliable way. The guiding tool is a docking mechanism with an advanced damping system. Active damping is needed in order to handle a heavy module, that cause extreme forces to the system, in a rigid and controlled way. SHS increases the design criteria of the operation and makes it possible to operate in harsher environmental conditions. Thus the operation season can be extended and waiting on weather periods can be reduced. The SHS has a SWL of 420 t at sea states with  $H_s$  of 4.5 m (AxTech, 2017b).

The SHS is able to pick up the module from the quayside such that an external crane is not needed. Figure 3.5 shows the 420t Special Handling System testing on board the North Sea Giant in rough weather outside Sandnessjøen in November 2015 (AxTech, 2017b).



Figure 3.5: A test of a Special Handling System on board the North Sea Giant outside Sandnessjøen (AxTech, 2017b)

SHS is an expensive system and marine lifting operations should therefore be carefully planned with regard to operational costs. The accessibility of vessels equipped with SHS, increase of design criteria and decrease in WOW should among others be accurately assessed during the cost planning.

AxTech has also developed a Light Module Handling System (LMHS) that is specially designed to deploy and recover light modules safely and efficiently. LMHS can be used for both over side crane operations and moonpool operations, and has a SWL of 25 t. LMHS consists of a *stand-alone* tower

with one connection to the vessel deck. Thus the LMHS can be installed on several vessel types. The lifted module is guided by an adjustable cursor frame during all the lifting phases and landing and lift-off are ensured by use of AHC, winches and guide wires (AxTech, 2017a).

Both SHS and LMHS have a slewing structure that allow them to pick up and land objects on several spots on the deck of the vessel.

## 4 Hydrodynamic Approach

This section focuses on the hydrodynamic approach for both manual estimation and simulation of the design criteria. Linear wave theory is often used for manual estimation. A simple regular wave does not give a realistic description of the sea state, hence irregular waves should be investigated and implemented in simulation models. Thus, the basics of both theories are explained. A dynamic model is based on time domain analyses and the equation of motion, which includes hydrodynamic parameters as added mass and drag. The manually estimated design criterion is found by use of DNV GL's Simplified Method. Hence these theories are explained in details in the following.

### 4.1 Linear Wave Theory

A regular wave propagates with permanent form. It has a distinct wave length, wave period and wave height. The wave profile for a regular sinusoidal incident wave is given by equation (4.1) (DNV GL, 2011b).

$$\zeta = \zeta_a \sin(\omega t - kx) \quad (4.1)$$

Due to the assumptions of incompressible and inviscid sea water, irrotational fluid motion, infinite water depth and that the pressure follows the Bernoulli equation, the velocity potential  $\phi$  for a regular wave can be given by equation (4.2).

$$\phi = \frac{g\zeta_a}{\omega} e^{kz} \cos(\omega t - kx) \quad (4.2)$$

The wave kinematics decreases with depth  $z$  and the water particles will move in paths formed as circles. At sea surface the radius will equal the wave amplitude, and with large depth the radius will be close to zero, as illustrated in Figure 4.1.

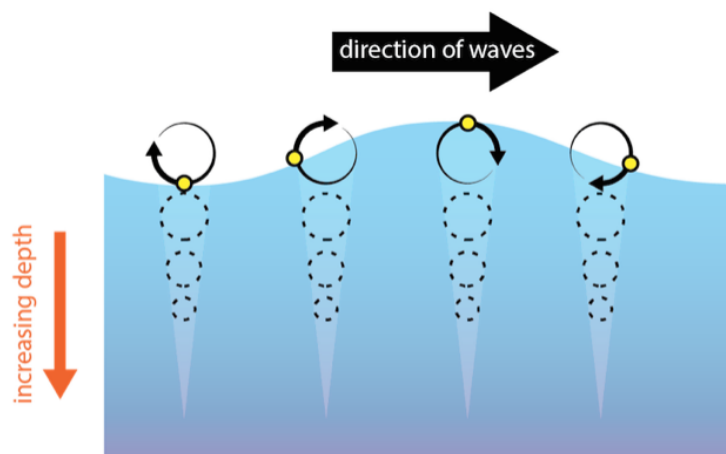


Figure 4.1: Water particles paths with water depth (TSI, 2016)

The water particle velocity  $v_w$  and acceleration  $\dot{v}_w$  is given by equation (4.3) and (4.4), where the wave number  $k$  equals  $\frac{\omega^2}{g}$ , derived from the dispersion relation (Faltinsen, 1990).

$$v_w = \omega \zeta_a e^{kz} \cos(\omega t - kx) \quad (4.3)$$

$$\dot{v}_w = -\omega^2 \zeta_a e^{kz} \sin(\omega t - kx) \quad (4.4)$$

## 4.2 Irregular Waves

Ocean waves are irregular and random in shape, height, length and propagation. They are generated by several regular waves of multiple frequencies, lengths and amplitudes in addition to swell. Short-term stationary irregular sea states can be described statistically by a frequency and directional wave spectrum, that is a power spectral density function of vertical sea surface displacement (Greco, 2012). A short-term sea state of short-crested waves was assumed, hence the sea surface is stationary for a duration of 3 hours, characterised by a constant *significant wave height*  $H_s$  and *spectral peak period*  $T_p$ . 3 hours is usually sufficient for achieving reliable statistical values (DNV GL, 2011b). A short-crested sea is characterised by a two-dimensional wave spectrum, where the wave energy is distributed over several directions, i.e. three-dimensional waves (Faltinsen, 1990).

Irregular sea can be simulated and statistical estimates can be estimated by use of linear wave theory. For linear conditions the superposition principle is valid and the random wave elevation can be split into several regular wave components. In other words, it is possible to study the response of irregular waves as the sum of the response of regular waves. This concept is illustrated in Figure 4.2 (Greco, 2012).

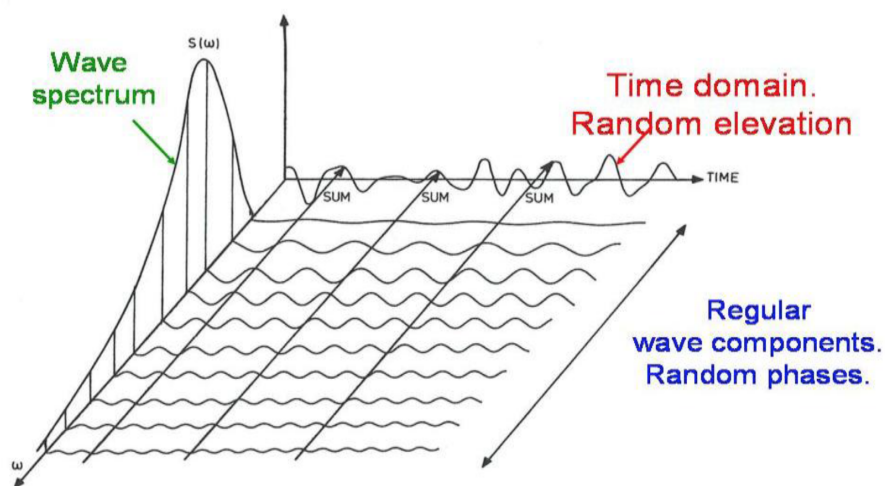


Figure 4.2: Connection between a frequency domain and time domain representation of waves in a long-crested short term sea state (Greco, 2012)

### 4.2.1 Wave Spectra

It is not possible to know the exact wave spectrum for a specified location, hence several standardised wave spectra have been developed. A directional wave spectrum  $S(\omega, \theta)$  distributes the wave amplitude for a given frequency and direction, and is often written as

$$S(\omega, \theta) = S(\omega) \frac{2}{\pi} \cos^n(\theta)$$

where  $n$  is the exponent of the cosine spreading and determines the spreading of the spectrum. The standardised wave spectrum is an average spectrum, but it is not necessarily valid for all wave frequencies. Different recommendations for  $S(\omega)$  has been developed to describe properly ocean waves (Greco, 2012). The choice of wave spectrum is determined by how well the estimated spectrum describes the true spectrum in terms of frequency range and if the spectrum is given with an adequate number of parameters (Myrhaug and Lian, 2014).

For short-crested irregular sea propagating along the positive  $x$ -axis, the wave elevation  $\zeta$  is given by equation (4.5), for several wave components.  $A_{ij}$  is the wave amplitude,  $\epsilon_{ij}$  is a random phase angle and  $\omega_i$  is the wave frequency for wave component  $i$ , uniformly distributed between 0 and  $2\pi$  and constant with time.  $k_i$  is the wave number and by using the dispersion relation for deep water  $k$  is equal to  $\frac{\omega_i^2}{g}$ .  $\theta_j$  indicates the direction of the wave propagation (Faltinsen, 1990).

$$\zeta = \sum_{i=1}^I \sum_{j=1}^I A_{ij} \sin(\omega_i t - k_i x \cos \theta_j - k_i y \sin \theta_j + \epsilon_{ij}) \quad (4.5)$$

The wave amplitude is defined as following

$$\frac{1}{2} A_{ij}^2 = S(\omega_i, \theta_j) \Delta \omega_i \Delta \theta_j$$

A wave spectrum can be estimated from wave measurements and contain all necessary information about statistical properties of the wave elevation (Myrhaug and Lian, 2014). Figure 4.2 illustrates the relation between the frequency domain, representing the waves by a wave spectrum  $S(\omega)$ , and a time domain solution of the waves, as found by equation (4.5).

Generally, in order to calculate the wave spectra  $S(\omega, \theta)$  recommended sea spectra from International Ship and offshore Structures Congress (ISSC) and International Towing Tank Conference (ITTC) are used. The ISSC spectral formulation for fully developed sea is recommended by the 15th ITTC and is also called the *Pierson-Moskowitz* (P-M) spectrum (Faltinsen, 1990). The spectrum is based on data from the North Atlantic and has *one* peak and a steep front at low frequencies (Myrhaug and Lian, 2014).

The 17th ITTC recommended a *Joint North Sea Wave Project* (JONSWAP) spectrum for limited fetch (Faltinsen, 1990). JONSWAP is a result of a multinational project where the generation, propagation and decay of the ocean surface waves in the south-east part of the North Sea were measured and investigated (Spiess, 1975). The results showed that the spectrum in the North Sea

had a fairly sharp peak. The JONSWAP spectrum is based on a peak frequency  $\omega_p$ , a significant wave height  $H_s$  and a peakedness parameter  $\gamma$ .  $\gamma$  is proportional to the ratio between maximum energy in the JONSWAP spectrum and in the P-M spectrum. The total energy in the sea state will be identical for both spectra, but the difference is how the energy is distributed along the frequency axis. (Myrhaug and Lian, 2014). Both spectra describe wind sea conditions that often occur for the harshest sea states. Examples of a modified P-M spectrum and a JONSWAP spectrum are shown in Figure 4.3. It can be seen that the peak value of the P-M (ISSC) spectrum occurs at a different  $\frac{\omega T_2}{2\pi}$ -value than for the JONSWAP spectrum, and that more energy is concentrated around the peak frequency for a JONSWAP spectrum (Faltinsen, 1990).

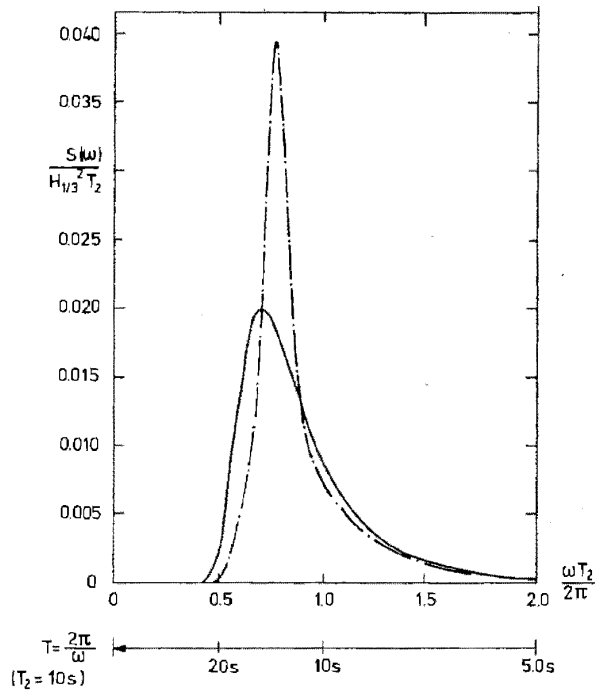


Figure 4.3: Examples of wave spectra. ( $H_{\frac{1}{3}}$  = significant wave height,  $T_2$  = mean wave period). Modified Pierson-Moskowitz spectrum -, JONSWAP spectrum -.- (see equation (4.6)) (Faltinsen, 1990)

The JONSWAP spectrum is a modification of the P-M spectrum and given by equation (4.6), where  $T_1$  is 1.073 times  $T$  used in the P-M spectrum (Faltinsen, 1990).

$$S(\omega) = 155 \frac{H_1^2}{T_1^4 \omega^5} \exp\left(\frac{-944}{T_1^4 \omega^4}\right) \gamma^Y \tag{4.6}$$

where:

$$Y = \exp\left(-\left(\frac{0.191\omega T_1 - 1}{\frac{1}{2^2}\sigma}\right)^2\right)$$

$$\sigma = 0.07 \text{ for } \omega \leq \frac{5.24}{T_1}$$

$$\sigma = 0.09 \text{ for } \omega > \frac{5.24}{T_1}$$

The spectral moments of the wave spectra can be found by equation (4.7).

$$M_n = \int_0^\infty \omega^n S(\omega) d\omega_n \tag{4.7}$$

### 4.2.2 Swell

Wave conditions are compounded of both local wind seas and swell. Swell has no relationship with local environmental conditions but is instead a series of regular waves that has been generated and formed by wind blowing over a long stretch of sea over a long period of time (Futura-Sciences, 2017). Swell is difficult to predict due to its independence of the local environment, and does usually propagate from a different direction than the local wind waves. The exact peak period that will arise at the operation location will be a combination of the local wind sea periods and the swell periods, and hence the actual peak period may be hard to predict.

### 4.2.3 Seed Numbers

Random irregular waves are not only determined by the significant wave height and peak period. It will also be dependent on the regular waves' phase, that can be determined by a random seed number. Various seed numbers result in different irregular waves based on the same significant wave height and peak period, within the same wave spectrum. An example of this concept is illustrated in Figure 4.4. In figure *B* the red sine wave is shifted towards the right and thus changes the total wave response.

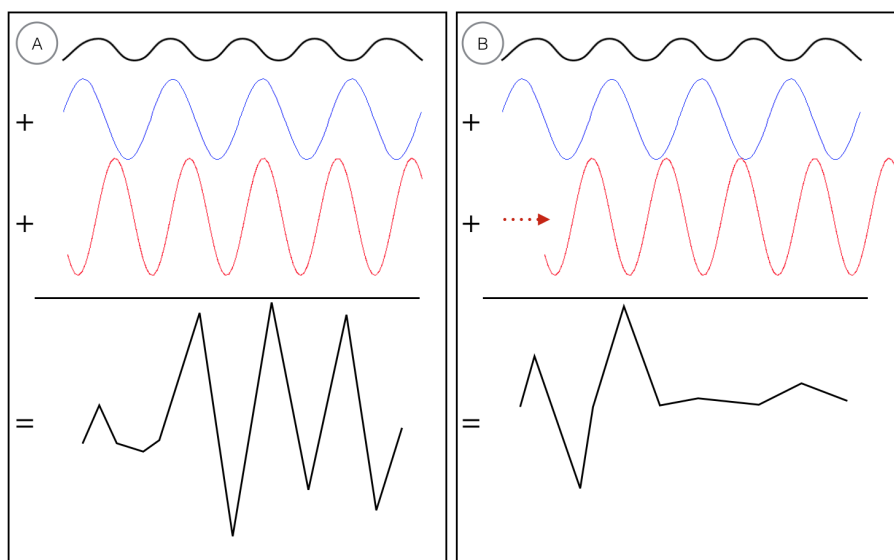


Figure 4.4: Illustration of the seed number concept

Excitation loads are environmental loads from waves, wind and current. Wind and current loads were neglected in this thesis, and the design criteria was only dependent on the maximum sea state, based on  $H_s$  and  $T_p$ .

### 4.3 Time Domain Analysis

There are generally two different methods to anticipate the dynamic responses of a marine operation, Frequency Domain (FD) and Time Domain (TD). The FD-method is described by the energy spectrum, as described in the previous section about irregular waves. The method is based on linearity and all non-linearities are eliminated. The TD-method is based on realisation of the response over time. The history of all the important parameters should be gathered from simulations, and the resulting time histories should be statistically processed in order to obtain extreme values. The TD-method takes non-linearity effects into account, and all the dynamic loads are calculated for each time step. Thus this method is a time consuming computation and complex simulation programs are needed in order to achieve adequate results.

The time domain method will be further described in the following subsection, for dynamic loads acting on a marine lifting operation.

#### 4.3.1 Equation of Motion

Dynamic loads vary with time and hence differ from static loads by implying a time dependent solution and introducing inertia loads throughout the structure (Langen and Sibjörnsson, 2009). The dynamic equation of motion in heave is given by equation (4.8).

$$(m + m_a)\ddot{\eta}_3 + c\dot{\eta}_3 + k\eta_3 = F_3\sin(\omega t) \quad (4.8)$$

- $m$  = total mass of lifted object and rigging [kg]
- $m_a$  = added mass coefficient [kg]
- $c$  = damping coefficient [ $\frac{kg}{s}$ ]
- $k$  = restoring coefficient [ $\frac{kg}{s^2}$ ]
- $\eta_3$  = translation in heave [m]
- $\dot{\eta}_3$  = velocity in heave [ $\frac{m}{s}$ ]
- $\ddot{\eta}_3$  = acceleration in heave [ $\frac{m}{s^2}$ ]
- $F_3$  = excitation force in heave [N]

The lifted object will have a heave motion defined as  $\eta = \eta_0\sin(\omega t - \varepsilon)$ .  $\eta_0$  is the vertical single amplitude motion of the lifted object and can be found by equation (4.9), and  $\varepsilon$  is the phase angle between the wave and crane tip motion.

$$\eta_0 = \frac{F_3}{k} \cdot DAF \quad (4.9)$$

The dynamic amplification factor (DAF) accounts for global dynamic effects that might arise during a lifting operation (DNV GL, 2014). The DAF is a dimensionless number and is defined as the ratio between dynamic and static displacement (Langen and Sibjörnsson, 2009). It is calculated by



equation (4.10) where  $\omega_0$  is the natural frequency.

$$DAF = \frac{1}{\sqrt{(1 - (\frac{\omega}{\omega_0})^2)^2 + \omega^2 \frac{c^2}{k^2}}} \quad (4.10)$$

Capacity checks have to be performed for the lift, and the following relation should be applied  $DAF = \frac{F_{dyn} + F_{stat}}{F_{stat}} = \frac{F_{tot}}{Mg}$  (Bøe, 2016). Global dynamic load effects can be found by using the DAF.

The natural frequency  $\omega_0$  is dependent on the system's mass, added mass and stiffness, and is found by equation (4.11).

$$\omega_0 = \sqrt{\frac{k}{(m + m_a)}} \quad (4.11)$$

The natural period is found by equation (4.12).

$$T_0 = \frac{2\pi}{\omega_0} = 2\pi \sqrt{\frac{(m + m_a)}{k}} \quad (4.12)$$

The damping ratio  $\zeta$  is the ratio between actual damping and critical damping, and can be calculated by equation (4.13). The critical damping coefficient  $c_{cr}$  is equal to  $2\sqrt{km} = 2m\omega$ , and is used to categorise the damping to *critical* ( $c = c_{cr}$ ), *supercritical* ( $c > c_{cr}$ ) or *subcritical* ( $c < c_{cr}$ ) (Langen and Sibjörnsson, 2009).

$$\zeta = \frac{c}{c_{cr}} = \frac{c}{2(m + m_a)\omega_0} \quad (4.13)$$

### 4.3.2 Static and Dynamic Equilibrium

The static load in the hoisting line  $F_{line,stat}$  will be the total weight of the lifted object, the hoisting line and the rigging equipment ( $Mg$ ), in addition to the buoyancy force ( $F_{B,mean}$ ) acting in opposite direction. A porous object will be filled with water when it is submerged, thus the mass will increase slowly with time ( $m(t)g$ ). The static equilibrium equation is given by equation(4.14).

$$F_{line,stat} = Mg + m(t)g - F_{B,mean} \quad (4.14)$$

The *total line force*  $F_{line,tot}$  is the sum of the static and dynamic forces acting on the line, and is given as equation (4.15). The dynamic line force  $F_{line,dyn}$  is the determined by the line's stiffness and the relative vertical motion between the crane tip and the waves.

$$F_{line,tot} = F_{line,stat} + F_{line,dyn} = Mg + m(t)g - F_{B,mean} + K(\eta_{ct} - \eta) \quad (4.15)$$

Dynamic equilibrium can be found by summing the dynamic line force  $F_{line,dyn}$  and the hydrodynamic forces; inertia, drag, slamming and varying buoyancy, as shown in equation (4.16) (Larsen, 2016). Drag and damping are based on the same parameter, but the relation between the two velocities are different. Drag and damping are considered to be the same for a small object oscillating in vertical

motion.

$$\begin{aligned}
 M\ddot{\eta} = & \underbrace{-\rho C_A V \dot{\eta} + \rho V(1 + C_A)\dot{v}}_{\text{Inertia}} + \underbrace{\frac{1}{2}\rho C_D S(v - \dot{\eta})|v - \dot{\eta}|}_{\text{Drag}} \\
 & + \underbrace{\frac{1}{2}\rho C_S A_p (\dot{\zeta} - \dot{\eta})^2}_{\text{Slamming}} + \underbrace{\rho g A_w \zeta}_{\text{Varying Buoyancy}} + \underbrace{K(\eta_{ct} - \eta)}_{F_{\text{line,dyn}}}
 \end{aligned} \tag{4.16}$$

The vertical motion  $\eta$  can be found and dynamic equilibrium can be achieved if equation (4.16) is rearranged to equation (4.17), where added mass  $A = \rho C_A V$ .

$$\begin{aligned}
 (M + A)\ddot{\eta} + K\eta = & \rho V_R(1 + C_A)\dot{v} + \frac{1}{2}\rho C_D S(v - \dot{\eta})|v - \dot{\eta}| \\
 & + \frac{1}{2}\rho C_S A_p (\dot{\zeta} - \dot{\eta})^2 + \rho g A_w \zeta + K\eta_{ct}
 \end{aligned} \tag{4.17}$$

$M$	=	mass of lifted object	$A_w$	=	waterplane area of object
$\rho$	=	sea water density	$\zeta$	=	wave elevation
$C_A$	=	added mass coefficient	$\dot{\zeta}$	=	wave velocity
$V_R$	=	added mass reference volume	$\eta_{ct}$	=	crane tip vertical motion
$K$	=	stiffness of hoisting cable	$\eta$	=	dynamic vertical motion
$C_D$	=	drag coefficient in oscillatory flow	$\dot{\eta}$	=	dynamic vertical velocity
$S$	=	projected area normal to force direction	$\ddot{\eta}$	=	dynamic vertical acceleration
$C_S$	=	slamming coefficient	$v$	=	fluid particle vertical velocity
$A_p$	=	horizontal projected area of object	$\dot{v}$	=	fluid particle vertical acceleration

## 4.4 Response Amplitude Operator

An Response Amplitude Operator (*RAO*) is a linear transfer function between wave and vessel motion. A transfer function  $|H(\omega, \theta)|$  defines a relation between an input and an output and can be defined as  $|H(\omega, \theta)| = \frac{\eta_a}{\zeta_a}$ , where  $\eta_a$  is the dynamic vertical motion and  $\zeta_a$  is the wave amplitude (Greco, 2012). There are several ways to determine the vessel motion. First order motion transfer functions (*RAOs*) for different motions and wave directions are commonly used. Another method is to define a dynamic equilibrium equation based on input from excitation forces, frequency dependent damping and added mass, stiffness matrices, retardation functions and fixed force elongations. The latter is a transfer function between excitation forces and vessel motion. In this paper the vessel *RAOs* will be used to determine the vessel motions. For a crane operation the motions in the crane tip are of significance and should be further investigated.

## 4.5 Crane Tip Motion

Pursuant to DNV GL's *Recommended Practice H103* (DNV GL, 2011b) the crane tip motions for a light lift operation can be determined directly from the wave induced motions of the vessel. The wave induced translational motions of the crane tip are given by the vessel RAOs for six degrees of freedom. They are defined at the vessel COG and the crane tip motion can be written as equation (4.18), where " $\times$ " means a vector product, and  $\mathbf{i}$ ,  $\mathbf{j}$  and  $\mathbf{k}$  are unit vectors along the x-, y-, and z-axis respectively (Faltinsen, 1990).

$$\mathbf{s} = \eta_1 \mathbf{i} + \eta_2 \mathbf{j} + \eta_3 \mathbf{k} + \boldsymbol{\omega} \times \mathbf{r} \quad (4.18)$$

$$\boldsymbol{\omega} = \eta_4 \mathbf{i} + \eta_5 \mathbf{j} + \eta_6 \mathbf{k}$$

$$\mathbf{r} = x \mathbf{i} + y \mathbf{j} + z \mathbf{k}$$

Equation (4.19) shows the derived translational motions at any point, where  $s_1$ ,  $s_2$  and  $s_3$  are the motions along the x-, y-, and z-axis respectively (Faltinsen, 1990). E.g. the vertical motion of the crane tip is determined by the vessel RAOs in heave, pitch and roll. Roll, pitch and yaw motion are given in radian.

$$\mathbf{s} = \underbrace{(\eta_1 + z\eta_5 - y\eta_6)}_{s_1} \mathbf{i} + \underbrace{(\eta_2 - z\eta_4 + x\eta_6)}_{s_2} \mathbf{j} + \underbrace{(\eta_3 + y\eta_4 - x\eta_5)}_{s_3} \mathbf{k} \quad (4.19)$$

The most probable largest crane tip motion that may occur during a time series is determined by equation (4.20) (Larsen, 2015).

$$\eta_{ct}^{max} = \sigma \sqrt{2 \ln(N)} \quad (4.20)$$

$\eta_{ct}^{max}$  is often denoted as the characteristic largest crane tip motion, and is only exceeded by *one* value during  $N$  waves.  $N$  is the number of individual waves during a period of time, usually 3 hours or 10 800 seconds,  $N = \frac{t}{T_z}$ .  $\sigma$  is the standard deviation of the crane tip motion (Myrhaug and Lian, 2014). The zero up-crossing period  $T_z$  is the average time interval between two successive up-crossings of the mean sea level, and defined by equation (4.21).

$$T_z = 2\pi \sqrt{\frac{M_0}{M_2}} \quad (4.21)$$

The zero and second moments of the JONSWAP spectrum,  $M_0$  and  $M_2$ , are defined as following.

$$M_0 = \frac{1}{16} H s^2$$

$$M_2 = \frac{1}{16} H s^2 \omega_p^2 \frac{11 + \gamma}{5 + \gamma}$$

Average values for the JONSWAP experiment non-dimensional peakedness parameter  $\gamma$  is 3.3 (DNV GL, 2011b).

The crane tip velocity  $\dot{\eta}_{ct}^{max}$  and acceleration  $\ddot{\eta}_{ct}^{max}$  are derived from the derivatives of  $\eta = \eta_a \sin \omega t$ .

$$\dot{\eta}_{ct}^{max} = \omega_p \eta_{ct}^{max}$$

$$\ddot{\eta}_{ct}^{max} = -\omega_p^2 \eta_{ct}^{max}$$

## 4.6 Hydrodynamic Parameters

Hydrodynamic parameters can be determined by theoretical and/or experimental methods. Added mass and drag forces are important hydrodynamic forces caused by forced harmonic rigid body motions (Faltinsen, 1990). They depend on the body geometry, perforation, sharp edges, oscillation, wave height, wave period and vicinity of free surface or sea bottom (DNV GL, 2011b). The hydrodynamic parameters will vary with depth, and experimental analyses should therefore be performed in order to ensure adequate depth dependent hydrodynamic parameters implemented in a numerical simulation model.

Hydrodynamic loads on slender elements can be estimated by summing up sectional forces acting on each strip of the element. Wave loads can be calculated by use of Morison's equation for slender elements with cross-sectional dimensions less than one fifth of the wave length (DNV GL, 2011b).

Experimental hydrodynamic parameters can be found by use of WAMIT, Computational Fluid Dynamics (CFD) analyses or model tests. WAMIT is a diffraction program that has been developed in order to do analysis of the interaction of surface waves with offshore structures, and gives adequate coefficients for added mass of complex structures (WAMIT, 2006). CFD-analyses are numerical experiments in terms of computational simulations of fluid motion described by the Navier-Stokes equations (DNV GL, 2011b).

### 4.6.1 Added Mass Value

Added mass is associated with a mass of fluid that is accelerated by the object due to generation of surface waves (Rahman and Bhatta, 1993). Added mass is highly dependent on the oscillation amplitude of the object and is difficult to determine for complex three-dimensional structures. Model tests are the most accurate method to determine added mass coefficients for such structures (DNV GL, 2011b).

Added mass is dependent on the body shape, current, depth, oscillation frequency and motion mode and will increase through splash zone when the object's projected area increases. Thereafter it will stay constant until it will start to increase again when the structure approaches the sea bottom (Nielsen, 2016).

Theoretical added mass values exist for simple geometries and can be found in Table A-2 in *DNV GL's Recommended Practice DNV-RP-H103, 2011b*, which is shown in Figure 4.5. For realistic geometries experimental data has to be relied on (Nielsen, 2016). Added mass calculations based upon superposition, which is summation of contributions from each element, is not recommended if the structure is densely compounded. Due to oscillation amplitude dependency and interaction effects, an underestimation of the calculated values may be expected (DNV GL, 2011b).

**Table A-2 Analytical added mass coefficient for three-dimensional bodies in infinite fluid (far from boundaries). Added mass is  $A_{ij} = \rho C_A V_R$  [kg] where  $V_R$  [m<sup>3</sup>] is reference volume**


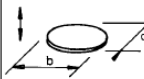
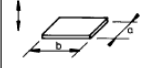
Body shape		Direction of motion	$C_A$				$V_R$
Flat plates	Circular disc 	Vertical	$2/\pi$				$\frac{4}{3} \pi a^3$
	Elliptical disc 	Vertical	$b/a$	$C_A$	$b/a$	$C_A$	$\frac{\pi}{6} a^2 b$
			$\infty$	1.000	5.0	0.952	
		14.3	0.991	4.0	0.933		
		12.8	0.989	3.0	0.900		
		10.0	0.984	2.0	0.826		
		7.0	0.972	1.5	0.758		
	Rectangular plates 	Vertical	$b/a$	$C_A$	$b/a$	$C_A$	$\frac{\pi}{4} a^2 b$
			1.00	0.579	3.17	0.840	
			1.25	0.642	4.00	0.872	
			1.50	0.690	5.00	0.897	
			1.59	0.704	6.25	0.917	
			2.00	0.757	8.00	0.934	
			2.50	0.801	10.00	0.947	
			3.00	0.830	$\infty$	1.000	

Figure 4.5: Table of added mass coefficients for a three-dimensional body (DNV GL, 2011b)

The added mass value is given in *kilogrammes* and can be found by equation (4.22), where  $A_{ij}$  is the added mass force in  $i$ -direction due to acceleration in  $j$ -direction,  $C_A$  is the dimensionless added mass coefficient and  $V_R$  is the reference volume in  $m^3$ , found in Figure 4.5.

$$A_{ij} = \rho C_A V_R \tag{4.22}$$

### 4.6.2 Drag Coefficient

Drag forces are flow resistance on the submerged parts of the structure and are related to relative velocity between the object and water particles (Bøe, 2016). The drag force is based on a drag coefficient  $C_D$  which in reality has to be empirically determined.  $C_D$  is dependent on several parameters such as the Reynold number and the Keulegan-Carpenter (KC) number. It is assumed that  $C_D$  is constant with depth for a constant submerged projected area. The drag coefficient can be found in Table B-2 in *DNV GL's Recommended Practice DNV-RP-H103, 2011b*, which is shown in Figure 4.6. In oscillatory flow the drag coefficient  $C_D$  is generally greater than 2.5 (DNV GL, 2011b).

**Table B-2**  
 Drag coefficient on three-dimensional objects for steady flow  $C_{DS}$ .  
 Drag force is defined as  $F_D = \frac{1}{2} \rho C_{DS} S u^2$ .  
 $S$  = projected area normal to flow direction [m<sup>2</sup>].  
 $Re$  =  $uD/\nu$  = Reynolds number where  $D$  = characteristic dimension.

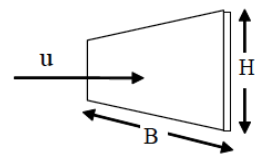
Geometry	Dimensions	$C_{DS}$
Rectangular plate normal to flow direction 	B/H	
	1	1.16
	5	1.20
	10	1.50
	$\infty$	1.90
		$Re > 10^3$

Figure 4.6: Table of drag coefficients for a three-dimensional body (DNV GL, 2011b)

## 4.7 The Simplified Method

The Simplified Method described in DNV GL's "Recommended practice for modelling and analysis of marine operations DNV GL-RP-H103 (DNV GL, 2011b) is used to estimate hydrodynamic forces and tension in the hoisting line in an efficient way. The Simplified Method can be applied on objects lowered through the water surface and down to the sea bottom. The aim with this method is to find allowable sea states limited by the crane and equipment capacity, and to achieve simple conservative estimates of the forces acting on the object, such as; drag, inertia, water entry (slamming) and varying buoyancy forces. By using the simplified method one assumes that the wave length is large relative to the horizontal length of the lifted object, that the vertical motion of the object follows the crane tip motion ( $\eta_{ct} = \eta$ ), and that the vertical motion of the object dominates such that all other motions can be disregarded (DNV GL, 2011b). Thus the added mass force in heave  $A_{33}$  and the drag force in vertical direction are the ones of interest. According to DNV GL the simplified method can be applied for the criteria shown in Figure 4.7, and is recommended when the length of the body is 4 times the wave length  $L$  (Bøe, 2016).

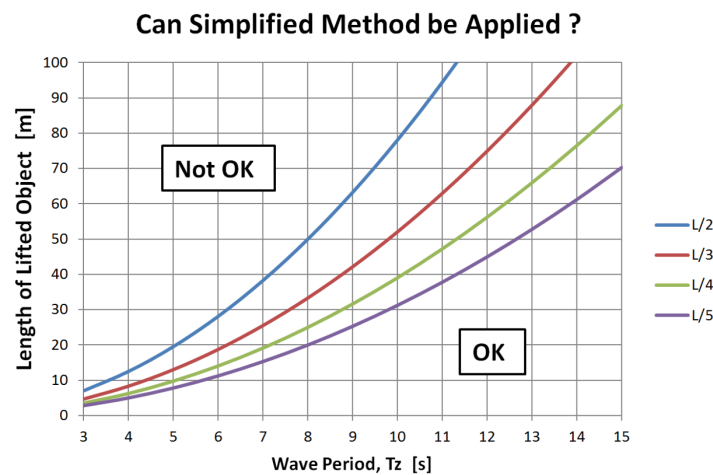


Figure 4.7: An overview of application of the Simplified Method

### 4.7.1 Wave Kinematics

The wave particle velocity and acceleration can be found by equation (4.23) and (4.24) respectively. The equations are derived from linear wave theory where  $\omega$  equals  $\frac{2\pi}{T_z}$ ,  $k$  equals  $\frac{\omega^2}{g}$  and  $d$  is the distance from sea surface to the centre of gravity of submerged part of object (Larsen, 2016).

$$v_w = \zeta_a \cdot \left(\frac{2\pi}{T_z}\right) \cdot e^{-\frac{4\pi^2 d}{T_z^2 g}} \quad (4.23)$$

$$\dot{v}_w = \zeta_a \cdot \left(\frac{2\pi}{T_z}\right)^2 \cdot e^{-\frac{4\pi^2 d}{T_z^2 g}} \quad (4.24)$$

For an operation where the duration of crossing the splash zone is less than 30 minutes, the wave

amplitude  $\zeta_a$  is  $0.9 \cdot H_S$ .  $T_z$  is the zero up-crossing period found by equation (4.21).

### 4.7.2 Drag Force

Drag forces are caused by relative velocity between the lifted object and water particles. The drag force can be calculated by equation (4.25), where the drag coefficient  $C_D$  can be found in Table B-2 in *DNV GL's Recommended Practice DNV-RP-H103, 2011b*, shown in Figure 4.6 (Larsen, 2016).

$$F_D = \frac{1}{2} \cdot \rho \cdot C_D \cdot A_p \cdot v_r^2 \quad (4.25)$$

- $\rho$  = density of sea water
- $C_D$  = drag coefficient in oscillatory flow of submerged part of object
- $A_p$  = projected area of submerged part of object in a horizontal plane
- $v_r$  = characteristic vertical relative velocity between object and water particles, found by equation (4.26).

$$v_r = v_c + \sqrt{\dot{\eta}_{ct}^2 + v_w^2} \quad (4.26)$$

- $v_c$  = hook hoisting/lowering velocity
- $\dot{\eta}_{ct}$  = characteristic vertical velocity of the crane tip
- $v_w$  = characteristic vertical water particle velocity

### 4.7.3 Water Entry (Slamming) Force

Slamming forces are impulse loads with high pressure peaks that occur during impact between an object and the water surface. Slamming is a non-linear phenomenon and will occur when an object is lifted through the splash zone and hits the water with a high velocity. Large slamming forces can be a problem for the global elastic behaviour and the local system strength. The object's dead rise angle and relative impact velocity  $v_r$  are two important parameters for slamming (Faltinsen, 1990). The slamming force can be calculated by equation (4.27), where  $\frac{dA(z)}{dz}$  is the rate of change of added mass with submergence.

$$F_S = v_s^2 \cdot \frac{dA(z)}{dz} \quad (4.27)$$

$F_S$  can also be written as following

$$F_S = \frac{1}{2} \cdot \rho \cdot C_s \cdot A_s \cdot v_s^2$$

- $C_s$  = slamming coefficient which may be determined by theoretical and/or experimental methods.
- $A_s$  = slamming area, identical projected area of submerged part of object in a horizontal plane  $A_p$
- $v_s$  = slamming impact velocity, which is identical to the relative velocity between object and water particles  $v_r$ , calculated in section 4.7.2

#### 4.7.4 Inertia Force

Inertia forces are caused by crane tip acceleration and the acceleration of water particles. The total inertia force is a combination of inertia, Froude-Kriloff and diffraction forces, and is calculated by equation (4.28) (Bøe, 2016). The relation between the crane tip and water particle accelerations is visualised in Figure 4.8.

$$F_I = \sqrt{[(M + A_{33})\ddot{\eta}_{ct}]^2 + [(\rho V + A)\dot{v}_w]^2} \quad (4.28)$$

- $M$  = mass of object
- $A_{33}$  = added mass in heave
- $\ddot{\eta}_{ct}$  = crane tip acceleration
- $V$  = volume of displaced water
- $\dot{v}_w$  = water particle acceleration

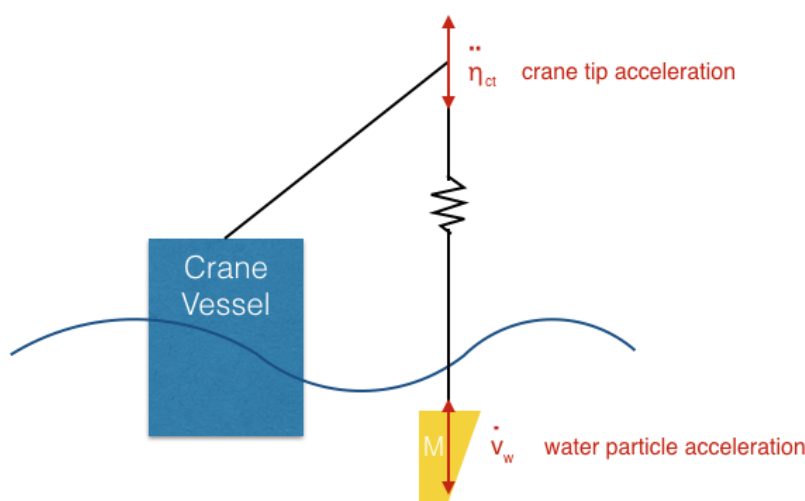


Figure 4.8: Relation between crane tip- and water particle acceleration

#### 4.7.5 Varying Buoyancy Force

When an object is lowered into the ocean a buoyancy force will instantly affect the lifting load. The buoyancy force varies due to change in geometry and buoyancy relative to water surface elevation. The varying buoyancy force  $F_B$  is calculated by equation (4.29), where wave amplitude  $\zeta_a$  and crane tip motion  $\eta_{ct}$  are important parameters and assumed statistically independent (Larsen, 2016). The relation between the crane tip motion and the wave amplitude is visualised in Figure 4.9.

$$F_B = \rho \cdot \delta V \cdot g \quad (4.29)$$

$\delta V$  is the varying volume due to oscillation and is given by equation (4.30), where  $A_w$  is the mean water line area in the wave surface zone.

$$\delta V = A_w \cdot \sqrt{\zeta_a^2 + \eta_{ct}^2} \quad (4.30)$$



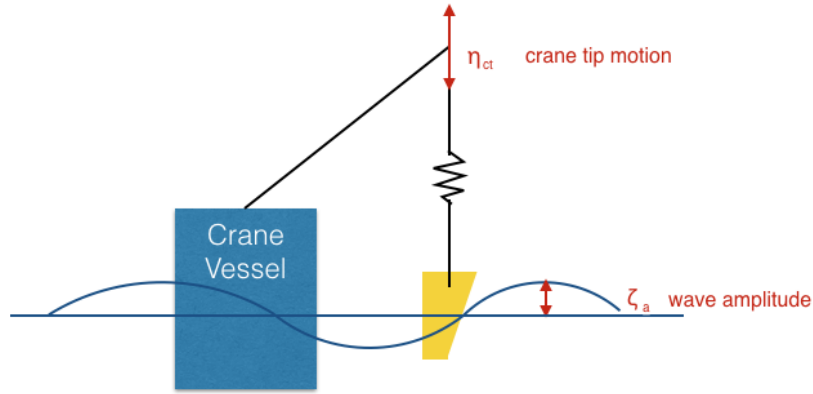


Figure 4.9: Relation between crane tip motion and wave amplitude

#### 4.7.6 Resulting Force

The hydrodynamic force acting on the system calculated by the Simplified Method is dependent on the lifting phase. Table 4.1 shows an overview of which forces that affect the hydrodynamic force during each lifting phase, where *phase 1* is *in-air*, *phase 2* is the *splash zone* and *phase 3* is when the lifted object is fully submerged. The inertia force and weight of the cover will be present at all times.

Table 4.1: Overview of significant forces acting during different lifting phases

	Drag	Slamming	Inertia	Varying Buoyancy	Buoyancy	Mg
Phase 1			✓			✓
Phase 2	✓	✓	✓	✓	✓	✓
Phase 3	✓		✓		✓	✓

During phase 2 the hydrodynamic force will be a combination of drag and inertia forces, slamming and varying buoyancy forces, as indicated in equation (4.31) (Larsen, 2016).

$$F_{Hyd} = \sqrt{(F_D + F_S)^2 + (F_I - F_B)^2} \quad (4.31)$$

The drag and slamming forces are summarised because they can occur simultaneously. Varying buoyancy and buoyancy forces will compensate for inertia and mass forces, hence they are subtracted.

The resulting force is the sum of the mass force, the buoyancy force and the total hydrodynamic forces. The mass force is the weight of the lifted object with rigging equipment. The resulting force is calculated by equation (4.32).

$$F_{Res} = Mg - F_{buoy} + F_{Hyd} \quad (4.32)$$



## 5 Statistical Models

Characteristic loads used during the design phase of an offshore operation are defined by means of probabilities. The variability of the environmental conditions should be described properly in order to determine consistent estimate of loads and predict probable future environmental conditions (Haver, 2012a). Most forcing processes are of random nature that cannot be specified with certainty, thus statistical methods are used. Statistical methods are not very valuable without good quality data. Good quality data is independent observations from identical test conditions that is representative for a problem (Haver, 2012b). For selecting an adequate probabilistic model, a solid theoretical basis is needed. The central part of several probability distributions may be equally valid, while the tails can be completely different. Usually, the tails are of main interest and the distributions should therefore be selected carefully (Haver, 2012a). Two distributions that are commonly used in reliability engineering are the *Weibull distribution* and the *Extreme Value distribution*.

### 5.1 Weibull Distribution

The Weibull distribution was introduced by Professor Waloddi Weibull in 1951 (Weibull, 1951) and has since then been widely studied. There are several methods in the objective analytical procedure, but in this paper *The Method of Moments* will be used and further described. The Weibull distribution is usually based on *two* parameters; the scale ( $\gamma$ ) and shape ( $\beta$ ) parameter. Different combinations of the parameters can result in several other distributions. The shape parameter is a numerical parameter of a parametric family of probability distributions (ReliaWiki, 2016). If  $\beta = 1$ , the distribution is identical to a decreasing exponential distribution with constant failure rate. The effect of the scale parameter  $\gamma$  is to stretch out the graph. The Weibull Probability Density Function (PDF) is described by equation (5.1) (van Voorthuysen, 2015). The area underneath a PDF is always equal to 1.

$$f(x) = \frac{\beta}{\gamma} \left(\frac{x}{\gamma}\right)^{\beta-1} e^{-\left(\frac{x}{\gamma}\right)^\beta} \quad (5.1)$$

The Weibull Cumulative Distribution Function (CDF) is the inverse of the PDF and described by equation (5.2). The CDF gives the probability  $p$  that  $X$  is less than or equal to a given value  $x$ .

$$F(x) = 1 - \exp\left(-\left(\frac{x}{\gamma}\right)^\beta\right) = p \quad (5.2)$$

The inverse cumulative distribution function, also called the quantile function, is described by equation (5.3). The quantile function gives the corresponding value to a given probability  $p$ .

$$Q(p) = \gamma(-\ln(1-p))^{\frac{1}{\beta}} \quad (5.3)$$

If  $x_1, x_2, \dots, x_n$  represent a data set, the expected value  $\bar{x}$  is called the *first moment of X*, and is calculated by equation (5.4), where  $\Gamma(\cdot)$  is a gamma function evaluated at  $n$  (Haver, 2012b).

$$\bar{x} = E[X] = \frac{1}{n} \sum_{i=1}^n x_i = \gamma \Gamma\left(1 + \frac{1}{\beta}\right) \quad (5.4)$$

The variance  $s_x^2$  is called the *second central moment of X*, and is calculated by equation (5.5) (Haver, 2012b). Both the expected value and standard deviation can be calculated for a data set.

$$s_x^2 = \frac{1}{n-1} \sum_{i=1}^n (x_i - \bar{x})^2 = \gamma^2 \left[ \Gamma\left(1 + \frac{2}{\beta}\right) - \Gamma^2\left(1 + \frac{1}{\beta}\right) \right] \quad (5.5)$$

The idea behind the method of moments is that the two Weibull parameters  $\gamma$  and  $\beta$  can be found by solving the two moment equations that are dependent on  $\gamma$  and  $\beta$ . Firstly  $s_x^2$  in equation (5.5) should be divided on  $\bar{x}^2$  in equation (5.4) such that the scale parameter  $\gamma$  disappears. Hence the equation will only be dependent on the shape parameter  $\beta$ , as shown in equation (5.6). Subsequently the scale parameter  $\gamma$  can be found from equation (5.4) (Haver, 2012b).

$$\left(\frac{s_x}{\bar{x}}\right)^2 = \frac{\Gamma\left(1 + \frac{2}{\beta}\right) - \Gamma^2\left(1 + \frac{1}{\beta}\right)}{\Gamma^2\left(1 + \frac{1}{\beta}\right)} \quad (5.6)$$

In order to get an indication of whether the selected distribution fits the data set adequately or not, an empirical distribution function can be plotted in a Weibull probability paper. The Weibull assumption can be supported if the plot is close to the straight empirical distribution line. The *Weibull-plot* is found by rearranging equation (5.2) to a linear equation dependent on the cumulative probability  $F(x)$ , as defined in equation (5.7) (Leira, 2009).

$$\ln[-\ln(1 - F(x))] = \beta \ln x - \beta \ln \gamma \quad (5.7)$$

The linear *Weibull-plot* should be plotted towards an empirical distribution function as described below, where  $n$  is the sample size of the data set and  $k = 1, 2, \dots, n$  (Leira, 2009).

$$\hat{F}(x_k) = \frac{x_k}{n+1}$$

Thereafter  $\hat{F}(x_k)$  is used in equation (5.7) and the empirical distribution function can be plotted for  $\ln(x_k)$  on the x-axis, for sorted  $x_k$ .

## 5.2 Extreme Value Distribution

Extreme value distributions are limiting distributions for maximums or minimums. There are several extreme value distributions, but the most common one is the type I, *standard Gumbel distribution* (UAH, 2017). In order to set realistic limiting sea states for an operation it is interesting to find the maximum or minimum tension that will arise in the slings during different  $H_s$ - $T_p$  conditions. The limiting sea states will be based on potential slack in slings and exceedance of material strength.

Figure 5.1 shows the distributions of a Gaussian Process ( $p[x(t)]$ ) from the left, an individual maxima ( $p[\eta]$ ) distribution and an extreme value distributions ( $p_{max}[\eta]$ ). The Gaussian process distribution is based on all data in a wave series, while the individual maxima distribution is based on only the wave crests above the mean.

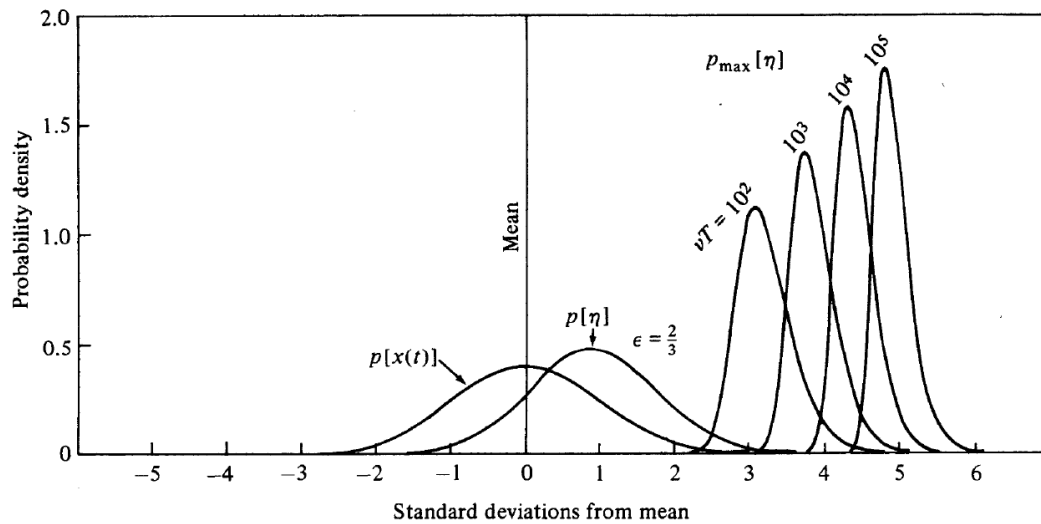


Figure 5.1: Distributions of the Gaussian Process ( $p[x(t)]$ ), Individual Maxima ( $p[\eta]$ ) and Extreme Values ( $p_{max}[\eta]$ ) (Larsen, 2015)

The extreme value of a wave series is its absolute maxima or minima. The extreme value distribution is based on a data set containing several extreme values found in multiple wave series with different seed numbers. This concept is visualised in Figure 5.2 for maximum extreme values and in Figure 5.3 for minimum extreme values. Several wave series with constant  $H_s$  and  $T_p$  should be run for several random seed numbers. The minimum tension arising in the slings should be stored for each wave series with different seed number. The extreme values  $X_{max}$  and  $X_{min}$  are stochastic variables that represent the maxima and minima respectively (Haver, 2012b).

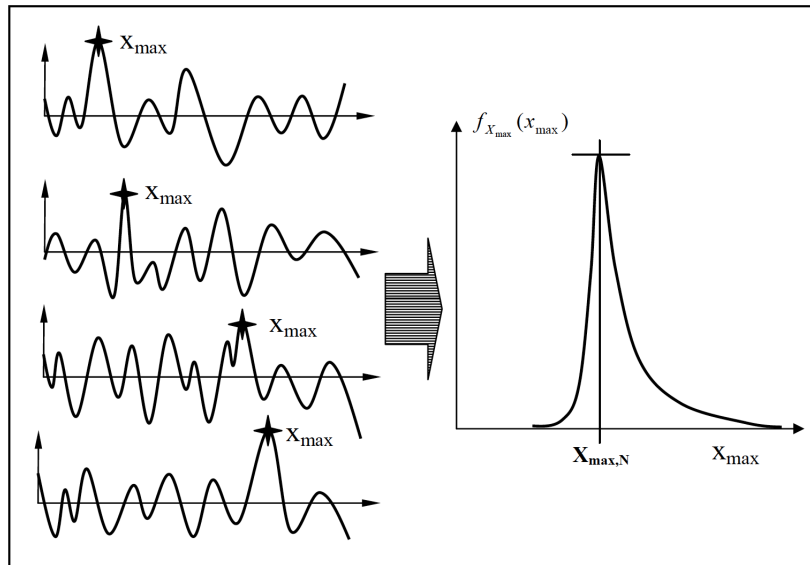


Figure 5.2: Establishment of the Extreme Value Distribution - Maxima (Larsen, 2015)

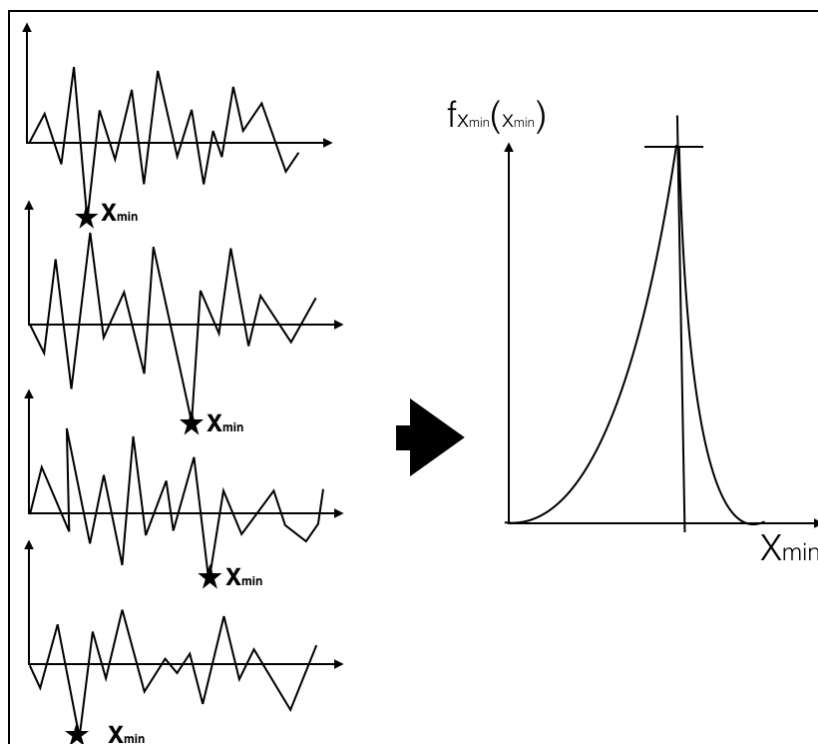


Figure 5.3: Establishment of the Extreme Value Distribution - Minima

A Gumbel probability density function can be created for the set of minima or maxima. The Gumbel PDF has a positive skewness for maxima and a negative skewness for minima (Haver, 2012a). Figure 5.4 *a* and *b* show the Gumbel PDF for minima and maxima respectively. One can clearly see that the minima PDF is skewed towards the left while the maxima PDF is skewed towards the right. Hence the PDF will be based on different equations for the two situations.

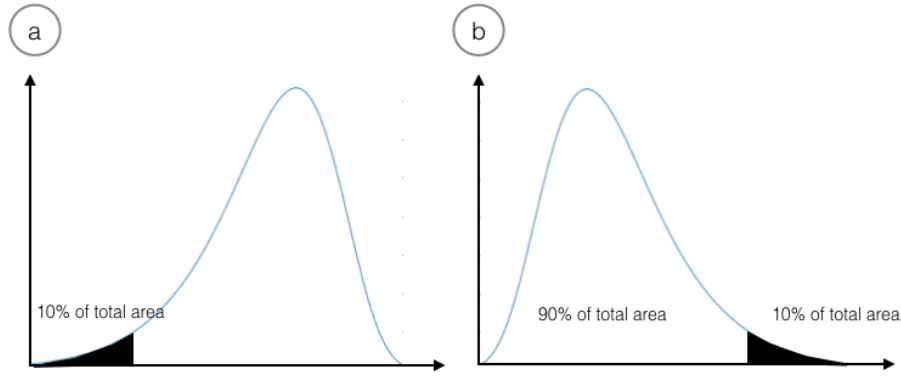


Figure 5.4: Gumbel PDF for a) Minima and b) Maxima

The PDFs for maxima and minima are given by equation (5.8) *a* and *b* respectively (UAH, 2017).

$$f(x_{max}) = \frac{1}{\beta} \exp(-z + \exp(-z)) \quad (5.8a)$$

$$f(x_{min}) = \frac{1}{\beta} \exp(z + \exp(z)) \quad (5.8b)$$

The variable  $z$  is identical to  $\frac{x-\mu}{\beta}$ , where  $x$  is  $x_{max}$  for maxima and  $x_{min}$  for minima.

The Gumbel PDF is based on two variables;  $\mu$  and  $\beta$ . These can be found by the distribution's expected value  $E[X]$  and standard deviation  $\sigma$ , described by equation (5.9) and (5.10) respectively.  $\gamma$  is the Euler-Mascheroni constant of 0.5772 (UAH, 2017).

$$E[X_{max}] = \mu + \gamma\beta \quad (5.9a)$$

$$E[X_{min}] = \mu - \gamma\beta \quad (5.9b)$$

$$\sigma = \beta \frac{\pi}{\sqrt{6}} \quad (5.10)$$

The Gumbel cumulative distribution function is given by equation (5.11) *a* and *b* for maxima and minima respectively (UAH, 2017).

$$F(x_{max}) = P(X \leq x_{max}) = \exp(-\exp(-z)) \quad (5.11a)$$

$$F(x_{min}) = P(X \leq x_{min}) = 1 - \exp(-\exp(z)) \quad (5.11b)$$

Figure 5.5 shows an example of how the CDF can be used. The probability that  $X$  is less than or equal to  $x_1$  ( $P(X \leq x_1)$ ) is 0.2. The equation can be rearranged such that the probability that  $X$  is greater  $x$  ( $P(X > x)$ ) can be found by subtracting  $P(X \leq x)$  from 1.

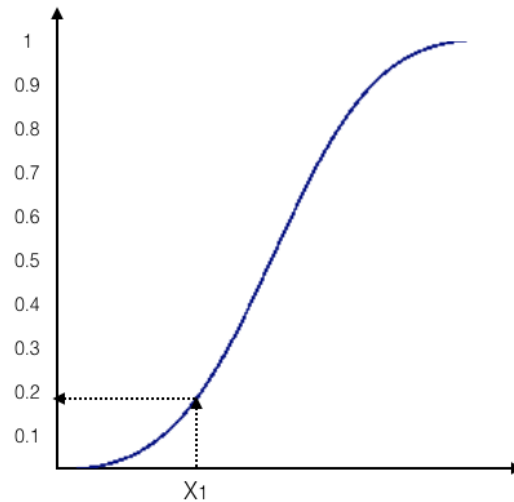


Figure 5.5: Gumbel CDF

The inverse cumulative distributions (quantile functions) for maxima and minima are given by equation (5.12)  $a$  and  $b$  respectively (UAH, 2017).

$$x_{max}(P) = \mu - \beta \ln [-\ln(P)] \tag{5.12a}$$

$$x_{min}(P) = \mu + \beta \ln [-\ln(1 - P)] \tag{5.12b}$$

An example of the quantile function is shown in Figure 5.6. The minimum tension that can occur with a 10% probability is found to be  $X_{10\%}$  and the maximum tension that can occur with a 90% probability is found to be  $X_{90\%}$ .

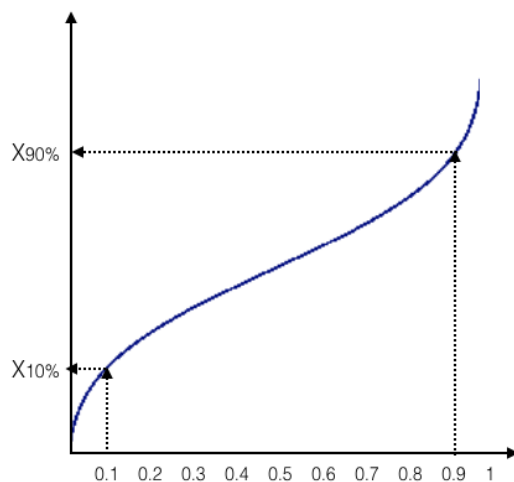


Figure 5.6: Gumbel Quantile Function

The two Gumbel parameters  $\mu$  and  $\beta$  will vary with increased sample size of extreme values. Hence the quantiles will vary for a given probability. One can assume that enough data has been gathered,



and enough simulations have been run, when the parameters and the quantile converge with 5-7% (Larsen, 2017). The converged parameters and quantile will be used for further calculations. The limiting sea state will be set to be the  $H_s-T_p$  condition where the converged quantile for minima gets below the minimum slack requirement or the converged quantile for maxima exceeds the material strength.

A *Gumbel-plot* is used to see how good the distribution fits a linear line. The Gumbel-plot is found by rearranging equation (5.12) to the linear function as in equation (5.13)  $a$  and  $b$  for maxima and minima respectively. The slope for minima is negative while the slope for maxima is positive.

$$-\ln[-\ln(P)] = \frac{x_{max} - \mu}{\beta} = \frac{1}{\beta}x - \frac{\mu}{\beta} \quad (5.13a)$$

$$-\ln[-\ln(1 - P)] = -\frac{x_{min} - \mu}{\beta} = -\frac{1}{\beta}x + \frac{\mu}{\beta} \quad (5.13b)$$

Usually  $P$  will be equal to 0.9 for maxima extreme values and 0.1 for minima extreme values. Hence  $-\ln[-\ln(P)]$  for maxima will be equal to  $-\ln[-\ln(1 - P)]$  for minima.

Polynomial fitting can be used to make the empirical distribution function as a straight reference line to the Gumbel-plot.  $P$  in equation (5.13) will be equal to  $\frac{k}{n-1}$ , where  $n$  is the sample size and  $k = 1, 2, \dots, n$  (Leira, 2009). MATLAB's built in function *polyfit* returns the best fitted polynomial to the data set, by use of the least-squared method (MathWorks-Nordic, 2017). The empirical distribution line from the data set should be compared with the Gumbel-plot from the distribution. If they are close to similar, one can assume that the data set fits the Gumbel distribution. An example of Gumbel-plots from distribution and polynomial fitting is shown in Figure 5.7. The empirical distribution function is based on the sample size, while the Gumbel-plot is based on the parameters achieved from the data set and distribution.

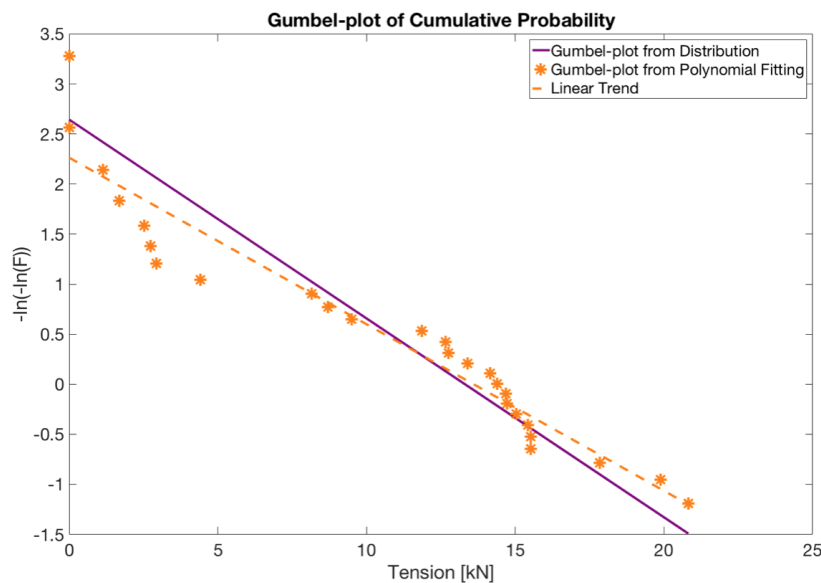


Figure 5.7: Gumbel-plot of cumulative probability with polynomial fitting



## 6 SIMA

SIMA is a software application developed by SINTEF Ocean, former MARINTEK, at the Norwegian Marine Technology Research Institute. SIMA is a non-linear time domain simulation program and is a common simulation workbench for multiple marine applications. All non-linearities are taken directly into account and the total motion, consisting of both low frequency and wave frequency, are solved simultaneously. The software is based on numerical integration and is a powerful tool for modelling and analysing tasks within the marine technology field (Levold, 2016). SIMA is generally used to build numerical models, run multiple simulations and post-process and report results.

Two main goals of the development of SIMA have been to "create a tool for beginners that shorten the time it takes to become proficient in modelling and analysis" and "to create a tool for experts that shorten the time from project initiation to conclusion" (SIMA, 2017). SIMA was also developed to give users the benefit of 3D visualisation of the model while working on conventional analyses (Levold, 2016). Before SIMA was developed, analyses were performed in SIMO or RIFLEX and the input was given by text editing. SIMO is used to create marine operation models and RIFLEX is used to model slender elements. SIMA makes it possible to combine SIMO and RIFLEX in order to archive a marine operation model that consist of slender elements.

SIMA has the ability to run simulations in batches or through workflows, and uses a post-processor to analyse the results. A batch simulation is a model parametrisation with variables and scripts that run defined sets of simulations. A workflow is a powerful tool for combination of several SIMA tasks. Complex workflows that consist of several analyses and post-processors can be established in order to save simulation time. The program does also have the functionality of interact with external programs without leaving the SIMA interface. The post-processor can process and analyse the results in many ways and is often used to extract statistical values and visualise the results graphically (Reinholdtsen and Aksnes, 2016).

SIMA performs both static and dynamic simulations. A static analysis assumes that the loads act on the system with no time-varying effects, and generally the results give information about the conditions of equilibrium. A dynamic analysis is time-varying and implies a time or frequency dependent response. Dynamic analyses are more complicated and more realistic compared to static analyses (Karnovsky and Lebed, 2010). Dynamic analyses are most commonly used in SIMA, but static analyses should be used regularly during the construction phase of the model in order to ensure adequate equilibrium conditions. The time domain simulation in SIMA is further described in the following subsection.

## 6.1 Time Domain Simulation

The time domain simulation should be performed for various  $H_s-T_p$  conditions that occur at the specified operation location. The simulation should be repeated for several seed numbers for generating waves. The simulation approach is based on a coupled system where the dynamic motion of the vessel and the lifting equipment dynamics are solved simultaneously. The vessel is described by a large volume body and the cover consists of slender elements. The SIMO model is a simplified model and consists of six lines with stiffness  $K$  and three masses  $M$ , as illustrated in Figure 6.1. The dynamic equation of motion described in *section 4.3 Time Domain Analysis* are implemented in the software.

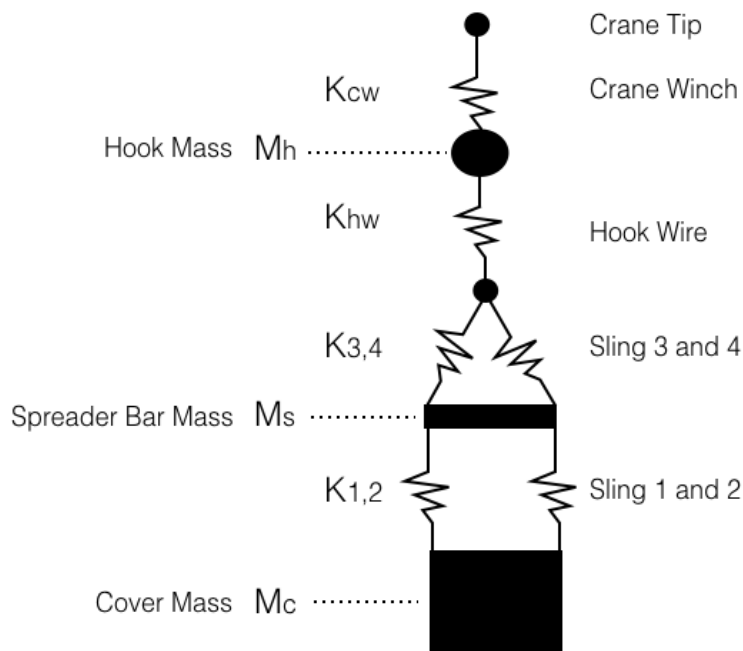


Figure 6.1: SIMO model of lifting system

Morison's equation is used to describe the hydrodynamic loads arising in the circular slender elements. According to DNV GL's recommended practice *H103* (DNV GL, 2011b) the hydrodynamic forces applied to a slender element can be estimated by summation of the forces acting on each strip of the structure. Wave loads can then be determined by use of Morison's formula if the ratio between the cross-sectional diameter and the wave length is small. Morison's equation is generally used to calculate wave forces on constructions with circular cross-section, and is given in equation (6.1).  $C_M$  and  $C_D$  are the mass and drag coefficient respectively (Pettersen, 2007).

$$dF = \rho \frac{\pi D^2}{4} C_M a_x dz + \frac{1}{2} \rho C_D D u |u| dz \quad (6.1)$$

The parameters used in the equation are defined as illustrated in Figure 6.2.

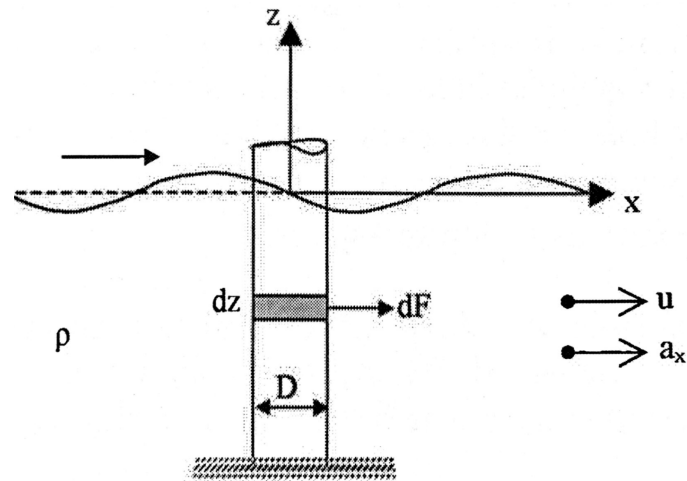


Figure 6.2: Parameters in Morison's equation defined on a cylinder (Pettersen, 2007)

The numerical procedure was based on the Runge-Kutta methods, which are a family of implicit and explicit iterative methods (Langen and Sibjörnsson, 2009).



## 7 The Simulation Model

The installation operation of the GRP pipeline protection cover should take place at two locations; Heidrun and Tanzania Block 2 and was simulated by use of SIMA. This section will contain information about the input data that was used in SIMA, in statistical models and in numerical calculations. This section describes environmental conditions, in terms of both locations and wave conditions, cover dimensions, hydrodynamic parameters, rigging system with coordinates and vessel dimensions and RAOs.

### 7.1 Environmental Conditions

#### 7.1.1 Locations

The Heidrun oil and gas field is located at Haltenbanken, west off the Norwegian coastline. Tanzania Block 2, hereinafter referred to as Tanzania, is located east off the African coastline. The locations are shown in the two maps in Figure 7.1 and 7.2.

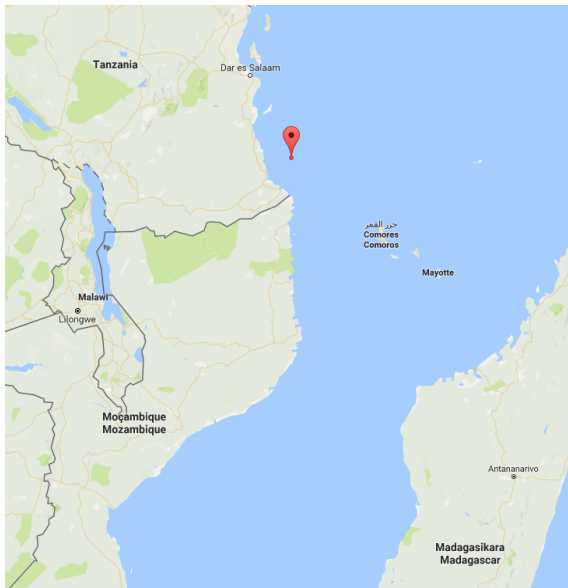


Figure 7.1: Location of the Tanzania field



Figure 7.2: Location of the Heidrun field

Local environmental conditions have been observed and stored every three hours for 52 years at Heidrun and 27 years at Tanzania. The Heidrun data set is gathered from the best hindcast data base for the Norwegian continental shelf, *NORA10* (NORwegian ReAnalysis 10 km) over a 10 km grid spacing (Reistad et al., 2011). The two location's geographical coordinates are listed in Table 7.1 in addition to the start and end date for the time series that were used. The water depth at Heidrun and Tanzania is approximately 360 m and 2 460 m respectively. Information about the

data sets is found in Statoil's Metocean reports for Heidrun (Eik and Nygaard, 2004) and Tanzania (Mathiesen, 2010).

Table 7.1: Information about time series at Heidrun and Tanzania

Field	Latitude	Longitude	Start date	End date
Heidrun	65.29N	7.32E	01.01 1958	31.12 2009
Tanzania	9.25S	40.38E	01.01 1987	31.12 2013

The time series were divided into seasons, and because Norway and Tanzania are located on the opposite side of equator, their respective seasons will be in the opposite time of the year. In Norway, planned operations do usually take place during late spring, summer, and early autumn. Late spring and early autumn will hereinafter be referred to as spring and autumn respectively, while the remaining months in these seasons will be referred to as *off-season*. In Tanzania the different seasons will contain the appurtenant three months. The correlation between months and *operation seasons* in Norway and Tanzania is shown in Table 7.2.

Table 7.2: Correlation between months and operation seasons in Norway and in Tanzania

	January	February	March	April	May	June	July	August	September	October	November	December
Heidrun	Off-Season		Spring		Summer			Autumn		Off-Season		
Tanzania	Summer		Autumn		Winter			Spring		Summer		

### 7.1.2 Wave Conditions

The wave conditions implemented in SIMA were not location dependent. Short-term sea states, conveniently defined by significant wave height, the spectral peak period and the direction of the propagating waves were used during the simulations. The environment was characterised by a JONSWAP wave spectrum with no swell, wind or current. Cosine series were used as a representation of the waves in order to take care of the depth dependent water particle motion, as in equation (4.23). The short-crested sea was given for 11 directions and varied from 90° to 270°. The direction of the propagating waves was determined to be 180 degrees to the vessel, also called head sea, and was constant throughout all the simulations. The significant wave height, peak period and seed number were all variables during the simulations. The simulated  $H_s-T_p$  conditions were based on observed  $H_s-T_p$  conditions at the Heidrun field. Figure 7.3 shows the observed wave conditions limited by  $H_s = 4$  m and  $T_p = 15$  s, determined by the 95% confidence interval, smoothed from a log-normal distribution (Nielsen, 2016).



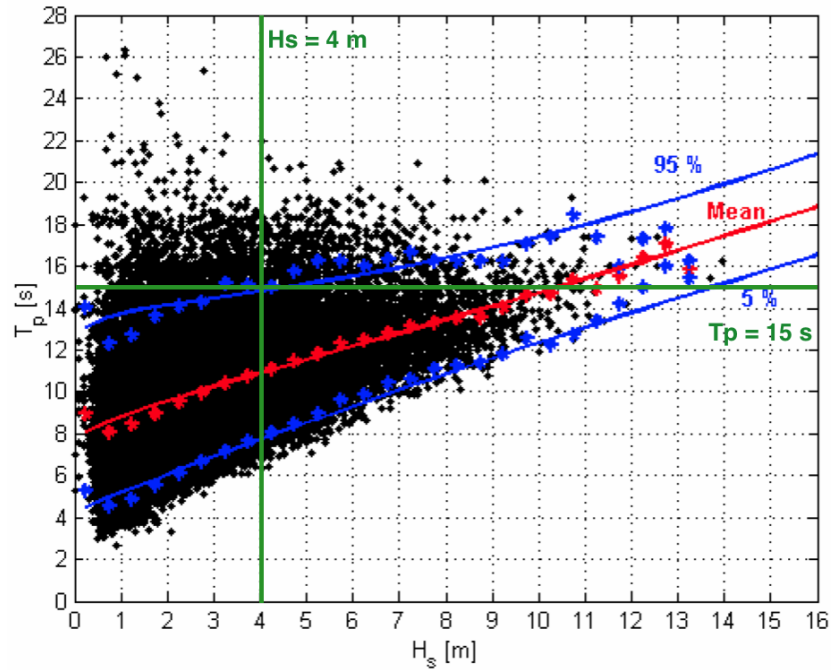


Figure 7.3: Conditional characteristics for the significant wave height and corresponding spectral peak period at Heidrun, with given upper boundaries (Eik and Nygaard, 2004)

The spectral peak periods and corresponding significant wave height occurring at the Tanzania well position during 1987 and 2009 are shown in Figure 7.4. The data-values enclosed by the red ellipse are outliers from the tropical storm Doloresse 16 – 17 February 1996 (Mathiesen, 2010).

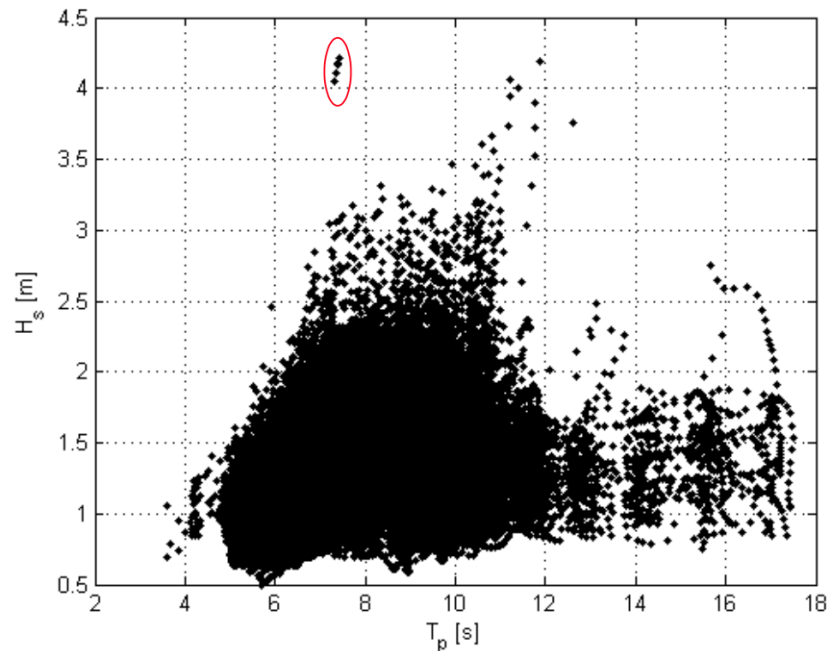
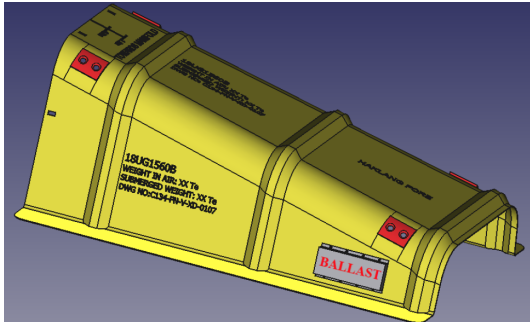


Figure 7.4: Spectral peak period and corresponding significant wave height at the Tanzania Block 2 well position (Mathiesen, 2010)

## 7.2 GRP Protection Cover

The subsea pipeline protection cover is made of Glass-Reinforced Plastic (GRP) and is shown in Figure 7.5 and has mass dimensions as described in Table 7.3.



	Mass	Density	Volume
<b>Cover</b>	7 144 kg	1 940 kg/m <sup>3</sup>	3.682 m <sup>3</sup>
<b>Ballast</b>	4 757 kg	7 866 kg/m <sup>3</sup>	0.605 m <sup>3</sup>
<b>Total</b>	<b>11 901 kg</b>		<b>4.287 m<sup>3</sup></b>

Figure 7.5: CAD model of cover (Tharigoupla, 2016) Table 7.3: Cover mass dimensions (Kendon, 2016)

The exact dimensions of the cover shown in Figure 7.6. In air, the COG is located 1.425 m above the flanges and 6.914 m from the biggest opening, while for a fully submerged cover the COG is located 1.297 m above the flanges and 7.303 m from the biggest opening.

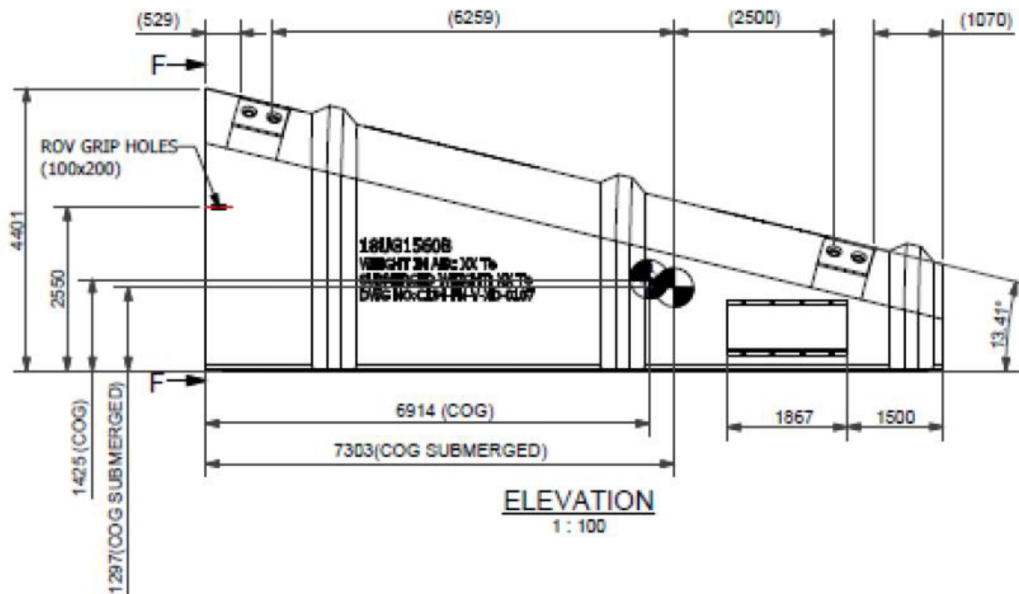


Figure 7.6: Cover dimensions with COG (Statoil, 2015)

The cover shape was simplified in order to do efficient, but adequate hand calculations. The simplified model is shown in Figure 7.7 and has dimensions as listed in Table 7.4.

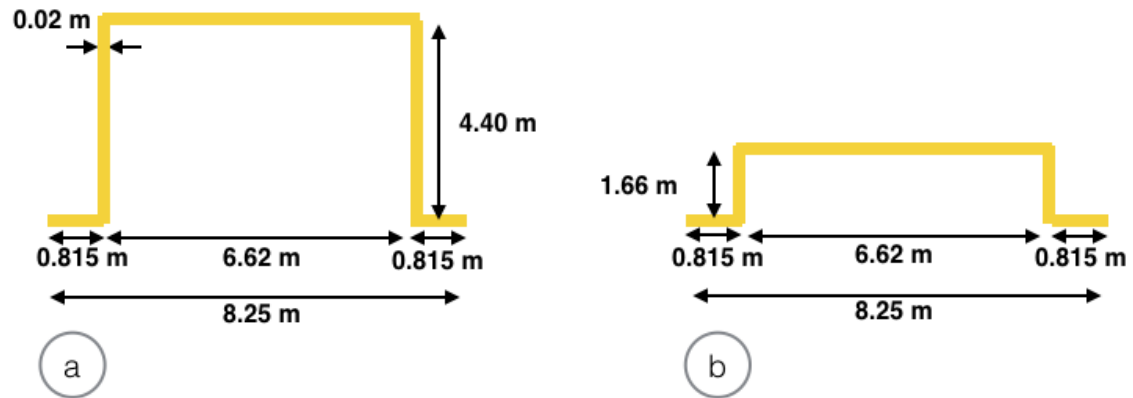


Figure 7.7: Dimensions of simplified cover, seen from the (a) front and (b) back

Table 7.4: Cover dimensions (Solaas et al., 2016)

Parameters	Values
Length	11.5 m
Total Breadth (flange included)	8.25 m
Breadth (flange excluded)	6.62 m
Height	4.40 m
Height (lower end)	1.66 m
Longitudinal COG	6.91 m
Longitudinal COG (submerged)	7.30 m
Vertical COG	1.43 m
Vertical COG (submerged)	1.30 m
Material Thickness	0.02 m

The COG coordinates with respect to the simulation model's origin are listed in Table 7.5 for translation and rotation. The cover's dimensions were defined in horizontal direction as illustrated in Figure 7.6. The rotation defines how the cover was lifted, hence  $68^\circ$  to the y-axis and  $90^\circ$  to the z-axis. Thus the bottom side of the cover was turned towards the vessel side.

Table 7.5: Cover COG with respect to origin

<b>Translation</b>	(x,y,z)	(-24.5, 23.9, 11.8)
<b>Rotation</b>	(rx,ry,rz)	(0, 68, 90)

## 7.3 Added Mass and Damping

Hydrodynamic parameters as added mass and damping were found by use of WAMIT and CFD. The hydrodynamic parameters that were implemented in the simulation model were based on the results gathered from the CFD-analysis. The WAMIT and CFD-analyses were performed by Solaas et al. (2016), and the results are described in the following section in addition to the implementation of the hydrodynamic parameters in SIMA.

### 7.3.1 From WAMIT- and CFD-analyses

The added mass and damping coefficients are dependent on the submerged depth of the object. WAMIT calculations were performed for different panel models; three simplified models with different thickness and one complex model with no thickness. The complex model with no thickness and the simplified model with a thickness of 2 cm are shown to the right and left respectively in Figure 7.8. Solaas et al. (2016) observed that there were generally a small difference between the results for the different models, hence the complex geometry with no thickness was used for further analyses.

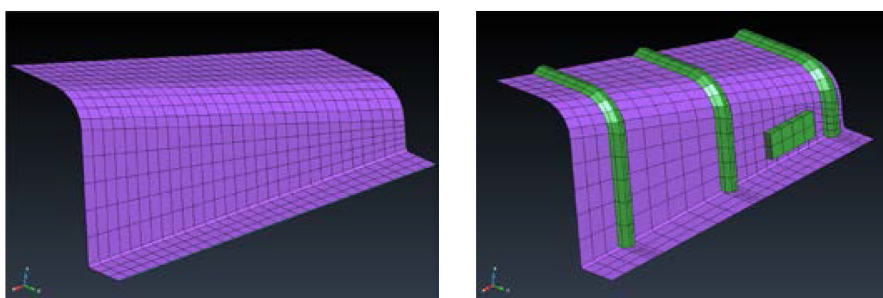


Figure 7.8: Panel models in WAMIT: Simplified model and Complex model (Solaas et al., 2016)

The obtained added mass values in three directions for a fully submerged cover with an angle of  $68^\circ$  are listed in Table 7.6, and the direction of the added mass are illustrated in Figure 7.9.

Table 7.6: Added mass values from WAMIT

Added Mass Direction	Value
$A_{11}$	440 t
$A_{22}$	210 t
$A_{33}$	23 t

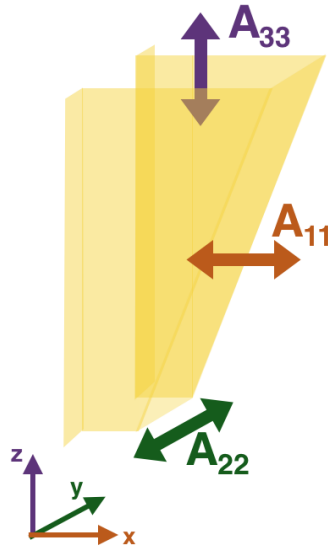


Figure 7.9: Directions of added mass

The change of added mass and damping with draught found from WAMIT analyses are shown in Figure 7.10 and 7.11 respectively for a period of 8 s. It can clearly be seen that the hydrodynamic coefficients increased with increasing draught through the splash zone until the cover was fully submerged. For further lowering the coefficients began to decrease and converge towards the value with no free surface (Solaas et al., 2016).

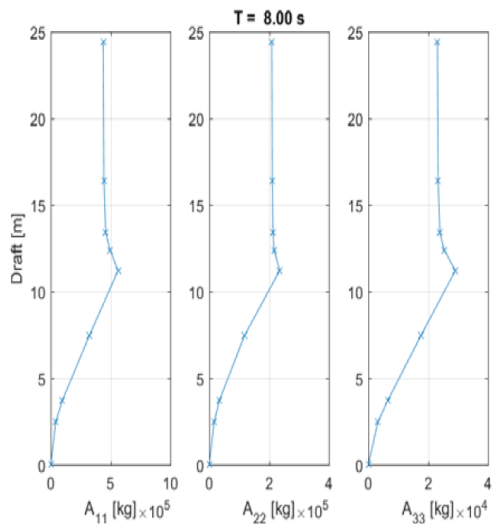


Figure 7.10: Draught dependent added mass (Solaas et al., 2016)

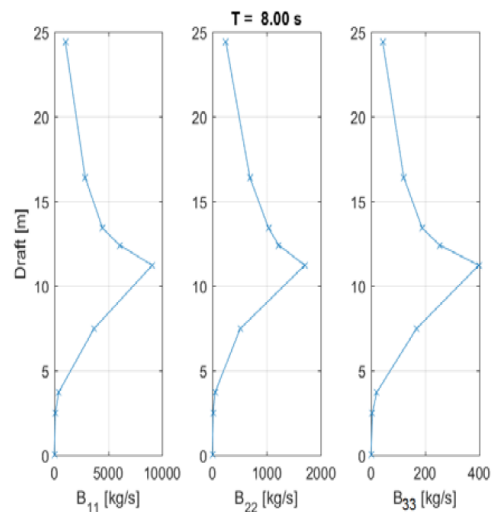


Figure 7.11: Draught dependent damping (Solaas et al., 2016)

The CFD calculations were performed with the CFD-software STAR CCM+ form CD-adapco version 11 that solve Navier-Stokes equations with appropriate turbulence models using Reynolds averaging (Solaas et al., 2016). The CFD-analyses were carried out for various amplitudes and periods. Solaas et al. (2016) observed that the added mass from CFD and forced oscillation tests differed with less than 5% and their results are presented in Figure 7.12, 7.13 and 7.14 for  $A_{11}$ ,  $A_{22}$  and  $A_{33}$  respectively.

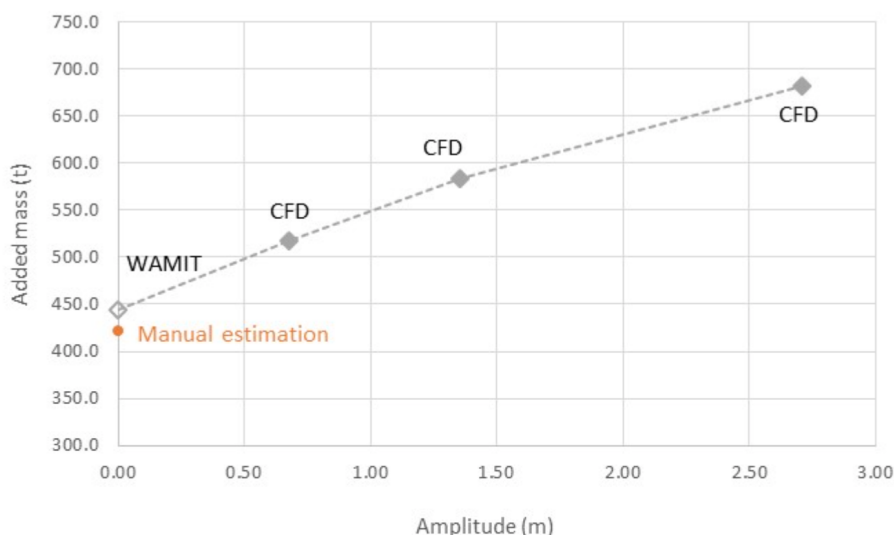


Figure 7.12: Added mass in surge  $A_{11}$  from CFD-analyses (Solaas et al., 2016)

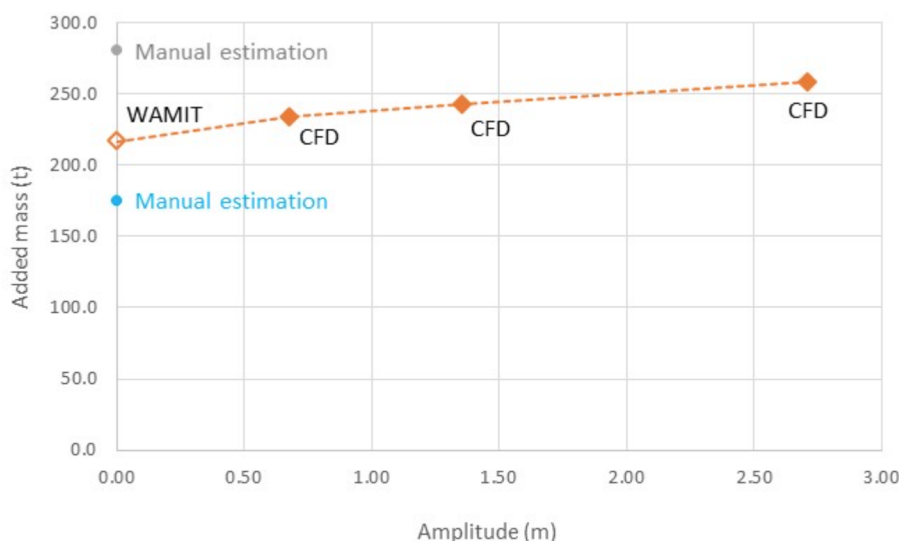


Figure 7.13: Added mass in sway  $A_{22}$  from CFD-analyses (Solaas et al., 2016)

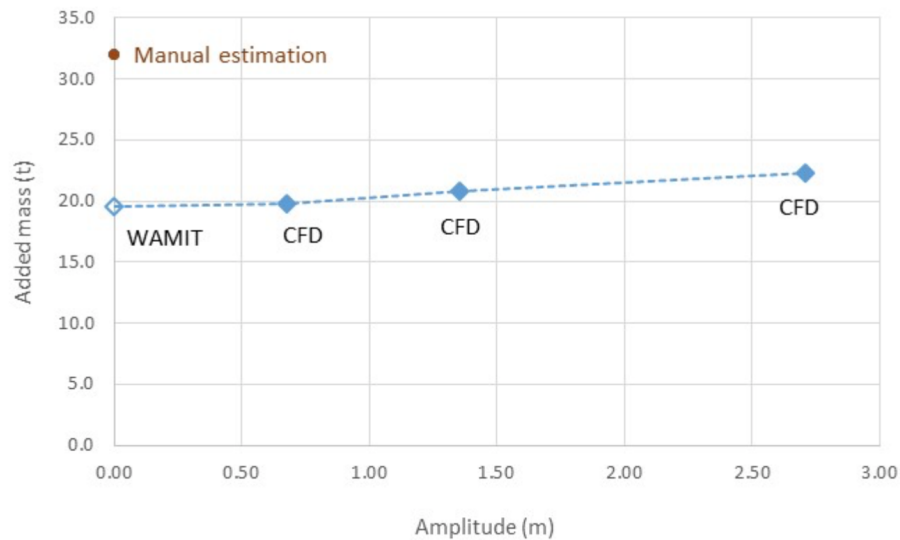


Figure 7.14: Added mass in heave  $A_{33}$  from CFD-analyses (Solaas et al., 2016)

The damping results from the CFD analyses are shown in Figure 7.15 and listed in Table 7.7.

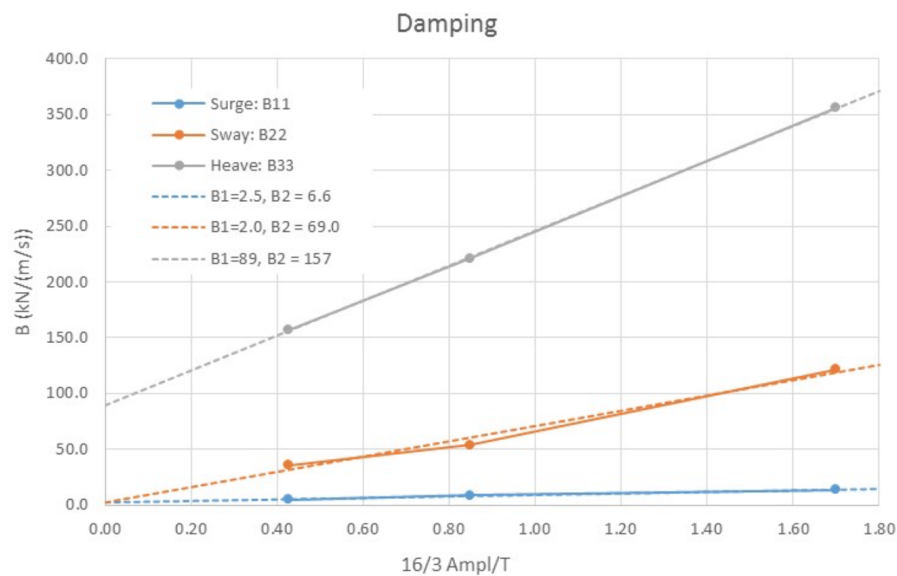


Figure 7.15: Damping for cover calculated by CFD-analyses. Results for different amplitudes of oscillation with period 8.5 s together with linear and quadratic damping estimated from the results (Solaas et al., 2016).

Table 7.7: Linear and quadratic damping for fully submerged cover from CFD (Solaas et al., 2016)

	Linear Damping [Ns/m]	Quadratic Damping [Ns <sup>2</sup> /m <sup>2</sup> ]
<b>Surge</b> $B_{11}$	2 400	6 600
<b>Sway</b> $B_{22}$	2 000	69 000
<b>Heave</b> $B_{33}$	89 100	156 900

### 7.3.2 Implemented in SIMA

The cover was modelled by slender elements in the simulation model. Eleven elements were used to model the cover, where four elements represented the side walls, two represented the *flanges* on each side, three represented the roof and two small ones represented the ballast. Each slender element was given coordinates to its end points. To obtain a realistic mass matrix, the cover's total volume, added mass and damping were distributed along each slender element (Solaas et al., 2016). The slender element's coordinates, total length, specific volume per meter, mass per meter and number of strips are listed in Table 7.8.

Table 7.8: Slender elements' coordinates, volume and mass

Slender Elements	End Point 1 (x,y,z)	End Point 2 (x,y,z)	Length [m]	Specific Volume [ $m^2$ ]	Distributed Mass [ $kg/m$ ]	Number of Strips
Skirt 1	(0, 3.8, 0)	(11.5, 3.8, 0)	11.50	0.04845	94	6
Skirt 2	(0, -3.8, 0)	(11.5, -3.8, 0)	11.50	0.04845	94	6
Roof 1	(0, 2, 4.4)	(11.5, 2, 1.75)	11.80	0.03660	71	6
Roof 2	(0, -2, 4.4)	(11.5, -2, 1.75)	11.80	0.03660	71	6
Roof 3	(0, 0, 4.4)	(11.5, 0, 1.75)	11.80	0.06701	130	6
Wall I 1	(0, 3, 2.4)	(7.5, 3, 2)	7.51	0.05052	98	3
Wall I 2	(0, -3, 2.4)	(7.5, -3, 2)	7.51	0.05052	98	3
Wall II 1	(7.5, 3, 2)	(11.5, 3, 1.8)	4.00	0.02268	43	3
Wall II 2	(7.5, -3, 2)	(11.5, -3, 1.8)	4.00	0.02268	43	3
Ballast1	(8.13, 3.3, 0.7)	(10, 3.3, 0.7)	1.87	0.16018	1260	2
Ballast2	(8.13, -3.3, 0.7)	(10, -3.3, 0.7)	1.87	0.16018	1260	2
<b>Total</b>				<b>4.308 <math>m^3</math></b>	<b>11 900 <math>kg</math></b>	

Each slender element was given added mass and damping per meter, in order to take care of depth dependency. Added mass and damping values gathered from CFD-analysis with amplitudes of 2.5 m were used in the simulation model. The added mass per meter and linear and quadratic damping per meter for each slender element are listed in Table 7.9 and 7.10 respectively.



Table 7.9: Slender elements' added mass

Slender Elements	Length [m]	Direction	Added mass [kg/m]
Skirt 1	11.50	z	12 000
Skirt 2	11.50	z	12 000
Roof 1	11.80	z	8 000
Roof 2	11.80	z	8 000
Roof 3	11.80	z	16 000
Wall I 1	7.51	y	14 000
Wall I 2	7.51	y	14 000
Wall II 1	4.00	y	4 600
Wall II 2	4.00	y	4 600

Table 7.10: Slender elements' linear and quadratic damping

Slender Elements	Length [m]	Direction	Linear Damping [Ns/m <sup>2</sup> ]	Quadratic Damping [Ns <sup>2</sup> /m <sup>3</sup> ]
Skirt 1	11.50	z	2 700	3 500
Skirt 2	11.50	z	2 700	3 500
Roof 1	11.80	z	800	2 250
Roof 1	11.80	x	20	60
Roof 2	11.80	z	800	2 250
Roof 2	11.80	x	20	60
Roof 3	11.80	z	800	2 350
Roof 3	11.80	x	40	80
Wall I 1	7.51	y	120	4 000
Wall I 2	7.51	y	120	4 000
Wall II 1	4.00	y	30	1 100
Wall II 2	4.00	y	30	1 100

Total added mass in vertical  $A_{11}$  and translational  $A_{22}$  direction (for the cover in initial position) implemented to the slender elements in SIMA are listed in Table 7.11.

Table 7.11: Total added mass implemented in SIMA

Total Added Mass	
$\mathbf{z}$ ( $A_{11}$ )	<b>653 600 kg</b>
$\mathbf{y}$ ( $A_{22}$ )	<b>247 080 kg</b>

Total linear and quadratic damping in vertical  $B_{33}$ , translational  $B_{22}$  and horizontal  $B_{11}$  direction implemented to the slender elements in SIMA are listed in Table 7.12.

Table 7.12: Total linear and quadratic damping implemented in SIMA

	Total Linear Damping	Total Quadratic Damping
$\mathbf{x}$ ( $B_{11}$ )	<b>944 <math>Ns/m</math></b>	<b>2 360 <math>Ns^2/m^2</math></b>
$\mathbf{y}$ ( $B_{22}$ )	<b>2 042 <math>Ns/m</math></b>	<b>68 880 <math>Ns^2/m^2</math></b>
$\mathbf{z}$ ( $B_{33}$ )	<b>90 420 <math>Ns/m</math></b>	<b>161 330 <math>Ns^2/m^2</math></b>

## 7.4 Lifting Equipment

The lifting equipment consisted of a main lifting wire, a hook, a double sling from the hook to a master link, two slings from the master link to a spreader bar and two more slings from the spreader bar to the cover. The double sling from the hook to the master link was omitted in the simulation model. Thus sling 3 and 4 were connected to the hook through the hook wire directly. The rigging is illustrated in Figure 7.16, where the slender elements are shown as the blue elements on the cover.

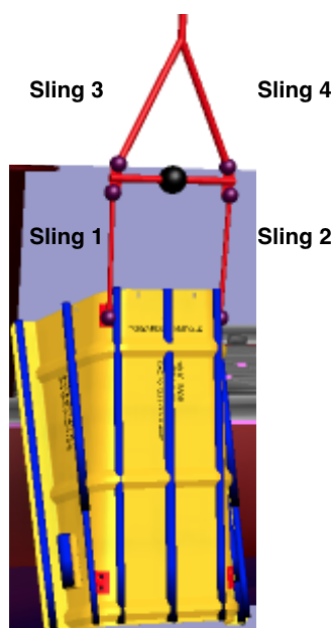


Figure 7.16: GRP cover with lifting equipment

The main hook's mass was 12 t and the spreader bar's mass was 2 t. Sling 1 and Sling 2 are the two slings located between the cover and the spreader bar, while Sling 3 and Sling 4 are located above the spreader bar. The forces arising in sling 3 and 4 will therefore include the weight of the spreader bar.

In SIMA the lifting equipment were given properties in addition to connection coordinates for the equipment's end points. The crane winch was given properties as listed in Table 7.13. The crane winch was connected to the crane tip and the *Hook Top*. The crane tip's global coordinates were (-24.5, 27.9, 32.6).

Table 7.13: Crane winch properties

Property	Values	Units
Length	4	<i>m</i>
Cross-Section Stiffness <i>EA</i>	$1.24 \cdot 10^9$	<i>N</i>
Material Damping	$1.00 \cdot 10^6$	<i>Ns</i>

The main hook was given two local connection points; the *hook top* located at (0, 0, 0.5) and the *hook bottom* located at (0, 0, -1.5). Hence the hook's vertical length was 2 m. The global connection point between the crane winch and the hook top was calculated by subtracting the crane winch length from the crane tip's vertical location. According to this the crane winch and hook top connection point was located at (-24.5, 27.9, 28.6).

The hook was given mass properties as listed in Table 7.14. The mass moments of inertia were defined about the origin and there was no linear damping nor any hydrostatic stiffness data implemented in the simulation model.

Table 7.14: Structural mass of hook

Parameters	Values	Units
Mass	12 000	<i>kg</i>
<i>I<sub>xx</sub></i>	48 000	<i>kgm<sup>2</sup></i>
<i>I<sub>yy</sub></i>	48 000	<i>kgm<sup>2</sup></i>
<i>I<sub>zz</sub></i>	24 000	<i>kgm<sup>2</sup></i>

The hook bottom was connected to a 4 m long hook wire with a cross-section stiffness of  $6 \cdot 10^6$  N. The global connection point between the hook bottom and the hook wire was therefore (-24.5, 27.9, 26.6). The other end of the hook wire was connected to sling 3 and 4 via a multiple connection located at (-24.5, 27.9, 22.6).

The slings were made of polyester and had a Safe Working Load of 15 t. The four slings' *EA* was  $3 \cdot 10^6$  N. Sling 1 and 2 was given a vertical length of 4.3 m while sling 3 and 4 were 4.4 m long with

an angle of approximately  $60^\circ$ . Hence the vertical length of sling 3 and 4 was approximately 3.8 m. The spreader bar was 1 m thick and 4.64 m wide and was given *four* local connection points, as listed in Table 7.15. SBAR\_pt3 and SBAR\_pt4 were connected to sling 3 and 4 respectively. Hence the global connection coordinates between the spreader bar and sling 3 were (-22.33, 27.9, 18.8) and the spreader bar and sling 4 were (-26.67, 27.9, 18.8).

Table 7.15: Body points of spreader bar

Name	(x, y, z)
SBAR_pt1	(2.32, 0.0, -0.5)
SBAR_pt2	(-2.32, 0.0, -0.5)
SBAR_pt3	(2.167, 0.0, 0.5)
SBAR_pt4	(-2.167, 0.0, 0.5)

The lower ends of the spreader bar; SBAR\_pt1 and SBAR\_pt2, were connected to sling 1 and 2 respectively. Hence their connection coordinates were (-22.18, 27.9, 17.8) and (-26.82, 27.9, 17.8). The spreader bar was given mass properties as listed in Table 7.16. The mass moments of inertia were defined about the origin and there was no linear damping nor any hydrostatic stiffness data implemented in the simulation model.

Table 7.16: Structural mass of spreader bar

Parameters	Values	Units
Mass	2 000	kg
Ixx	2 000	kgm <sup>2</sup>
Iyy	4 000	kgm <sup>2</sup>
Izz	4 000	kgm <sup>2</sup>

The cover was connected to the other ends of sling 1 and 2 via to shackles. The cover was given local coordinates for horizontal direction along the x-axis. It was thereafter given a rotation of  $68^\circ$  around the y-axis and  $90^\circ$  around the z-axis. The shackles were attached to the cover and given local coordinates as listed in Table 7.17. After the cover was rotated the global connection coordinates between the slings and the shackles were calculated to be (-22.28, 27.9, 13.5) and (-26.72, 27.9, 13.5).

Table 7.17: Body points of shackle

Name	(x, y, z)
Shackle1	(0.966, -2.216, 4.0)
Shackle2	(0.966, 2.216, 4.0)

The vertical dimensions of the cover hanging with an angle of  $68^\circ$  are illustrated in Figure 7.17. With a vertical distance of approximately 6.5 m from the shackles to the cover COG, it was assumed that the cover's lower end was located approximately 2.2 m above the sea surface.

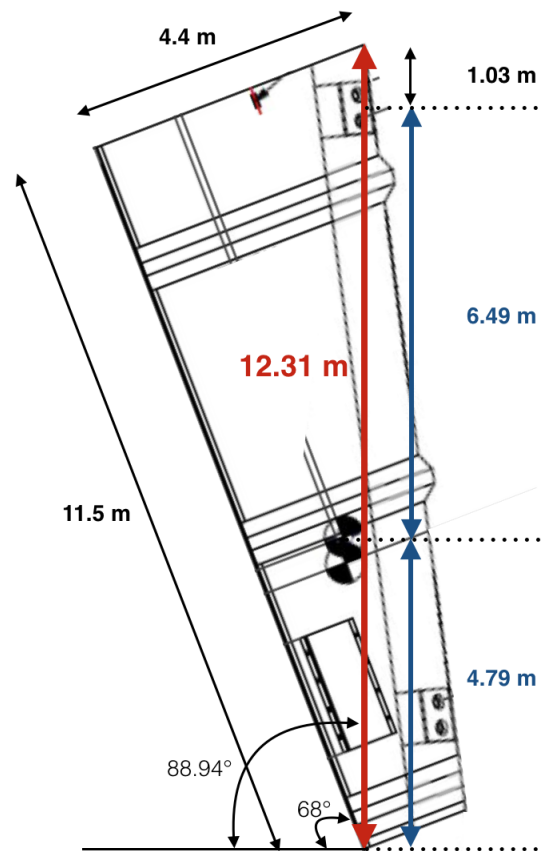


Figure 7.17: Vertical dimensions of cover with an angle of  $68^\circ$

The rigging system with global coordinates are shown in Figure 7.18 for the upper part of the system and 7.19 for the lower part of the system.

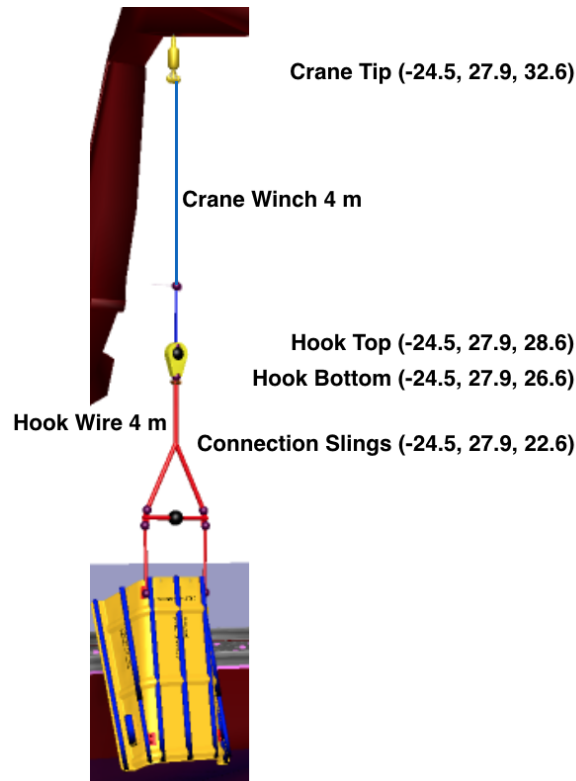


Figure 7.18: Upper part of rigging system with global coordinates

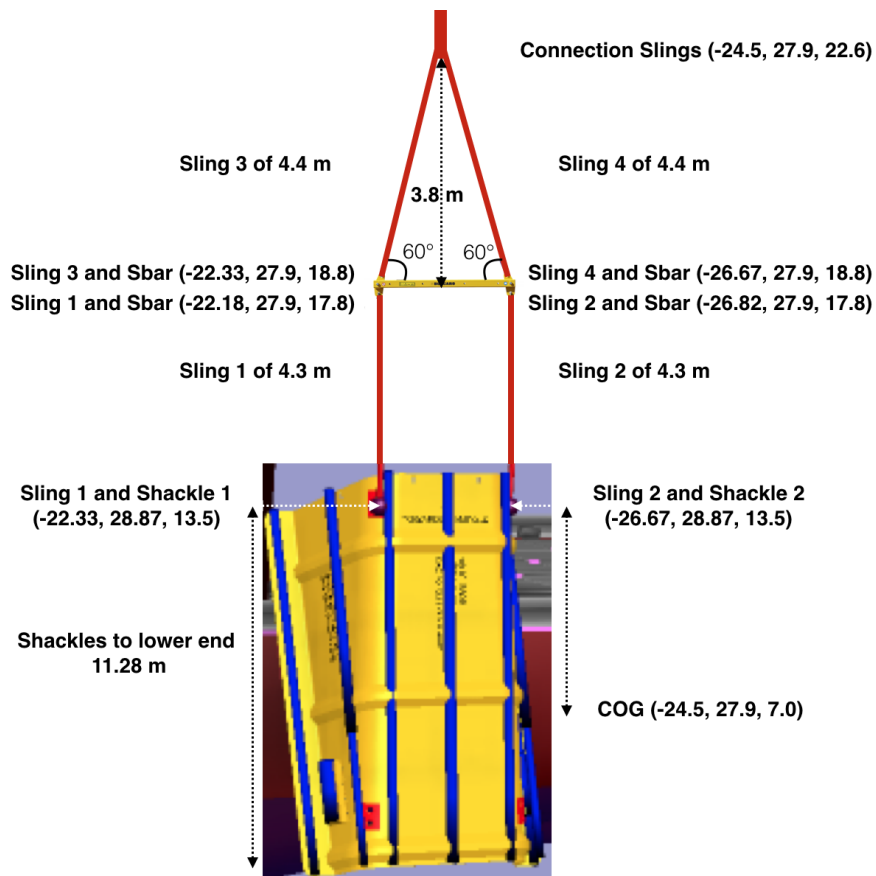


Figure 7.19: Lower part of rigging system with global coordinates

## 7.5 Installation Vessel

Scandi Acergy is a typical crane vessel and was used in the simulation model. Scandi Acergy was given dimensions as listed in Table 7.18. A typical crane vessel does usually have a Dynamic Positioning (DP) system that uses its own propellers and thrusters to maintain the vessel's position and heading. With DP one is able to minimise the motion of the vessel in certain directions by altering the heading of the ship into desired direction (Insight, 2017). A DP system, that is independent of mooring and anchors, is not easy to implement into a simulation model. Thus the vessel in the simulation model was kept in position by use of a horizontal mooring system that consisted of four mooring lines with stiffness and damping equivalent to the ones that would have arose due to a DP system (Solaas et al., 2016). The vessel that was used in the simulation is shown in Figure 7.20.

Table 7.18: Installation vessel dimensions - Scandi Acergy

Parameters	Values
Length ( $L_{pp}$ )	137.7 m
Breadth	27 m
Draught	6.438 m

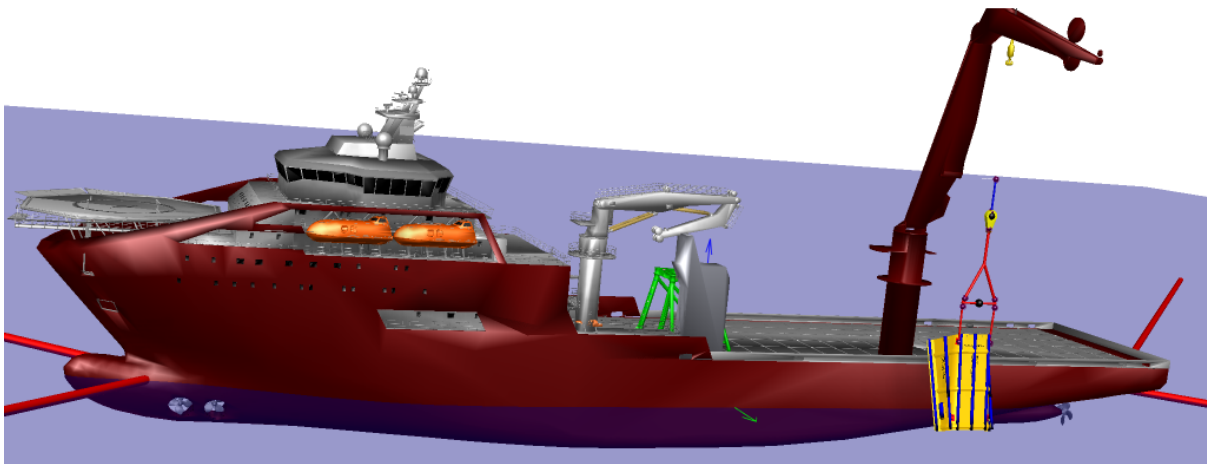


Figure 7.20: Vessel used in the simulation model with rigging system

The installation vessel's was given mass properties as listed in Table 7.19. The mass moments of inertia were defined about the origin.

Table 7.19: Structural mass of installation vessel

Parameters	Values	Units
Mass	$1.69 \cdot 10^7$	kg
$I_{xx}$	$1.93 \cdot 10^9$	$kgm^2$
$I_{yx}$	0	$kgm^2$
$I_{yy}$	$2.35 \cdot 10^{10}$	$kgm^2$
$I_{zx}$	$8.78 \cdot 10^6$	$kgm^2$
$I_{zy}$	0	$kgm^2$
$I_{zz}$	$2.31 \cdot 10^{10}$	$kgm^2$

The vessel's COG was located at (0.12, 0.0, 4.25) with its crane tip located at (-24.5, 27.9, 32.6). Hence the relative difference between the crane tip and the vessel was (-24.62, 27.90, 28.35). Figure 7.21 illustrates the simulation model's locations of the COG, the origin and the crane tip with respect to each other. The origin in the simulation model is the intersection between the water plane and the vessel for  $y = 0$ .

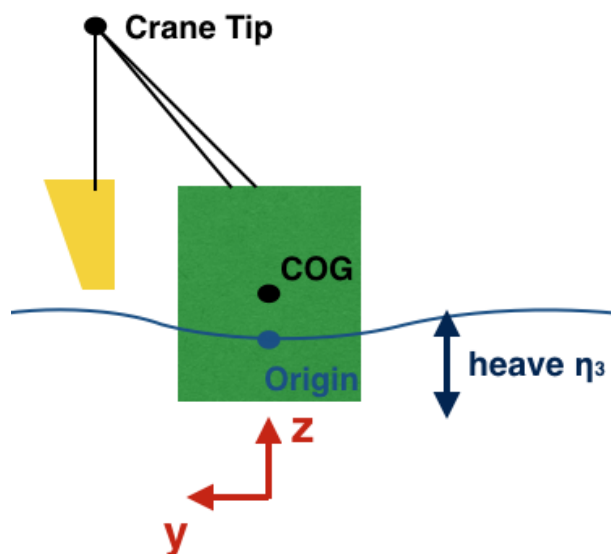


Figure 7.21: Illustration of the simulation model's origin, vessel COG and crane tip (the vessel is seen from the aft)

The crane winch was given a predefined acceleration of  $0.1 \text{ m/s}^2$ , maximum speed of  $0.5 \text{ m/s}$ , maximum length of  $100 \text{ m}$  and drum length of  $100 \text{ m}$ , but throughout all simulations the winch speed was set to  $0.2 \text{ m/s}$ .

The installation vessel was given first order motion transfer functions (RAOs) as found in Figure 7.24-7.29. The RAOs were given in the simulation model's origin and were dependent on the direction of the waves and the vessel motion in six degrees of freedom, as defined in Figure 7.22.



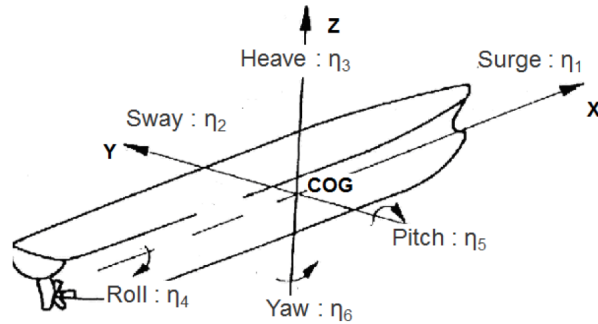


Figure 7.22: Coordinate system and definition of motions (Larsen, 2017)

The vessel was symmetric with respect to the x-axis, hence the RAOs between  $0^\circ$  and  $180^\circ$  were equal to the RAOs between  $360^\circ$  and  $180^\circ$ . The three or four most critical RAOs are visualised for their respective directions of propagating waves. Figure 7.23 shows how the wave directions and vessel motions were defined in the simulation model. Waves propagating  $90^\circ$  to the vessel is called *beam sea*, while incoming waves  $180^\circ$  and  $0^\circ$  to the vessel is called *head sea* and *following sea* respectively.

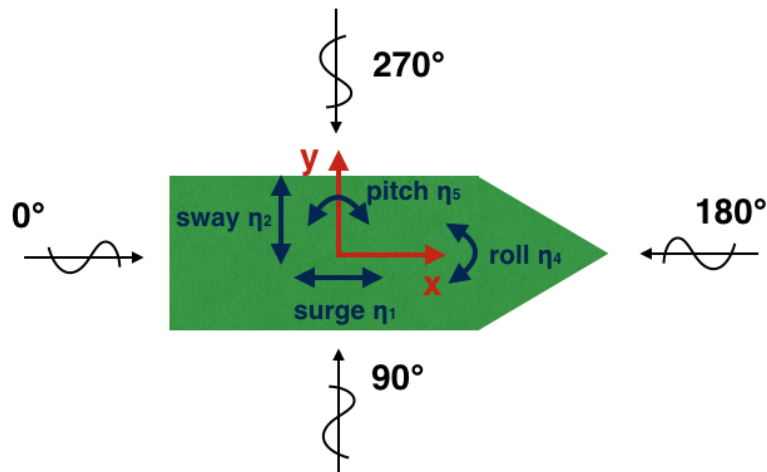


Figure 7.23: Given wave direction and vessel motion (vessel seen from above)

For an over side crane operation the motions of the crane tip are of significance and were investigated. The motions of the crane tip followed the rigid body motion equation (4.19) for the vessel motion and the relative distance between the vessel COG and the crane tip.

The RAOs for the vessel in surge motion are shown in Figure 7.24 for following sea, ( $0^\circ$ ), beam sea ( $90^\circ$ ) and head sea ( $180^\circ$ ). Beam sea will not have any significant impact on the vessel's surge motion. Head sea and following sea will on the other hand have a small impact. Waves with a peak period around 7 seconds will give the vessel a surge amplitude of 0.1 meter per meter wave height ( $\frac{m}{m}$ ), which is a negligible motion. As the wave peak period approaches 20 seconds the

surge amplitude converges towards 1 m/m, e.g. the vessel will move one meter per meter wave height along the x-axis. According to the rigid body motion equation (4.19) the crane tip motion in longitudinal direction will be dependent on the vessel's surge, pitch and yaw motion. Small surge motions will not be of huge risk during the lifting operation because the lifted object will move along the vessel side.

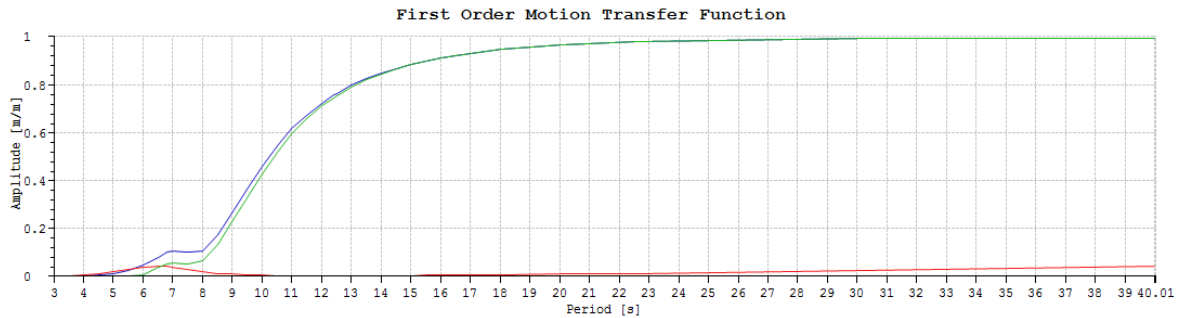


Figure 7.24: RAO for surge motion: blue = 0°, red = 90°, green = 180°

RAOs for the vessel's sway motion are visualised in Figure 7.25. Beam sea with a peak period of 15 seconds will result in a sway amplitude of approximately 1.5  $\frac{m}{m}$  before it converges towards 1  $\frac{m}{m}$  for peak periods around 19 s. It is assumed that the peak arises for the vessel's eigenperiod, which in sway motion is 15 s. Resonance arises for this peak period. This was also the case for incoming waves of 68°, which is not visualised in this Figure. The RAO for waves propagating 158° to the vessel will have a curvature similar to the aforementioned ones, but the peak amplitude converges towards 0.4  $\frac{m}{m}$ . Following sea and head sea will not have any significant impact on the vessel's sway motion. The crane tip motion in translational direction will be dependent on the vessel's sway, roll and yaw motion. Sway motions can be of huge risk during a lifting operation because the lifted object will move along the y-axis towards the vessel side, and a collision between the object and the vessel can occur.

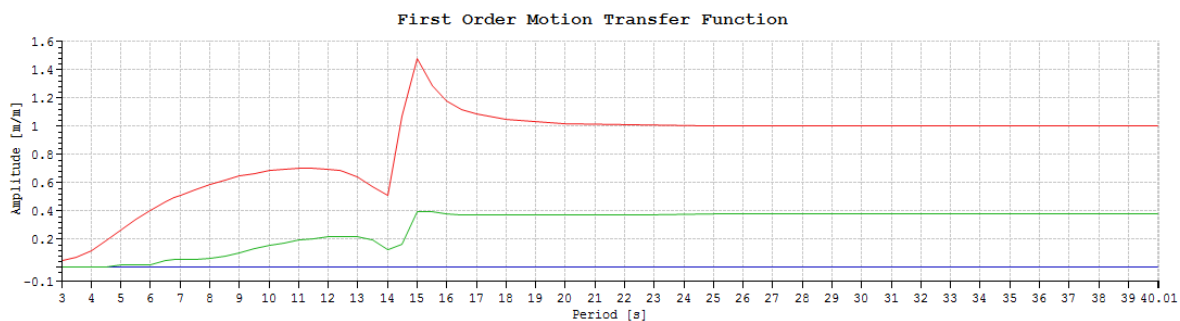


Figure 7.25: RAO for sway motion: blue = 0°, red = 90°, green = 158°

RAOs for the vessel's heave motion are shown in Figure 7.26. Beam sea with a  $T_p$  of approximately 8 s will result in a heave amplitude of 1.2  $\frac{m}{m}$  before it converges towards 1  $\frac{m}{m}$  around 13 s. The RAOs for waves propagating with a heading of 68° and 113° will converge towards 1  $\frac{m}{m}$  around 12 s. The crane tip motion in vertical direction will be dependent on the vessel's heave, roll and pitch motion.

Heave motions can be of huge risk during a lifting operation due to sudden submergence of the lifted object, large slamming forces in the splash zone and possible slack in slings that may result in large snap forces.

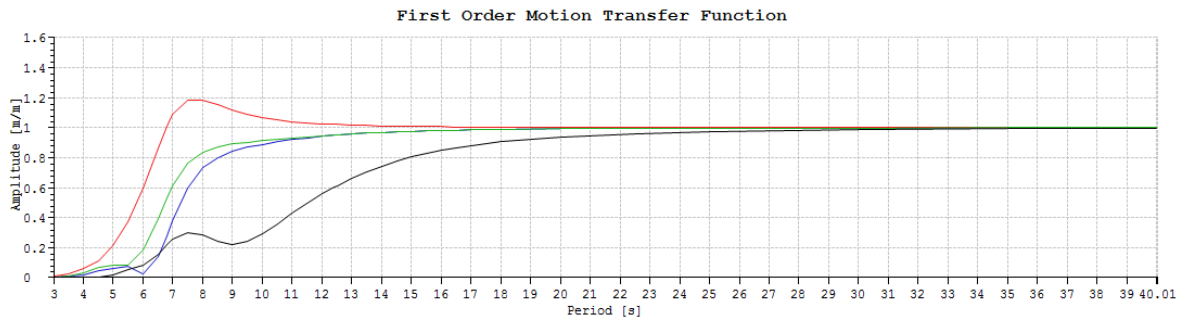


Figure 7.26: RAO for heave motion: blue =  $68^\circ$ , red =  $90^\circ$ , green =  $113^\circ$ , black =  $180^\circ$

RAOs for the vessel's roll motion are shown in Figure 7.27. The roll motion is significantly affected by beam sea with a peak period of 14.5 s, where the roll amplitude is approximately 12 degrees per meter wave height ( $\frac{deg}{m}$ ). Hence one can assume that the vessel gets resonance in roll for wave periods around 14.5 s, and that the vessel's eigenperiod in roll lays around this period. Incoming waves  $68^\circ$  and  $113^\circ$  to the vessel will have similar curves and peaks as the aforementioned one, and are not shown in this Figure. Incoming waves  $158^\circ$  to the vessel will have a similar curvature as the aforementioned one, but with a max roll amplitude of  $5 \frac{deg}{m}$  for a  $T_p$  of 14.5 s. Roll has a great impact on the translational and vertical motion of an object, and it can clearly be seen in Figure 7.25 that the RAO for sway motion is affected by the roll motion's RAO. Large roll motions will result in sway and heave motions for the crane tip and hence for the lifted object. As mentioned above this is not a desired case and should be prevented.

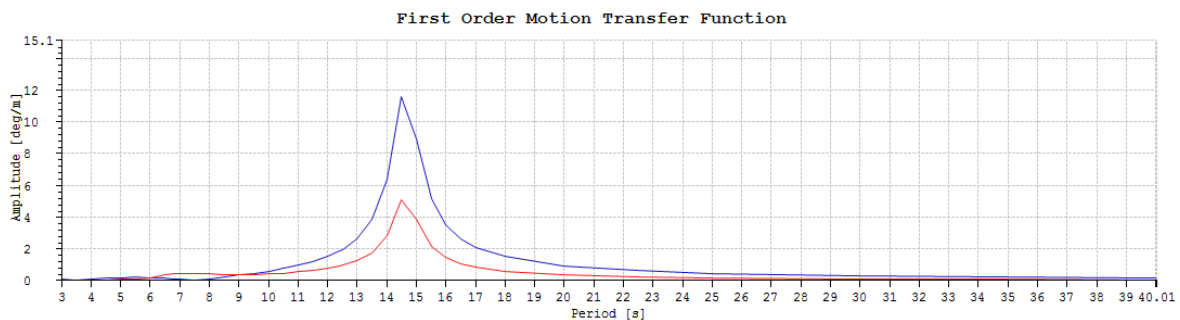


Figure 7.27: RAO for roll motion: blue =  $90^\circ$ , red =  $158^\circ$

RAOs for the vessel's pitch motion are shown in Figure 7.28. The pitch motion will be affected by incoming waves  $68^\circ$  to the vessel with  $T_p$  of approximately 7 s, resulting in a pitch amplitude of  $1.4 \frac{deg}{m}$ . It converges towards  $0 \frac{deg}{m}$  for peak periods around 30 s, and will also be the case for incoming waves  $113^\circ$  to the vessel. Incoming waves with a heading of  $135^\circ$  and head sea will have a similar curvature as the aforementioned ones, but with a pitch amplitude of  $1.3 \frac{deg}{m}$  for peak periods of 9

s and 11 s respectively. Beam sea will have an insignificantly impact on the pitch motion. Large pitch motions will result in surge and heave motions of the crane tip, that are transferred to the lifted object. As mentioned above small surge motions do not have a huge impact on the lift, but heave motions can be critical and should be prevented. It can be seen in Figure 7.26 that the RAO for heave motion has the same peak period as the RAO in pitch motion.

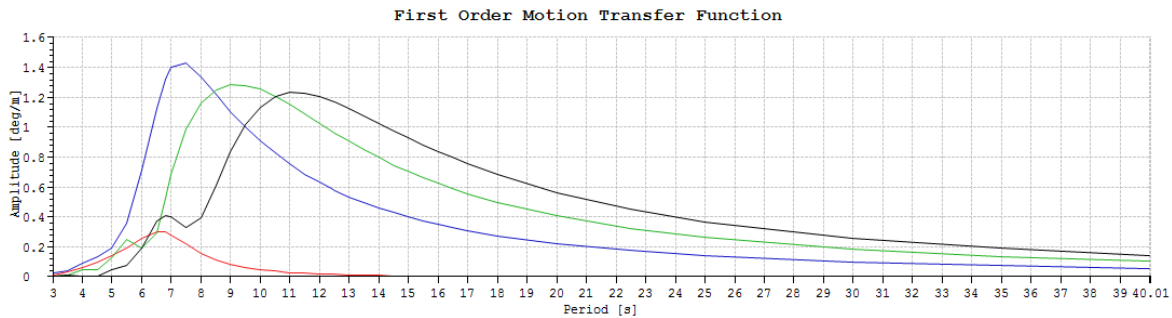


Figure 7.28: RAO for pitch motion: *blue* = 68°, *red* = 90°, *green* = 135°, *black* = 180°

RAOs for the vessel’s yaw motion are shown in Figure 7.29. Incoming waves with a heading of 113° result in an RAO with two peaks around periods of 8 s and 14.5 s. Both peaks have yaw amplitudes of approximately  $0.5 \frac{deg}{m}$  before it converges towards  $0 \frac{deg}{m}$  for peak periods of 30 s. Incoming waves 135° to the vessel will have a similar curvature as the aforementioned one but with peaks around 9.5 s and 15 s. Incoming waves with headings of 158° and 90° result in RAOs with similar curvature as the aforementioned ones, but with lower yaw amplitudes. Large yaw motions will result in surge and sway motions of the crane tip and hence of the lifted object. As mentioned above small surge motions do not have a huge impact on the operation, while large yaw motions should be avoided in order to prevent a potential collision between the lifted object and the vessel side.

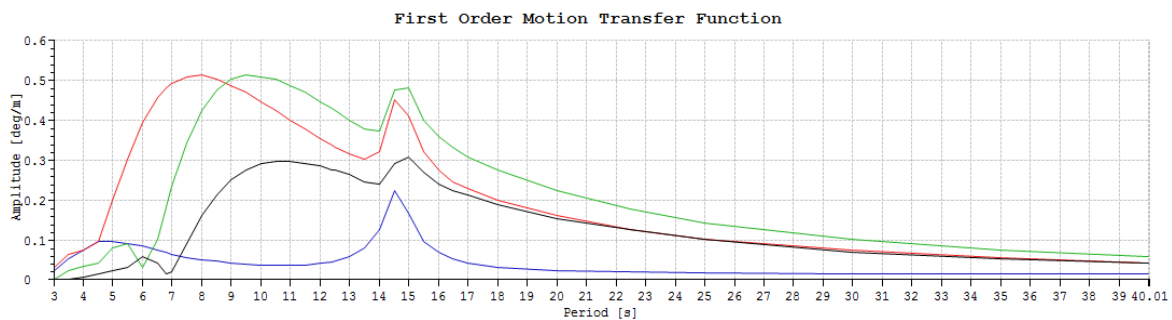


Figure 7.29: RAO for yaw motion: *blue* = 90°, *red* = 113°, *green* = 135°, *black* = 158°

The variables that were held constant throughout all the simulations in SIMA are listed in Table B.1 in Appendix B - *Variables as Input to SIMA*.

## 8 Establishment of Hydrodynamic Parameters

When the maximum limiting sea state for a marine lifting operation should be set, different methods to determine the hydrodynamic coefficients could be investigated. Such methods are estimation by use of WAMIT, CFD or model tests, or manual estimation by use of known methods. WAMIT and CFD-analyses were carried out by Solaas et al. (2016). The largest tension that arose in the slings during the simulated lift occurred just after the cover was fully submerged. Hence DNV GL's *Simplified Method* was used to manually estimate the hydrodynamic parameters just after the cover was fully submerged. The simulation results are further described in *section 9.3 Installation Simulation*. All the four hydrodynamic forces that act during *the splash zone* phase were calculated, because the cover was located in the interface between the splash zone phase and fully submerged phase. Added mass and drag are central hydrodynamic parameters and were obtained for both horizontal and vertical rigging.

Because not all the simulated wave conditions could be visualised, three wave conditions were selected for further calculations and visualisations. The three wave conditions are listed in Table 8.1.

Table 8.1: Selected wave conditions

Condition	Hs	Tp
<b>Cond I</b>	3 m	8 s
<b>Cond II</b>	3 m	12 s
<b>Cond III</b>	2 m	6 s

The hydrodynamic forces were all dependent on the crane tip motion, velocity or acceleration. Hence the crane tip motion was estimated in the following subsection, for the three wave conditions.

### 8.1 Crane Tip Motion

The vertical crane tip motion was calculated by equation (4.19), and was determined by the vessel's body motions in heave, roll and pitch, in addition to the relative location between the crane tip and the vessel COG. The vertical motion of the vessel and crane tip for head sea are plotted in Figure 8.1, 8.2 and 8.3 for the three wave conditions *cond I*, *cond II* and *cond III* respectively.

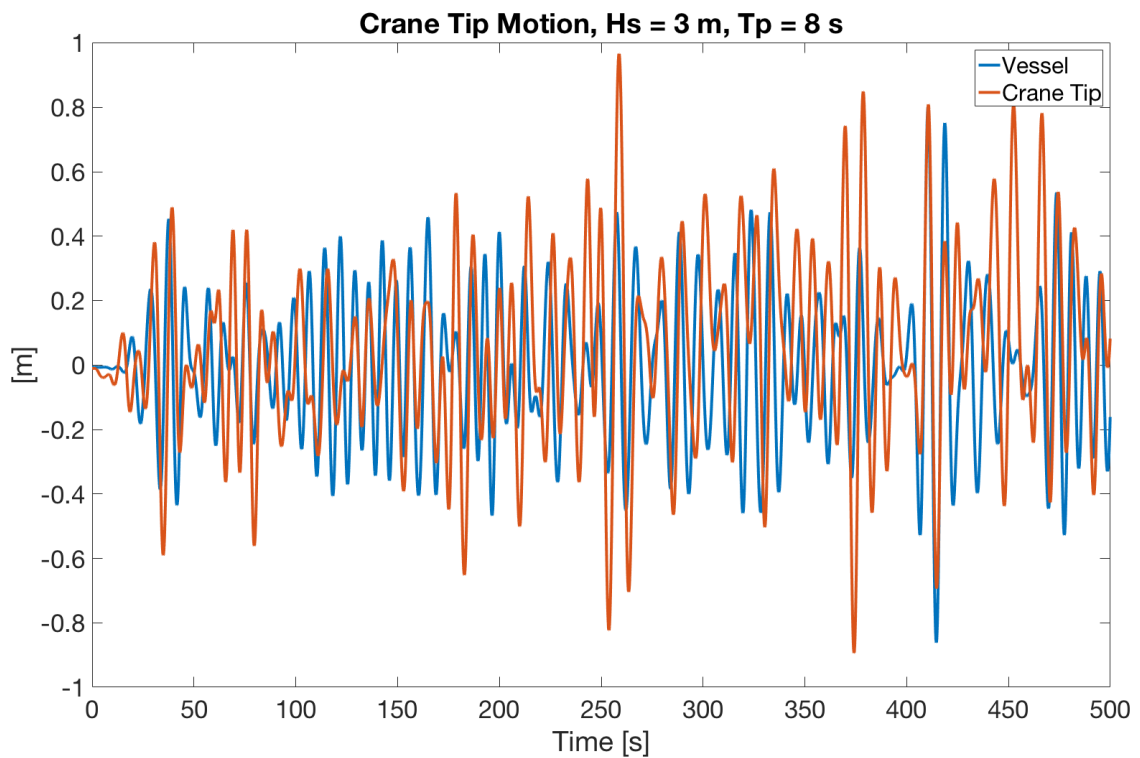


Figure 8.1: Vertical motion of the vessel COG and crane tip,  $H_s = 3$  m,  $T_p = 8$  s

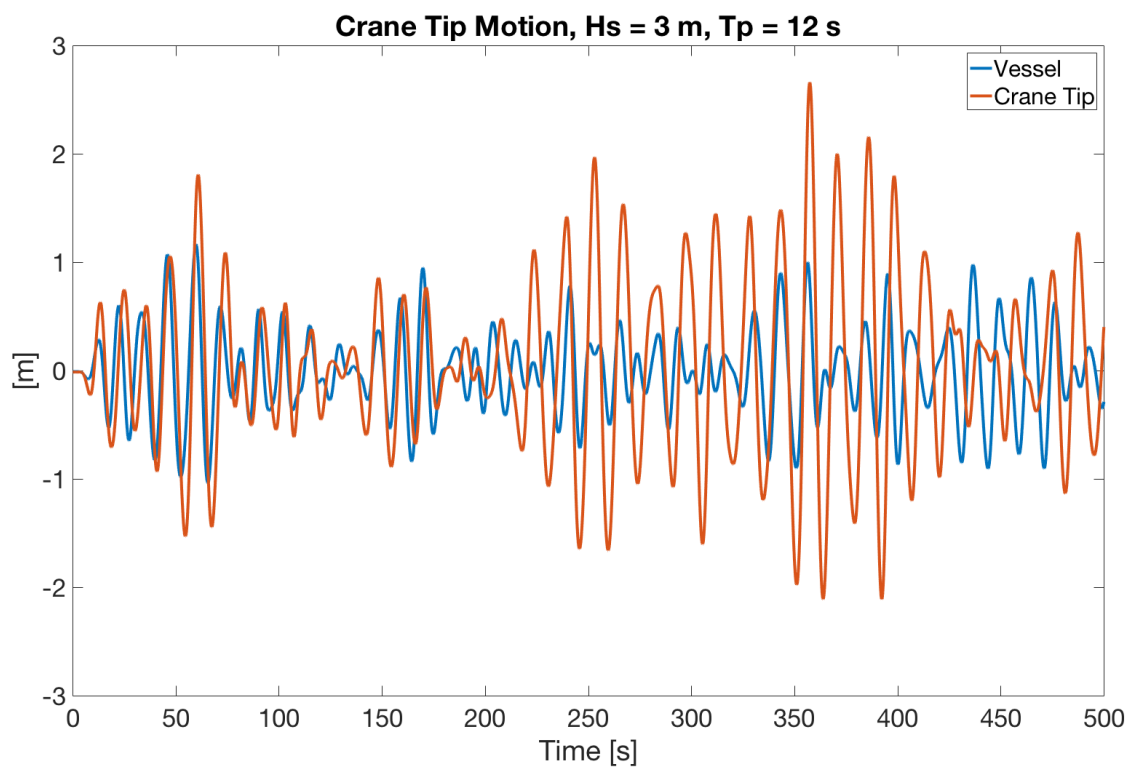


Figure 8.2: Vertical motion of the vessel COG and crane tip,  $H_s = 3$  m,  $T_p = 12$  s

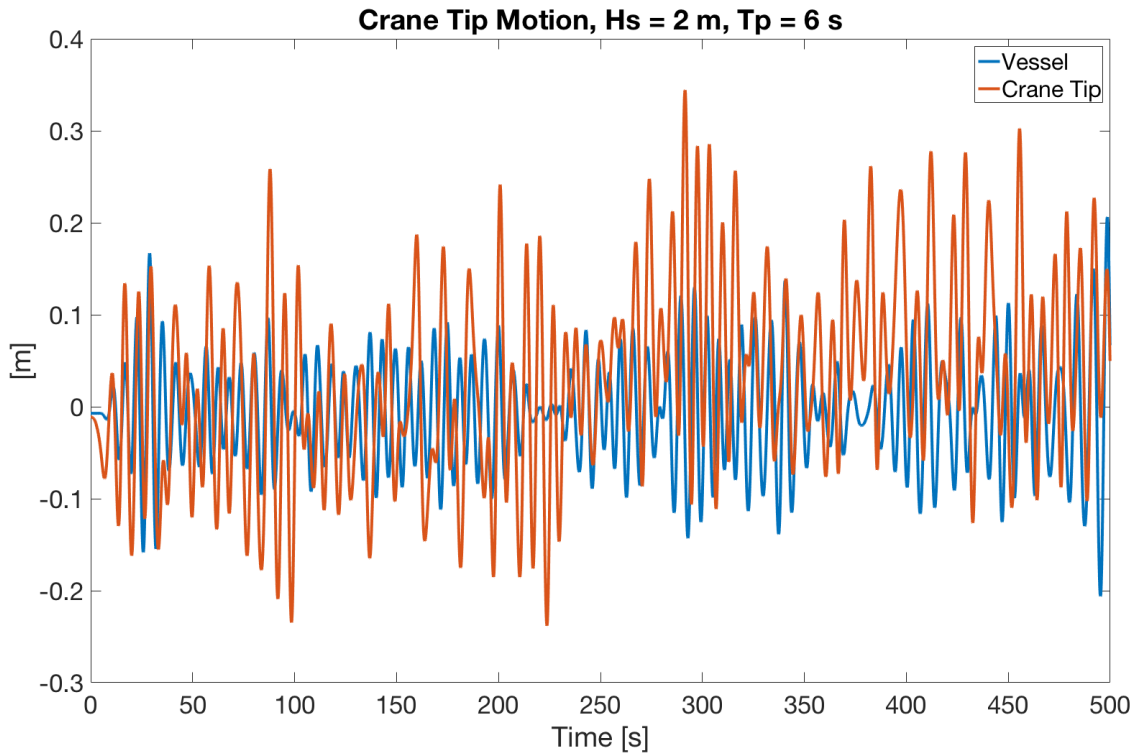


Figure 8.3: Vertical motion of the vessel COG and crane tip,  $H_s = 2$  m,  $T_p = 6$  s

The vertical crane tip motion that will be used for further calculation is the most probable crane tip motion that would occur during  $N$  waves,  $\eta_{ct}^{max}$ , where  $N$  is the ratio between 3 hours and  $T_z$ . The most probable crane tip motion was found by equation (4.20), where  $\eta_{ct}^{max} = \sigma \sqrt{2 \ln(N)}$ . The crane tip motion, velocity and acceleration for the three wave conditions are listed in Table 8.2.

Table 8.2: Crane tip motion, velocity and acceleration

	$T_z$	$N$	$\sigma$	$\eta_{ct}^{max}$	$\dot{\eta}_{ct}^{max}$	$\ddot{\eta}_{ct}^{max}$
<b>Cond I</b>	6.09 s	1 772	0.283 m	1.094 m	0.859 $\frac{m}{s}$	-0.675 $\frac{m}{s^2}$
<b>Cond II</b>	9.14 s	1 181	0.800 m	3.009 m	1.576 $\frac{m}{s}$	-0.825 $\frac{m}{s^2}$
<b>Cond III</b>	4.57 s	2 363	0.102 m	0.401 m	0.420 $\frac{m}{s}$	-0.440 $\frac{m}{s^2}$

## 8.2 The Simplified Method

### 8.2.1 Added Mass and Inertia Force

The inertia force  $F_I$  was dependent on the cover's vertical added mass, the submerged volume and the acceleration of the crane tip and water particles. The added mass was calculated by use of DNV GL's procedure for a rectangular flat plate, as further explained in *section 4.6.1 Added mass*. For rectangular plates the reference volume  $V_R$  is  $\frac{\pi}{4}a^2b$ , and the vertical added mass value  $A_{33}$  was calculated by equation (8.1). The added mass coefficient  $C_A$  was found by interpolating in Table A-2, found in Figure 4.5 for rectangular plates.

$$A_{33} = \rho \cdot C_A \cdot \underbrace{\frac{\pi}{4}a^2b}_{V_R} \quad (8.1)$$

Correction of a three-dimensional body with vertical sides was not applied. Effect of perforation on the added mass was neither taken into account because of the perforation rate  $p$  was less than 5% (DNV GL, 2011b).

An added mass force is a mass of fluid that is accelerated by the object. The cover had added mass in three directions and they were all acting perpendicular to their respective projected areas. The cover accelerated in vertical direction due to the crane tip's and water particle's vertical motion. When the cover was rotated  $68^\circ$  the added mass value in  $kg$  was still working perpendicular to the cover and did accelerate in vertical direction. Figure 8.4 *a* and *b* shows how the added mass force is defined on the rotated cover.  $A_{11}$  is the perpendicular added mass value to the cover flanges and  $A_{33}$  is the cover's longitudinal added mass value.

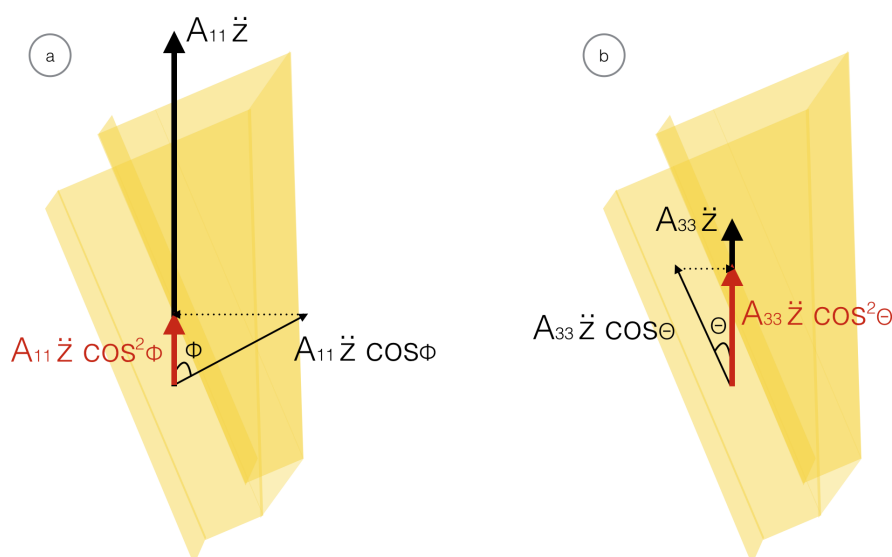


Figure 8.4: Decomposing of added mass for a)  $A_{33}$  and b)  $A_{11}$

The vertical added mass forces  $A_{11}\ddot{z}$  and  $A_{33}\ddot{z}$  were the product of the respective added mass value



and the vertical acceleration. The forces were decomposed in order to obtain the added mass force acting perpendicular to the respective projected area, as defined as  $A_{11}\ddot{z}\cos\phi$  and  $A_{33}\ddot{z}\cos\theta$  in the figure. In order to achieve the actual added mass force acting in vertical direction (marked in red), the perpendicular added mass forces were decomposed once more. The sum of the two double decomposed vertical added mass forces were used to calculate the inertia force.

Longitudinal added mass  $A_{33}$  and perpendicular added mass  $A_{11}$  are calculated in the following subsections. The parameters used to determine the added mass were not dependent on the wave conditions. The cover was fully submerged when the depth  $z$  was 11.5 m and the distance from the sea surface to the centre of gravity of the cover  $d$  was 7.303 m. The cover was lifted with an angle of  $68^\circ$  and the vertical inertia force was determined relative to this.

### 8.2.1.1 Longitudinal Added mass

The added mass value in longitudinal direction was dependent on the vertical projected area as illustrated in Figure 8.5. The parameters used to calculate this added mass value  $A_{33}$  are listed in Table 8.3.

Table 8.3: Added mass in longitudinal direction - fully submerged

Parameters	Values
$a$	2.74 m
$b$	6.62 m
$\frac{b}{a}$	2.416
$C_A$	0.802
$V_R$	39.03 m <sup>3</sup>
<b><math>A_{33}</math></b>	<b>32 088 kg</b>

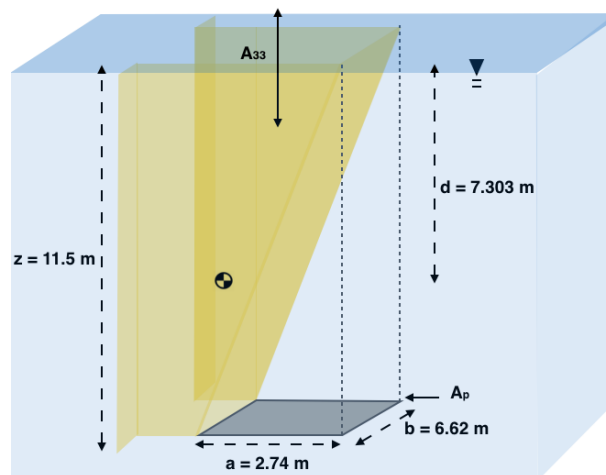


Figure 8.5: Dimensions for estimation of longitudinal added mass

### 8.2.1.2 Perpendicular Added Mass

The added mass value perpendicular to the cover flanges was dependent on the horizontal projected area as illustrated in Figure 8.6. The parameters used to calculate this added mass value  $A_{11}$  are listed in Table 8.4.

Table 8.4: Added mass perpendicular to cover flanges - fully submerged

Parameters	Values
$a$	8.25 m
$b$	11.50 m
$\frac{b}{a}$	1.394
$C_A$	0.670
$V_R$	614.75 m <sup>3</sup>
<b><math>A_{11}</math></b>	<b>422 177 kg</b>

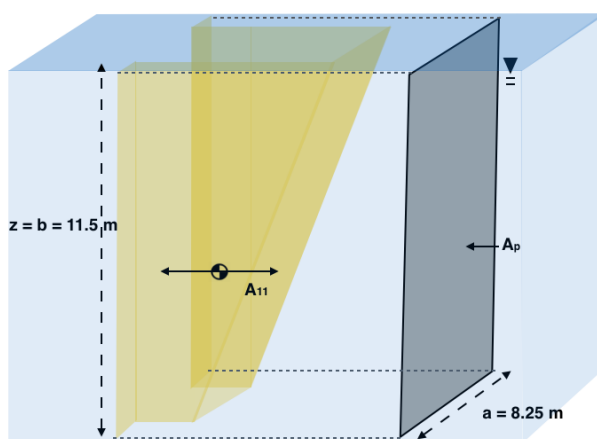


Figure 8.6: Dimensions for estimation of perpendicular added mass

### 8.2.1.3 Inertia Force

The inertia force  $F_I$  was found by equation 8.2. The cover's mass and volume were 11 901 kg and 4.287 m<sup>3</sup> respectively.

$$F_I = \sqrt{[(M_{air} + A_{33,tot})\ddot{y}_{ct}]^2 + [(\rho V + A_{33,tot})\dot{v}_w]^2} \quad (8.2)$$

The water particle acceleration  $\dot{v}_w$  was found by equation (4.24) and was dependent on the distance  $d$ , from the sea surface to the lifted object's centre of gravity. For a fully submerged cover lifted with an angle of 68° the vertical distance  $d$  was 7.82 m. The crane tip and water particle acceleration were both dependent on the wave condition.

The total vertical added mass used to determine the inertia force were based on the two double decomposed vertical added mass forces, dependent on the added mass values  $A_{33}$  and  $A_{11}$ , calculated in Table 8.3 and 8.4 respectively.

Figure 8.4 shows how the decomposition was performed, where  $\ddot{z}$  was vertical acceleration and  $\phi$  and  $\theta$  were  $68^\circ$  and  $22^\circ$  respectively. The total vertical added mass was the sum of  $A_{11}\cos^2\phi$  and  $A_{33}\cos^2\theta$ , that were calculated as below.

$$A_{11}\cos^2\phi = 422\cos^2(68) = 59.22t$$

$$A_{33}\cos^2\theta = 32\cos^2(22) = 27.51t$$

Hence the total vertical added mass  $A_{33,tot}$  was calculated to be 86.73 t. The inertia forces calculated for the three wave conditions are listed in Table 8.5.

Table 8.5: Inertia forces

	$\ddot{\eta}_{ct}$	$\dot{v}_w$	$F_I$
<b>Cond I</b>	-0.675 $\frac{m}{s^2}$	1.230 $\frac{m}{s^2}$	<b>130 350 N</b>
<b>Cond II</b>	-0.825 $\frac{m}{s^2}$	0.875 $\frac{m}{s^2}$	<b>113 936 N</b>
<b>Cond III</b>	-0.440 $\frac{m}{s^2}$	0.754 $\frac{m}{s^2}$	<b>81 257 N</b>

### 8.2.2 Drag Force

The parameters used to determine the drag coefficient were not dependent on the wave conditions and are listed in Table 8.6 for a fully submerged cover. The drag coefficient  $C_D$  was found by interpolating between the drag coefficients found in DNV GL's Table B-2 for rectangular flat plates.

Table 8.6: Parameters used to calculate the drag coefficient in vertical direction

Parameters	Values
$H$	2.74 m
$B$	6.62 m
$\frac{B}{H}$	2.416
$C_D$	1.174
$A_P$	18.14 m <sup>2</sup>

The drag force was found by equation (8.3).

$$F_D = \frac{1}{2} \cdot \rho \cdot C_D \cdot A_P \cdot v_r^2 \quad (8.3)$$

The characteristic vertical relative velocity between the object and water particles  $v_r$  was found by equation (4.26). It was assumed that the lifting speed  $v_c$  was 0.2 m/s and the wave amplitude  $\zeta_a = 0.9 \cdot Hs$ . The relative velocity and drag force calculated for each wave condition are listed in Table 8.7.

Table 8.7: Drag forces

	$v_r$	$F_D$
<b>Cond I</b>	1.670 $\frac{m}{s}$	<b>30 448 N</b>
<b>Cond II</b>	2.230 $\frac{m}{s}$	<b>54 075 N</b>
<b>Cond III</b>	0.891 $\frac{m}{s}$	<b>8 661 N</b>

### 8.2.3 Slamming Force

The slamming force is dependent on the slamming velocity  $v_s$ , which is equal to the relative velocity  $v_r$  between the object and water particles. The slamming force is also dependent on the rate of change of added mass with submergence  $\frac{dA(z)}{dz}$ .

A force is the product of a mass and acceleration. The acceleration in the added mass force will work in vertical direction due to the vertical crane tip motion, and is denoted as  $a_z$ . The acceleration normal to the cover  $a_n$  will be a component of  $a_z$  as following:

$$a_n = a_z \cdot \cos\phi$$

The added mass force normal to the cover  $F_n$  was therefore described as equation (8.4), where  $A_n(z)$  is the depth-dependent added mass normal to the cover.

$$F_n = A_n(z) \cdot a_n \Rightarrow F_n = A_n(z) \cdot a_z \cdot \cos\phi \quad (8.4)$$

The vertical added mass force  $F_z$  was found to be a component of  $F_n$  described as following

$$F_z = F_n \cdot \cos\phi \Rightarrow F_z = \underbrace{A_n(z) \cdot \cos^2\phi}_{A_z(z)} \cdot a_z$$

$F_z$  can therefore be written as the product of the depth-dependent vertical added mass  $A_z(z)$  and the vertical acceleration  $a_z$ , where  $A_z(z)$  is described as in equation (8.5).

$$A_z(z) = A_n(z) \cdot \cos^2\phi \quad (8.5)$$

Figure 8.7 *a* and *b* illustrates the directions of the given variables, forces and accelerations.

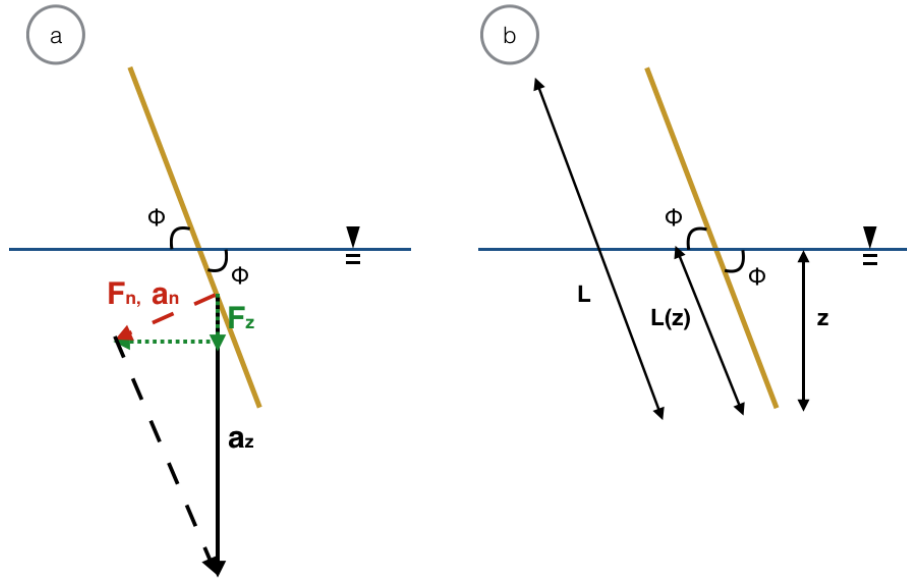


Figure 8.7: Illustration of slamming forces and accelerations. (Yellow inclined line is partly submerged cover.)

By use of trigonometry one can say that

$$\frac{A_n(z)}{A_n} = \frac{l(z)}{l} = \frac{z}{\sin\phi \cdot l}$$

where  $l$  is the total length of the cover. Hence  $A_n(z)$  will be described as in equation (8.6).

$$A_n(z) = \frac{z}{\sin\phi \cdot l} \cdot A_{11} \quad (8.6)$$

By combining equation (8.5) and (8.6)  $A_z(z)$  can be described as in equation (8.7).

$$A_z(z) = \frac{z}{\sin\phi \cdot l} \cdot A_{11} \cdot \cos^2\phi \quad (8.7)$$

The change in vertical added mass with depth will therefore be as following:

$$\frac{dA_z(z)}{dz} = \frac{A_{11}}{\sin\phi \cdot l} \cdot \cos^2\phi$$

Hence the vertical slamming force  $F_{S,z}$  could be found by multiplying the squared slamming velocity with the change in vertical added mass as following:

$$F_{S,z} = \frac{dA_z(z)}{dz} \cdot v_s^2$$

The added mass normal to the cover  $A_n$  was equal to  $A_{11}$  of 422 t. The length of the cover  $l$  was 11.5 m and the angle  $\phi$  was for simplicity assumed to be  $75^\circ$ , which is the average angle between the cover roof of  $81^\circ$  and the cover flanges of  $68^\circ$ .  $\frac{dA_z(z)}{dz}$  was hence calculated to be  $2\,545 \frac{\text{kg}}{\text{m}}$ .

The slamming force was calculated for an immediately fully submerged cover with a vertical distance  $d$  from the sea surface to the cover COG of 7.82 m. The slamming forces that arose for the three wave conditions are listed in Table 8.8.

Table 8.8: Vertical slamming force for three wave conditions

	$v_s$	$F_{s,z}$
<b>Cond I</b>	1.670 $\frac{m}{s}$	<b>7 047 N</b>
<b>Cond II</b>	2.226 $\frac{m}{s}$	<b>12 516 N</b>
<b>Cond III</b>	0.891 $\frac{m}{s}$	<b>2 005 N</b>

### 8.2.4 Varying Buoyancy Force

Varying buoyancy was calculated by equation (8.8), where  $A_w$  was the mean waterline area and determined to be approximately  $0.3 \text{ m}^2$ .

$$F_B = \rho \cdot A_w \cdot \sqrt{\zeta_a^2 + \eta_{ct}^2} \cdot g \quad (8.8)$$

The wave amplitude, crane tip motion and calculated varying buoyancy force are listed in Table 8.9 for the three wave conditions.

Table 8.9: Vertical varying buoyancy force for three wave conditions

	$\zeta_a$	$\eta_{ct}$	$F_B$
<b>Cond I</b>	2.7 m	1.09 m	<b>8 788 N</b>
<b>Cond II</b>	2.7 m	3.01 m	<b>12 196 N</b>
<b>Cond III</b>	1.8 m	0.40 m	<b>5 563 N</b>

### 8.3 Manually Estimated Design Criteria

The total hydrodynamic force  $F_{hyd}$  was calculated by  $\sqrt{(F_D + F_S)^2 + (F_I - F_B)^2}$ . The inertia force was dominating the total hydrodynamic force for all wave conditions. The inertia force is proportional with the water particle velocity, hence linear scaling was used to determine the maximum design criteria  $H_{sLIM}$ . In order to stay within the slack criterion, the hydrodynamic force could not exceed 90% of the total submerged weight of the lifted object of 73 600 N, that is equal to 66 240 N. The corresponding  $H_{sLIM}$  was found linearly as illustrated in Figure 8.8 for wave condition I, where  $H_s$  was 3 m. According to this  $H_{sLIM}$  was found to be 1.56 m.

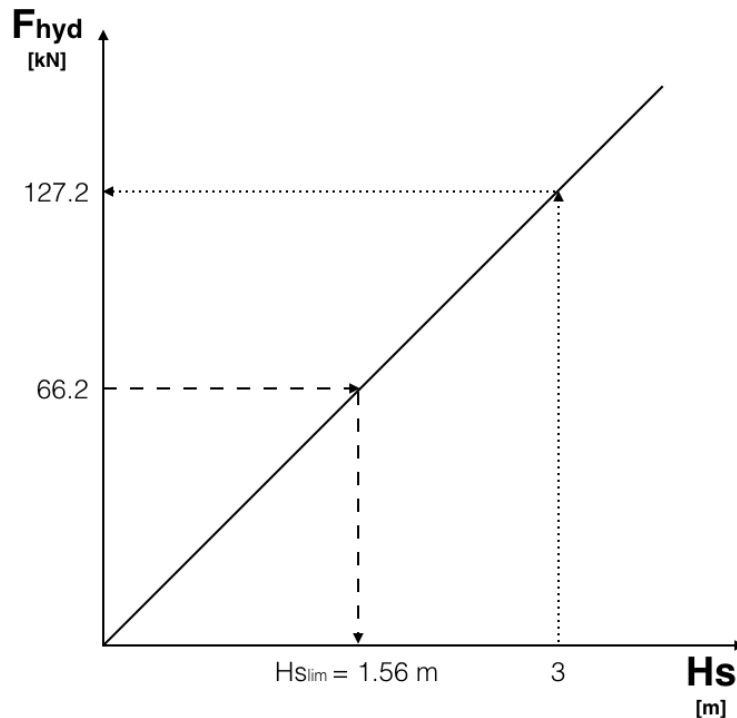


Figure 8.8: Linear scaling of hydrodynamic force, wave condition I

All the hydrodynamic forces that arose for the three wave conditions, when the cover was immediately fully submerged are listed in Table 8.10. The total hydrodynamic forces and the design criteria are listed in the same table. The average  $H_{sLIM}$  was found to be 1.643 m and determined to be constant for all peak periods.

Table 8.10: Total hydrodynamic force and manually estimated design criteria

	$F_D$	$F_S$	$F_I$	$F_B$	$F_{hyd}$	$H_{sLIM}$
<b>Cond I</b>	30 448 N	7 047	130 350 N	8 788 N	<b>127 213 N</b>	<b>1.562 m</b>
<b>Cond II</b>	54 075 N	12 516 N	113 936 N	12 196 N	<b>125 947 N</b>	<b>1.634 m</b>
<b>Cond III</b>	8 661 N	2 005 N	81 257 N	5 563 N	<b>76 442 N</b>	<b>1.733 m</b>





## 9 Simulation Results

The tension that arose in the lifting slings and wires during each simulation was investigated. This was done such that the maximum design criteria could be determined and to ensure that the system was adequately designed in terms of strength and slack requirements.

The hydrodynamic parameters achieved from CFD-analysis for an amplitude of 2.5 m were used as input to the numerical model in SIMA. Slamming and varying buoyancy were omitted. The simulation model contained the installation vessel, the lifting gear and the GRP protection cover. The simulation was performed for the *through splash zone* phase for *Hs-Tp* conditions as listed in Table 9.1.

Table 9.1: *Hs-Tp* conditions used in simulations

<b>Hs [m]</b>	<b>2.0</b>	<b>2.1</b>	<b>2.2</b>	<b>2.3</b>	<b>2.4</b>	<b>2.5</b>	<b>2.6</b>	<b>2.8</b>	<b>3.0</b>	<b>4.0</b>
<b>5</b>	✓	✓	✓	✓		✓				
<b>6</b>	✓	✓	✓	✓	✓	✓	✓	✓		
<b>7</b>	✓	✓	✓	✓	✓	✓	✓	✓	✓	
<b>8</b>	✓	✓	✓	✓	✓	✓	✓	✓	✓	✓
<b>9</b>	✓				✓	✓	✓	✓	✓	✓
<b>10</b>	✓					✓			✓	✓
<b>11</b>	✓								✓	✓
<b>12</b>	✓								✓	✓
<b>13</b>	✓								✓	✓
<b>14</b>	✓								✓	✓
<b>15</b>	✓								✓	✓

Between 20 and 60 lowering simulations were performed for each *Hs – Tp* condition, with random seed numbers. The simulation time step was set to 0.001 s due to low wire stiffness and small mass of lifting equipment and object.

The simulation started with the cover COG hanging approximately 7 m above sea surface. Thus the vertical distance from the sea surface to the lower end of the cover was 2.2 m. The winch speed was 0.2 m/s and started to run after 200 s, such that the system was able to stabilise. The GRP cover reached the sea surface after 209 s and was fully immersed at  $t = 276$  s. The winch stopped after 400 s when the cover COG was lowered to a depth of approximately 33 m. The simulation stopped after 500 s.

The spreader bar and the cover were exposed to large motions during the in-air phase. Figure 9.1 to 9.4 are snap shots from the simulation where the spreader bar's and cover's surge, pitch, sway and yaw motions are visualised.

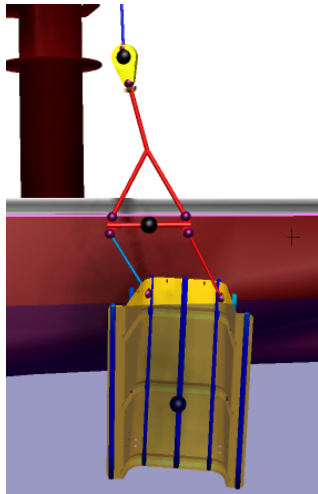


Figure 9.1: Surge motion

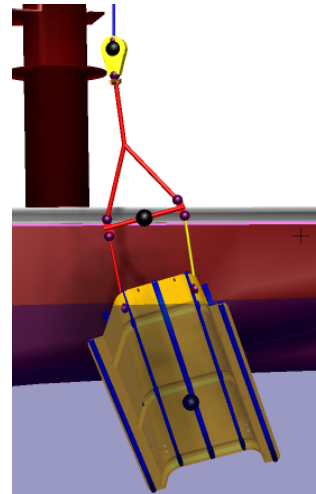


Figure 9.2: Pitch motion

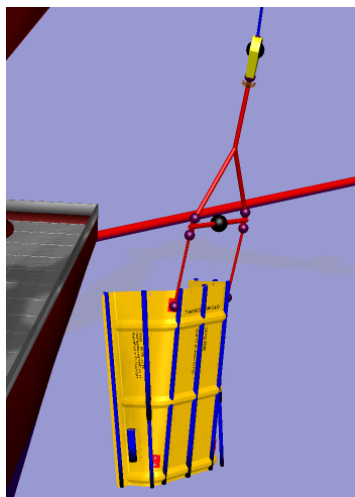


Figure 9.3: Sway motion

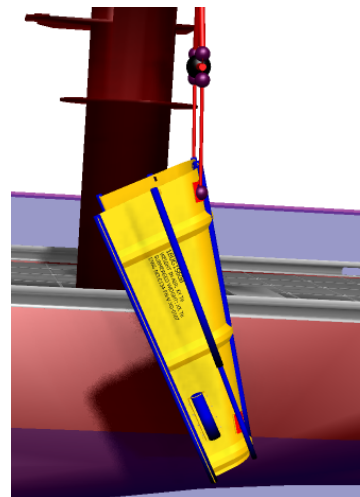


Figure 9.4: Yaw motion

Many simulations for small peak periods failed due to large acceleration in the spreader bar's intrinsic second degree of freedom (sway). The spreader bar was connected to four slings with 6 dofs each, and was hence exposed to large motions. Figure 9.5 shows the defined motions of the spreader bar.

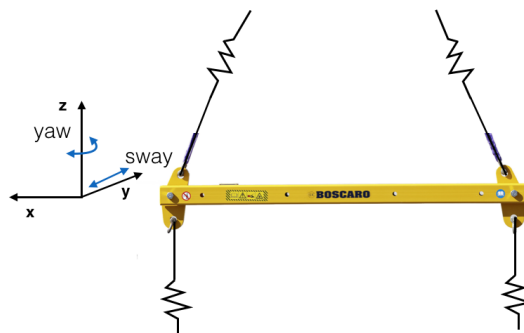


Figure 9.5: Sway and yaw motion of spreader bar

In order to decrease the number of failures in the simulation, the intrinsic sway motion of the spreader bar, that corresponds to the global sixth degree of freedom (yaw), was damped. It was assumed that the eigenperiod of the spreader bar  $T$  was 5 s. The spreader bar stiffness was found by rearranging equation (4.12) to the following

$$K = \frac{4\pi^2}{T^2} \cdot I_{zz}$$

The spreader bar's mass moment of inertia in z-direction  $I_{zz}$  was 4 000  $kgm^2$ . The critical damping coefficient was defined as  $c_{cr} = 2\sqrt{K \cdot I_{zz}}$  and calculated to be approximately 10 kNm. 10% of  $c_{cr}$  (1 000 Nm) was added to the spreader bar in rz-direction. The rate of failed simulations did not decay.

The spreader bar did also rotate a lot during the in-air phase. In order to reduce this rotation, stiffness was added to the spreader bar in rz-direction. The stiffness was calculated as above, and found to be approximately 6 300 Nm.

The minimum slack criterion is 10% of the static submerged tension in the slings. The static submerged tension in the slings were found by running simulations with no environmental loads as waves, wind or current. The static tension in sling 1 and 2 is visualised in Figure 9.6 and was read off to be approximately 36 800 N. The static tension in sling 3 and 4 is visualised in Figure 9.7 and was read off to be approximately 53 800 N. Hence the minimum slack criterion was 3 680 N for sling 1 and 2 and 5 380 N for sling 3 and 4.

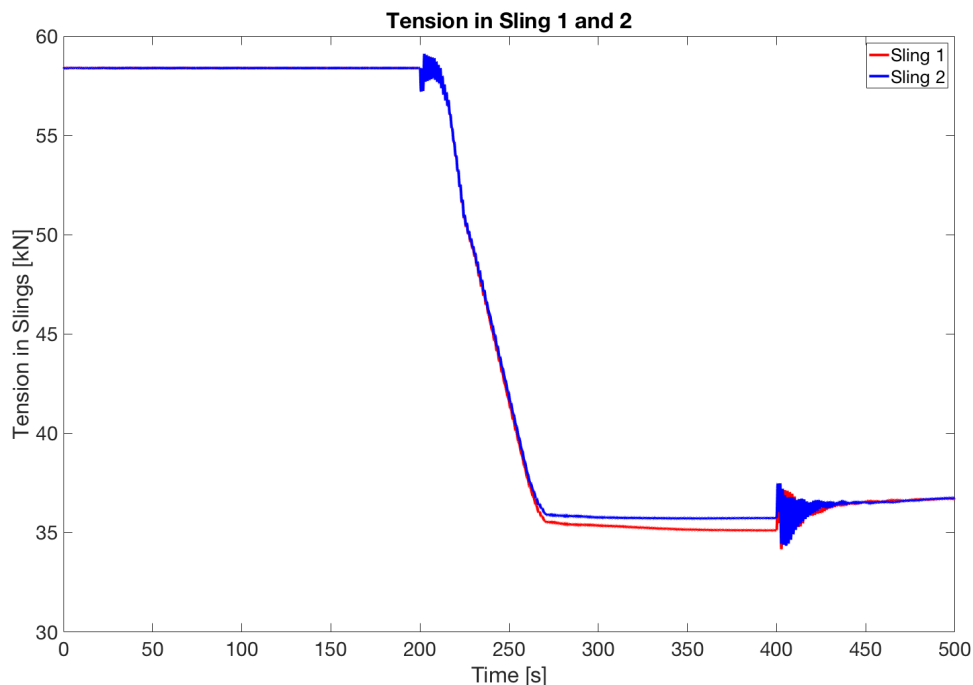


Figure 9.6: Tension in sling 1 and 2 with no environmental loads

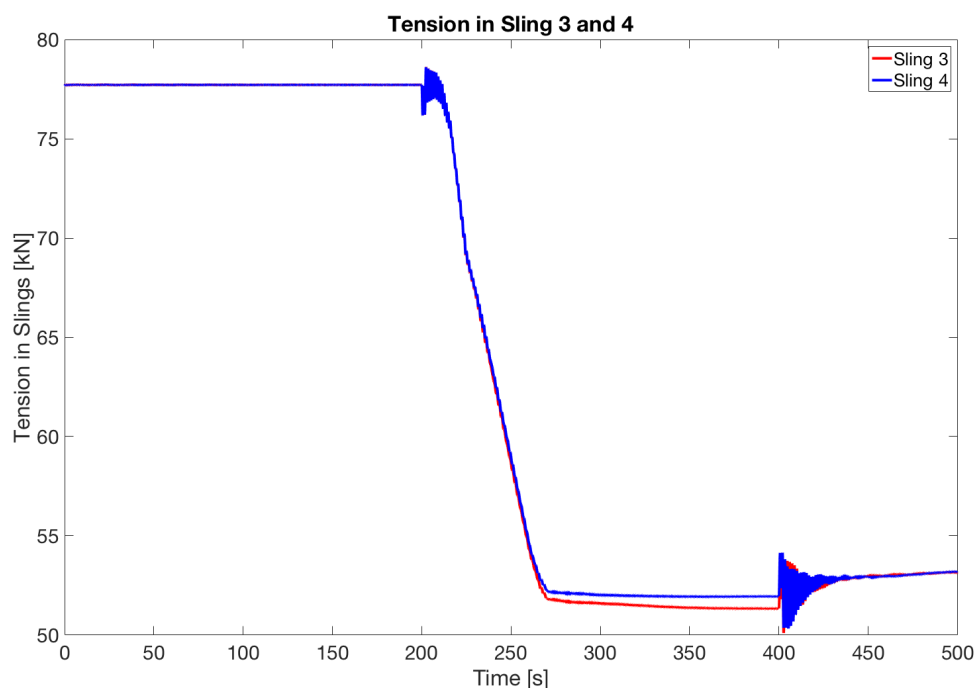


Figure 9.7: Tension in sling 3 and 4 with no environmental loads

Simulations were run for all the wave conditions listed in Table 9.1, where 20-30 simulations did not fail. The results from all the wave conditions were processed, but are described and visualised for only three selected wave conditions.

## 9.1 Wave Conditions

The three wave conditions that were further looked into in this thesis were categorised as; below slack criterion, above slack criterion and above slack criterion even when slack occurred, and are listed in Table 9.2.

Table 9.2: Wave conditions below or above the slack criterion

	Hs	Tp	Seed Number	Below/Above Slack Criterion
<b>Condition I</b>	3 m	8 s	19	<b>Sling 1 Below</b>
<b>Condition II</b>	3 m	12 s	22	<b>Both Slings Above</b>
<b>Condition III</b>	2 m	6 s	15	<b>Both Slings Above (Slack Occurs)</b>

For each seed number the minimum tension that occurred in the slings were stored and used to develop extreme value distributions. The 10% quantile was calculated and compared towards the minimum slack criterion of 3 680 N in sling 1 and 2 and 5 380 N in sling 3 and 4. Figure 9.8, 9.9 and 9.10 show the 10% quantile found for peak periods between 5 s and 15 s, for  $H_s$  of 2, 3 and 4 m.

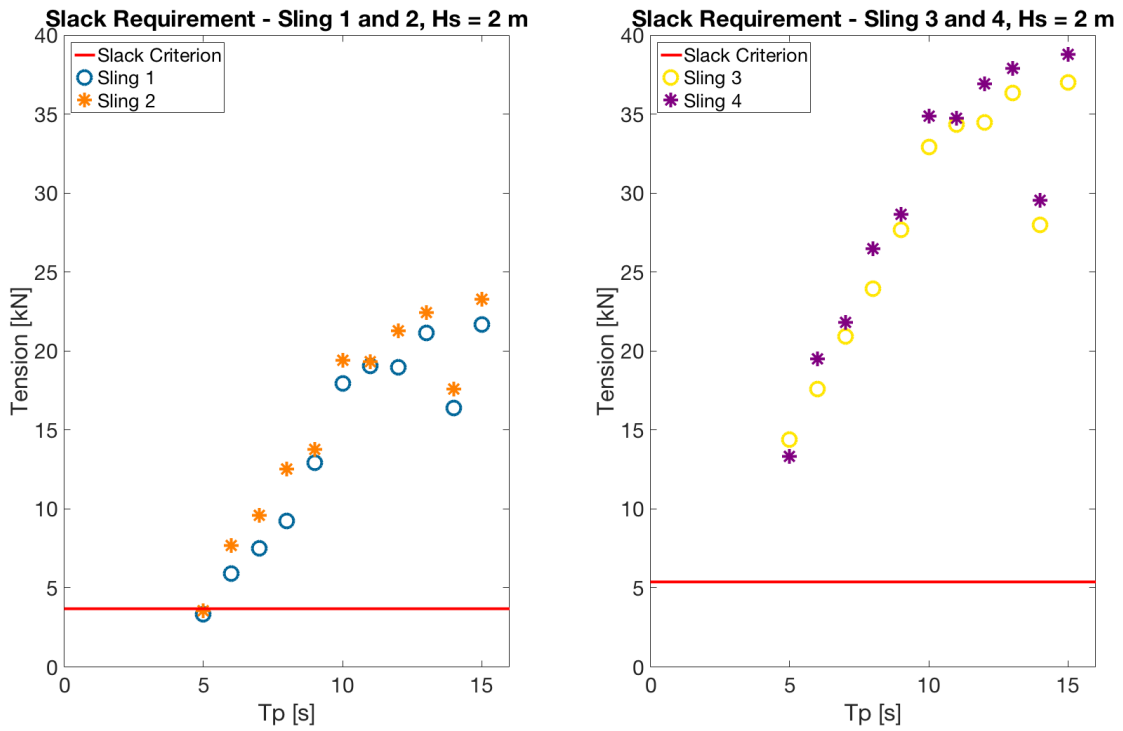


Figure 9.8: 10% quantiles for various  $T_p$  compared to slack requirement,  $H_s = 2$  m

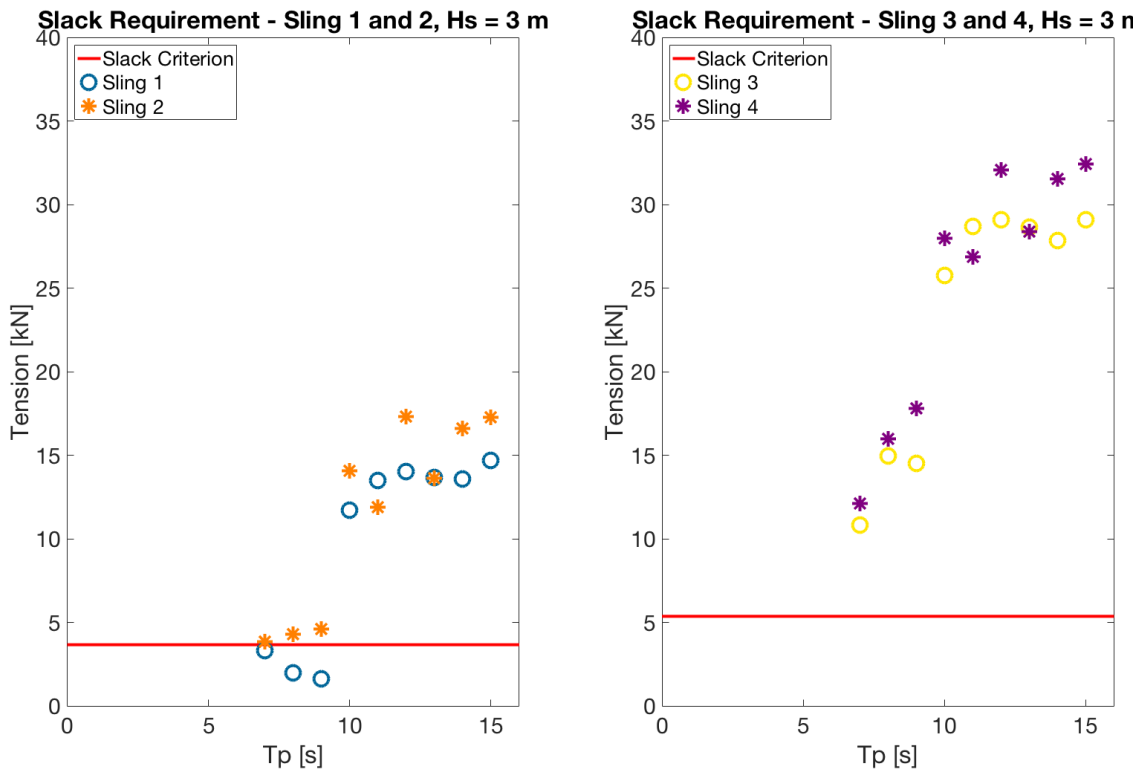


Figure 9.9: 10% quantiles for various  $T_p$  compared to slack requirement,  $H_s = 3$  m

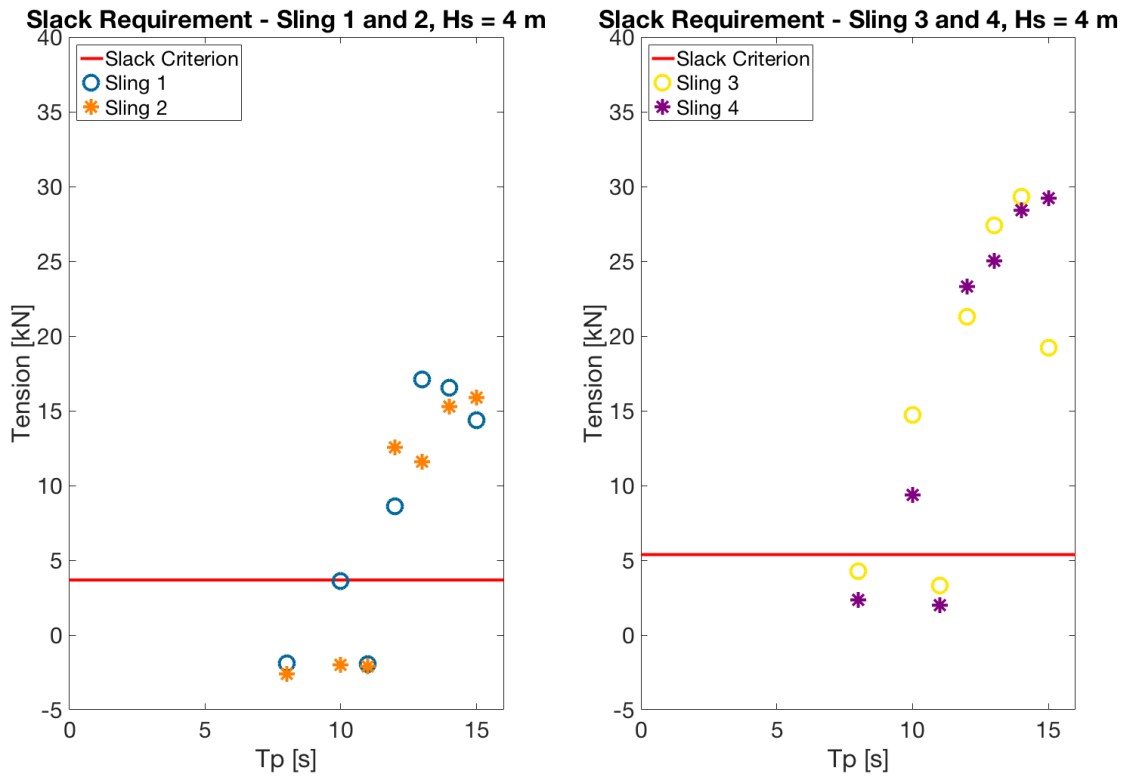


Figure 9.10: 10% quantiles for various  $T_p$  compared to slack requirement,  $H_s = 4$  m

The wave elevation for the three wave conditions are plotted in Figure 9.11. The following subsections will describe the spreader bar's and cover's translation and rotation for the different wave series, and illustrate the tension that arose in the slings and wires.

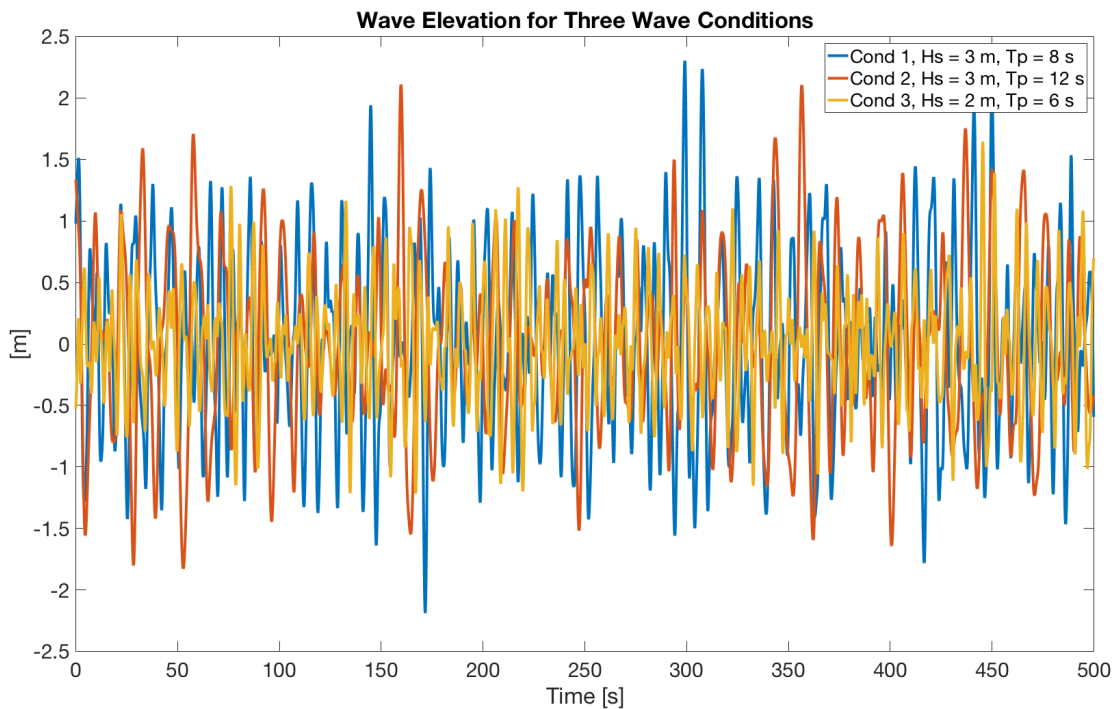


Figure 9.11: Wave elevation for the three wave conditions

### 9.1.1 Motions

Figure 9.12, 9.13 and 9.14 show the translation in x-, y- and z-direction for the spreader bar and the cover with wave condition *I*, *II* and *III* respectively.

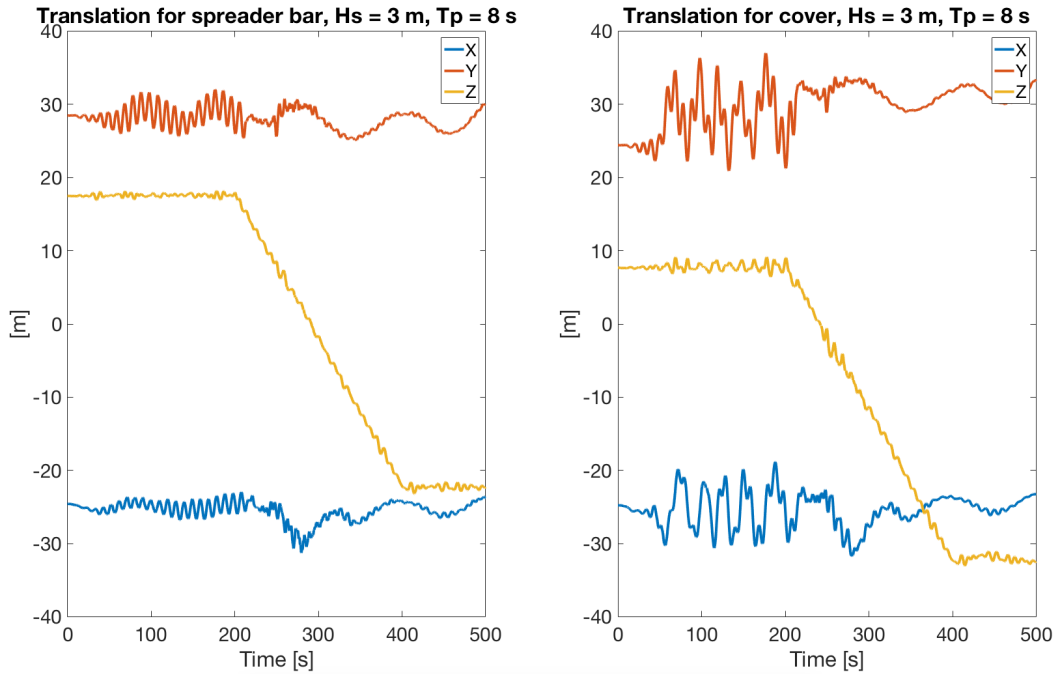


Figure 9.12: Translation of spreader bar and cover,  $H_s = 3$  m,  $T_p = 8$  s

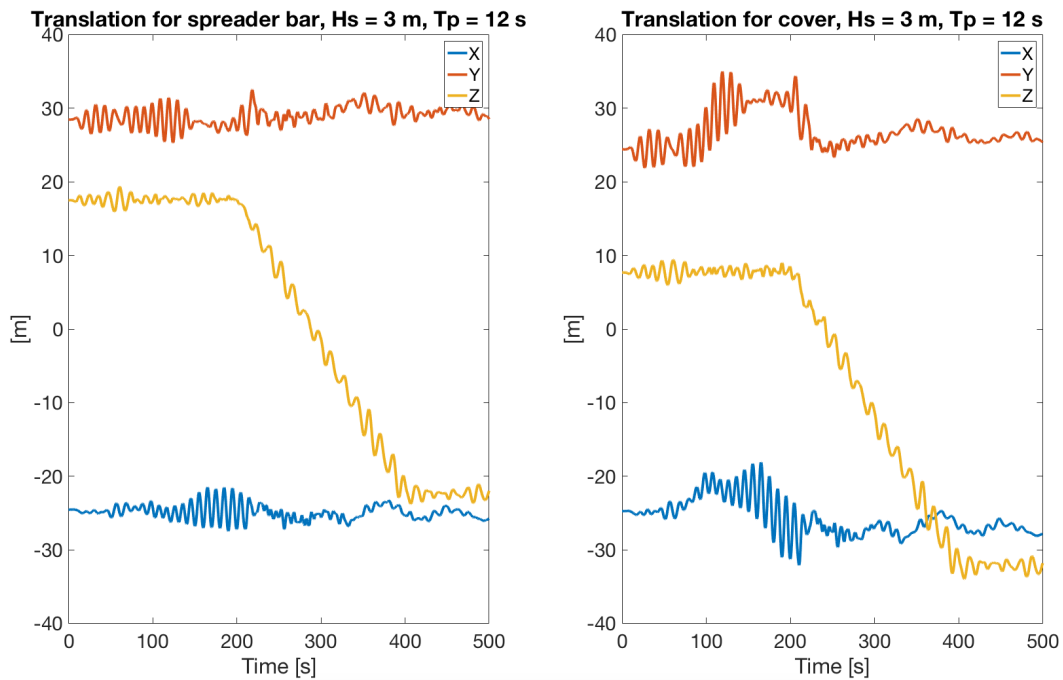


Figure 9.13: Translation of spreader bar and cover,  $H_s = 3$  m,  $T_p = 12$  s

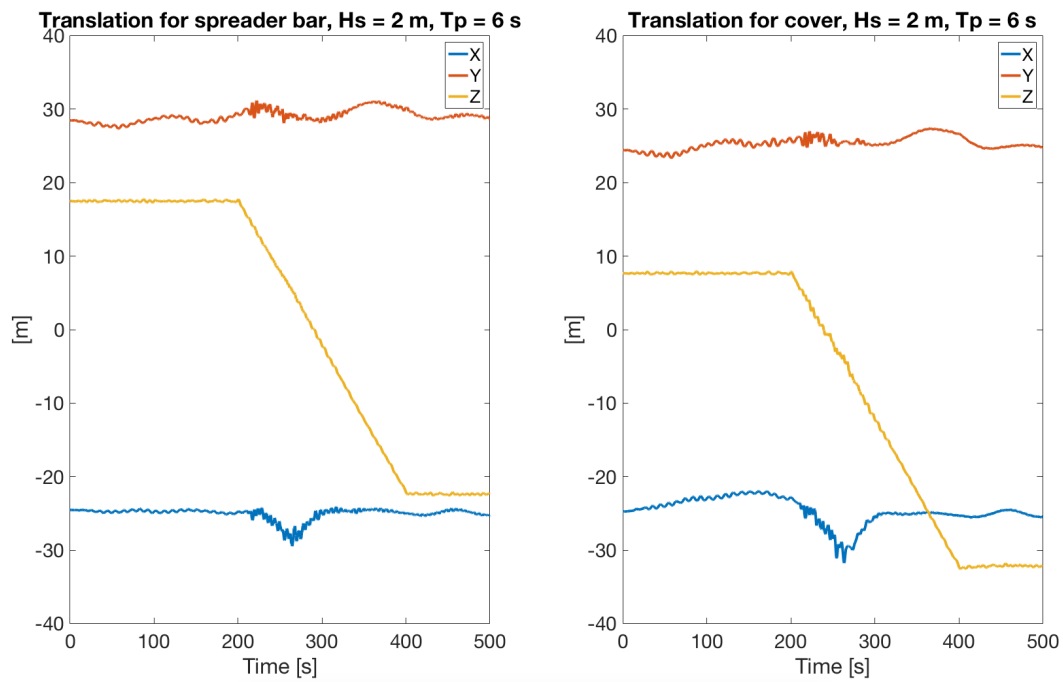


Figure 9.14: Translation of spreader bar and cover, Hs = 2 m, Tp = 6 s

The location of the cover's COG with time is illustrated in Figure 9.15, 9.16 and 9.17 for the three wave conditions respectively. The plots show when the cover COG hits the sea surface. The splash zone is assumed to be  $\pm 2$  m.

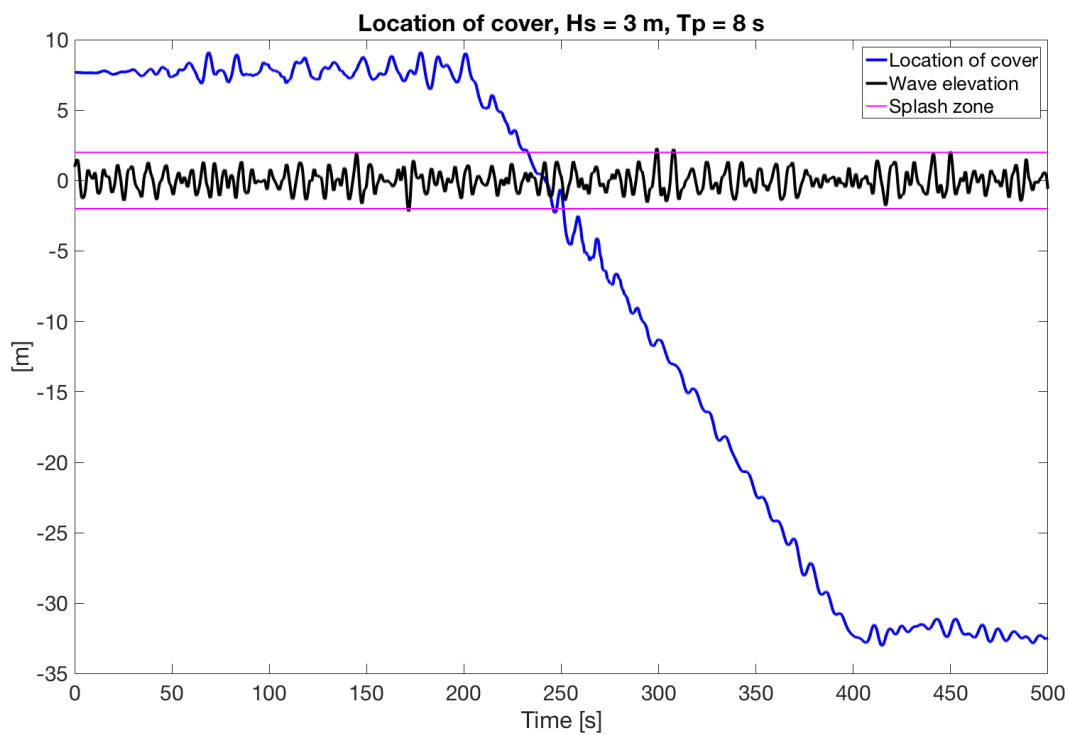


Figure 9.15: Location of cover, Hs = 3 m, Tp = 8 s



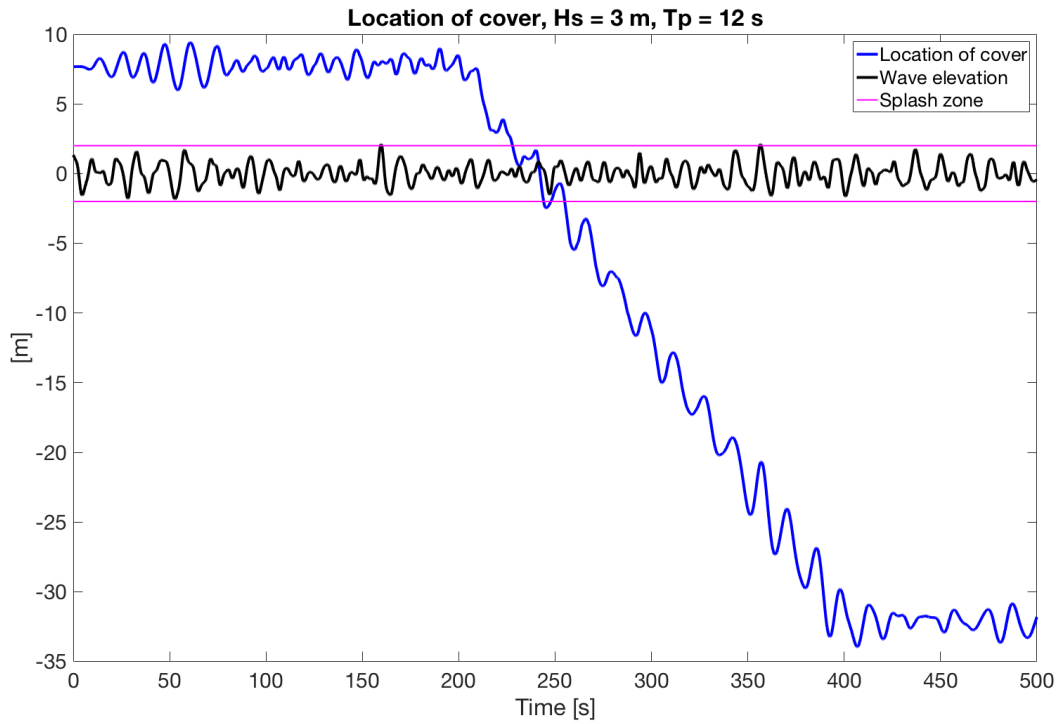


Figure 9.16: Location of cover,  $H_s = 3$  m,  $T_p = 12$  s

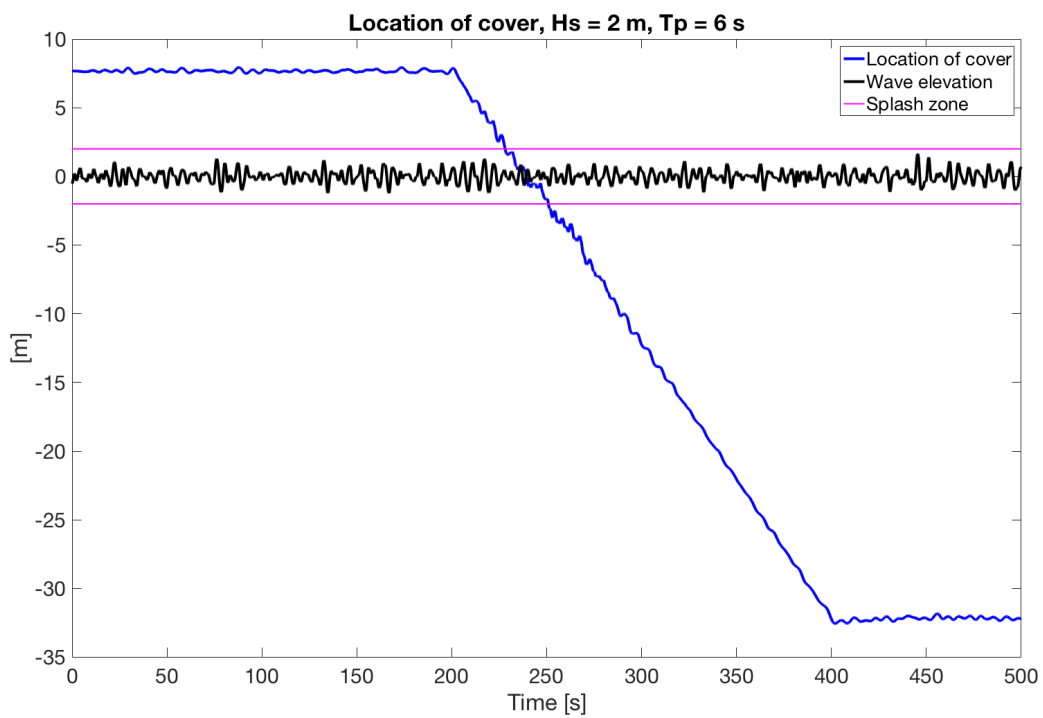


Figure 9.17: Location of cover,  $H_s = 2$  m,  $T_p = 6$  s

Figure 9.18, 9.19 and 9.20 show the rotation about the x-, y- and z-axis for the spreader bar and cover for the three wave conditions respectively.

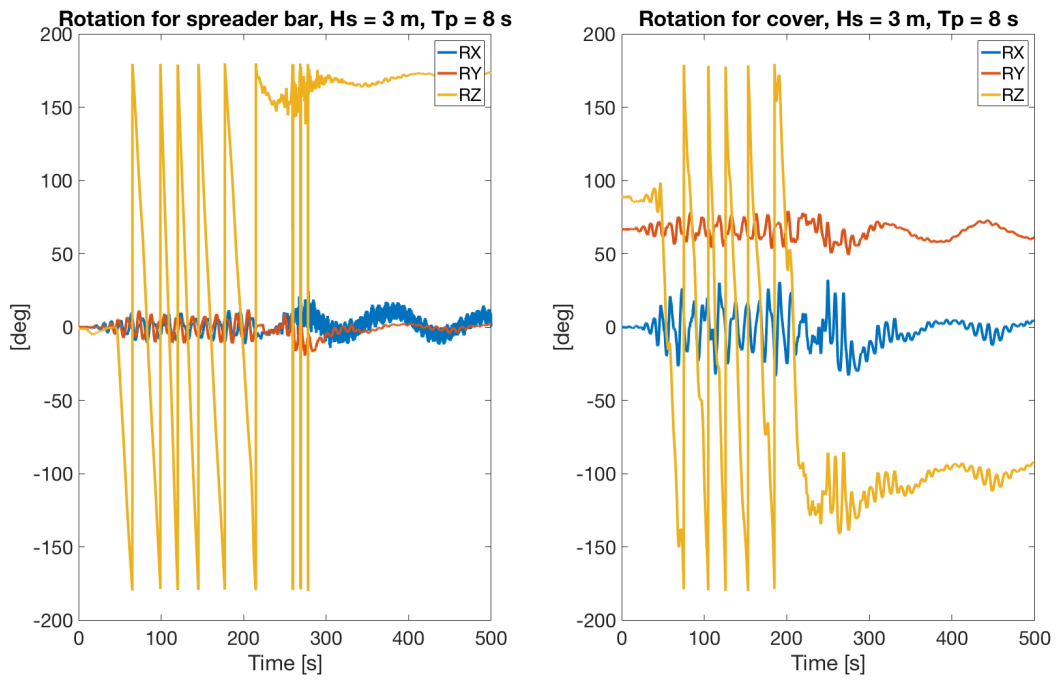


Figure 9.18: Rotation of spreader bar and cover, Hs = 3 m, Tp = 8 s

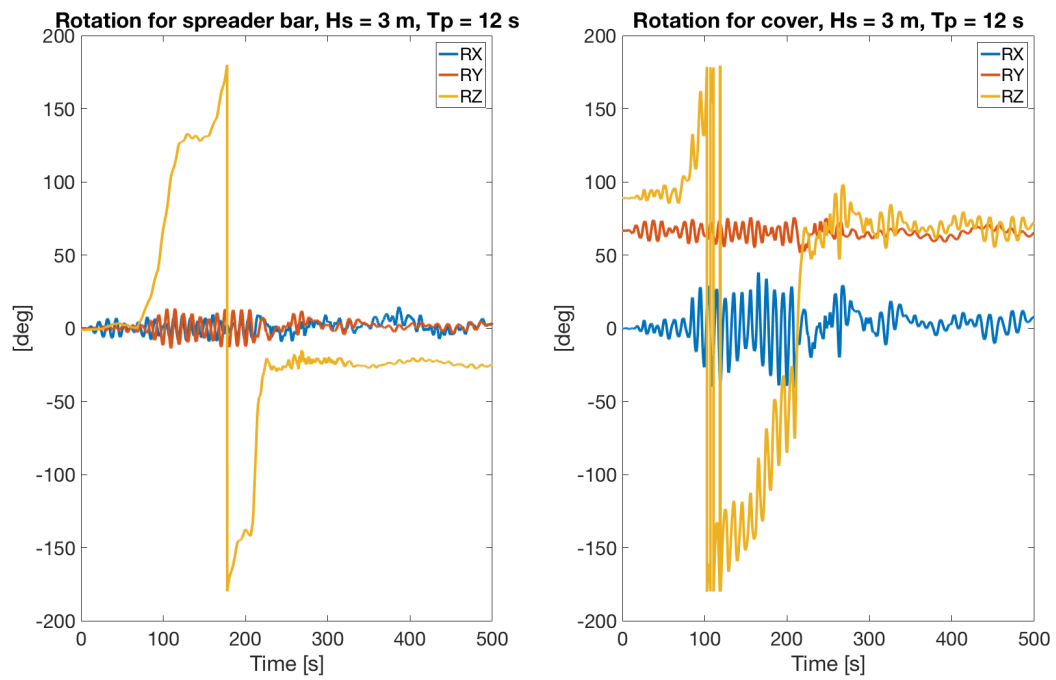


Figure 9.19: Rotation of spreader bar and cover, Hs = 3 m, Tp = 12 s

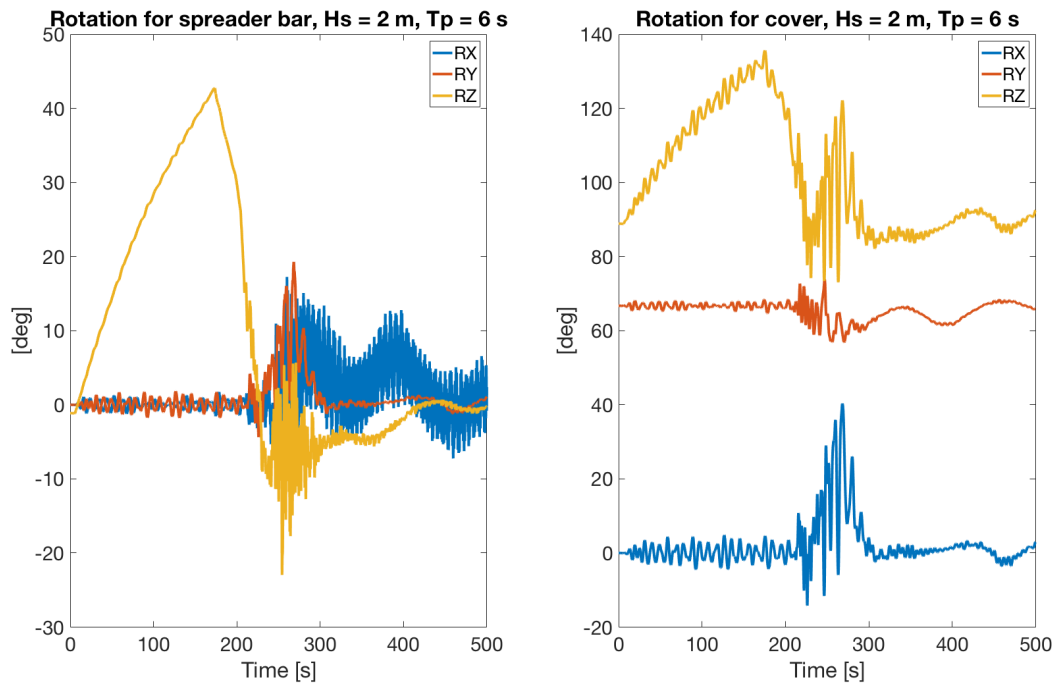


Figure 9.20: Rotation of spreader bar and cover,  $H_s = 2$  m,  $T_p = 6$  s

Stiffness was added to the spreader bar in rz-direction with a magnitude of 6 300 Nm. The rotation of the spreader bar and cover reduced significantly and are visualised in Figure 9.21, 9.22 and 9.23 for the three wave conditions *I*, *II* and *III* respectively.

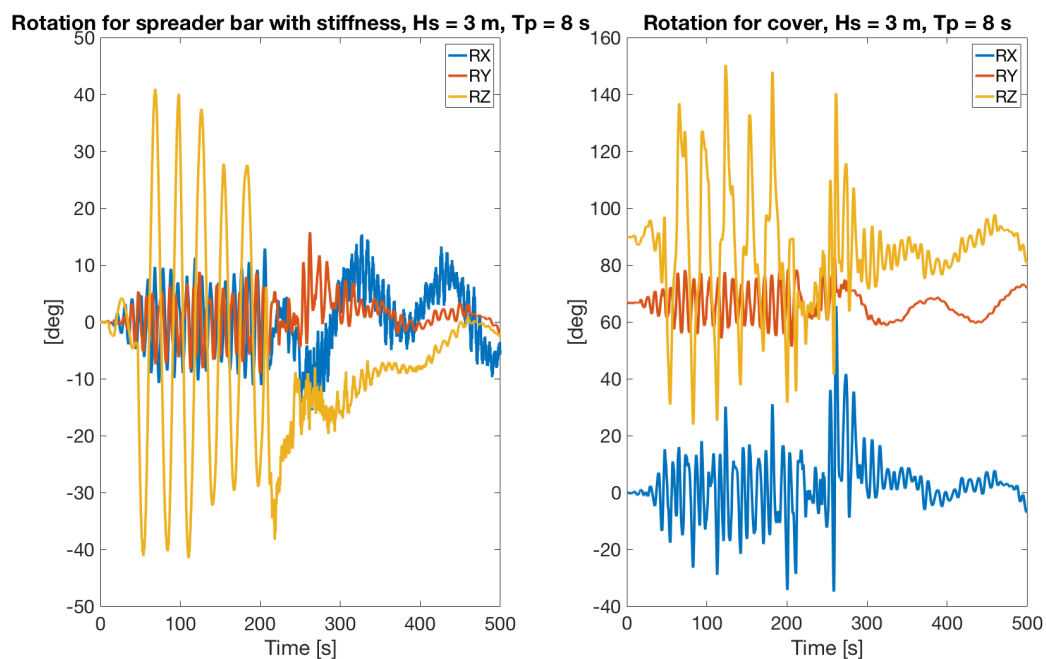


Figure 9.21: Rotation of spreader bar and cover with added stiffness,  $H_s = 3$  m,  $T_p = 8$  s

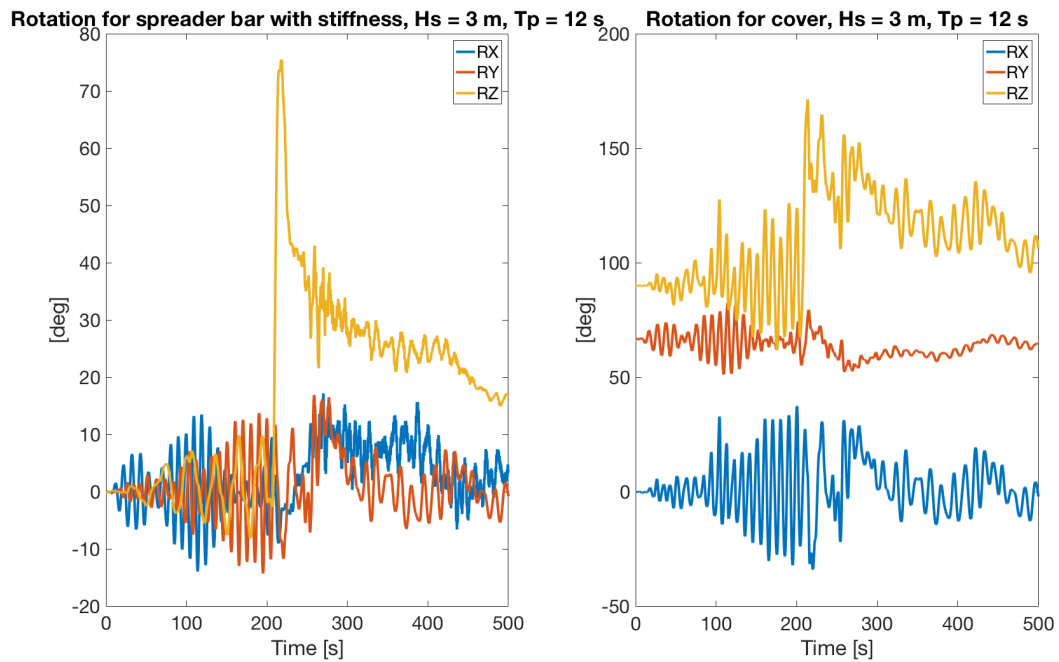


Figure 9.22: Rotation of spreader bar and cover with added stiffness,  $H_s = 3\text{ m}$ ,  $T_p = 12\text{ s}$

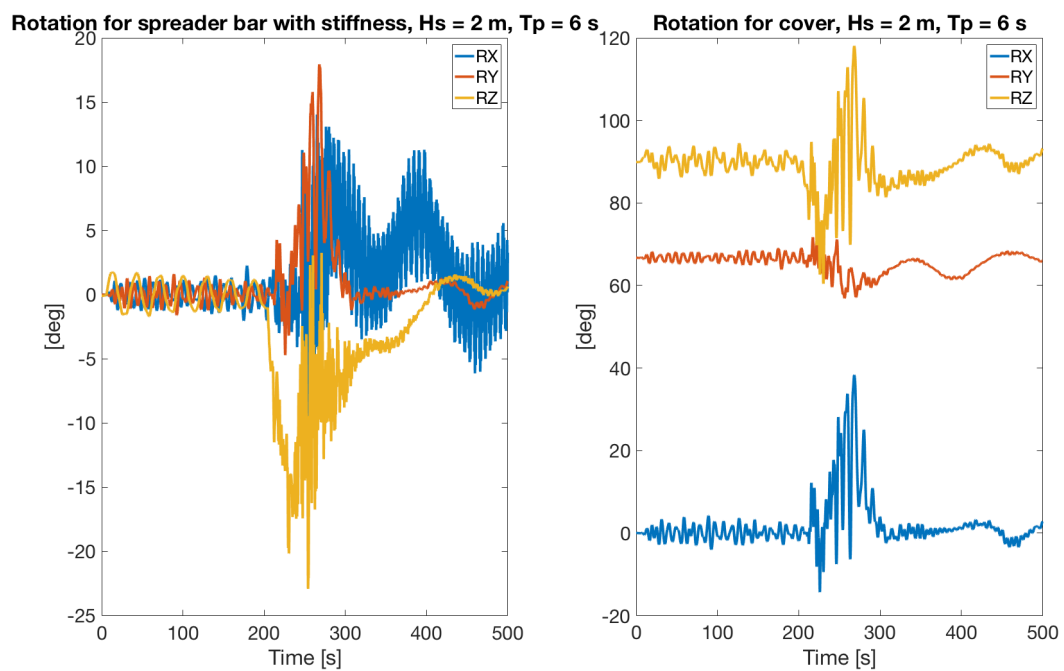


Figure 9.23: Rotation of spreader bar and cover with added stiffness,  $H_s = 2\text{ m}$ ,  $T_p = 6\text{ s}$

### 9.1.2 Tension in Slings and Wires

Figure 9.24, 9.25 and 9.26 visualise the tension that arose in the crane wire and the forces that acted on the hook during the three wave conditions *I*, *II* and *III* respectively.

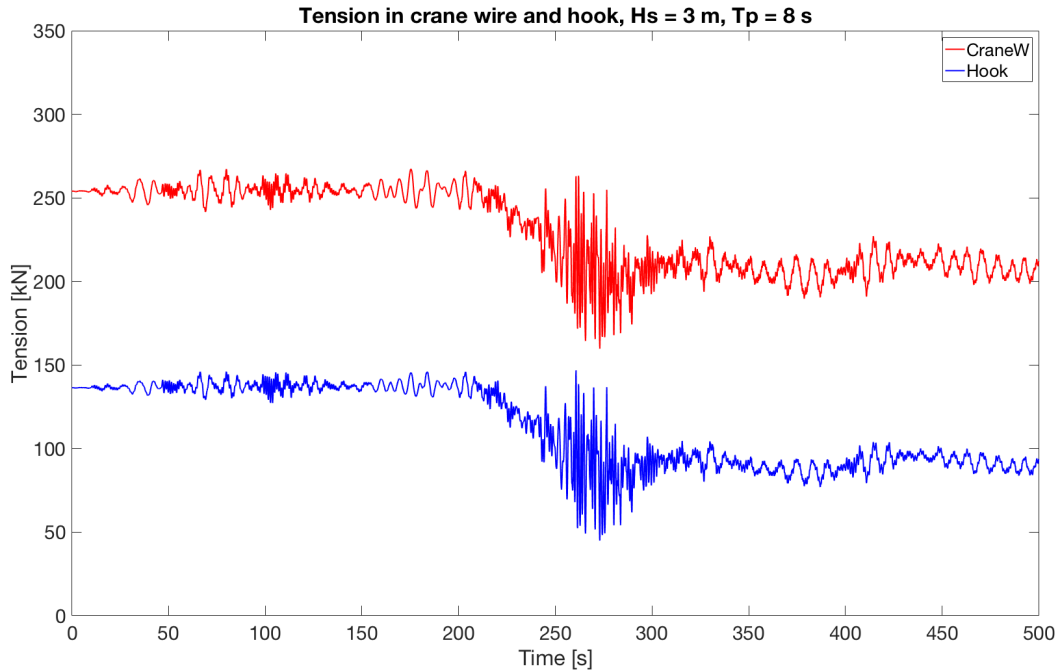


Figure 9.24: Tension in crane wire and force acting on hook, Hs = 3 m, Tp = 8 s

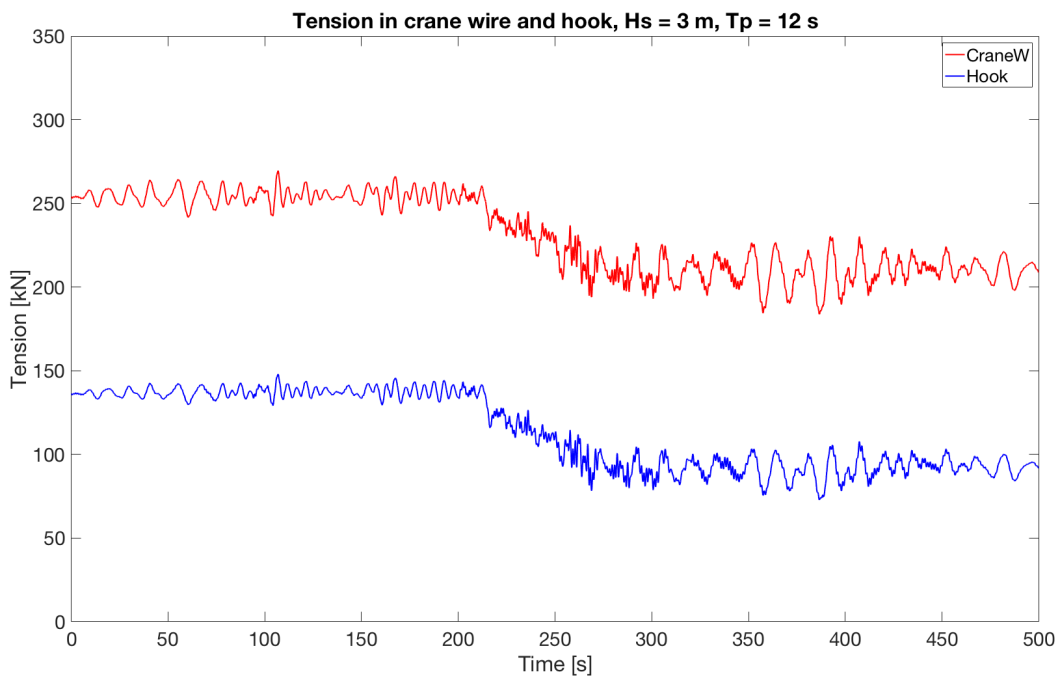


Figure 9.25: Tension in crane wire and force acting on hook, Hs = 3 m, Tp = 12 s

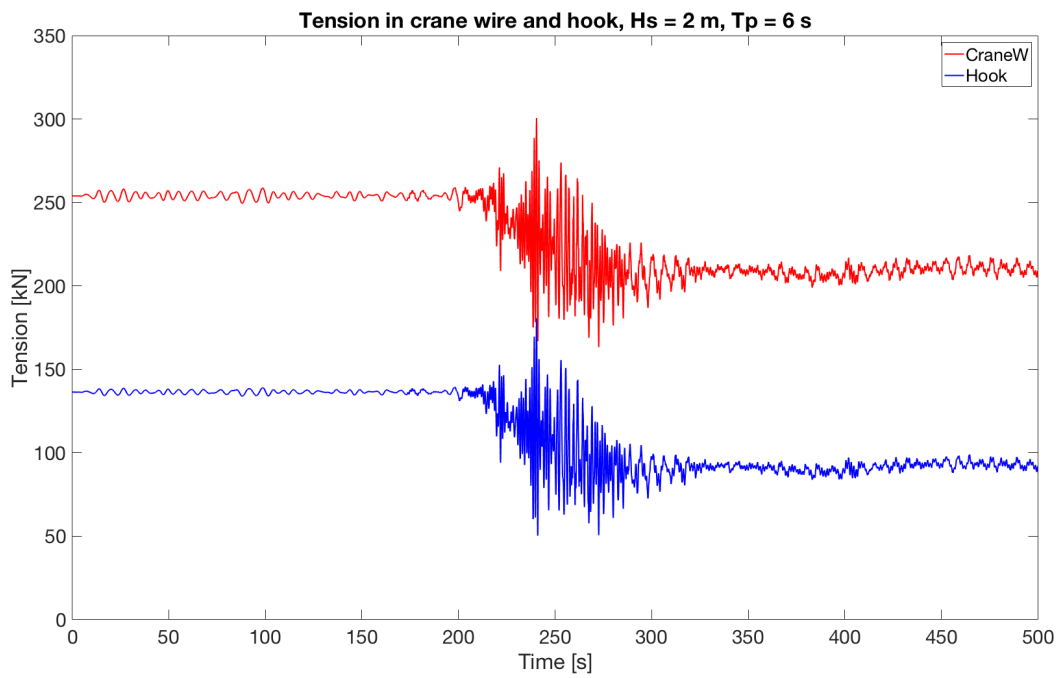


Figure 9.26: Tension in crane wire and force acting on hook,  $H_s = 2\text{ m}$ ,  $T_p = 6\text{ s}$

Figure 9.27, 9.28 and 9.29 visualise the tension that arose in the slings for the three wave conditions respectively.

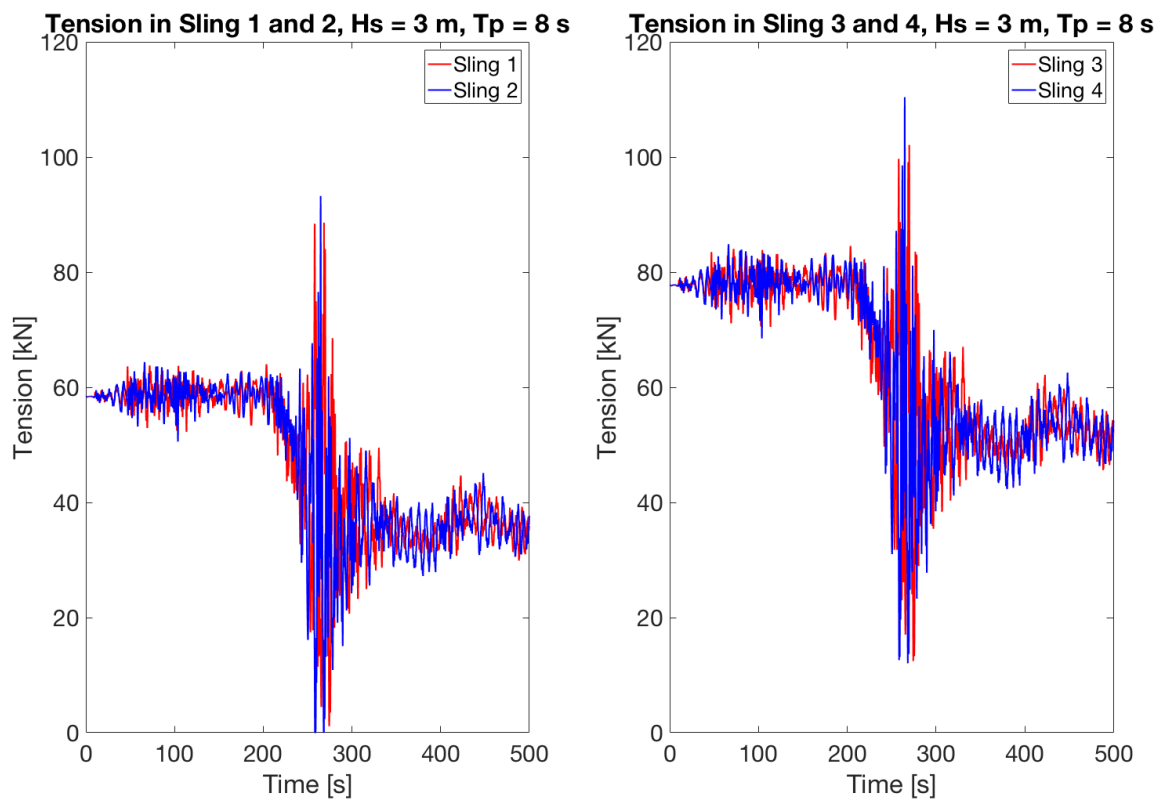


Figure 9.27: Tension arising in slings,  $H_s = 3\text{ m}$ ,  $T_p = 8\text{ s}$

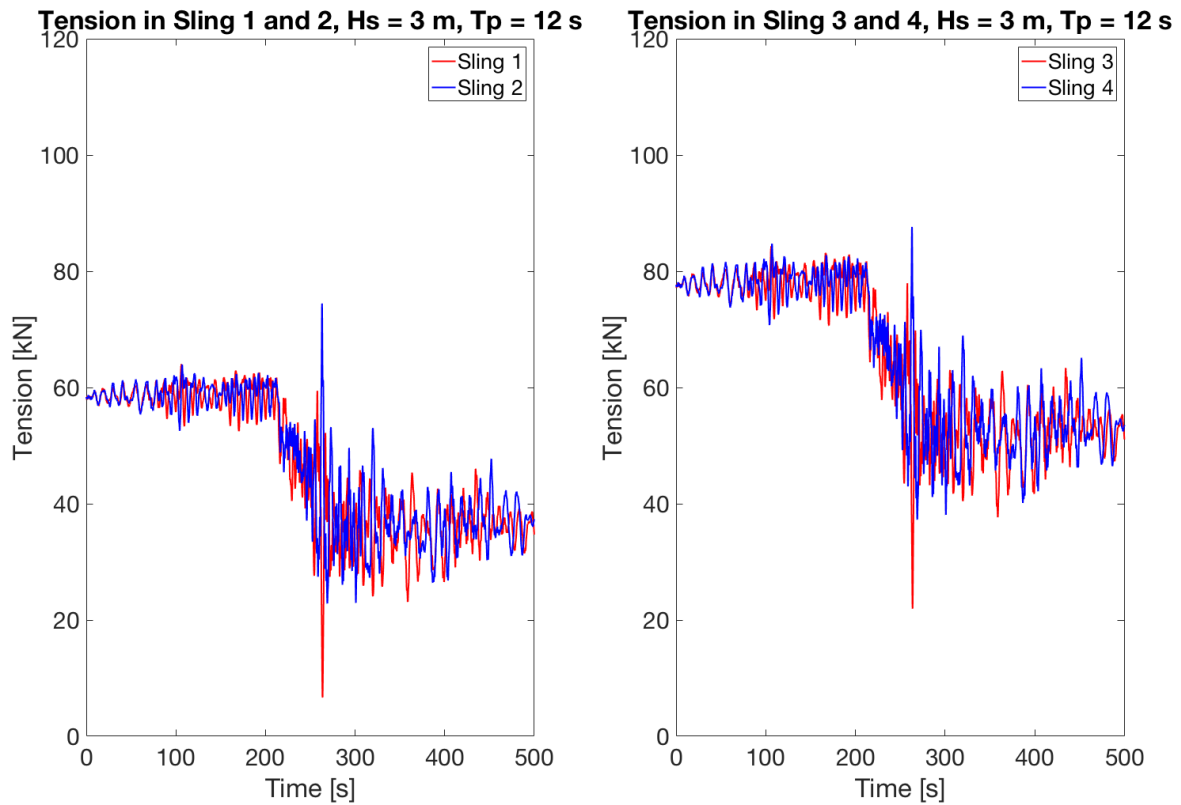


Figure 9.28: Tension arising in slings,  $H_s = 3$  m,  $T_p = 12$  s

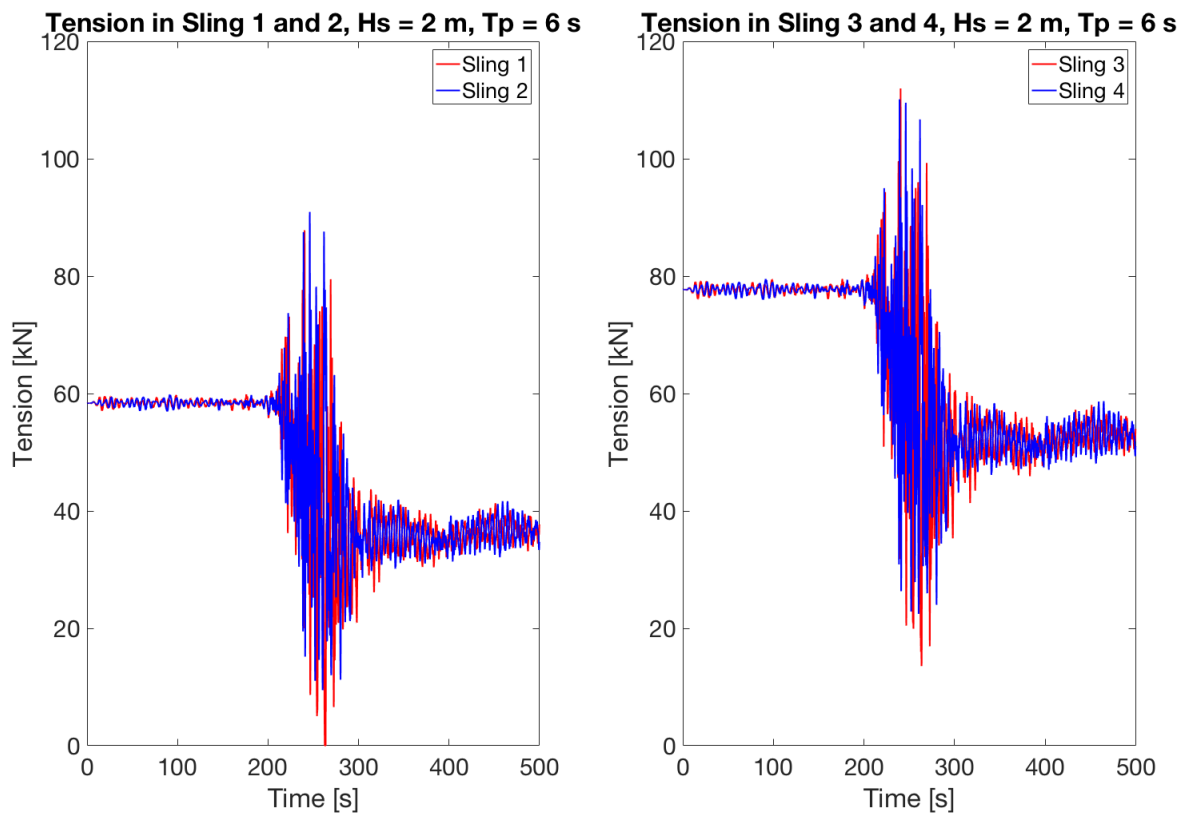


Figure 9.29: Tension arising in slings,  $H_s = 2$  m,  $T_p = 6$  s

The minimum and maximum tension that arose in the slings for the three wave conditions are listed in Table 9.3.

Table 9.3: Minimum and maximum tension in slings

		Sling 1	Sling 2	Sling 3	Sling4
<b>Comb I</b>	<b>Min</b>	1 140 N	0 N	12 439 N	12 058 N
	<b>Max</b>	88 607 N	93 239 N	102 094 N	110 398 N
<b>Comb II</b>	<b>Min</b>	6 665 N	22 845 N	21 943 N	37 274 N
	<b>Max</b>	64 039 N	74 455 N	84 338 N	87 637 N
<b>Comb III</b>	<b>Min</b>	0 N	9 466 N	13 578 N	22 473 N
	<b>Max</b>	87 830 N	90 934 N	111 979 N	110 122 N

## 9.2 Gumbel Distributions

The Gumbel distribution is based on two Gumbel parameters;  $\mu$  and  $\beta$ . These parameters are determined by the data set's mean and standard deviation and will thus change with increased sample size. The 10% quantile is also dependent for the two Gumbel parameters, hence the 10% quantile differed with increased sample size. *Convergence tests* were performed on the two Gumbel parameters and the 10% quantile in order to determine how many simulations with random seed numbers that were necessary to run before adequate results could be achieved. Convergence was assumed when the remaining samples deviated with less than 7%. The 10% quantile converged towards a different amount of seed numbers for the three wave conditions, and the results are listed in Table 9.4.

Table 9.4: Amount of seed numbers needed for 7% convergence

Condition	Converged Amount
Cond I	26
Cond II	12
Cond III	20

The convergence tests were calculated by use of the MATLAB code *Gumbel Plots*, found in Appendix C.1. The 10% quantiles were plotted towards the slack criterion for sling 1 and 2 and are shown in Figure 9.30, 9.31 and 9.32 for the three wave conditions *I*, *II* and *III* respectively.



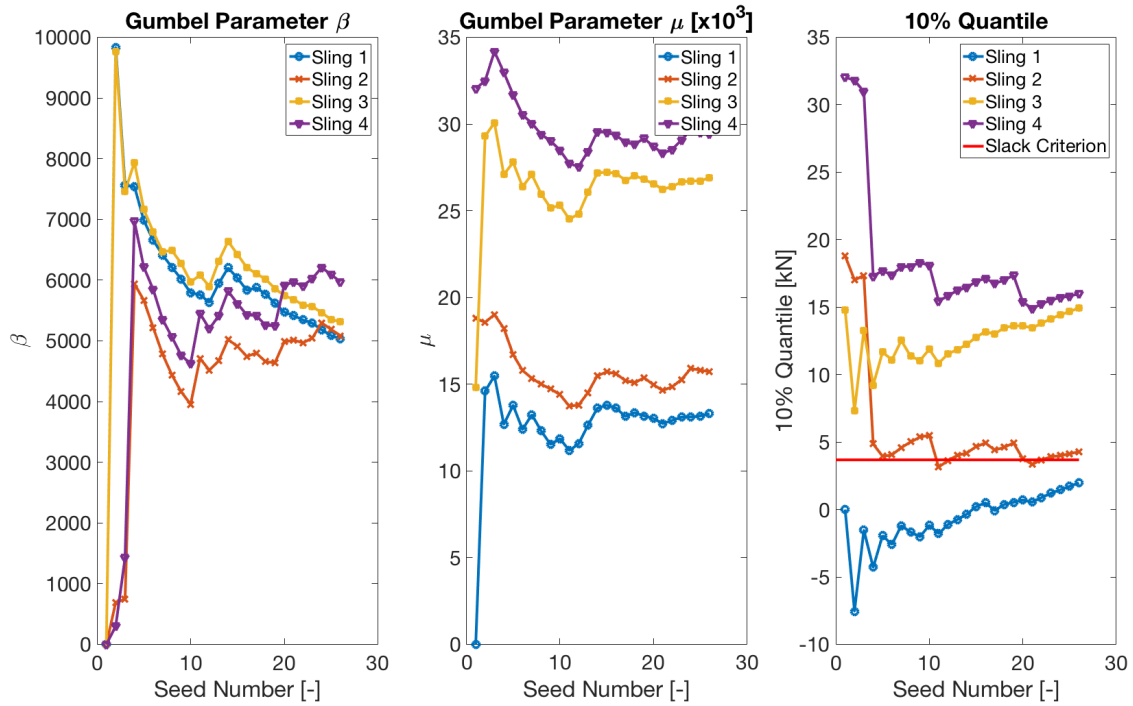


Figure 9.30: Convergence test of Gumbel parameters and 10% quantile,  $H_s = 3\text{ m}$ ,  $T_p = 8\text{ s}$

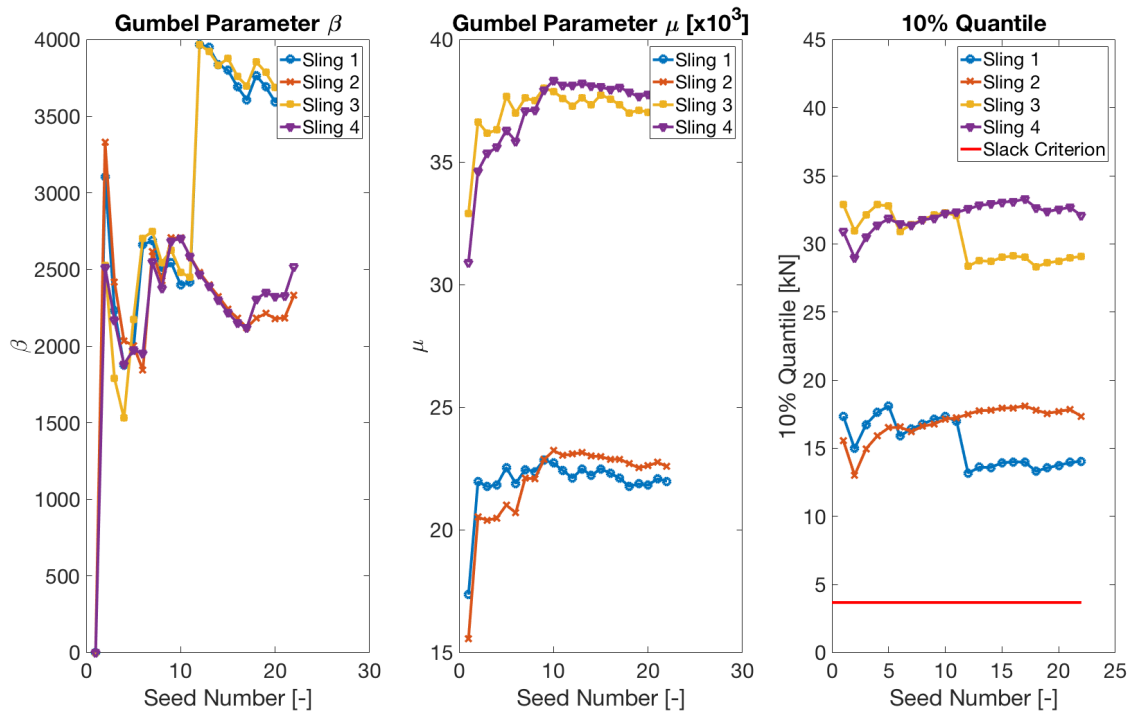


Figure 9.31: Convergence test of Gumbel parameters and 10% quantile,  $H_s = 3\text{ m}$ ,  $T_p = 12\text{ s}$

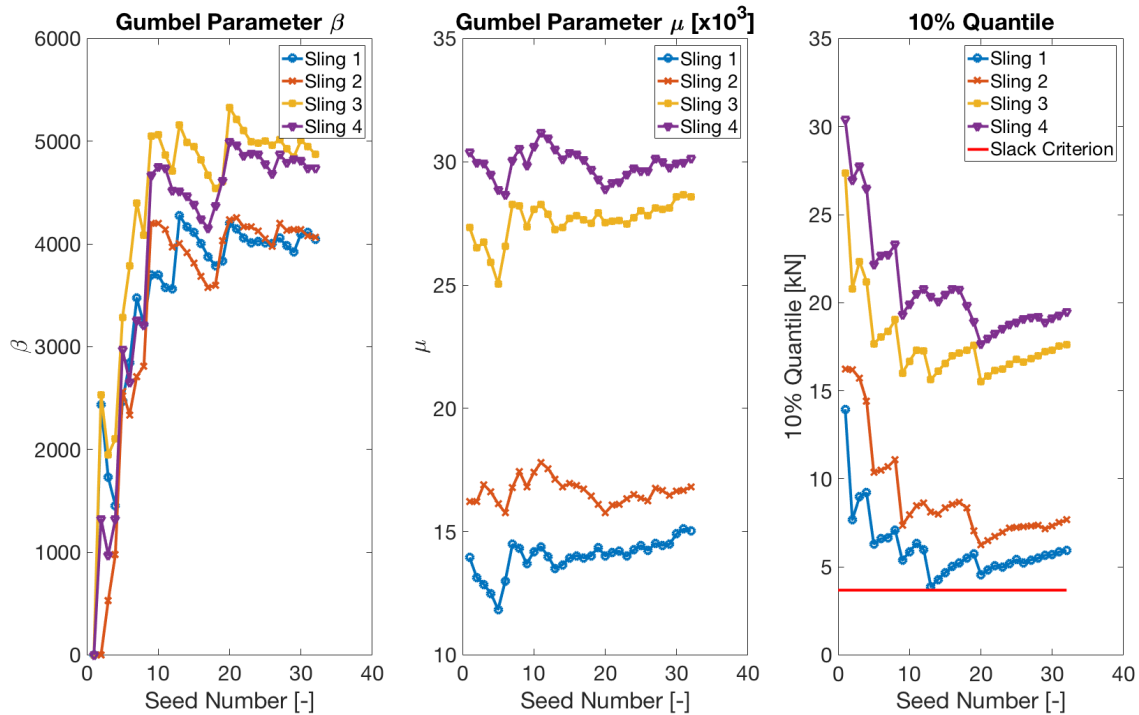


Figure 9.32: Convergence test of Gumbel parameters and 10% quantile,  $H_s = 2 \text{ m}$ ,  $T_p = 6 \text{ s}$

The converged Gumbel parameters were used to create the Gumbel PDF and CDF for the three wave conditions, and were calculated by use of the same aforementioned MATLAB code. The converged parameters that arose in each sling are listed in Table 9.5.

Table 9.5: 7% convergence for 10% quantile

Condition	Parameter	Sling 1	Sling 2	Sling 3	Sling 4
Cond I	$\mu$	13 305	15 732	26 913	29 437
	$\beta$	5 032	5 084	5 317	5 970
Cond II	$\mu$	21 986	22 590	37 227	37 742
	$\beta$	3 530	2 333	3 612	2 517
Cond III	$\mu$	15 036	16 822	28 572	30 142
	$\beta$	4 047	4 065	4 873	4 735

The Gumbel PDF's are shown in Figure 9.33, 9.34 and 9.35 for wave condition I, II and III respectively.

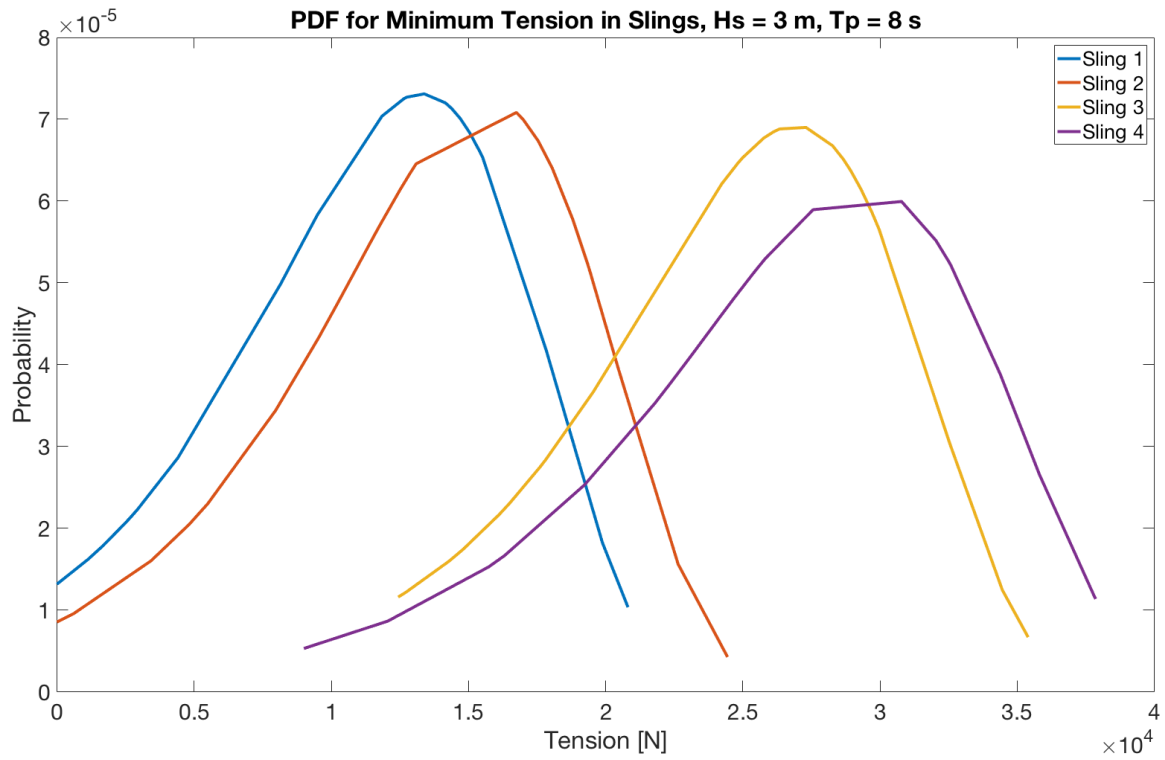


Figure 9.33: Gumbel PDF,  $H_s = 3$  m,  $T_p = 8$  s

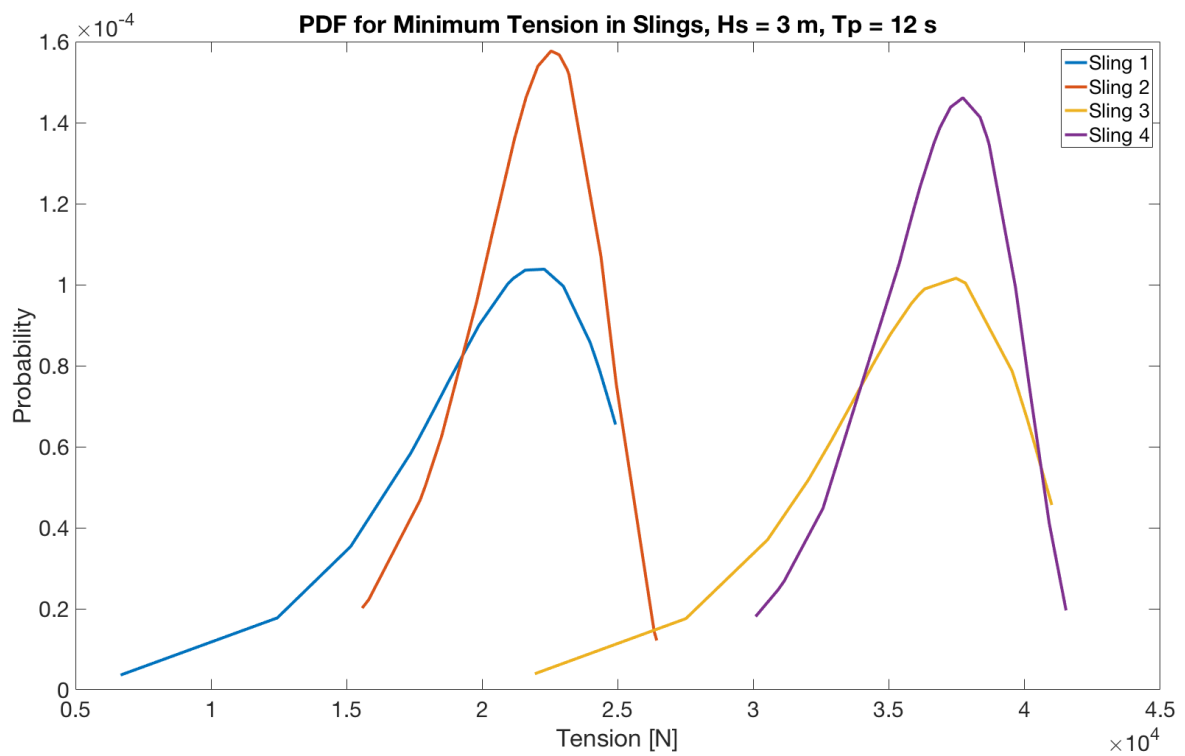


Figure 9.34: Gumbel PDF,  $H_s = 3$  m,  $T_p = 12$  s

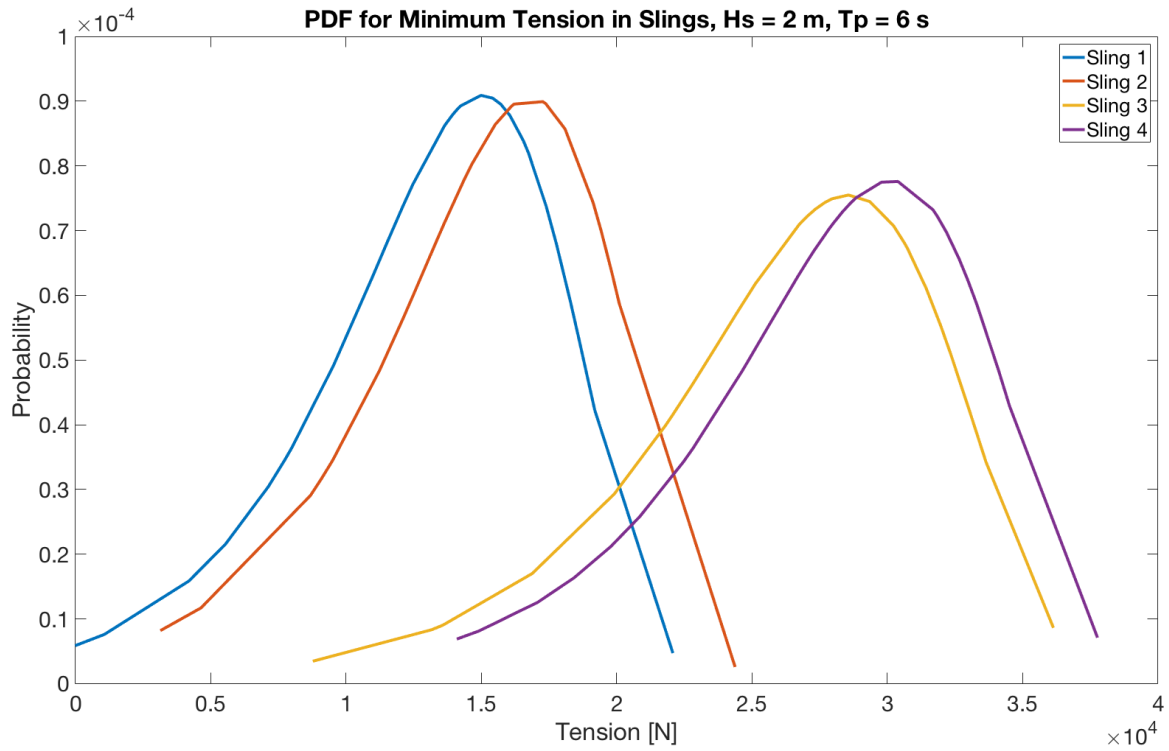


Figure 9.35: Gumbel PDF,  $H_s = 2\text{ m}$ ,  $T_p = 6\text{ s}$

The Gumbel CDF's are shown in Figure 9.36, 9.37 and 9.38 for wave condition I, II and III respectively.

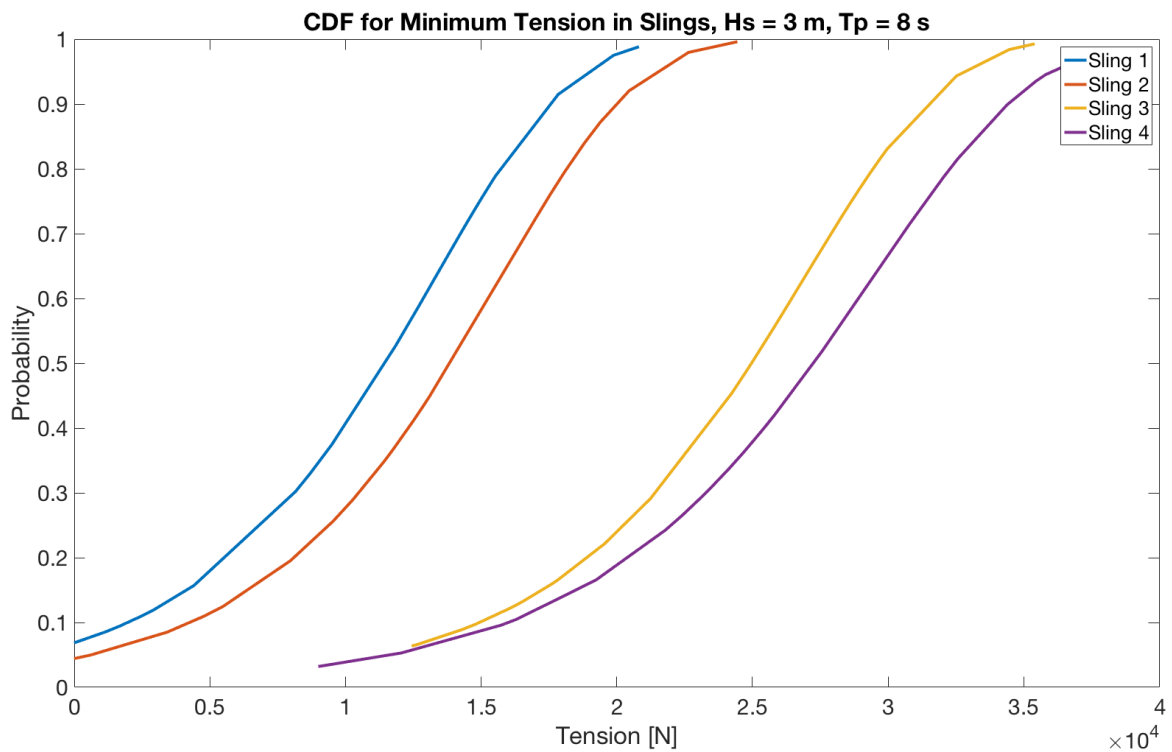


Figure 9.36: Gumbel CDF,  $H_s = 3\text{ m}$ ,  $T_p = 8\text{ s}$

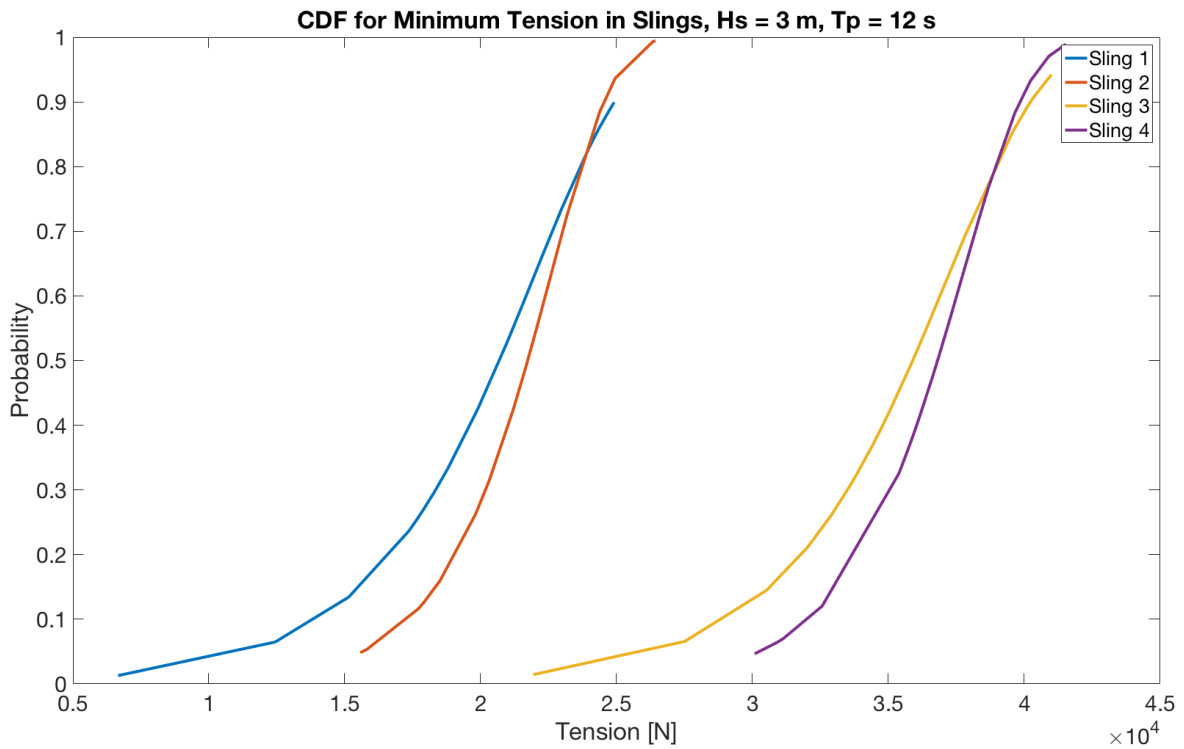


Figure 9.37: Gumbel CDF,  $H_s = 3$  m,  $T_p = 12$  s

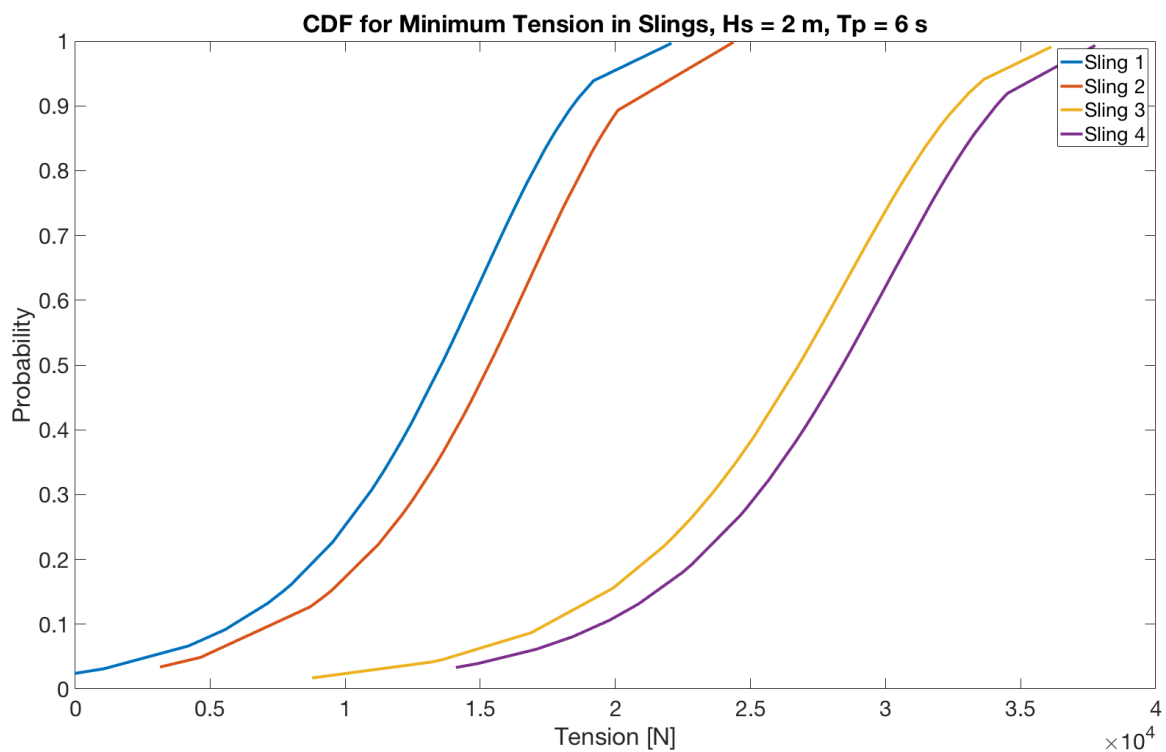


Figure 9.38: Gumbel CDF,  $H_s = 2$  m,  $T_p = 6$  s

Figure 9.39, 9.40 and 9.41 show the calculated Gumbel-plot from both distribution and empirical polynomial fitting. The 10% quantile and the minimum slack limit were added into the same plots.

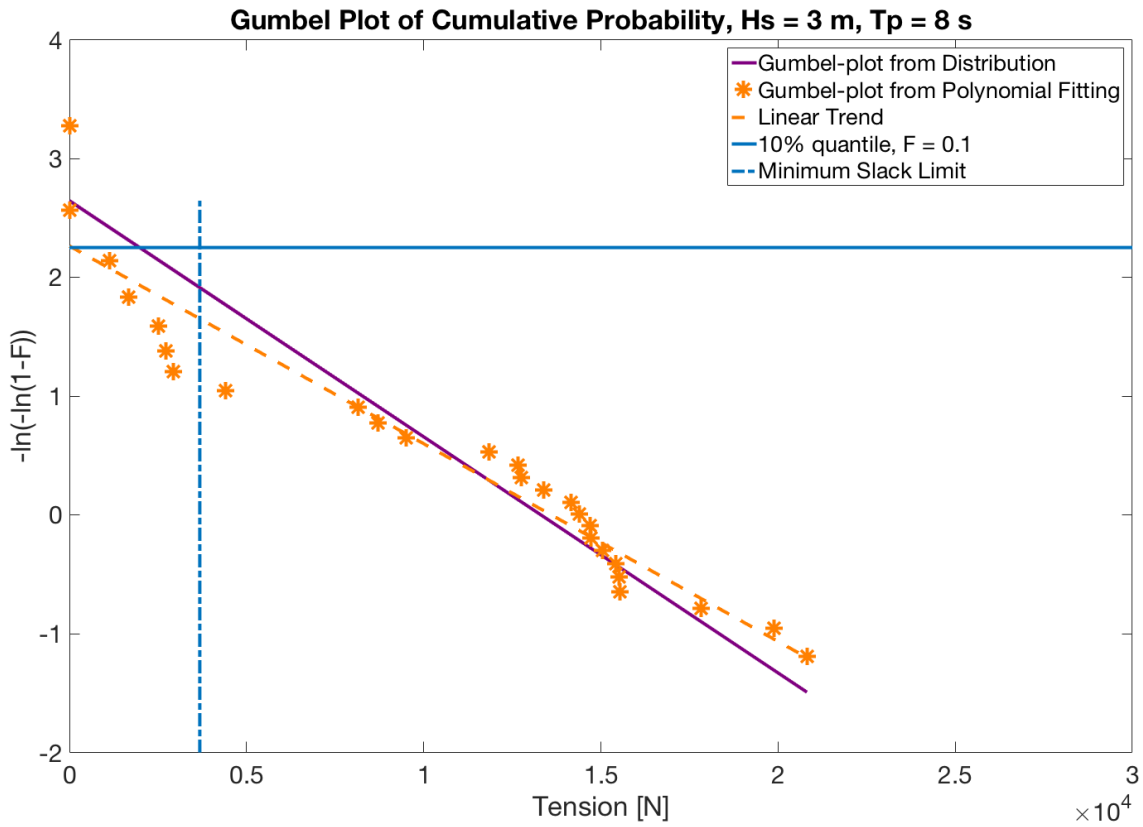


Figure 9.39: Gumbel-plot for tension in sling 1,  $H_s = 3\text{ m}$ ,  $T_p = 8\text{ s}$

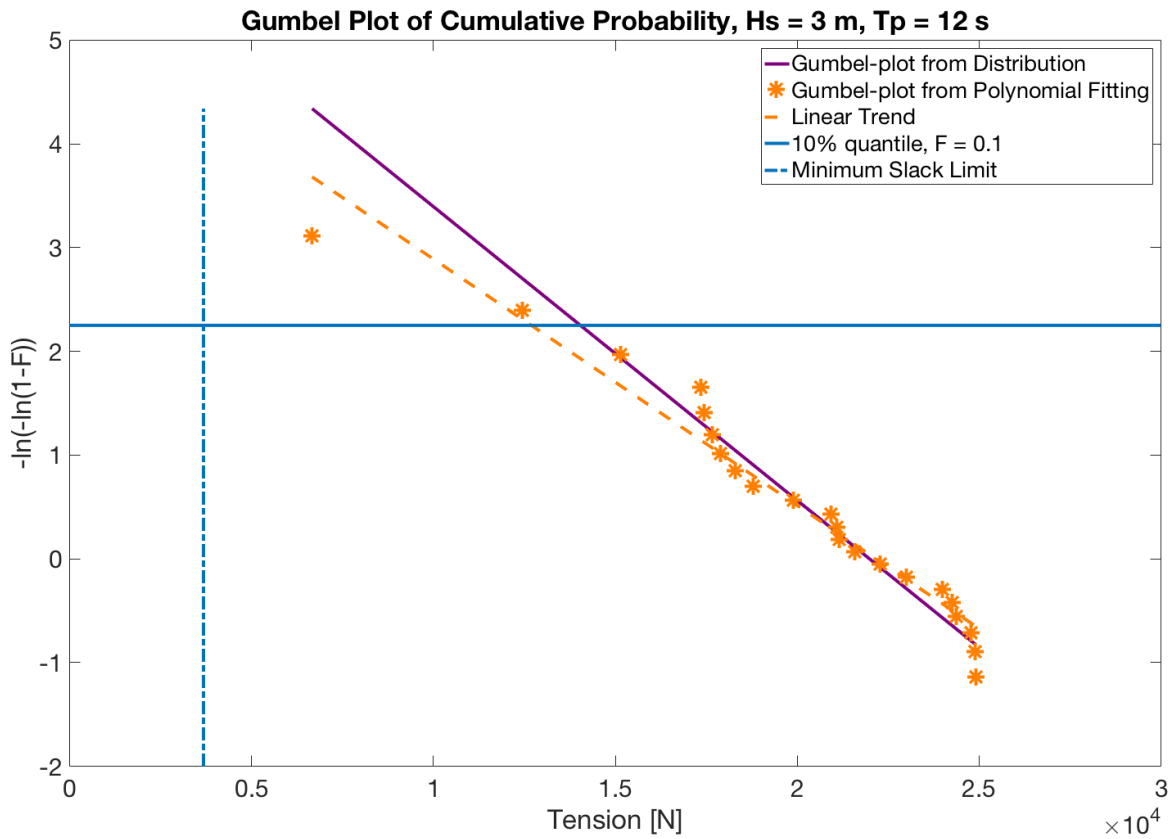


Figure 9.40: Gumbel-plot for tension in sling 1,  $H_s = 3\text{ m}$ ,  $T_p = 12\text{ s}$

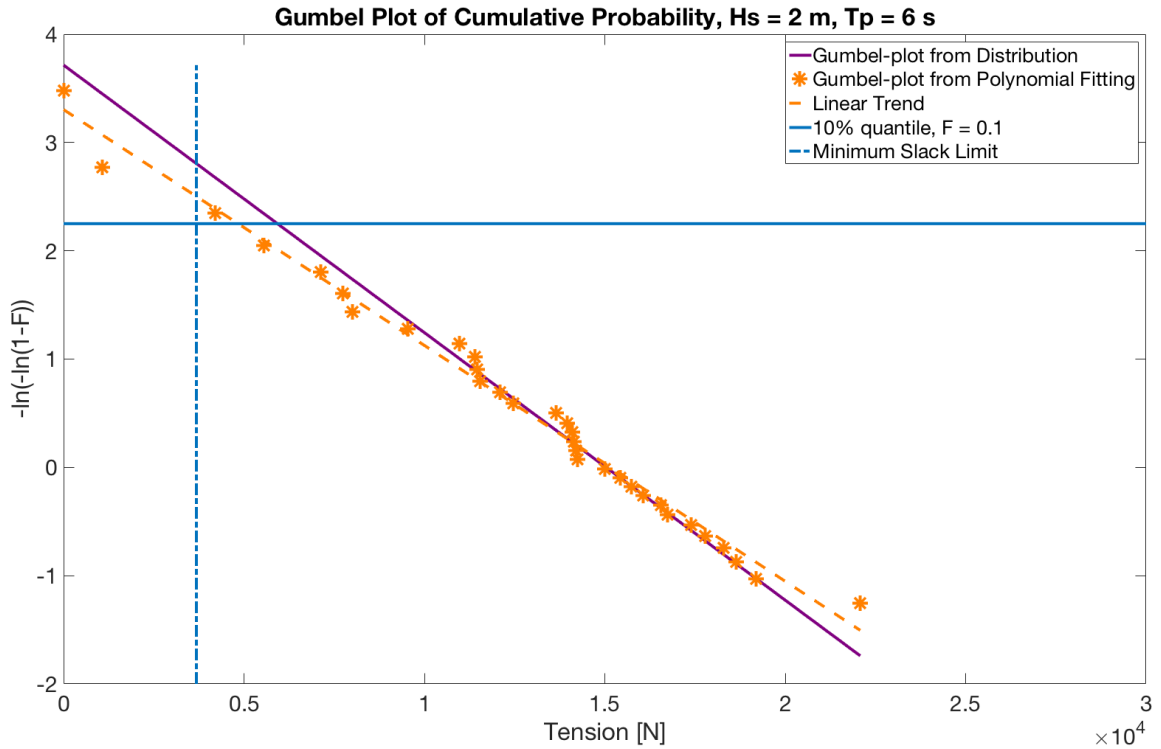


Figure 9.41: Gumbel-plot for tension in sling 1,  $H_s = 2$  m,  $T_p = 6$  s

### 9.3 Simulated Design Criteria

The simulated design criteria were determined by the four slings' 10% quantiles, as shown in Figure 9.8-9.10. The simulated design criteria were dependent on both  $H_s$  and  $T_p$  and are shown in Figure 9.42. The yellow line illustrates the lower wave condition boundary found in Figure 7.3 from the Heidrun Metocean report (Eik and Nygaard, 2004). No wave conditions below the yellow line have occurred at the Heidrun field. For further calculations the simulated design criteria was assumed to be 2.5 m, and constant for all peak periods.

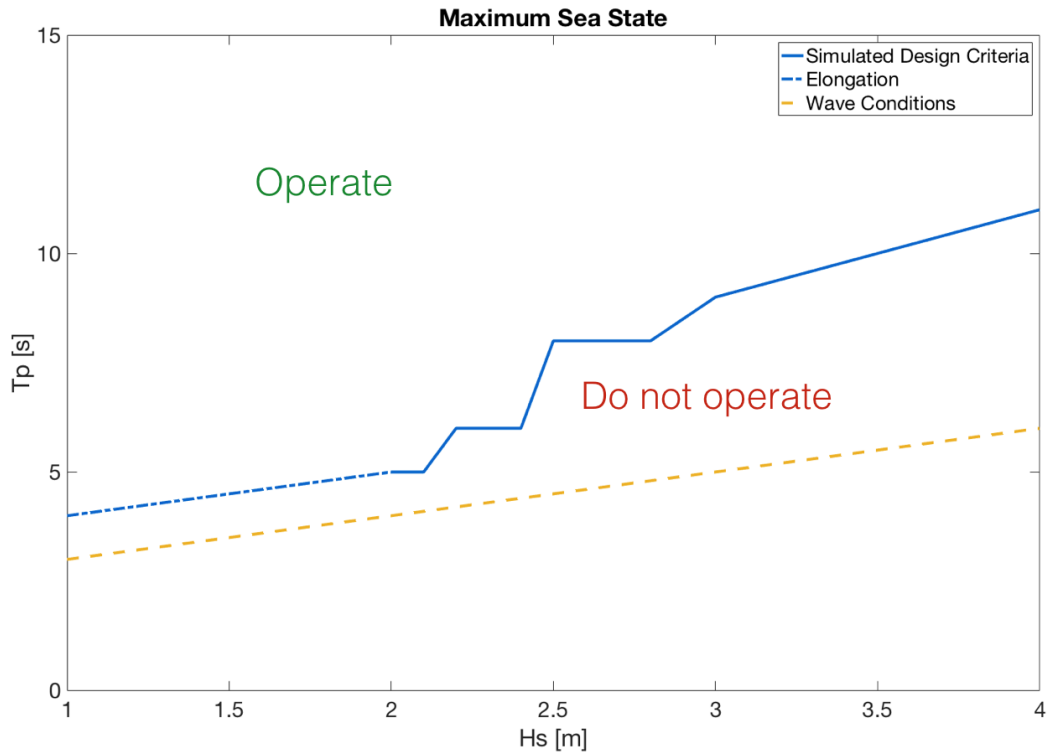


Figure 9.42: Simulated design criteria

Both the manually estimated and simulated design criteria are shown in Figure 9.43. The purple line indicates the average  $H_s$ -limit found from manual estimation by use of DNV GL's Simplified Method.

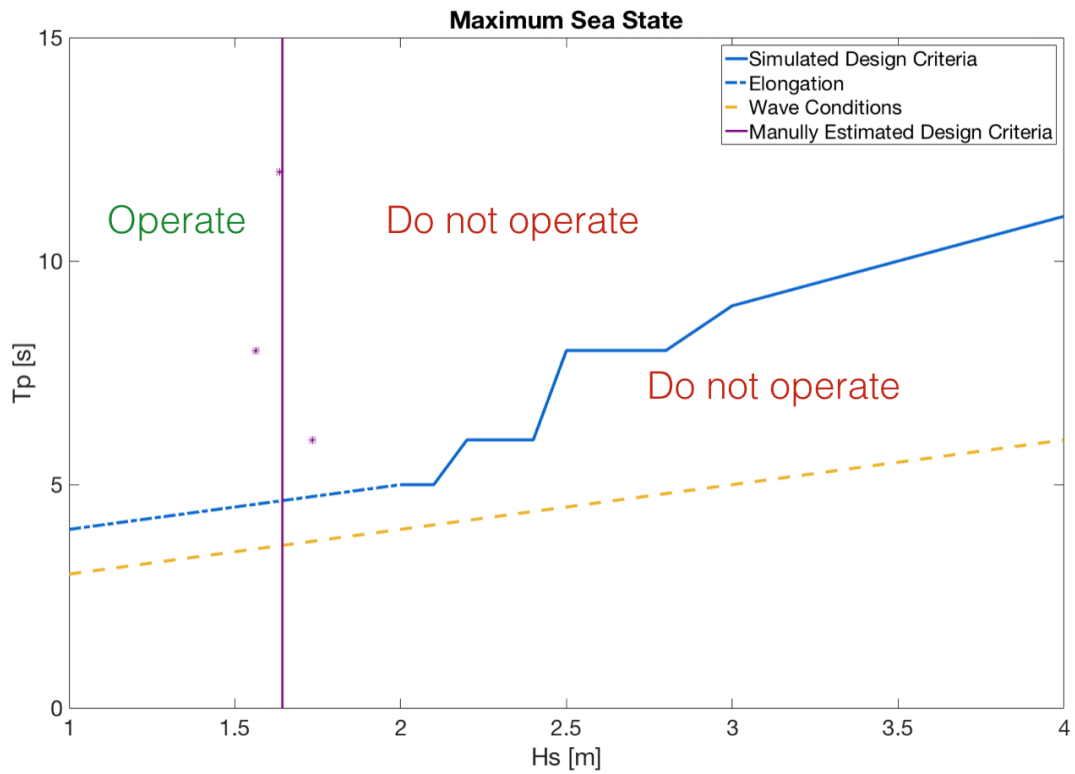


Figure 9.43: Manually estimated and simulated design criteria



## 10 Planning

Before the marine operation could take place three important parameters were determined; the operation's reference period  $T_R$ , the design criterion  $OP_{LIM}$  and the  $\alpha$ -factor. The various planning phases were examined separately before  $T_{POP}$  could be estimated.  $T_C$  consider all uncertainties and  $T_R$  summarise  $T_{POP}$  and  $T_C$ . A marine operation shall always be designed to bring an object from one safe condition to another safe condition, and for this operation the first safe condition was when the cover was safely fastened on deck (1) and the other one when the cover was safely landed on the seabed (2), as illustrated in Figure 10.1.

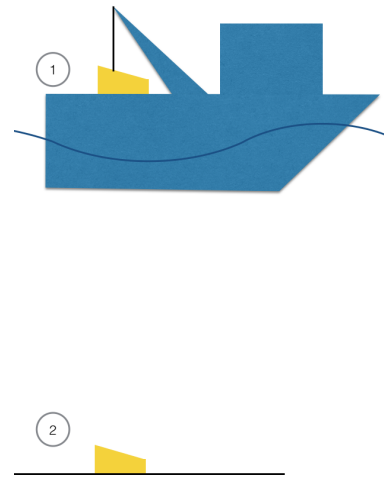


Figure 10.1: Illustration of safe conditions

The planned operation period  $T_{POP}$  for the different lifting phases at Heidrun and Tanzania are listed in Table 10.1. The lowering phase is depth dependent and was therefore different for Heidrun and Tanzania. Due to Tanzania's deep water and stronger current, the probability of any offset was greater at Tanzania compared to at Heidrun. The landing on seabed phase was therefore different for the two fields.

Table 10.1: Planned operation period for different phases

Phase	Heirun	Tanzania
Loosen sea fastening and prepare rigging	15 min	15 min
Lift-off, In-air and Through splash zone	15 min	15 min
Lowering	30 min	205 min
Landing	15 min	45 min
$T_{POP}$	<b>1 hours and 15 min</b>	<b>4 hours and 40 min</b>

If uncertainties in the planned operation period and required time for contingency situations were not assessed in detail  $T_C$  should be similar to  $T_{POP}$  (DNV GL, 2011a). Hence  $T_R$  was determined to be **2.5 hours at Heidrun** and **9 hours and 20 minutes at Tanzania**. Planning was performed for both the manually estimated and the simulated design criteria of 1.64 m and 2.5 m respectively.

Offshore lifting and installation of a GRP protection cover was determined to be a level B marine

operation. If the available weather forecasting services could be regarded as level B, and the highest forecasted wave heights from at least two recognised and pre-defined sources were considered, the  $\alpha$ -factor could be determined according to Table 10.2 (DNV GL, 2011a).

Table 10.2:  $\alpha$ -factor for waves, level B highest forecast (DNV GL, 2011a)

Operational Period [hours]	Design Wave Height [m]				
	$H_S = 1$	$H_S = 2$	$H_S = 3$	$H_S = 4$	$H_S = 6$
$T_{POP} \leq 12$	0.68	0.80	0.82	0.83	0.84
$T_{POP} \leq 24$	0.66	0.77	0.79	0.80	0.82
$T_{POP} \leq 36$	0.65	0.75	0.76	0.77	0.80
$T_{POP} \leq 48$	0.63	0.71	0.73	0.75	0.78
$T_{POP} \leq 72$	0.58	0.66	0.69	0.71	0.76

The planned operation period was less than 12 hours for both fields, thus the  $\alpha$ -factor was determined to be 0.76 and 0.81 for a design wave height  $H_{sLIM}$  of 1.64 m and 2.5 m respectively. This resulted in an operational wave height criterion  $H_{sWF}$  of 1.25 m and 2.0 m respectively.

The cover can be installed in several ways; over side lifting, lift through moonpool or with special handling systems. If possible it was desired to install the cover with a traditional over side crane operation. The cover can also be installed with different angles and was given an angle of  $68^\circ$  to the horizontal, as shown in Figure 10.2.



Figure 10.2: Vessel lifting cover in vertical direction (Statoil, 2015)

## 10.1 Operability

Weather conditions may affect and delay marine operations. The weather proved to be season dependent and during summer one was more likely to observe lower significant wave heights and calmer weather windows compared to the winter season.

During the planning process it can be interesting to have knowledge about the weather window, the operation's operability for a specified location and how long one should estimate to wait on weather during the operation. The determined weather criteria, based on the resulting force acting on the system during the lift, could give an estimate of when the operation can and cannot be carried out. In order to decide whether or not it is important and profitable to increase the operational criteria of the operation, it is important to have knowledge about the operation field. Figure 10.3 shows wave series for four years at Tanzania (to the left) and Heidrun (to the right) with an design criteria of 1.64 m and 2.5 m.

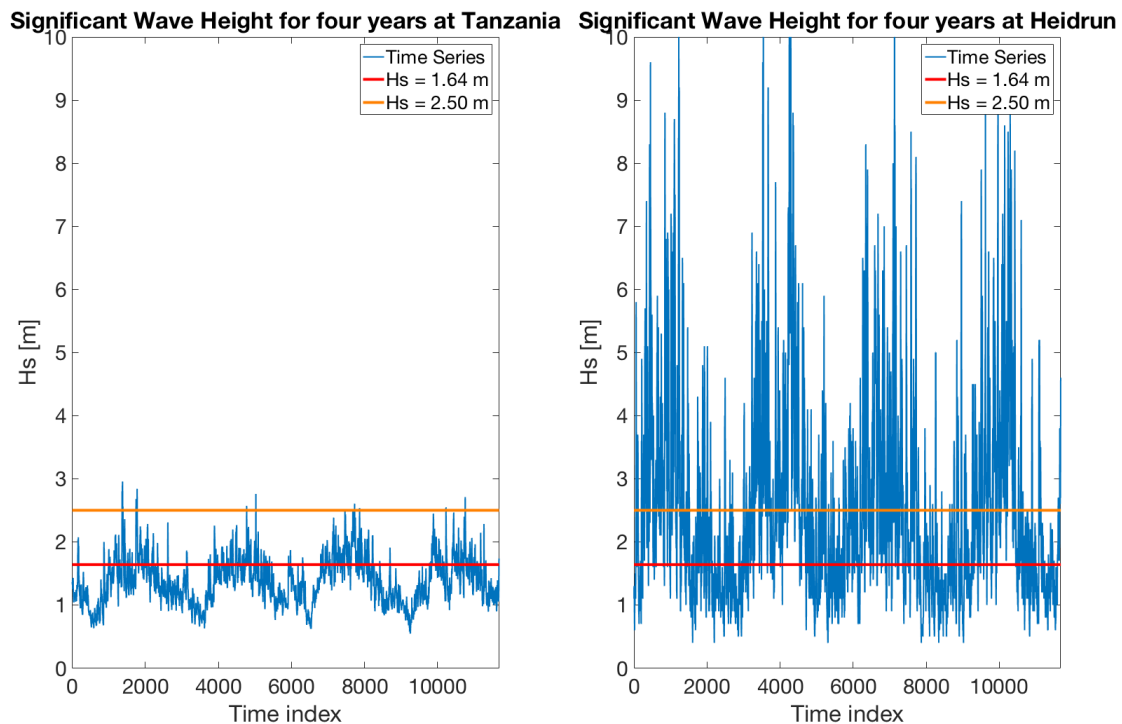


Figure 10.3: Wave conditions at Tanzania (to the left) and Heidrun (to the right) for four years and two wave criteria

In order to differentiate between season variation, the time series that contained environmental data were separated into four seasons; spring, summer, autumn and off-season/winter. Observed significant wave heights during each season were stored in separate vectors. To be able to visualise the duration of calms for various operational criteria a *calm vector* was established. Every observed  $H_s$  was compared with  $H_{S_{WF}}$  for every season and the total length of the calm periods were stored in the *calm vector* and subsequently plotted. This was repeated for  $H_{S_{WF}}$  varying between 0.5

m and 10 m with a step of 0.025 for Heidrun and 0 m and 5 m with a step of 0.01 for Tanzania. Operational significant wave height was plotted against the duration of calms for each season, by use of the MATLAB code *Season Dependent Duration of Calms* found in Appendix C.3. The plots are shown in Figure 10.4 and 10.5 for Heidrun and Tanzania respectively.

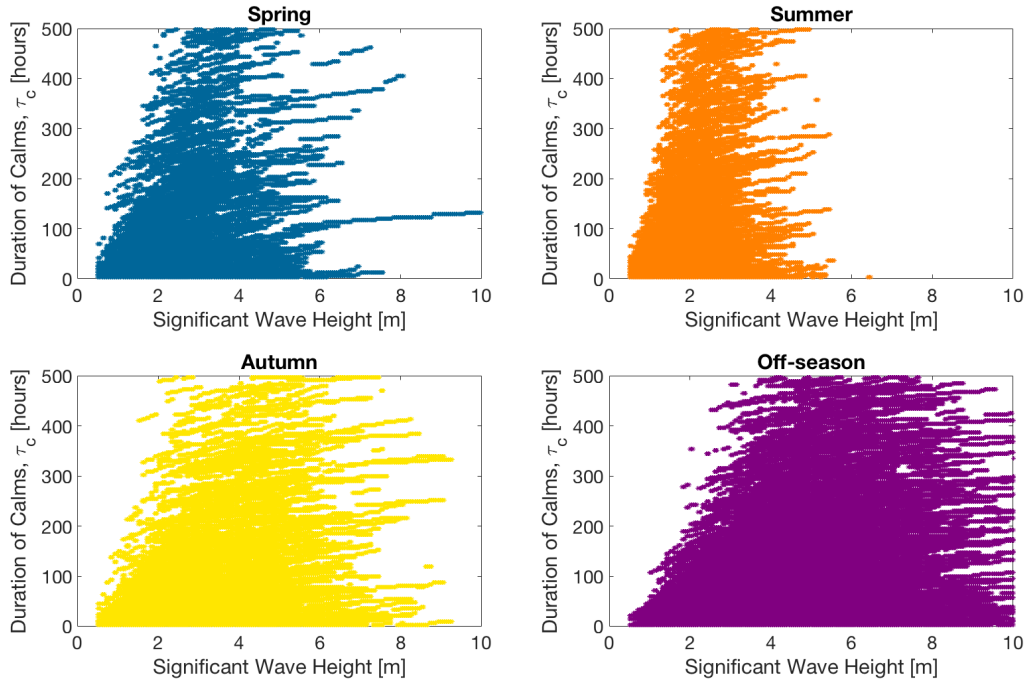


Figure 10.4: Observed duration of calms vs. operational criterion for various seasons at Heidrun

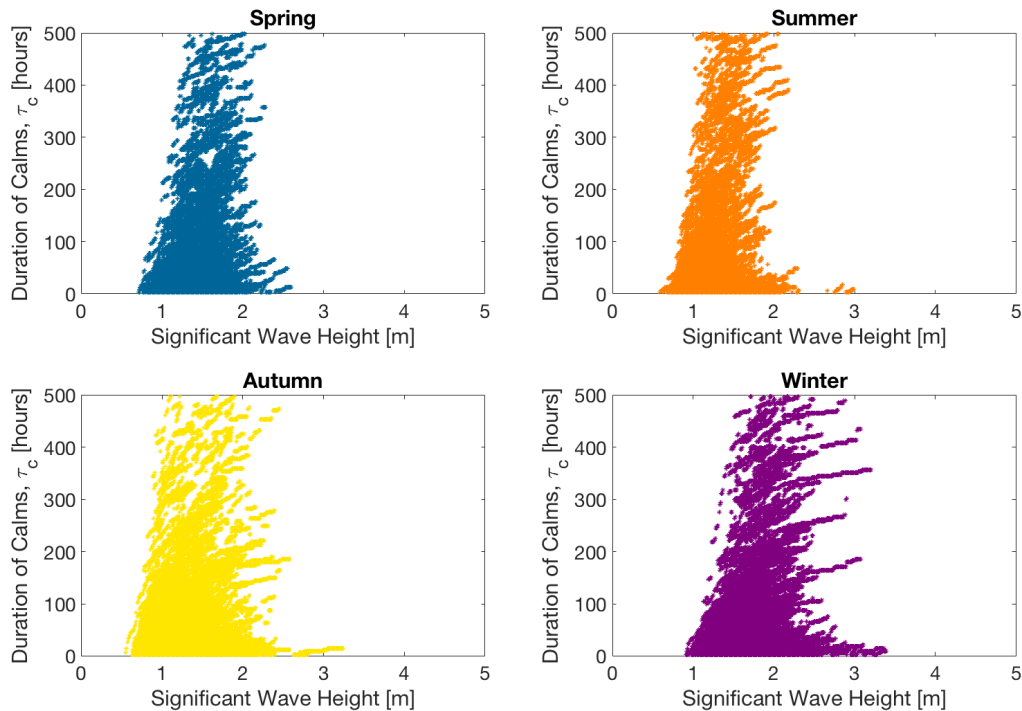


Figure 10.5: Observed duration of calms vs. operational criterion for various seasons at Tanzania

The observed length of calms were compared to the given reference period  $T_R$  and subsequently divided into four categories; *Calm*, *Calm-Wait*, *Storm-Wait* and *Storm*. The appurtenant criteria are listed in Table 10.3.

Table 10.3: Weather categories with appurtenant criteria

Category	Criteria
Calm	$(H_s \leq H_{s_{WF}}) \cap (\tau_c \geq T_R)$
Calm-Wait	$(H_s \leq H_{s_{WF}}) \cap (\tau_c < T_R)$
Storm-Wait	$(H_s > H_{s_{WF}}) \cap (\tau_c \geq T_R)$
Storm	$(H_s > H_{s_{WF}}) \cap (\tau_c < T_R)$

The categories are visualised in Figure 10.6, where observed duration of calms at Heidrun and Tanzania are plotted against significant wave height. The approach was the same as the season dependent one, but segregation of seasons was in this case not included.

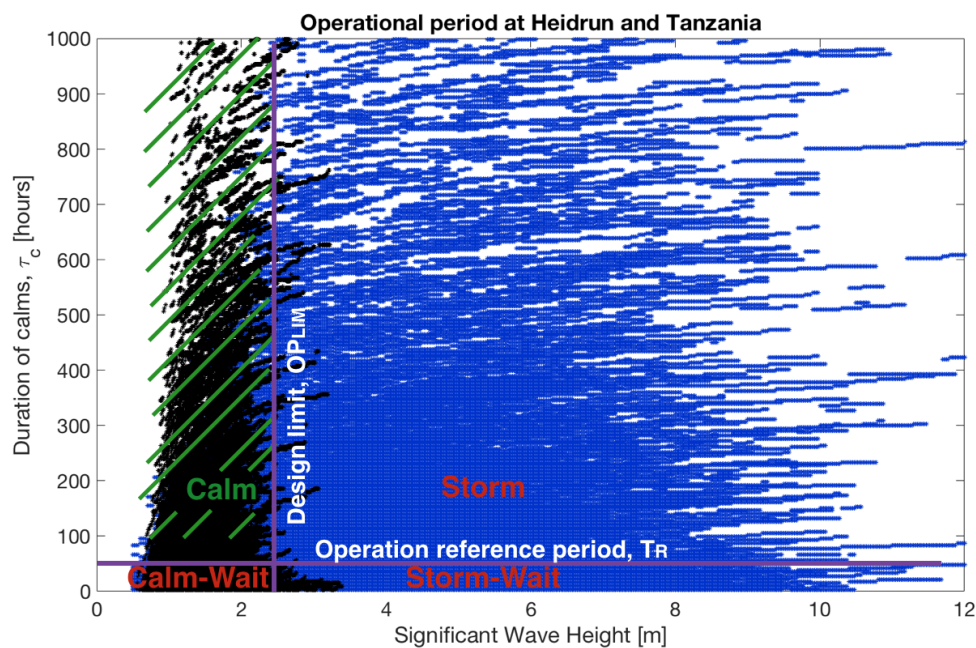


Figure 10.6: Observed duration of calms vs.  $H_s$  at Heidrun (blue) and Tanzania (black), with categories

Average operability for the marine operation was found by summing the calm periods of longer duration than the reference period, and divide it by the total amount of hours during each season. The average operational downtime is the average probability of waiting on weather, and was found by summing the storm periods and the calm periods of lower duration than the reference period, and divide it by the total amount of hours during each season.

The probability that the operation could be carried out at Heidrun during different seasons, for the manually estimated operational criterion  $H_{s_{WF}} = 1.25$  m and  $T_R = 2.5$  hours, are listed in Table

10.4.

Table 10.4: Average operability at Heidrun,  $T_R = 2.5$  hours,  $H_{s_{WF}} = 1.25$  m

	Spring	Summer	Autumn	Off-season
<b>Operability</b>	<b>21.1%</b>	<b>38.6%</b>	<b>11.3%</b>	<b>2.8%</b>

The average operation downtime for an identical operation is listed in Table 10.5, in addition to the reason of WOW.

Table 10.5: Average downtime at Heidrun,  $T_R = 2.5$  hours,  $H_{s_{WF}} = 1.25$  m

<b>Downtime</b>	Spring	Summer	Autumn	Off-season
Calm-Wait	0.0%	0.0%	0.0%	0.0%
Storm-Wait	0.0%	0.0%	0.0%	0.0%
Storm	78.9%	61.4%	88.7%	97.2%
<b>WOW</b>	<b>78.9%</b>	<b>61.4%</b>	<b>88.7%</b>	<b>97.2%</b>

For the simulated operational criterion of 2 m, the operability and downtime are listed in Table 10.6 and 10.7 respectively.

Table 10.6: Average operability at Heidrun,  $T_R = 2.5$  hours,  $H_{s_{WF}} = 2$  m

	Spring	Summer	Autumn	Off-season
<b>Operability</b>	<b>58.9%</b>	<b>79.9%</b>	<b>41.0%</b>	<b>18.7%</b>

Table 10.7: Average downtime at Heidrun,  $T_R = 2.5$  hours,  $H_{s_{WF}} = 2$  m

<b>Downtime</b>	Spring	Summer	Autumn	Off-season
Calm-Wait	0.0%	0.0%	0.0%	0.0%
Storm-Wait	0.0%	0.0%	0.0%	0.0%
Storm	41.1%	20.3%	59.0%	81.3%
<b>WOW</b>	<b>41.1%</b>	<b>20.3%</b>	<b>59.0%</b>	<b>81.3%</b>

The season dependent operability and downtime when  $T_R$  increased to 7.25 hours, are listed in Table 10.8 and 10.9 respectively, for  $H_{s_{WF}} = 1.25$  m.

Table 10.8: Average operability at Heidrun,  $T_R = 7.25$  hours,  $H_{s_{WF}} = 1.25$  m

	Spring	Summer	Autumn	Off-season
<b>Operability</b>	<b>20.5%</b>	<b>37.9%</b>	<b>10.9%</b>	<b>2.6%</b>

Table 10.9: Average downtime at Heidrun,  $T_R = 7.25$  hours,  $H_{s_{WF}} = 1.25$  m

<b>Downtime</b>	Spring	Summer	Autumn	Off-season
Calm-Wait	0.6%	0.7%	0.4%	0.1%
Storm-Wait	0.2%	0.4%	0.2%	0.0%
Storm	78.7%	61.0%	88.5%	97.3%
<b>WOW</b>	<b>79.5%</b>	<b>62.1%</b>	<b>89.1%</b>	<b>97.4%</b>

For the simulated operational criterion of 2 m, the operability and downtime are listed in Table 10.10 and 10.11 respectively for  $T_R = 7.25$  hours.

Table 10.10: Average operability at Heidrun,  $T_R = 7.25$  hours,  $H_{s_{WF}} = 2$  m

	Spring	Summer	Autumn	Off-season
<b>Operability</b>	<b>58.4%</b>	<b>79.4%</b>	<b>40.6%</b>	<b>18.0%</b>

Table 10.11: Average downtime at Heidrun,  $T_R = 7.25$  hours,  $H_{s_{WF}} = 2$  m

<b>Downtime</b>	Spring	Summer	Autumn	Off-season
Calm-Wait	0.5%	0.3%	0.5%	0.5%
Storm-Wait	0.6%	0.5%	0.4%	0.2%
Storm	40.5%	19.8%	58.5%	81.3%
<b>WOW</b>	<b>41.6%</b>	<b>20.6%</b>	<b>59.4%</b>	<b>82.0%</b>

The operability for a marine operation with a reference period of 2.5 hours at Heidrun and 9.3 hours at Tanzania, for various  $H_s$ -criteria were calculated by use of the MATLAB code *Operability* found in Appendix C.4, and are visualised in Figure 10.7 and 10.8 respectively. The plots show the probability of experiencing a calm period of longer duration than  $T_R$ .

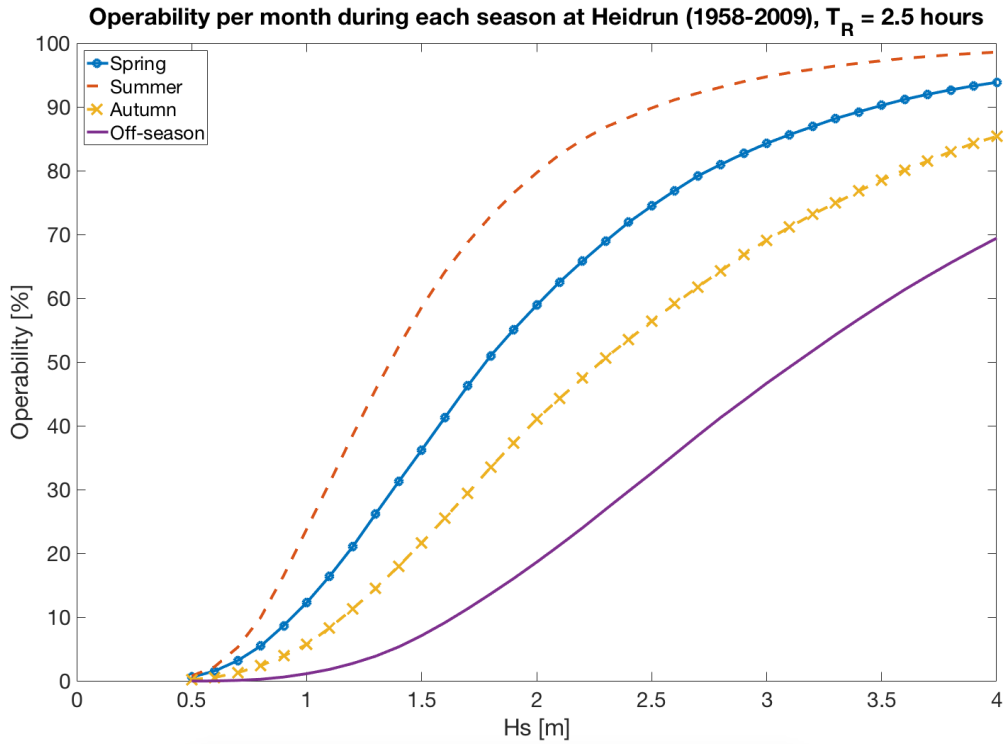


Figure 10.7: Operability for each season at Heidrun

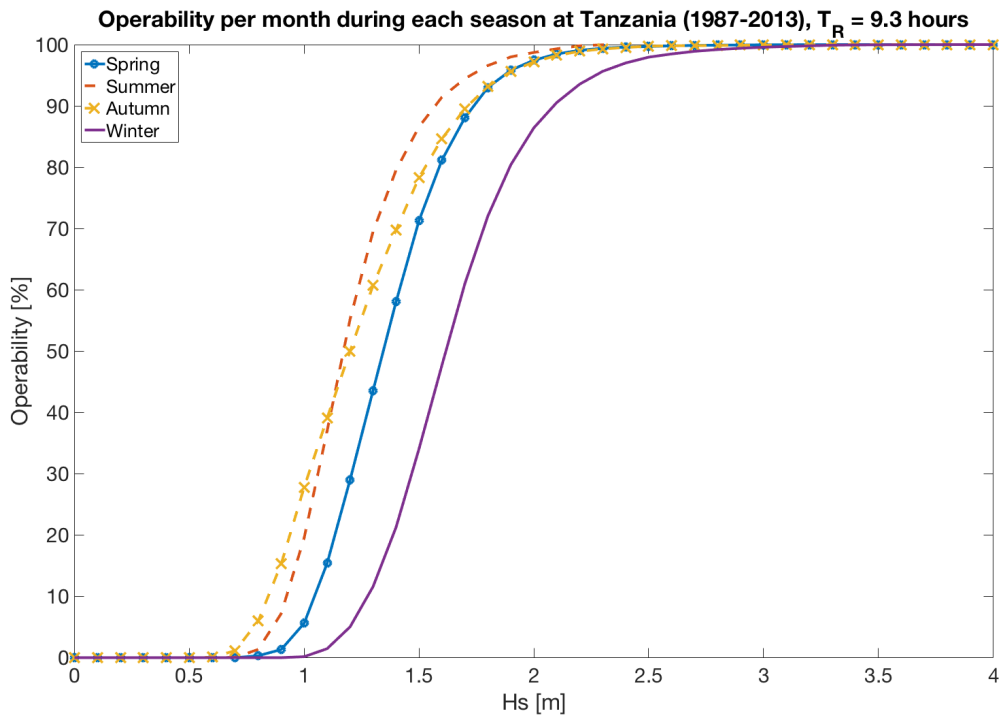


Figure 10.8: Operability for each season at Tanzania

The operability and downtime of an operation is highly dependent on  $H_{s_{WF}}$  and  $T_R$ . By having a monitoring system and a meteorologist on board the vessel during the operation the  $\alpha$ -factor can increase with approximately 0.15, as listed in Table A.3 in Appendix A -  $\alpha$ -factor for Waves. The



operability and downtime for a regular level B operation and a level A operation with monitoring systems and meteorologist (*m&m*), are listed in Table 10.12 and 10.13 for  $T_R = 2.5$  hours and  $H_{S_{LIM}} = 1.64$  m and 2.5 m respectively, in addition to the respective  $\alpha$ -factor and  $H_{S_{WF}}$ .

Table 10.12: Operability and downtime for multiple  $\alpha$ -factors,  $T_R = 2.5$  hours,  $H_{S_{LIM}} = 1.64$  m

	$\alpha$	$H_{S_{WF}}$		Spring	Summer	Autumn	Off-season
<b>Level B</b>	0.76	1.25 m	<b>Operate</b>	21.1%	38.6%	11.3%	2.8%
			<b>WOW</b>	78.9%	61.4%	88.7%	97.2%
<b>Level A (m&amp;m)</b>	0.93	1.53 m	<b>Operate</b>	36.2%	58.6%	21.7%	7.0%
			<b>WOW</b>	63.8%	41.4%	78.3%	93.0%

Table 10.13: Operability and downtime for multiple  $\alpha$ -factors,  $T_R = 2.5$  hours,  $H_{S_{LIM}} = 2.5$  m

	$\alpha$	$H_{S_{WF}}$		Spring	Summer	Autumn	Off-season
<b>Level B</b>	0.81	2.03 m	<b>Operate</b>	58.9%	79.7%	41.0%	18.7%
			<b>WOW</b>	41.1%	20.3%	59.0%	81.3%
<b>Level A (m&amp;m)</b>	0.96	2.40 m	<b>Operate</b>	71.9%	88.3%	53.6%	29.8%
			<b>WOW</b>	28.1%	11.7%	46.4%	70.2%

## 10.2 Distribution of Calm Periods

By use of *the method of moments* a PDF for length of calms and wait-periods at Heidrun, fitted a Weibull distribution with scale  $\gamma$  and shape  $\beta$  parameters as listed in Table 10.14 and 10.15 for  $T_R = 2.5$  hours and 7.25 hours respectively. The operational criteria found for a level B marine operation were used.

Table 10.14: Weibull parameters fitting length of calms at Heidrun,  $T_R = 2.5$  hours

$H_{S_{WF}}$	Parameters	Spring	Summer	Autumn	Off-season
<b>1.25 m</b>	Scale - $\gamma$	32.9	41.1	26.3	21.4
	Shape - $\beta$	1.07	1.04	1.06	1.24
<b>2 m</b>	Scale - $\gamma$	61.3	111.0	47.7	30.8
	Shape - $\beta$	0.96	0.93	0.98	1.09

Table 10.15: Weibull parameters fitting length of calms at Heidrun  $T_R = 7.25$  hours

$H_{s_{WF}}$	Parameters	Spring	Summer	Autumn	Off-season
1.25 m	Scale - $\gamma$	42.0	50.3	33.7	27.6
	Shape - $\beta$	1.31	1.23	1.25	1.55
2 m	Scale - $\gamma$	72.3	125.2	56.9	38.1
	Shape - $\beta$	1.10	1.03	1.11	1.29

The mean and standard deviation of the calms and WOW-periods for  $T_R = 2.5$  hours and 7.25 hours are listed in Table 10.16 and 10.17 respectively.

Table 10.16: Mean and standard deviation of length of calms and WOW,  $T_R = 2.5$  hours

$H_{s_{WF}}$			Spring	Summer	Autumn	Winter
1.25 m	Operate	Mean	32.0	40.4	25.6	19.9
		Std	33.1	42.7	29.1	17.9
	WOW	Mean	119.5	64.4	199.7	692.5
		Std	141.0	66.7	259.9	1 021.7
2 m	Operate	Mean	62.5	114.9	48.2	29.7
		Std	69.9	127.6	56.8	31.2
	WOW	Mean	43.5	29.3	69.3	129.7
		Std	46.9	27.4	80.9	174.4

Table 10.17: Mean and standard deviation of length of calms and WOW,  $T_R = 7.25$  hours

$H_{s_{WF}}$			Spring	Summer	Autumn	Winter
1.25 m	Operate	Mean	38.4	46.7	31.0	24.5
		Std	33.7	43.4	30.3	17.9
	WOW	Mean	148.3	76.4	252.1	900.9
		Std	166.2	77.7	311.8	1 227.4
2 m	Operate	Mean	67.5	123.3	54.4	34.9
		Std	70.9	128.6	58.1	31.9
	WOW	Mean	49.3	31.9	79.7	157.5
		Std	53.2	30.1	95.4	219.4

The fitted Weibull distribution of calms at Heidrun during spring, for the simulated operational criterion of 2 m, is visualised to the left in Figure 10.9 and 10.10 for  $T_R = 2.5$  hours and 7.25 hours respectively. The empirical Weibull plot found from the sample size was plotted towards the linear

Weibull plot found from the distribution to the right in the two respective figures. The distributions were calculated and plotted by use of the MATLAB code *Duration* found in Appendix C.5. There are evidence to believe that the Weibull distribution is a good fit to the length of calms if the empirical data points are close to the linear Weibull plot.

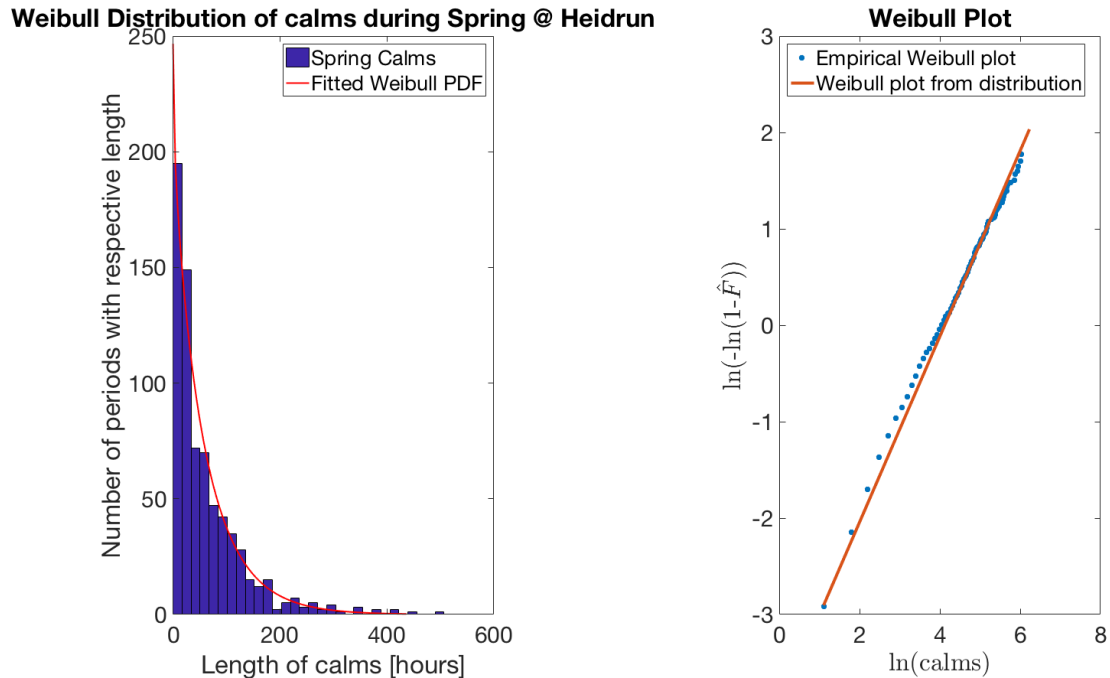


Figure 10.9: Weibull distribution of calm periods at Heidrun during spring for  $H_{s_{WF}} = 2 \text{ m}$ ,  $T_R = 2.5$

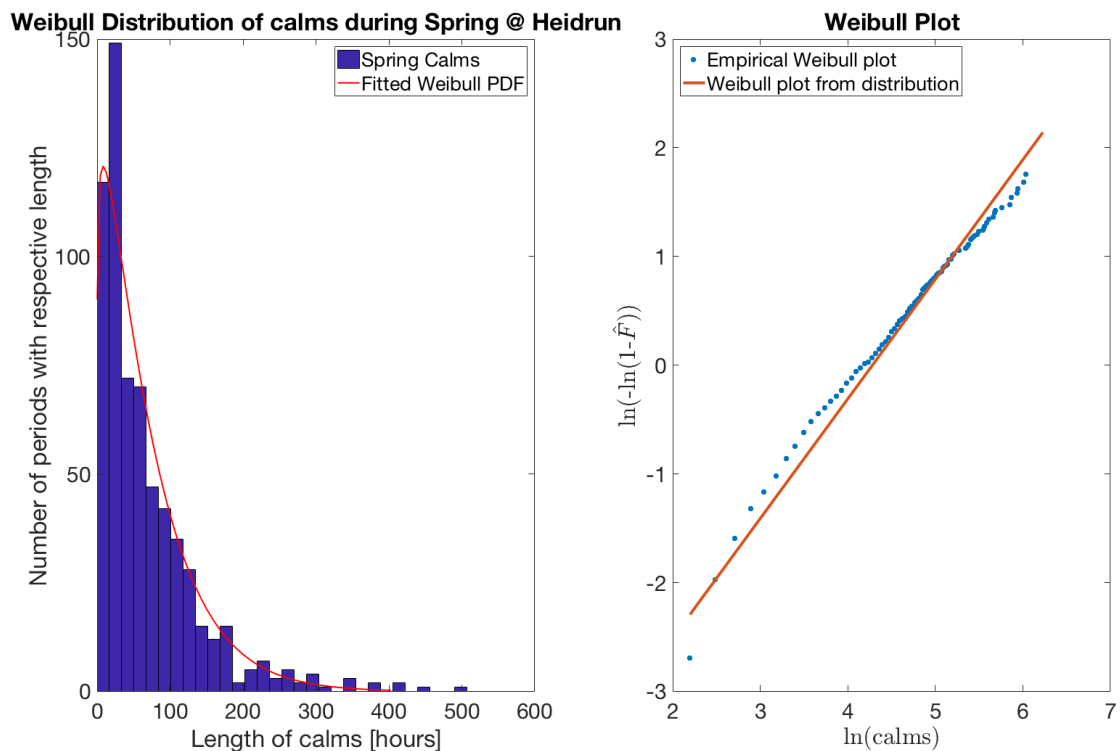


Figure 10.10: Weibull distribution of calm periods at Heidrun during spring for  $H_{s_{WF}} = 2 \text{ m}$ ,  $T_R = 7.25$

### 10.3 Actual Duration of Operation with Random Start

The actual duration of operation  $T_{op}$  was based on an operation with random start and included the operation time in addition to appurtenant WOW-periods. The *method of moments* were used to fit the total duration of operations to a Weibull distribution, and the parameters are listed in Table 10.18.

Table 10.18: Weibull parameters for actual duration of operations with random start at Heidrun

$T_R$	$H_{sWF}$	Spring		Summer		Autumn		Off-Season	
		$\gamma$	$\beta$	$\gamma$	$\beta$	$\gamma$	$\beta$	$\gamma$	$\beta$
2.5 hrs	1.25 m	93	0.70	33	0.67	212	0.78	979	0.84
	2 m	16	0.66	7	0.78	35	0.63	116	0.67
7.25 hrs	1.25 m	134	0.85	55	0.86	284	0.90	1 202	0.90
	2 m	30	0.86	16	0.91	59	0.78	174	0.76

$T_{op}$  was predicted for three probabilities by use of the Weibull quantile function. The three probabilities were 90%, 50% and 10%, in addition to the mean.  $T_{op}$  is tabulated for  $T_R = 2.5$  hours and 12 hours in Table 10.19 and 10.20 respectively. E.g.  $P_{90}$  means that there was a 90% probability that the duration of operation was shorter than 55.2 hours during spring, when  $T_R$  is 2.5 hours. According to this, waiting on weather was calculated to be 52.7 hours. If any probability resulted in  $T_{op} < T_R$ ,  $T_{op}$  was set to be equivalent with  $T_R$ .

$T_{op}$  was calculated by use of the MATLAB code *Actual Duration of Operation* found in Appendix C.6. The results were only tabulated for  $T_{op}$  at Heidrun, but were visualised graphically for both Heidrun and Tanzania.

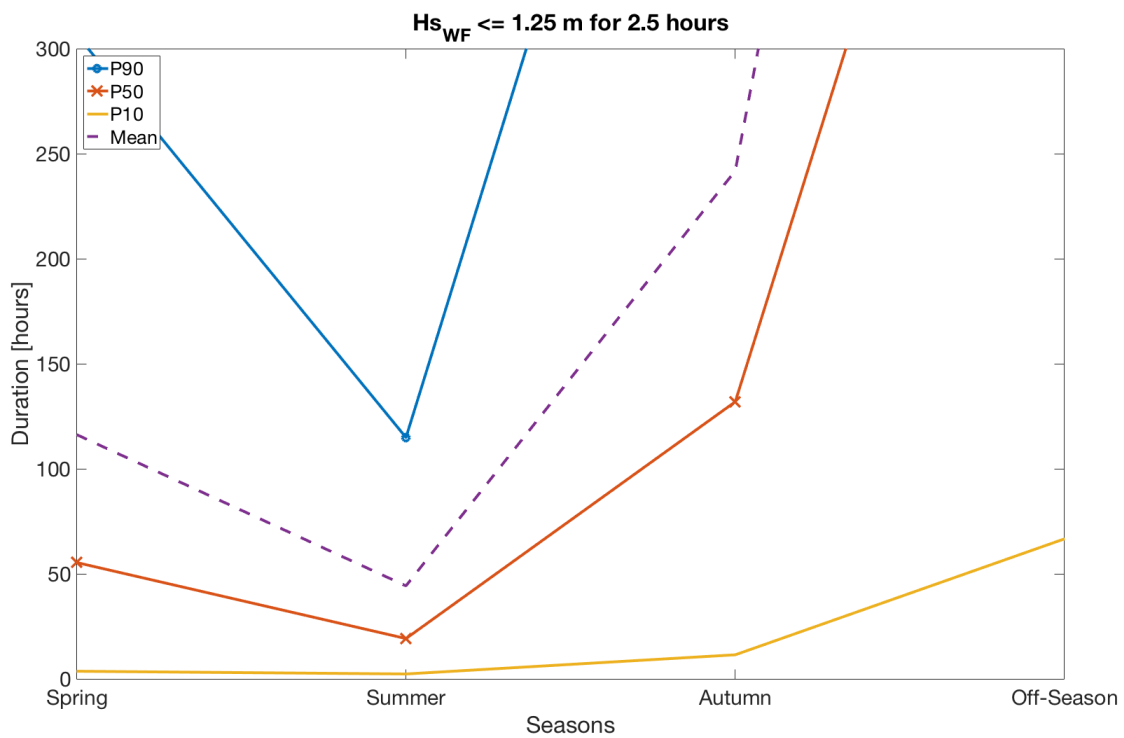
Table 10.19: Actual duration of operation with random start at Heidrun in hours,  $T_R = 2.5$  hours

$H_{sWF}$	Probability	Spring	Summer	Autumn	Off-Season
1.25 m	$P_{90}$	306	115	621	2 648
	$P_{50}$	55	19	132	632
	$P_{10}$	4	2.5	12	67
	<b>Mean</b>	116	44	242	1 071
2 m	$P_{90}$	55	20	134	400
	$P_{50}$	9	4	20	67
	$P_{10}$	2.5	2.5	2.5	4
	<b>Mean</b>	22	8	51	152

Table 10.20: Actual duration of operation with random start at Heidrun in hours,  $T_R = 7.25$  hours

$H_{s_{WF}}$	Probability	Spring	Summer	Autumn	Off-Season
1.25 m	$P_{90}$	359	146	715	3 033
	$P_{50}$	87	36	189	800
	$P_{10}$	9	7.25	23	99
	Mean	146	60	297	1 262
2 m	$P_{90}$	78	41	172	517
	$P_{50}$	19	11	37	107
	$P_{10}$	7.25	7.25	7.25	9
	Mean	33	18	69	206

The actual duration of operation with random start at Heidrun, is visualised in Figure 10.11 and 10.12 for  $T_R = 2.5$  hours and  $H_{s_{WF}}$  of 2 m and 3 m respectively, and in Figure 10.13 and 10.14 for  $T_R = 12$  hours and  $H_{s_{WF}}$  of 2 m and 3 m respectively.

Figure 10.11: Actual duration of operation with random start at Heidrun,  $T_R = 2.5$  hours,  $H_{s_{WF}} = 1.25$  m

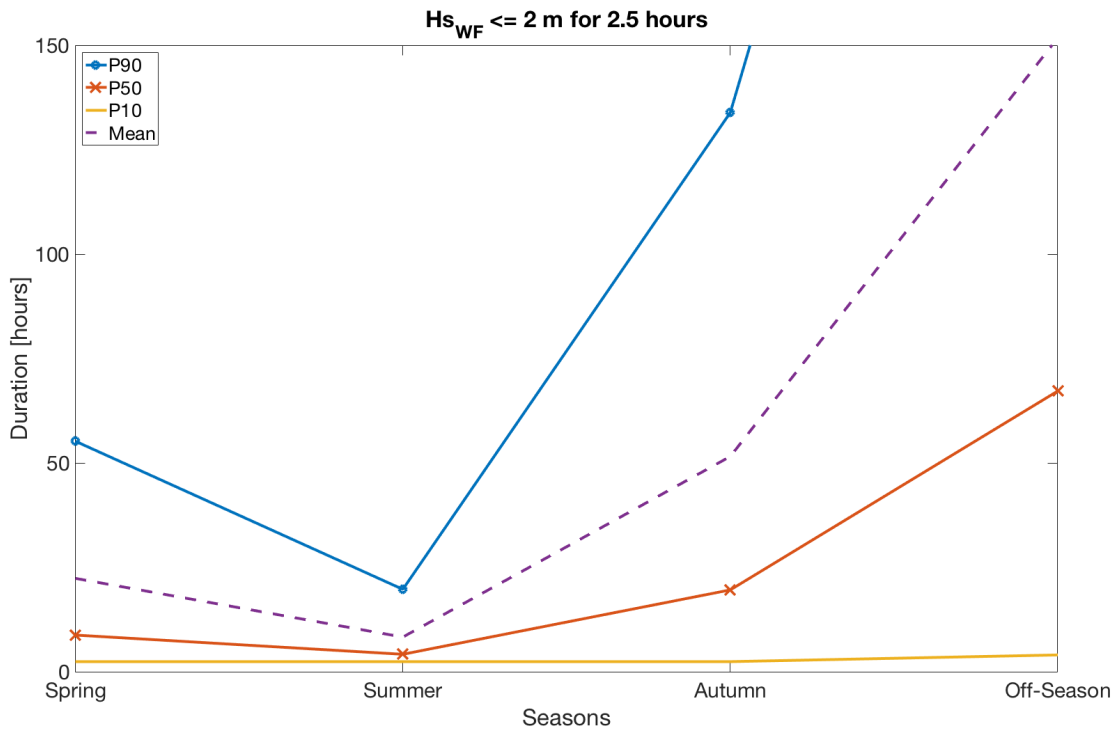


Figure 10.12: Actual duration of operation with random start at Heidrun,  $T_R = 2.5 \text{ hours}$ ,  $H_{s_{WF}} = 2 \text{ m}$

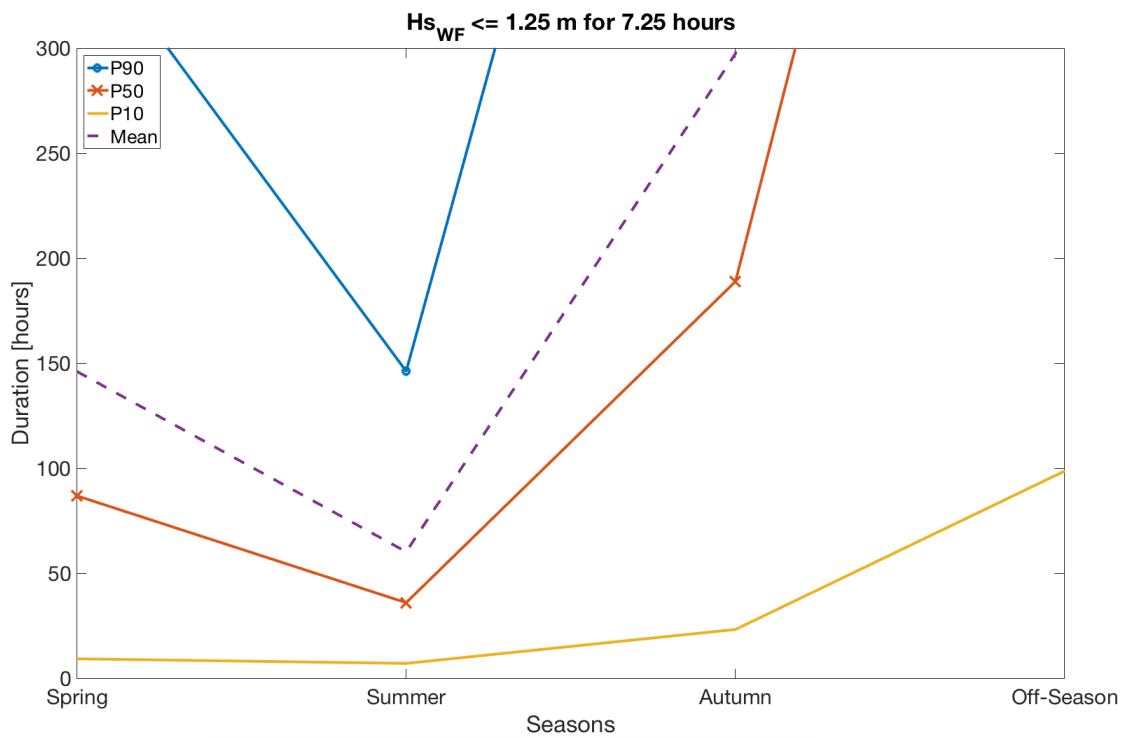


Figure 10.13: Actual duration of operation with random start at Heidrun,  $T_R = 7.25 \text{ hours}$ ,  $H_{s_{WF}} = 1.25 \text{ m}$

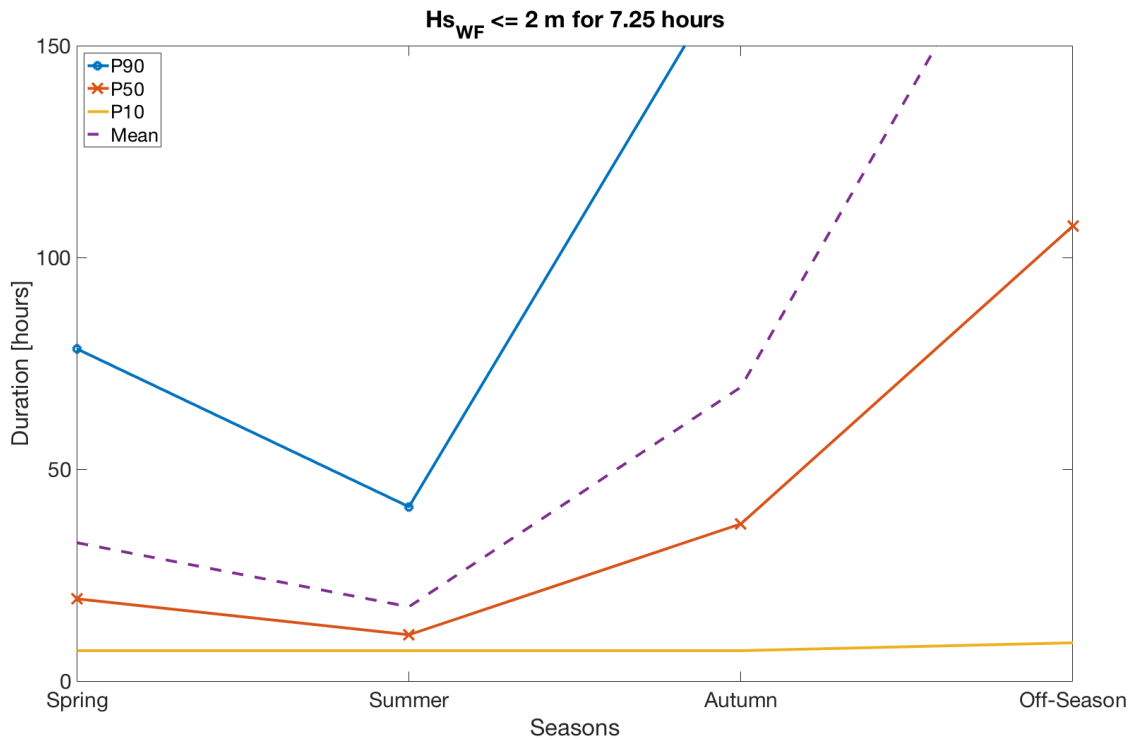


Figure 10.14: Actual duration of operation with random start at Heidrun,  $T_R = 7.25 \text{ hours}$ ,  $H_{s_{WF}} = 2 \text{ m}$

The actual duration of operation with random start at Tanzania, is visualised in Figure 10.15 and 10.16 for  $T_R = 9.3 \text{ hours}$  and  $H_{s_{WF}}$  of 2 m and 3 m respectively.

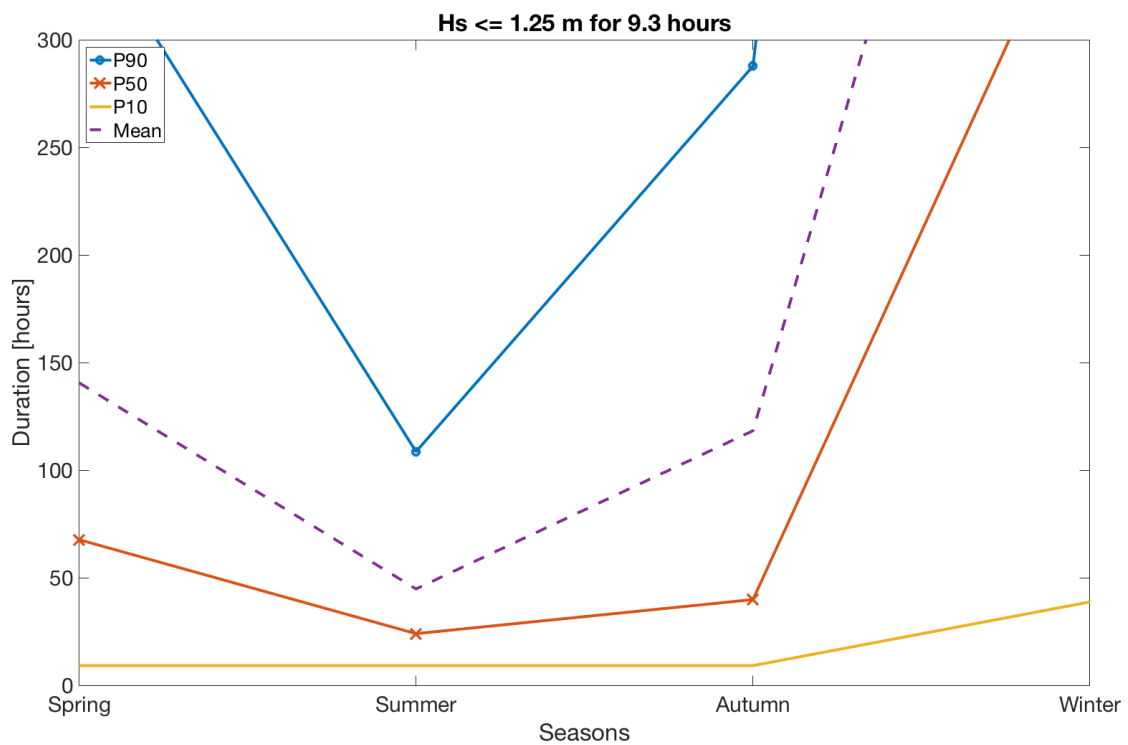


Figure 10.15: Actual duration of operation with random start at Tanzania,  $T_R = 9.3 \text{ hours}$ ,  $H_{s_{WF}} = 1.25 \text{ m}$

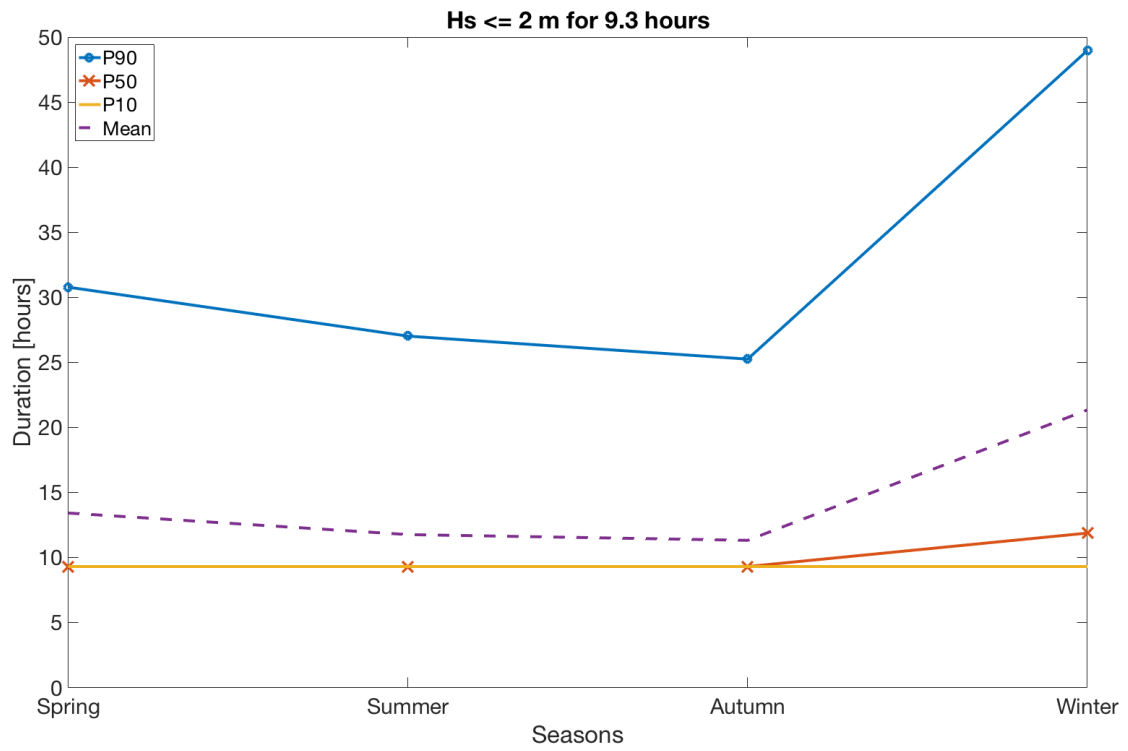


Figure 10.16: Actual duration of operation with random start at Tanzania,  $T_R = 9.3$  hours,  $H_{s_{WF}} = 2$  m



## 11 Model Validation

Model validation is performed in order to check whether the results from the simulations are reliable and accurate, and are checked up against the real model. It is important to check whether the assumptions that have been made are reasonable with respect to the real system, and to ascertain whether or not the model applies the assumptions properly within the simulation tool. Model validation should also be conducted in order to detect any mistakes that have been made during the modelling (Pearce, 2015). Model validation was performed on both input and output parameters, and are described in the following.

### 11.1 Static Analysis

To ensure that the model was implemented into SIMA in a proper way, the initial and static position of the cover were compared. The deviations are listed in Table 11.1.

Table 11.1: Static analysis positions

	Initial Position	Static Position	Deviation
<b>(x, y, z)</b>	(-24.5, 23.9, 11.8)	(-24.558, 24.412, 11.922)	(-0.2%, 2.1%, 1.0%)
<b>(rx, ry, rz)</b>	(0, 68, 90)	(0.028, 66.704, 88.882)	(2.8%, -1.9%, -1.2%)

A difference between initial and static position of less than 5% is usually acceptable (Zhao, 2017), and the implementation of all the coordinates were therefore considered adequate.

### 11.2 GRP Protection Cover

The cover was implemented in SIMA as slender elements with various dimensions. To ensure that correct volume, mass and hydrodynamic parameters were implemented properly, the total values were validated.

The total volume of all the slender elements was found by summation of the elements' product of specific volume and actual length. The total volume of the cover implemented in SIMA was 4.308  $m^3$ . The exact volume of the cover is 4.287  $m^3$ , that is a deviation of 0.5%.

The total mass was calculated with the same approach as for the volume, and found to be 11 899.96 kg. The exact mass of the cover was 11 901 kg, that is approximately 0% deviation.

The total implemented added mass and damping should be equal to the ones gathered from CFD-analysis, with an amplitude between 2.5 and 3 m. Total added mass in initial z-direction and y-

direction were calculated to be 653.5 t and 247.1 t respectively. Added mass from CFD-analyses with an amplitude of 2.5 m was approximately 660 t for  $A_{11}$  and 255 t for  $A_{22}$ . The total added mass deviated with approximately 1% and 3% respectively.

Total implemented linear and quadratic damping are listed in Table 11.2 and 11.3 respectively. The results from the CFD-analyses and the corresponding deviation are listed in the same tables.

Table 11.2: Linear damping validation

	Implemented	CFD-analysis	Deviation
<b>Surge</b> $B_{11}$	0.9 $kNs/m$	2.4 $kNs/m$	62.5%
<b>Sway</b> $B_{22}$	2.0 $kNs/m$	2.0 $kNs/m$	0.0%
<b>Heave</b> $B_{33}$	90.4 $kNs/m$	89.1 $kNs/m$	1.5%

Table 11.3: Quadratic damping validation

	Implemented	CFD-analysis	Deviation
<b>Surge</b> $B_{11}$	2.4 $kNs^2/m^2$	6.6 $kNs^2/m^2$	63.6%
<b>Sway</b> $B_{22}$	68.9 $kNs^2/m^2$	69.0 $kNs^2/m^2$	0.2%
<b>Heave</b> $B_{33}$	161.3 $kNs^2/m^2$	156.9 $kNs^2/m^2$	3.0%

### 11.3 Most Probable Largest Motion

Pursuant to DNV GL (2011b) Recommended Practice *DNV-RP-H102*, the most probable largest vertical single amplitude crane tip motion  $\eta_{ct}$  for an applied zero up-crossing period  $T_z$  can be taken as  $\eta_{ct} = 3.8\sigma_{ct}$  [m]. Hence  $\sqrt{2\ln(N)}$  should be equal to 3.8.  $\sqrt{2\ln(N)}$  was calculated to be 3.87, 3.76 and 3.94 for the three wave conditions *I*, *II* and *III* respectively. Hence the deviation was approximately 1%-4%.

### 11.4 Forces Acting on the System

In order to ensure reliable results from the simulations, *one* simulation was run without environmental loads as waves, wind or current. These results were compared against hand-calculated static tension in the lifting slings.

The rigging equipment's and cover's mass and weight are illustrated in a simplified rigging sketch in Figure 11.1. The cover's submerged volume was approximately  $4.3 m^3$ , that resulted in a fully submerged buoyancy force of 43.2 kN, acting in the opposite direction of the cover weight.

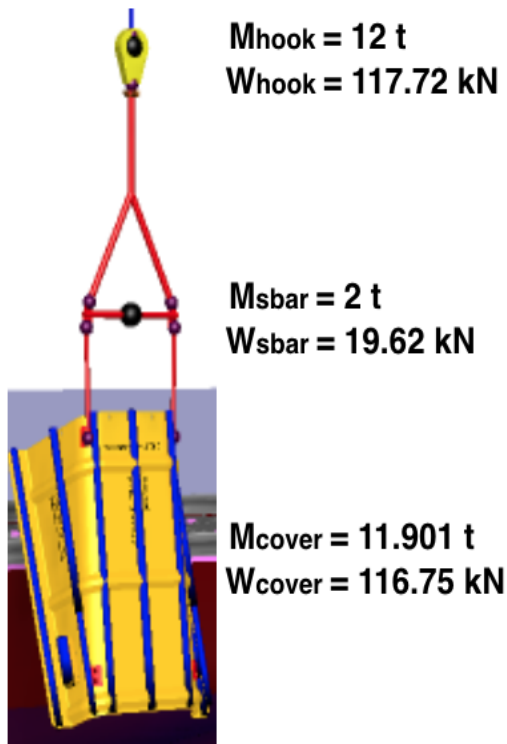


Figure 11.1: Forces on lifting equipment

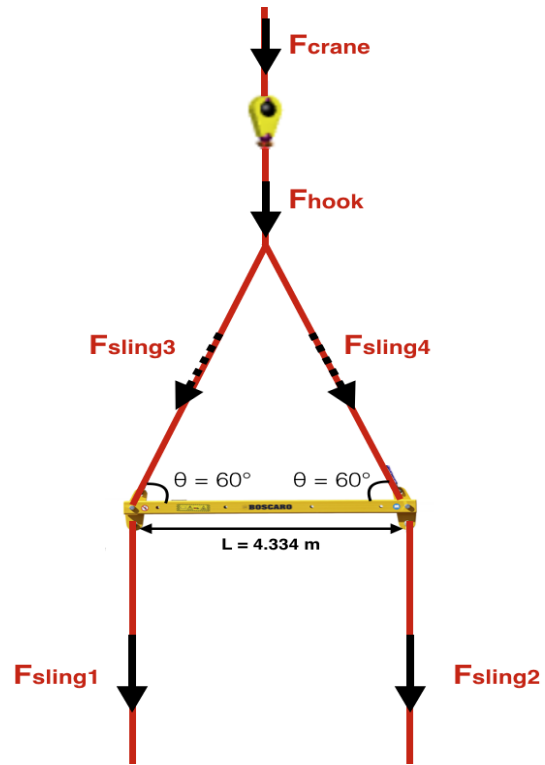


Figure 11.2: Defined forces of lifting equipment

There are six predefined forces acting on the system, as illustrated in Figure 11.2;  $F_{crane}$ ,  $F_{hook}$ ,  $F_{slings3}$ ,  $F_{slings4}$ ,  $F_{slings1}$  and  $F_{slings2}$ .

The force acting in the crane wire  $F_{crane}$  was the weight of the hook, spreader bar and cover, and was calculated as follows:

$$F_{crane,air} = (12t + 2t + 11.901t) \cdot 9.81 \frac{m}{s^2} = \underline{\underline{254.1 \text{ kN}}}$$

$$F_{crane,subm} = 254.1kN - 43.2kN = \underline{\underline{210.9 \text{ kN}}}$$

The force acting on the hook  $F_{hook}$  was the weight of the spreader bar and cover, and was calculated as follows:

$$F_{crane,air} = (2t + 11.901t) \cdot 9.81 \frac{m}{s^2} = \underline{\underline{136.4 \text{ kN}}}$$

$$F_{crane,subm} = 136.4kN - 43.2kN = \underline{\underline{93.2 \text{ kN}}}$$

Figure 11.3 shows the tension that arose in the crane wire and in the hook winch when the cover was lowered through the sea with no environmental loads. The tension in the crane wire was read off to be approximately 250 kN and 210 kN, in air and submerged respectively. The tension in the hook winch was read off to be approximately 135 kN and 93 kN, in air and submerged respectively.

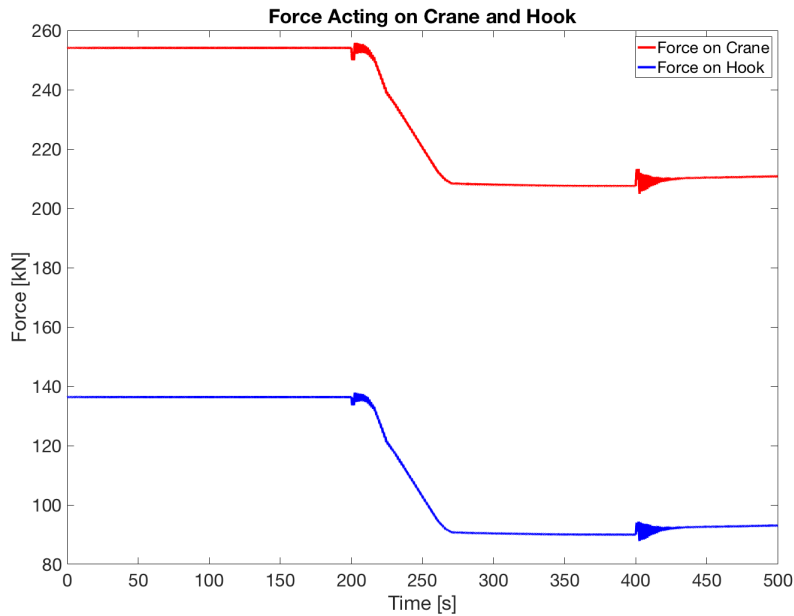


Figure 11.3: Forces acting on hook and tension in crane winch with no environmental loads

The vertical tension that arose in the hook winch was equally distributed between sling 3 and 4. The slings have an angle of  $60^\circ$ , hence the vertical tension was decomposed in order to achieve the axial tension  $F_{sling3}$  and  $F_{sling4}$  in sling 3 and 4 respectively.  $F_{sling3}$  and  $F_{sling4}$  were calculated as follows:

$$F_{sling3,air} = F_{sling4,air} = \frac{1}{2} \cdot \frac{136.4}{\sin(60)} = \underline{\underline{78.8 \text{ kN}}}$$

$$F_{sling3,subm} = F_{sling4,subm} = \frac{1}{2} \cdot \frac{93.2}{\sin(60)} = \underline{\underline{53.8 \text{ kN}}}$$

Figure 11.4 shows the tension that arose in sling 3 and 4 when the cover was lowered through the sea with no environmental loads.

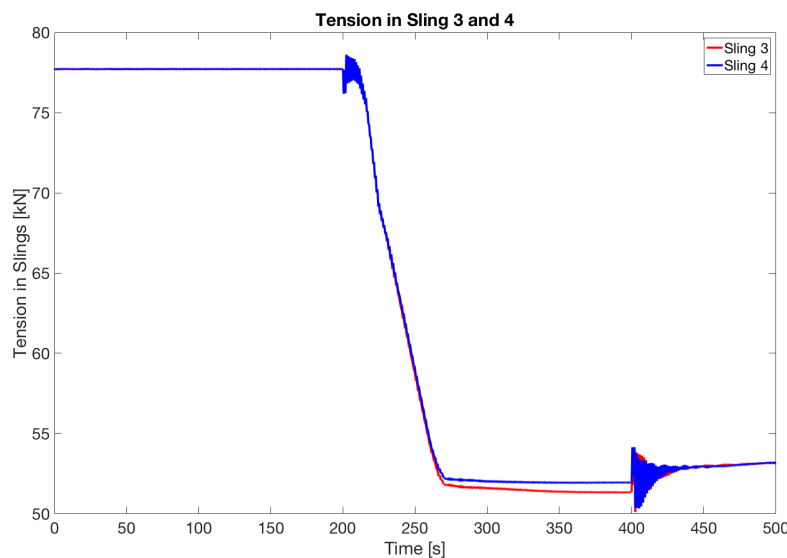


Figure 11.4: Tension arising in sling 3 and 4 with no environmental loads

The two axial forces in sling 3 and 4 were read off to be approximately 78 kN for the lifting system in air and 54 kN submerged.

The vertical tension in sling 1 and 2,  $F_{sling1}$  and  $F_{sling2}$ , was half the weight of the cover, and were calculated as follows:

$$F_{sling1,air} = F_{sling2,air} = \frac{116.75}{2} = \underline{\underline{58.4 \text{ kN}}}$$

$$F_{sling1,subm} = F_{sling2,subm} = \frac{116.75 - 43.2}{2} = \underline{\underline{36.8 \text{ kN}}}$$

Figure 11.5 shows the tension that arose in sling 1 and 2 when the cover was lowered through the sea with no environmental loads.

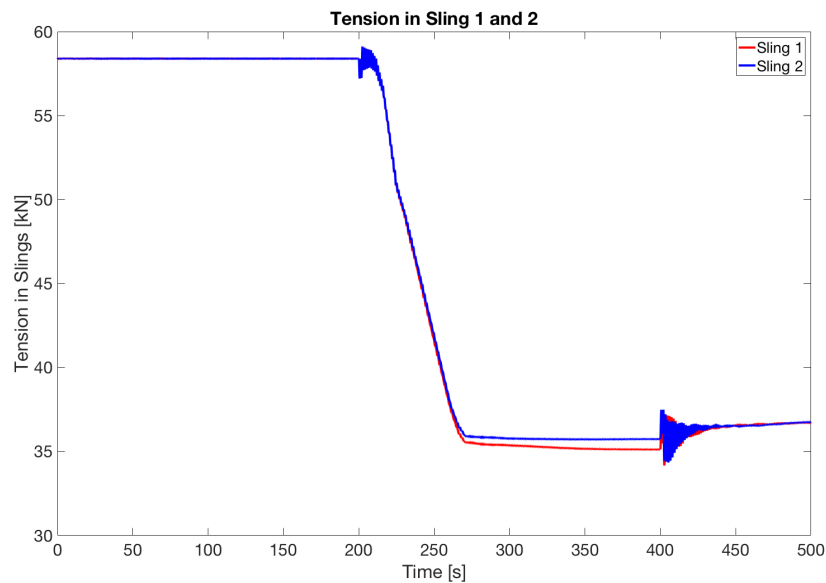


Figure 11.5: Tension arising in sling 1 and 2 with no environmental loads

The two axial forces in sling 1 and 2 were read off to be approximately 58 kN for the lifting system in air and 37 kN submerged.

The arising forces were found to be similar to the ones gathered by Solaas et al. (2016).

## 11.5 Operability

The operation's operability and downtime summed up to be 100% in all cases. The developed codes were therefore determined to be adequate.

## 11.6 Distributions

The mean and standard deviation found from the fitted Weibull distribution for the length of calms when  $H_{sLIM}$  was 2.5 m, are listed in Table 11.4. The mean and standard deviation obtained from the real data set can be found in the same table. The two means were found to be approximately equal, while the two standard deviations deviated with up to 14%.

*Table 11.4: Mean and standard deviation of calms for distribution and data set at Heidrun,  $T_R = 2.5$  hours,  $H_{sLIM} = 2.5$  m*

		Spring	Summer	Autumn	Off-season
<b>Distribution</b>	Mean	62.5	114.9	48.2	29.7
	Std	69.9	127.6	56.8	31.2
<b>Data set</b>	Mean	62.4	114.7	48.2	29.8
	Std	64.9	123.2	49.2	27.3

## 12 Discussion

The installation of a GRP pipeline protection cover is weather sensitive due to its low weight and large projected area. Even in low sea states the hydrodynamic forces can exceed the submerged weight and slack in lifting wires might occur. This can result in large snap loads. In order to increase the acceptable design criterion, ballast in terms of steel blocks were attached to the cover to increase its weight. The cover will also be installed at a steep angle to reduce hydrodynamic forces. The decisions and assumptions that have been made and the results gathered from this Master Thesis will be further discussed in the following.

### 12.1 The $\alpha$ -factor

The  $\alpha$ -factor is based on few locations but is used to plan operations worldwide. The wave conditions at Heidrun and Tanzania are highly different. The waves that arise outside Tanzania are rarely higher than 3 m, and the ones that arise outside Heidrun are significantly higher. Nevertheless, the same  $\alpha$ -factor is used. By using a local  $\alpha$ -factor instead of those gathered from the North Sea, more adequate operational criteria might be achieved at Tanzania. The water depth outside Tanzania is significantly deeper compared to Heidrun, and strong currents arise here. Therefore, an idea could be to use a factor for currents, instead of, or in addition to, the  $\alpha$ -factor for waves.

The  $\alpha$ -factor has not been revised since 2006, for many reasons because it will be an expensive and long process. The industry must be willing to invest in such a process, and for them to accept this, the return of the investment has to be positive. The changes in the  $\alpha$ -factors have to result in an economic benefit in terms of increased operational limits, that can extend the operational season and reduce the time for waiting on weather.

### 12.2 Weather Window

Generally, weather forecasts and thus the design criteria are based on the significant wave height  $H_s$  alone. The peak period of a wave series can be difficult to predict due to the combination of swell and local wind waves.  $T_p$  is therefore only in some cases used to plan an operation. During the actual operation it is up to the Captain and the Deck Foreman to decide whether the environmental conditions are within the planned operational criteria, in such a way that the operation can take place safely or not. This decision is based upon practical experience and the real motions of the vessel, in addition to the weather forecasts. In some cases, this decision results in a lower operational criterion than planned. A way of avoiding this can be by determine an operational criteria based on the actual response that will arise in the system.

## 12.3 Lifting Techniques

To decide whether or not heave compensation should be used during the operation, the possibility of resonance was investigated. It was assumed that a light lift of approximately 26 t, including the rigging equipment, followed a line below the green line in Figure 3.2. With a depth of 360 m it was assumed that no resonance would occur at Heidrun. At Tanzania the water depth was approximately 2 500 m and the system's resonance period was closer, but not equal to, the typical oscillation periods for crane tip motions. Hence it was decided that heave compensation systems were not necessary for this lifting operation.

It was determined that the GRP pipeline protection cover should be installed by a traditional over side crane operation. The installation is a light lift operation, hence special handling systems for heavy objects were omitted. A large number of protection covers have been and will be installed subsea. Thus, as long as the safety is ensured, the cheapest and easiest installation method is preferred. Not all vessels have a moonpool and in order to be independent on vessel accessibility, in terms of extra specifications, installation through moonpool and by use of LMHS was omitted.

## 12.4 The Simulation Model

### 12.4.1 Environmental Conditions

Due to the locations of Norway and Tanzania, with respect to equator, their seasons were occurring in the opposite time of the year. In Norway, the arising sea states are usually operable between April and October, and the implemented operational seasons were determined based on this.

The wave conditions at Heidrun and Tanzania are considerably different as shown in Figure 7.3 and 7.4. At Tanzania the waves do seldom exceed 3 m, and most of the waves are concentrated around 1 to 2 meter and 5 to 12 seconds. At Heidrun the waves are concentrated around 1 to 9 meter and 4 to 16 seconds. The wave conditions used in the simulation model were determined to be between 2 and 4 m and 5 and 15 s, based on counselling with supervisor. Wave conditions outside of these boundaries will most likely not occur, or be below the maximum design criteria.

The sea states that were used in the simulation model were characterised by a JONSWAP spectrum with cosine spreading with an exponent of 2, for 11 directions between 90° and 270°. A low cosine exponent will spread the wave energy evenly between the directions and result in a spectrum with a small peak. This is realistic for a marine operation that usually take place in normal sea conditions. Higher exponents are used for extreme wave conditions where the wave energy have a significant peak around 180°.

The simulations were performed for 58 different wave conditions. Some of the results from the



simulations were below the slack criterion, some were above and some were above even when slack occurred. In order to give a brief representation of the results, all results from one wave condition in each category were determined to be visualised. The selected wave conditions are listed in Table 8.1.

#### 12.4.2 GRP Protection Cover

The total volume of the slender elements implemented in the simulation model was  $4.308 \text{ m}^3$  while the total estimated volume of the CAD-model was  $4.287 \text{ m}^3$ , which is a difference of less than 0.5%. The deviation might have arisen due to simplification of the cover when it was implemented as slender elements into the simulation model. The cover mass was close to perfectly implemented in the simulation model, with a deviation of 1 kg.

The cover was lifted with an initial angle of  $68^\circ$  to the horizontal. This resulted in a maximum vertical length of the cover of 12.3 m, and was calculated by use of Pythagoras for the dimensions in the cover sketch in Figure 7.17.

#### 12.4.3 Hydrodynamic Parameters

Added mass is dependent on acceleration and wave amplitude. Hydrodynamic parameters as added mass and damping were analysed by use of WAMIT and CFD. The depth dependency of the hydrodynamic coefficients was estimated by use of WAMIT calculations for multiple draughts. The WAMIT analysis was performed for a sea state with zero amplitude, while CFD-analyses were performed for three wave amplitudes; 0.7 m, 1.4 m and 2.7 m, as shown in Figure 7.12-7.14. The added mass in sway  $A_{22}$  and in heave  $A_{33}$  did not vary much with amplitude. The added mass in surge  $A_{11}$  increased from 440 t to 680 t, when the amplitude increased from zero to 2.7 m. The added mass force is dependent on both projected area and acceleration, thus the added mass force is assumed to increase with greater area and amplitude.

Added mass and damping found from CFD-analysis with an amplitude of 2.5 m were implemented in SIMA through slender elements.  $A_{11}$ ,  $A_{22}$  and  $A_{33}$  for 2.5 m were 660 t, 255 t and 22 t respectively. The total implemented added mass in surge  $A_{11}$  and in sway  $A_{22}$  were 653.6 t and 247.1 t respectively, and respective deviations of 1% and 3% were seen. Added mass in heave was small compared to the added mass in other directions, and was therefore neglected.

Both linear and quadratic damping was found by CFD-analyses and implemented in SIMA. The deviations between damping found from CFD-analyses and damping implemented in SIMA were 1.5%-3% for  $B_{33}$ , approximately zero for  $B_{22}$  and approximately 60% for  $B_{11}$ .  $B_{11}$  was still small compared to damping in other directions.

The deviations from CFD-analyses to implementation in SIMA for both added mass and damping, are most likely due to the simplification that was done when the cover was implemented as slender elements into SIMA.

#### 12.4.4 Vessel and Crane Tip Motion

Due to the crane tip's location far away from the vessel COG, the crane tip motion was heavily affected by the vessel motion in its six degrees of freedom. Any motion in the crane tip will transfer to the rigging system and thus contribute to motion of the lifted object. Some motions cause more risk than others.

The vessel RAOs illustrate the vessel's eigenperiod for all motions in multiple directions. Resonance may occur if the sea state matches the vessel eigenperiod for a certain motion. This should be avoided at all time, and a combination of weather forecasts, experience and dynamic position of the vessel is used to prevent resonance.

Large vertical motions of the crane tip can result in sudden submergence of the lifted object and hence large slamming forces and potential slack in slings may occur. Vertical motion of the crane tip arises for the vessel's heave, roll and pitch motion and should as far as possible be prevented. The vessel's roll motion is shown in Figure 7.27 and has a significant peak for beam sea around 14.5 s. This peak period is very critical and should be avoided at all times in order to prevent large vertical motions of the lifted object. Heave compensation is often used to prevent vertical motion of a lifted object, but due to the cover's light weight heave compensation was omitted for this operation.

Sway motion of the lifted object is of huge risk because the cover may collide with the vessel side and get damaged. Sway motion should be prevented and tugger wires can be used to control such motion. Sway motion arises due to the vessel's sway, roll and yaw motion in addition to wind loads. The sway motion of the lifted object is dependent on the vessel's roll motion that has a peak around 14.5 s.

Surge motion of the lifted object will not be as risky as the two aforementioned motions, because the object is moving alongside the vessel. The crane tip surge motion is a result of the vessel's surge, pitch and yaw motion. The vessel RAOs in these motions do not have peaks of significant amplitudes, but the most critical pitch motion occurs for waves propagating  $68^\circ$  to the vessel with a peak period of approximately 7 s.

Because the rigging system consists of several components, each with six dofs, any motion may contribute to motions of the component, and hence result in critical situations as slack. Offshore lifts will always be a risk to personnel and equipment, and large motions should therefore be avoided at all times if possible.

As mentioned above waves are generated from both local wind and swell. Generally, weather

forecasts are based on local wind waves. Swell does usually have a greater peak period than local wind waves, thus the exact sea state can be difficult to predict. The operation was simulated for head sea. This will not always be the case in real scenarios, even when the vessel can reposition with dynamic positioning. Hence one should be aware of that the vessel motion, and thus the crane tip motion, can be significantly different from the simulated results.

## 12.5 Manual Estimation with the Simplified Method

The hydrodynamic force that determined the manually estimated design criteria was calculated by use of DNV GL's Simplified Method, and was dependent on several hydrodynamic parameters such as; added mass, drag, slamming and varying buoyancy. The Simplified Method assumes that the vertical motion of the lifted object dominates thus all other motions can be disregarded. The design criterion was therefore determined based on the total hydrodynamic force in vertical direction. The largest tension variations in the slings occurred right after the cover was fully submerged, hence the hydrodynamic force was calculated for an immediately fully submerged cover.

The time series of the crane tip motion in Figure 8.1-8.3 were calculated by use of the rigid body equation. The crane tip motion was greater than the vessel motion for all wave conditions, but was definitely greatest for higher significant wave height and longer wave period. Short wave periods resulted in more frequent vessel motion and crane tip motion. The hydrodynamic parameters were dependent on the most probable largest crane tip motion  $\eta_{ct}^{max}$ , that should occur only *one* time during a time series.  $\eta_{ct}^{max}$  does not occur in any of the time series, but it can be seen that there is *one* peak that is close to  $\eta_{ct}^{max}$ .

### 12.5.1 Added Mass

The added mass is highly dependent on the projected area of the submerged part of the cover. Minimum added mass will most likely occur when the cover is lifted in such a way that the projected area is minimised. Hence the cover was lifted with an angle to the flanges of  $68^\circ$  and an angle to the cover roof of  $81^\circ$ .

The total vertical added mass force accelerates in vertical direction. In order to yield the added mass force normal to the rotated cover, the acceleration was decomposed. In order to get the exact vertical force from the added mass, a new decomposition was needed, as seen in Figure 8.4. The total added mass in vertical direction was the sum of the vertical components of the perpendicular  $A_{11}$ -force and the longitudinal  $A_{33}$ -force.  $A_{11}$  and  $A_{33}$  were calculated to be 422 t and 32 t respectively and with an angle of  $68^\circ$  and  $22^\circ$ , the total vertical added mass was 86.73 t.

The WAMIT results deviated with 18 t and 9 t from the manually estimated parameters for  $A_{11}$  and  $A_{33}$  respectively. The deviation was most likely due to the cover's inclined shape. The manually

estimated added mass was not based on an inclined plate, because only estimates for flat plates are given rules or standards. The WAMIT analysis was on the other hand performed for the cover positioned in the free surface with an angle of  $68^\circ$  to the horizontal. Development of rules and standards for inclined plates should be investigated, but due to the small deviation the profit and benefit from doing this should be carefully looked into.

### 12.5.2 Manually Estimated Design Criteria

The largest tension variation in the slings occurred right after the cover was fully submerged, in the interface between two lifting phases; through splash zone and fully submerged. Slamming and varying buoyancy will not occur when the cover is fully submerged, but were calculated in order to determine whether or not they were of significance.

The total hydrodynamic force was dependent on the sum of the drag and slamming force, and the difference between the inertia and the varying buoyancy force. Thus the two pairs of forces were compared. The varying buoyancy was 7-10% of the inertia force and the slamming force was approximately 25% of the drag force. The slamming and varying buoyancy forces seemed to be moderate but not dominating.

The design criteria could be found by use of linear scaling if the hydrodynamic force was proportional with the water particle velocity. The slamming force was dependent on the squared slamming velocity, thus linear scaling would not have been an adequate approach if the slamming term was included. With the fact that slamming and varying buoyancy most likely would not occur for a fully submerged cover, the two terms were omitted. Hence linear scaling could be used as an adequate method to determine the design criteria. The estimated design criteria was not significantly affected by the omission.

The inertia force was the dominating term in the total hydrodynamic force for all wave conditions. The design criteria deviated with approximately  $\pm 5\%$  for the different wave conditions. The design criterion was therefore determined to be the average of 1.643 m, independent on  $T_p$ .

## 12.6 Installation Simulation

Pursuant to DNV GL's rules and standards for determination of marine operation design criteria, computer programs applying non-linear time domain simulations should be used for accurate solutions and the largest and smallest observed tension in slings should be stated (DNV GL, 2011b). SIMA met these requirements and was determined to be an adequate simulation tool for such simulations. Due to the cover's light weight, the risk of exceeding the rigging equipment's material strength was not present. Hence maximum loads in slings were not critical and thus omitted in this Master Thesis. However, maximum loads should be looked into before the design criteria can be

accepted.

The crane winch started to run first after 200 s. This was done in order to make the global system stable before the installation of the cover started. Usually, a simulation needs some time to reach equilibrium when it starts to run.

The simulation started with the cover's lower end hanging 2.2 m above sea surface. With a winch speed of 0.2 m/s the cover should have reached the sea surface after 11 s. During one simulation the cover did reach the sea surface after 9 s. The crane tip motions have amplitudes between  $\pm 1$  m between 200 and 210 s. Thus it is reasonable to say that this submergence deviation is due to waves and crane tip motion.

The environmental conditions that determine the design criteria will be different at Heidrun and Tanzania. Waves will play a significant role at Heidrun while current loads will be an issue at Tanzania. The through splash zone simulation with waves characterised by a JONSWAP spectrum and no current will be a good model if the operation is carried out at Heidrun. A simulation model for the operation at Tanzania should include current loads, and the simulation should last for a longer duration, where the lowering phase of the object is in focus. Potential offset will be of high risk and may determine the operational criteria at Tanzania.

### 12.6.1 Motions

Large motions of the spreader bar and cover were observed in the in-air phase because no tag or tugger wires were used in the simulation. In real life scenarios these motions can be controlled by the crane operator, and will therefore be significantly smaller.

For some sea states the spreader bar was exposed to such a large acceleration in sway that the simulation failed. Usually, the failure rate was higher for sea states with higher significant wave height and shorter peak periods. The spreader bar had four connection points to four slings, where each point consisted of six degrees of freedom. The spreader bar's stiffness matrix was large and its motion was affected by local motion in each sling. Lower peak periods did result in more frequent motions of all lifting equipment. Thus the spreader bar motion exceeded the limits of the simulation tool.

In order to reduce the failure rate, damping was added to the spreader bar's global yaw motion. The damping did not result in less failures, and it is therefore assumed that the damping was either too small or implemented incorrectly. Due to the simulations' high failure rates, extra simulations with several extra seed numbers were needed to be run in order to yield enough results to develop acceptable extreme value distribution. This was time consuming and should definitely be further looked into.

According to Figure 9.12-9.20 the motions of the spreader bar contributed to cover motion, but

the cover motion did not necessarily contribute to the spreader bar motion. The spreader bar and cover did experience heavy rotation during the in-air phase. Wind was not added to the simulation model, thus it is expected that the spreader bar and cover motion will increase if wind loads are implemented. In order to decrease this rotation, stiffness was added to the spreader bar in yaw motion. As a result, the rotations decreased significantly, as seen in Figure 9.21-9.23, but the tension and the forces in the system did also change. If a simulation with stiffness should be used for further analyses, the arising tension and forces should be investigated once more in order to achieve adequate results.

The motions calmed down when the cover entered the water. When the cover was submerged the hook motions increased and contributed to motions of slings, spreader bar and cover. Figure 9.24-9.29 show that the tension variation in the crane wire, hook winch and the four slings increased when the cover entered the splash zone, and calmed down when the cover was lowered to approximately 20 m.

## 12.6.2 The Gumbel Distribution

Tension variation arose in the slings when the cover entered the sea surface. This is due to hydrodynamic forces that suddenly starts to act on the system. The largest tension variation in the slings occurred right after the cover was fully submerged. A slack condition occurred when the tension in the slings was below 10% of the submerged weight of the cover. This was assumed to be an adequate safety level with respect to the load factors and load combinations stated at DNV GL's ultimate limit strength criteria. If slack occurred in more than 10% of the simulations for a given  $H_s$  and  $T_p$ , the sea state was determined to be non-operational. According to this slack could occur during a simulation even when the sea state was defined as operational.

Non-operational and operational sea states were determined by use of the Gumbel distribution. Two Gumbel parameters determined the Gumbel PDF and CDF, and hence the quantile function. The parameters varied with the sample size, thus the converged parameters should be used to create all the distribution functions. A sea state was operational if the quantile was above 10% and non-operational if the quantile was below 10%. Because the quantile changed with different Gumbel parameters, the 10% quantiles for each sling were plotted. Convergence was assumed if the 10%-quantile deviated with 7% or less. In some cases, e.g. condition 1, the 10%-quantile did not converge, but it can be clearly seen in Figure 9.30 that the 10%-quantile for sling 1 will be less than the slack criterion at all times, and this will most likely not change with a further increased sample size. Hence some exceptions were made in terms of convergence.

The Gumbel PDFs developed from the converged parameters did have a negative skewness for all wave conditions. This should be the case when the extreme values are based on minima instead of maxima. If 10% of the area below the PDF was below the slack criterion, the sea state was

categorised as non-operational. It was usually sling 1 that exceeded the slack criterion and thus determined the maximum operational sea state.

In order to determine whether or not the Gumbel distribution was a good fit to the extreme values, a Gumbel-plot was developed. Empirical values dependent on the sample size were plotted and fitted to a linear line based on *the least squared method*. The Gumbel-plot was only created for the tension in sling 1 because this was the most critical sling in all wave conditions. The empirical Gumbel-plot was similar to the linear line made from the Gumbel parameters, and thus the Gumbel distribution was found to be a good fit to the extreme values obtained from the simulations.

By comparing the results from the simulation by hand calculations it is clearly evident that the total forces and tension in the system were correctly distributed in the various components and slings. Hence the simulation model in SIMA was adequate.

Even when the simulations were run without any environmental conditions during model validation, tension variation occurred twice in the lifting equipment, as visualised in Figure 9.6 and 9.7. The tension variation is due to acceleration when the crane winch started and stopped. The magnitude is approximately  $\pm 1\%$  of the converged tension and is therefore not a big issue compared to other arising forces.

### 12.6.3 Slack and Snap Loads

As mentioned above slack conditions did occur in some operational sea states. Appurtenant to DNV GL's Recommended Practice H103 snap forces shall be avoided as far as possible, and the hydrodynamic force can therefore not exceed 90% of the submerged static weight of the lifted object. Snap forces did arise after slack during the simulations, but the snap forces did not exceed 100 kN, which is far away from the sling's material strength. According to this one can say that snap forces are not always critical, and the criterion should not always be as strict as it is. However, slack can be critical in some cases. When the tension disappears the sling can bend, which can result in fibre damage and decrease in material strength. The lifted object can also move uncontrolled in all degrees of freedom when the sling tension disappears.

The slack criterion should be further investigated and challenged. In some cases, it does not necessarily need to be so strict, if snap loads, bending and uncontrolled motions do not occur.

### 12.6.4 Simulated Design criteria

Large snap loads were not observed and the rigging system consisted of light equipment, hence the the design criteria were only investigated for minimum tension in slings.

The simulated design criteria varied with  $T_p$  and were determined based on simulation results for

$H_s$  between 2 and 4 m. In order to plot the simulated design criteria towards the manually estimated design criteria, the simulated graph was elongated to 1 m and 4 s, as illustrated in Figure 9.42. The design criteria were plotted towards the wave conditions that would actually occur at Heidrun, gathered from the conditional characteristics in Figure 7.3. The non-operational wave conditions are below the blue line, but since wave conditions below the yellow line would not occur, the actual waiting conditions will be between the two lines.

The manually estimated design criterion was plotted into the same figure, and by use of this criterion it can be seen that the operational wave conditions decreased to approximately one third of the simulated operational conditions.

## 12.7 Planning

The lifting operation was divided into phases that were given separate  $T_{POP}$ . The lift-off and in-air phases were determined to last for 15 minutes in total. The landing phase at Heidrun was also determined to be 15 minutes. The landing phase at Tanzania was determined to be 45 minutes in order to be able to relocate the cover in case of potential offset.  $T_{POP}$  of the lowering phase was determined based on the which speed of 0.2 m/s. 15 minutes was added in order to account for loosening sea fastening and prepare rigging. This can sometimes be performed before the operation starts. The whole operation's  $T_{POP}$  was determined to be 1 hour and 15 minutes at Heidrun and 4 hours and 40 minutes at Tanzania.  $T_C$  was determined to be equivalent to  $T_{POP}$  because the required time for contingency situations was not assessed in detail. According to DNV GL (H101)  $T_C$  less than 6 hours is not usually acceptable. The difference in operability and actual duration of operation with  $T_C = T_R$  and  $T_C = 6$  hours will be further discussed in the following.

### 12.7.1 Operability

In order to have an efficient planning process one should have some knowledge about the environmental conditions at the operation field. At Tanzania the waves do not exceed 3 m, but there is a significant difference in the operability for  $H_{SWF}$  of 1.25 m and 2 m, as one can see in Figure 10.3. The time series is given for four years where each peak represent the winter season at one year. Lower significant wave heights will arise during summer compared to winter at both fields. Thus, operations with strict operational criteria should take place during summer season. At Tanzania it will be of high importance trying to increase the  $\alpha$ -factor, and hence the operational criteria, up to approximately 3 m where the operability increases to 100%. A further increase of  $H_{SWF}$  will be pointless. At Heidrun it will be of high importance trying to increase the operational criteria as much as possible, in order to extend operational seasons. The money should therefore be spent wisely during the planning process, dependent on its operation location.



At Heidrun there is a distinct season variation in terms of duration of calms, as seen in Figure 10.4. During spring and summer the duration of calms exceed 500 hours and is therefore not shown in the figure. At Tanzania the season variation is not as clear as for Heidrun.

At Heidrun there is also a significant season variation in terms of operability, as seen in Figure 10.7. An increase of the operational criteria can result in an extension of the operational seasons, which is the time of the year where the installation can be carried out. At Tanzania this is not entirely the case because there are small differences in season operability, except from the winter season. Despite this, there are large differences between the operability for a design criterion  $H_{sLIM}$  of 1.64 m and 2.5 m at both locations. For such an increase in  $H_{sLIM}$  and hence  $H_{sWF}$ , the operability at Heidrun and Tanzania increases with 50-70% for all seasons. The operability at Tanzania converges towards 100% for  $H_{sLIM}$  of 3 m.

The time of waiting on weather is due to both storm periods and calm periods of shorter duration than the reference period, also called *Calm-Wait* periods. Both at Heidrun and Tanzania the contribution from *Calm-Wait* was minimal, because the duration of the operation was quite short.

Due to the ratio between the light weight of the cover in air and the large added mass and drag forces that arose when the cover was submerged, strict design criteria were given to the operation. The simulated design criterion was determined to be 2.5 m for all  $T_p$ . For a level B marine operation with  $T_{POP}$  less than 12 hours, the  $\alpha$ -factor was found to be 0.76 for  $H_{sLIM} = 1.64$  m and 0.81 for  $H_{sLIM} = 2.5$  m. Hence  $H_{sWF}$  was 1.25 m and 2.03 m respectively. The differences in operability by use manual estimation and simulation are listed in the tables below for Heidrun and Tanzania.

Table 12.1: Operability at Heidrun for manually estimated and simulated design criteria

Season	Manually Estimated	Simulation	Deviation
Spring	21%	59%	38%
Summer	39%	80%	41%
Autumn	11%	41%	30%
Off-Season	3%	19%	16%

Table 12.2: Operability at Tanzania for manually estimated and simulated design criteria

Season	Manually Estimated	Simulation	Deviation
Spring	40%	98%	58%
Summer	70%	99%	29%
Autumn	62%	98%	36%
Winter	10%	85%	75%

The operability increases significantly during all seasons at both Heidrun and Tanzania when the design criterion increases from the manually estimated one to the simulated one. But the operability will still be low at Heidrun during autumn and off-season.

If DNV GL's recommendation of having  $T_C$  of 6 hours is taken into consideration,  $T_R$  increases to 7.25 hours. The operability did not change much when  $T_R$  increased from 2.5 hours to 7.25 hours.

By categorising the installation as a level A marine operation and introduce a meteorologist and monitoring systems (*m&m*), the  $\alpha$ -factor increased significantly. At Heidrun, where  $T_{POP}$  was less than 4 hours, the  $\alpha$ -factor was calculated to be 0.932 for  $H_{SLIM}$  of 1.64 m and 0.96 for  $H_{SLIM}$  of 2.5 m. Hence  $H_{SWF}$  was calculated to be 1.53 m and 2.4 m respectively. The operability at Heidrun increased with approximately 15-20% for the manually estimated operational criterion and approximately 10% for the simulated operational criterion for all seasons. Before the operation should be categorised as a level A operation with *m&m* systems, the expenditure from introducing such systems should be compared to the profit from increasing the operability and WOW reduction.

### 12.7.2 Distribution

The Weibull distribution was fitted to the length of calms by use of the method of moments of expected value and standard deviation. Both Weibull parameters varied with increased  $H_s$ . At Heidrun, when  $T_R$  was 2.5 hours, the shape parameter  $\beta$  was close to 1 for all seasons, except off-season. Hence the distribution of the length of calms was similar to a decreasing exponential distribution, as shown in Figure 10.9. The scale parameter  $\gamma$  varied between 31 and 11 for the different seasons when  $H_{SWF}$  was 2 m. A large scale parameter will stretch out the probability density function which indicates that the length of calms was widely spread. When  $T_R$  increased to 7.25 hours, the shape parameter did also increase, and the distribution changed shape to a positively skewed distribution with one peak, as shown in Figure 10.10.

At Heidrun the mean length of calms did not vary much when  $T_R$  increased from 2.5 hours to 7.25 hours. However, the length of calms deviated significantly between the two different  $H_{SWF}$ . By increasing the operational criteria from the 1.25 m to 2 m, the mean wait periods decreased with up to 5 days.

The standard deviation was slightly greater than the mean for all conditions, thus there is evidence to believe that the length of calms was fairly spread out. This complies well to the Weibull parameters. The mean and standard deviation gathered from the Weibull distribution were compared to the ones found from the real data set. The means were approximately equal while the standard deviations deviated with up to 14%. Hence the real data set is slightly less spread out.

In order to determine whether or not the length of calms fitted the Weibull distribution, an empirical Weibull-plot was developed. The empirical points were dependent on the sample size. The time

series were given with a three-hour interval, hence the length of calms for  $T_R$  of 2.5 hours were 3, 6, 9,... etc. hours long. The double natural logarithm of the estimated probability  $\ln(-\ln(1-\hat{F}))$  was plotted on the y-axis. The maximum empirical value was plotted for each  $\ln(\tau_c)$ . The empirical points were close to the linear line from the Weibull distribution, hence there are evidence to say that the length of calms fitted the Weibull distribution certainly. The distribution of the length of calms were only visualised for Heidrun, but the length of calms at Tanzania did also fit the Weibull distribution.

### 12.7.3 Actual Duration of Operation with Random Start

The actual duration of operation  $T_{op}$  was based on an operation that is carried out at a random time, and was the total duration of the operation in addition to any appurtenant waiting periods. Waiting occurred when  $H_s$  was above the operational criteria or the calm period was of shorter duration than the reference period. The method of moments was used to fit  $T_{op}$  to a Weibull distribution. For all wave conditions  $T_{op}$  was found to fit the Weibull distribution adequately.

The actual duration of operation decreased during summer and increased during autumn and even more during winter/off-season. It is desirable to have a total duration of operation close to the reference period in order to minimise waiting on weather. The actual duration of operation was found for several probabilities; 10%, 50% and 90% in addition to the mean for both the manually estimated and the simulated operational criteria. For an operation taking place during spring at Heidrun with  $H_{s_{WF}}$  of 2 m and  $T_R$  of 2.5 hours, there was a 90% probability that the duration of operation was less than 55 hours, a 50% chance that the duration of operation was less than 9 hours and a 10% chance that the duration of operation was 2.5 hours. The respective WOW-periods were 52.5 hours, 6.5 hours and 0 hours.  $T_{op}$  was widely spread out because the probability that the operation lasted for more than 55 hours was equivalent to the probability that there was no waiting at all.

By decreasing the operational criterion to 1.25 m at Heidrun,  $T_{op}$  increased with approximately 80% for all seasons. For constant  $T_R$  this means that the WOW-periods will increase with the corresponding. Even during summer there is a 90% probability that the operation will last for up to 115 hours, which means that one has to wait more than 4 days in order to safely carry out the operation with an initial duration of 2.5 hours.

When  $H_{s_{WF}}$  was 1.25 m at Tanzania, there was a 50% probability that the waiting time was 70 hours during spring, which is equal to approximately *three* days. If the operational criterion increased to 2 m, the probability for zero waiting was 50%.  $T_{op}$  stabilised more for all probabilities when the operational criterion increased, which compiles with the operability plots and the wave conditions at Tanzania.

When  $T_R$  increased from 2.5 hours to 7.25 hours, the actual duration of operation with random start did also increase. However,  $T_{op}$  did for many probabilities increase with more than the difference of

4.75 hours, hence the WOW-periods became longer for increased  $T_R$ .

The simulated design criteria were both  $H_s$  and  $T_p$  dependent. The variation in operability between the upper and lower limit of the criteria was considerable. For a peak period of 5 s the design criterion was 2 m and the operability was 40-80% for the three operational seasons; spring, summer and autumn. For a peak period of 11 s the design criterion was 4 m and hence the operability was 85-98% for the three operational seasons. By being able to predict and rely on an actual wave peak period, the operability can be increased with up to 45%.

## 12.8 Error Sources

Errors will always be present when working with a model. It is not possible to make a perfect model of a real system and some of the assumptions that are introduced will result in modelling errors. However, if the assumptions are adequate and reliable, these errors will be limited.

Average operability is found on season basis, and because of leap years small deviations will be present in the operation's operability, WOW and actual duration of operation.

Wind and current have not been included in the planning process. For light structures wind can limit the operational criteria in the in-air phase, and current can result in large offset which will increase  $T_{POP}$  due to relocation of the cover. The simulated design criteria gathered in this thesis will therefore not be 100% reliable.

Uncertainties have arose in the choice of applied analysis method and coefficients. During manual estimation of the design criteria the hydrodynamic parameters were calculated by linear wave theory for regular waves. Real waves are irregular and non-linear, but manual estimations based on this theory is difficult and time-consuming, and should be considered when the operation is simulated, which they were.

The manually estimated added mass is calculated based on many assumptions. Surface effects and the cover wall's affect are neglected and the effect of water trapped inside the cover is not taken into consideration. These assumptions introduce errors that will follow in further calculation for the total hydrodynamic force.

Added mass and drag coefficients are well known for two-dimensional and three-dimensional compact bodies with simple geometry. They are adequately well understood for two-dimensional porous plates, but not for three-dimensional complex structures. The manually estimated hydrodynamic parameters are therefore not equal to the ones gathered from WAMIT and CFD-analyses.

The drag coefficients given by DNV GL are valid for a steady current, and corrections must be made for oscillatory flow. According to this, errors will be introduced. Some deviations have also occurred due to rounding errors.

## 13 Conclusion

Three wave conditions were described in this Master Thesis, where each one was either below the calculated slack criterion, above or above even when slack occurred.

Hydrodynamic parameters were manually estimated by use of DNV GL's Simplified Method. Crane tip motions were affected by the vessel motion and the most probable crane tip motion was determined to be 1.1 m, 3.0 m and 0.4 m for the three selected wave conditions.

The longitudinal and perpendicular added mass were double decomposed in order to allow for the cover's installation angle of  $68^\circ$ . The total added mass in vertical direction was calculated to be 86.7 t. Slamming was calculated for a flat plate with an angle of  $75^\circ$ , that is the average angle between the cover flanges and roof. The slamming force was small compared to the inertia force and was determined to be omitted in the simulation model. Due to fully submergence of the cover the varying buoyancy force was also omitted.

The manually estimated design criterion  $H_{S_{LIM}}$  for a GRP pipeline protection cover installation was found by use of linear scaling, and calculated to be 1.64 m, independent on  $T_p$ .

The installation of the cover was simulated in SIMA for several wave conditions, dependent on  $H_s$  and  $T_p$ . Only the *through splash zone* phase for was simulated. 20-30 lowering simulations were performed for each  $H_s$ - $T_p$  condition, with random seed numbers. The cover was exposed to large motions in air and the largest tension variation arose just after the cover was fully submerged. The converged 10% quantile from the Gumbel quantile function determined the simulated design criteria. Condition 1 was found to be below the slack criterion, where there was more than 10% chance of experiencing slack. Condition 2 and 3 were found to be above the slack criterion, but condition 3 experienced slack without exceeding the 10% requirement. The simulated design criteria were dependent on both  $H_s$  and  $T_p$  and were found to be significantly higher than the manually estimated design criteria. An average simulated design criterion was determined to be 2.5 m. The Gumbel distribution was found to be a good fit to the extreme values obtained from the simulations.

It was determined that the cover should be installed by a traditional over side crane operation. The installation was determined to be a level B marine operation.  $T_{POP}$  at Heidrun was 1 hour and 15 min and  $T_{POP}$  at Tanzania was 4 hours and 40 min. Hence  $T_R$  was 2 hours and 30 min, and 9 hours and 20 min respectively.

At Heidrun there was seen a significant season variation in terms of operability. At Tanzania the season variation was moderate but not significant. The operability increased with approximately 30-40% for spring, summer and autumn at Heidrun when  $H_{S_{WF}}$  increased from 1.25 m to 2 m. At Tanzania the operability increased from approximately 45% to 95%. Further increase of the operational criterion at Tanzania will be unnecessary in terms of operability.

By extending  $T_R$  to 7.25 hours the operability decreased with 1% during all seasons. Hence DNV GL's recommendation about having  $T_C$  greater than 6 hours can be implemented without affecting the operability significantly.

By upgrading the installation to a level A operation with meteorologist and monitoring systems, the  $\alpha$ -factor increased considerably. The operability increased with up to 20% for the manually estimated operational criterion and approximately 10% for the simulated operational criterion. Monitoring systems and a meteorologist should be used if the profit of increasing the operability is greater than the expenditures of implementing such systems.

Both at Heidrun and Tanzania the reason of WOW was usually due to *Storm* periods and not *Storm-Wait* or *Calm-Wait* periods. The planned length of the operation was therefore not an issue.

The actual duration of operation with a random start  $T_{op}$  decreased with approximately 80% when  $H_{SWF}$  increased from 1.25 m to 2 m. With a constant reference period, WOW increased with the corresponding. WOW increased when  $T_R$  increased to 7.25 hours for both the manually estimated and simulated operational criteria. The duration of operation was heavily season dependent, where WOW decreased towards summer and increased towards autumn and off-season/winter. For both fields there was a 10% probability of zero waiting during spring, summer and autumn for an operation with  $H_{SWF}$  of 2 m.

Both the length of calms and the actual duration of operation fitted a Weibull distribution by use of the method of moments.

The operational limit was determined by several factors; the installation method, the environmental conditions, the crane tip motion, the  $\alpha$ -factor and the tension airing in the slings. According to this one can say that an operation should be short in order to be able to take place often. For increased operational criteria the operability increased and waiting on weather decreased. The  $\alpha$ -factor should therefore be determined carefully.

If the operation should take place at a random time, waiting on weather will increase. Usually, a marine operation is planned ahead of execution and is based on weather forecasts. Such planning will often reduce waiting on weather and increase the operation efficiency, as shown in Figure 10.7 and 10.8.

In order to determine the highest operational sea state as possible, in such a way that waiting on weather can be reduced, simulations should absolutely be performed prior to installations of pipeline protection covers. Hence operational costs, engine idling and pollution can be significantly reduced compared to only relying on the simplified method.

## 13.1 Recommendations for Further Work

In order to do the simulations more efficiently, the reason for failures for short peak periods should be further investigated. If stiffness is added in order to decrease rotation of the spreader bar, all simulations should be run again due to changes in sling tension. Motions can also be reduced by increasing the weight of the lifting equipment. This will change the dynamics of the whole system and thus all simulations should be performed again.

SIMA should in the longer term be able to take in amplitude dependent hydrodynamic parameters, in order to ensure accurate added mass and damping for a certain sea state.

The motions that occur due to wind should also be investigated before the operation can be executed. The use of tugger wires should be taken into consideration if large motions in air is a problem.

The manually estimated design criteria is significantly lower than the simulated one. Hence the Simplified Method should be further looked into for complex geometries, and empirical values for inclined plates should be listed. An installation of a GRP pipeline protection cover is a common marine operation. However, no empirical values of tension and forces arising in the system have been established. In order to increase the operational criterion, more reliable data should be used in the planning process. A form of feedback loop should be developed for such operations and the forces and tension arising in the system should be documented for others to use.

The reason why slack is not allowed is generally due to subsequently large snap forces. In cases where these snap loads do not exceed the material strength, the slack criterion should not be as strict as it is today. Perhaps slack should be dependent on the material's bending strength instead.

Before the operation can take place capacity checks have to be performed on the crane, rigging equipment and structure. Also maximum tension in wires and slings should be looked further into in order to ensure tension below material strength at all time.

Advantages or disadvantages of using light module handling systems or other methods to transfer the cover safely through the splash zone should be examined, in terms of efficiency and cost. New methods of installing the covers can also be investigated. Perhaps more than one cover can be installed at the same time.





## References

- Alv er, P. (2008). DNV  $\alpha$ -Factor. *KTF - Subsea Lifting Operations, Stavanger 2008 - 03.12.2008*.
- AxTech (2017a). 25t Light Module Handling System. Marine and Offshore Lifting Equipment. [ONLINE] Available at: <http://www.axtech.no/index.php/system-solutions/25t-light-module-handling-system> [Accessed 21 May 2017].
- AxTech (2017b). 420t Special Handling System. Marine and Offshore Lifting Equipment. [ONLINE] Available at: <http://www.axtech.no/index.php/system-solutions/420t-special-handling-system> [Accessed 21 May 2017].
- Brandsvoll, R. A. (2016). The Different Phases of a Subsea Lift. *Subsea 7 presentation at Subsea Lifting Operations Seminar, Stavanger - 06.12.2016*.
- B e, T. (2016). Estimation of Hydrodynamic Forces during Subsea Lifting. *DNV GL Oil & Gas - Presentation at Subsea Lifting Operations Seminar, Stavanger - 06.12.2016*.
- Dahle, M., Meignan, L., Rossi, R., and Ludvigsen, A. (2016). Large Module Installation and Intervention System at Aasgard. Technical Report OTC-27078-MS, Offshore Technology Conference, Houston, Texas, USA, 2-5 May 2016.
- DNV (2007). Marine Operations Rules, Revised Alpha Factor - Joint Industry Project. Technical Report 2006\_1756, DNV. Rev 3, 27.06.2007.
- DNV GL (2008). Offshore Standard - Design of offshore steel structures, general (LRFD method). *DNV-OS-C101*.
- DNV GL (2011a). Offshore Standard - Marine Operations - General. *DNV-OS-H101*.
- DNV GL (2011b). Recommended Practice - Modelling and Analysis of Marine Operations. *DNV-RP-H103*.
- DNV GL (2014). Offshore Standard - Lifting Operations (VMO Standard - Part 2-5). *DNV-OS-H205*.
- Eik, K. J. and Nygaard, E. (2004). Heidrun - Metocen Design Basis. Technical Report PTT-NKG-RA 0058, Statoil.
- Faltinsen, O. M. (1990). *Sea Loads On Ships and Offshore Structures*. Cambridge Ocean Technology. Cambridge University Press.
- Futura-Sciences (2017). Ocean Swell. Definition > Swell - Ocean swell. [ONLINE] Available at: <http://www.futura-sciences.us/dico/d/oceanography-swell-50000971/> [Accessed 11 May 2017].
- Gjersvik, T. B. (2015). TPG4200 Subsea Production Systems - NTNU. *Lecture notes*.
- Greco, M. (2012). TMR4215 Sea Loads - NTNU. *Lecture Notes*.
- Haver, S. (2012a). From Probabilities to Design of Offshore Structures. Lecture Notes in TMR4195 - Design of Offshore Structures at NTNU. January 20, 2012.

- Haver, S. (2012b). Introducing probabilistic methods applied in design of offshore structures. *Statoil ASA*.
- Insight, M. (2017). What is a Dynamic Positioning Ship? [ONLINE] Available at: <http://www.marineinsight.com/types-of-ships/what-is-a-dynamic-positioning-ship/> [Accessed 25 April 2017].
- Karnovsky, I. A. and Lebed, O. (2010). *Advanced Methods of Structural Analysis*. Springer.
- Kendon, T. E. (2016). Determination of mass matrix for the GRP cover. Technical report, Statoil. 24.10.2016.
- Langen, I. and Sibjörnsson, R. (2009). *Dynamic analysis of structures*. NTNU - Faculty of Engineering Science and Technology.
- Larsen, C. M. (2015). *Marin Dynamikk - Kompendium for bruk i faget TMR4182 Marin Dynamikk*. Institutt for marin teknikk, Fakultet for ingeniørvitenskap og teknologi, NTNU.
- Larsen, K. (2016). TMR4225 Marine Operations - NTNU. *Lecture Notes*.
- Larsen, K. (2017). TMR4225 Marine Operations - NTNU. *Lecture Notes*.
- Leira, B. J. (2009). *Probabilistic Modelling and Estimation*. Faculty of Marine Technology. Compendium in "Stochastic Theory of Sea Loads", NTNU, Trondheim.
- Levold, P. (2016). SIMA Software Development at MARINTEK. *KTF - Subsea Lifting Operations, Stavanger - 07.12.2016*.
- Lundby (2006). DNV Marine Operations Revised Alpha Factors. *Presentation - Kranteknisk forening 23.11.2006*.
- MARIN (2017). JIP Moonpool. Maritime Research Institute Netherlands. [ONLINE] Available at: <http://www.marin.nl/web/JIPs-Networks/JIPs-public/Moonpool.htm> [Accessed 22 May 2017].
- Mathiesen, M. (2010). Tanzania Block 2 - Metocen Design Basis. Technical Report Metocaen RE-2010-006, Statoil and Polytec Foundation.
- MathWorks-Nordic (2017). Polynomial curve fitting - MATLAB polyfit. [ONLINE] Available at: <https://se.mathworks.com/help/matlab/ref/polyfit.html>. [Accessed 01 May 2017].
- Messineo, S., Celani, F., and Egeland, O. (2007). Crane Feedback Control in Offshore Moonpool Operations. Technical Report 16 (2008) 356-364, ScienceDirect, Elsevier, Control Engineering Practice.
- Myrhaug, D. and Lian, W. (2014). *TMR4182 Marine Dynamics, Irregular Waves, Lecture Notes 2009 NTNU*. Kompendiumforlaget.
- Natskår, A., Moan, T., and Alvær, P. (2015). Uncertainty in forecasted environmental conditions for reliability analyses of marine operations. *Ocean Engineering 108 (2015) 636-647*.
- Nielsen, F. G. (2007). *Lecture Notes in Marine Operations*. NTNU - Akademika Forlag.
- Nielsen, F. G. (2016). Installation of Sub-Sea Structures - Estimation of Hydrodynamic Forces. Technical report, Norsk Hydro O&E. Research Centre, Bergen, Field Development. 27.12.02.
- NTIS (1973). Snap loads in lifting and mooring cable systems induced by surface wave conditions. Technical

- Report AD-772 515, Naval Civil Engineering Laboratories. Distributed by National Technical Information Service (NTIS), U.S Department of Commerce, September 1973.
- Pearce, G. (2015). MMAN4410 Finite Element Method - UNSW. *Lecture Notes at University of New South Wales, Sydney, Australia.*
- Pettersen, B. (2007). *TMR4247 Marin Teknikk 3 - Hydrodynamikk, Department of Marine Technology. Akademika.*
- Rahman, M. and Bhatta, D. D. (1993). Evaluation of added mass and damping coefficient of an oscillating circular cylinder. *Applied Mathematical Modelling*, 17:70–79.
- Reinholdtsen, S.-A. and Aksnes, V. (2016). Simulation of Marine Operations using SIMA. *Lecture Notes in TMR4225 Marine Operations at NTNU in Cooperation with Statoil, MARINTEK and SINTEF.*
- Reistad, M., Aarnes, O. J., and Breivik, Ø. (2011). Wave Extremes In The Northeast Atlantic. Meteorological Institute of Bergen, University of Bergen, Norway, [ONLINE] Available at: [https://www.sintef.no/globalassets/project/nowitech/poster-phd-2011/ole-johan-aarnes\\_postera4\\_jan2011.pdf](https://www.sintef.no/globalassets/project/nowitech/poster-phd-2011/ole-johan-aarnes_postera4_jan2011.pdf) [Accessed 27 March 2017].
- ReliaWiki (2016). *The Weibull Distribution.* [ONLINE] Available at: [http://reliawiki.org/index.php/The\\_Weibull\\_Distribution](http://reliawiki.org/index.php/The_Weibull_Distribution) [Accessed 11 December 2016].
- SIMA (2017). *SIMA User Guide.* [Accessed 20 February 2017].
- Solaas, F., Sandvik, P. C., Pâkozdi, C., Kendon, T., Larsen, K., and Myhre, E. (2016). Limiting Sea States for Installation of GRP Protection Covers. Technical Report OMAE2017-62499, MARINTEK.
- Spiess, F. N. (1975). Joint North Sea Wave Project (JONSWAP) Progress – An Observer’s Report. Technical Report ADA010132, Office Of Naval Research - London, England.
- Statoil (2015). Aasta Hansteen Subsea Lines and Marine Operations. Technical Report C134-FN-V-KA-0110\_02, Statoil. Rev 2, 17.04.2015.
- Tharigoupla, V. (2016). E-mail correspondence "Aasta Hansteen marine operations - GRP cover installation. E-mail from VETH@statoil.com to erlmy@statoil.com. Received 08.09.2016 08:49.
- Thurston, K. W., Swanson, R. C., and Kopp, F. (2011). Statistical Characterization Of Slacking And Snap Loading During Offshore Lifting And Lowering In A Wave Environment. *Proceedings of the ASME 2011 30th International Conference on Ocean, Offshore and Arctic Engineering - OMAE2011-49.*
- TSI (2016). *Wave Energy and Wave Changes with Depth.* Exploring our fluid earth, Teaching Science as Inquiry (TSI) [ONLINE] Available at: <https://manoa.hawaii.edu/exploringourfluidearth/physical/waves/wave-energy-and-wave-changes-depth> [Accessed 13 December 2016].
- UAH (2017). The Extreme Value Distribution. University of Alabama in Huntsville (UAH), Department of Mathematical Sciences. [ONLINE] Available at: <http://www.math.uah.edu/stat/special/ExtremeValue.html> [Accessed 8 March 2017].
- van Voorthuysen, E. (2015). MANF4430 Reliability and Maintenance Engineering - UNSW. *Lecture notes.*

WAMIT (2006). WAMIT User Manual. *Versions 6.4, 6.4PC, 6.3S, 6.3S-PC, WAMIT, Inc., Massachusetts Institute of Technology.*

Weibull, W. (1951). A Statistical Distribution of wide Applicability. *ASME Journal of Applied Mechanics, Transactions of the American Society Of Mechanical Engineers, September 1951, pages 293-297.*

Zhao, Y. (2017). SIMA Guidance - Tutorial Class. NTNU - Spring 2017.

# Appendices

## A $\alpha$ -factors for Waves

Table A.1:  $\alpha$ -factor for waves, level B highest forecast (DNV GL, 2011a)

Operational Period [Hours]	Design Wave Height [m]				
	$H_S = 1$	$H_S = 2$	$H_S = 3$	$H_S = 4$	$H_S = 6$
$T_{POP} \leq 12$	0.68	0.80	0.82	0.83	0.84
$T_{POP} \leq 24$	0.66	0.77	0.79	0.80	0.82
$T_{POP} \leq 36$	0.65	0.75	0.76	0.77	0.80
$T_{POP} \leq 48$	0.63	0.71	0.73	0.75	0.78
$T_{POP} \leq 72$	0.58	0.66	0.69	0.71	0.76

Table A.2:  $\alpha$ -factor for waves, level A with meteorologist at site (DNV GL, 2011a)

Operational Period [Hours]	Design Wave Height [m]			
	$H_S = 1$	$H_S = 2$	$H_S = 4$	$H_S = 6$
$T_{POP} \leq 12$	0.72	0.84	0.87	0.88
$T_{POP} \leq 24$	0.69	0.80	0.84	0.86
$T_{POP} \leq 36$	0.68	0.78	0.80	0.84
$T_{POP} \leq 48$	0.66	0.75	0.78	0.81
$T_{POP} \leq 72$	0.61	0.69	0.75	0.79

Table A.3:  $\alpha$ -factor for waves, monitoring & level A with meteorologist (DNV GL, 2011a)

Operational Period [Hours]	Design Wave Height [m]			
	$H_S = 1$	$H_S = 2$	$H_S = 4$	$H_S = 6$
$T_{POP} \leq 4$	0.9	0.95	1.0	1.0
$T_{POP} \leq 12$	0.78	0.91	0.95	0.96
$T_{POP} \leq 24$	0.72	0.84	0.87	0.90
$T_{POP} > 24$	According to table A.2			

## B Input to SIMA

Table B.1: Input variables

Variable	Value	Unit
Skirt_vol	0.04845	$m^2$
Wall_I_vol	0.05052	$m^2$
Wall_II_vol	0.02268	$m^2$
Roof_vol	0.0366	$m^2$
Roof_mid_vol	0.067001	$m^2$
Ballast_vol	0.16018	$m^2$
Skirt_mass	94.0	$kg/m$
Wall_I_mass	98.0	$kg/m$
Wall_II_mass	43.0	$kg/m$
Roof_mass	71.0	$kg/m$
Roof_mid_mass	130.0	$kg/m$
Ballast_mass	1 260.0	$kg/m$
Skirt_amz	12 000.0	$kg/m$
Wall_I_amy	14 000.0	$kg/m$
Wall_II_amy	4 600.0	$kg/m$
Roof_amz	8 000.0	$kg/m$
Roof_mid_amz	16 000.0	$kg/m$
Skirt_c2z	3 500.0	$Ns^2/m^3$
Wall_I_c2y	4 000.0	$Ns^2/m^3$
Wall_II_c2y	1 100.0	$Ns^2/m^3$
Roof_c2z	2 250.0	$Ns^2/m^3$
Roof_c2x	60.0	$Ns^2/m^3$
Roof_mid_c2z	2 350.0	$Ns^2/m^3$
Roof_mid_c2x	80.0	$Ns^2/m^3$
Skirt_c1z	2 700.0	$Ns/m^2$
Wall_I_c1y	120.0	$Ns/m^2$
Wall_II_c1y	30.0	$Ns/m^2$
Roof_c1z	800.0	$Ns/m^2$
Roof_c1x	20.0	$Ns/m^2$
Roof_mid_c1z	800.0	$Ns/m^2$
Roof_mid_c1x	40.0	$Ns/m^2$
startTimeWinch	200.0	s
stopTimeWinch	400.0	s
speedWinch	0.2	$m/s$
Wavedir	180.0	$deg$

## C MATLAB codes

### C.1 Gumbel Plots

```

1 % ONLY SLING 1 IS PLOTTED IN THIS CODE. THE OTHER SLINGS CAN BE FOUND BY SAME
  APPROACH
2
3 %                               CONVERGENCE PLOTS
4 % S1_min = vector of minimum tension in sling 1 for random seed numbers
5 % n = number of simulations/random seed numbers
6 for i = 1:n
7     % Standard deviation
8     sig_S1_min(i) = std(S1_min);
9     % Espected value
10    E_S1_min(i) = mean(S1_min);
11    % Varying Gumbel parameter: beta
12    beta_S1_min(i) = sig_S1_min(i) * sqrt(6)/pi;
13    % Varying Gumbel parameter: mu
14    mu_S1_min(i) = E_S1_min(i) + 0.5772*beta_S1_min(i);
15    % 10% quantile varying with varying Gumbel parameters
16    quant_S1(i) = mu_S1_min(i) + beta_S1_min(i)*log(-log(1-0.1));
17 end
18
19 figure(1); clf
20 % Plot convergence test for beta
21 subplot(1,3,1)
22 plot(1:n,beta_S1_min,'o-')
23 xlabel('Seed Number [-]')
24 ylabel('\beta')
25 title('Gumbel Parameter \beta')
26 legend('Sling 1')
27
28 % Plot convergence test for mu
29 subplot(1,3,2)
30 plot(1:n,mu_S1_min,'o-')
31 xlabel('Seed Number [-]')
32 ylabel('\mu')
33 title('Gumbel Parameter \mu')
34 legend('Sling 1')
35
36 % Plot convergence test for 10% quantile
37 subplot(1,3,3)
38 plot(1:n,quant_S1,'o-')

```

```

39 line([0 n],[3680 3680]) % Line of the slack requirement
40 xlabel('Seed Number [-]')
41 ylabel('10% Quantile [N]')
42 title('10% Quantile')
43 legend('Sling 1','Slack Criterion')
44
45 %           GUMBEL PDF AND CDF AND LINEAR GUMBEL-PLOT
46 x1 = sort(S1_min);
47 mS1min = mu_S1_min(n);           %converged Gumbel parameter mu
48 bS1min = beta_S1_min(n);        %converged Gumbel parameter beta
49 quartS1min = mS1min + bS1min*log(-log(1-0.1)); %converged 10% quantile
50
51 for j = 1:n
52     z_S1_min(j) = (x1(j) - mS1min)/bS1min;
53     % Gumbel PDF
54     f_S1_min(j) = (1/bS1min) * exp((z_S1_min(j) - exp(z_S1_min(j))));
55     % Gumbel CDF
56     F_S1_min(j) = 1-exp(-exp(z_S1_min(j)));
57     % Estimated linear Gumbel-plot
58     G_S1_min(j) = mS1min/bS1min - x1(j)/bS1min;
59 end
60
61 % Plot PDF
62 figure(2); clf
63 plot(x1,f_S1_min,'o-')
64 xlabel('Tension [N]')
65 ylabel('Probability')
66 title('PDF for Minimum Tension in Slings')
67 legend('Sling 1')
68
69 % Plot CDF
70 figure(3); clf
71 plot(x1,F_S1_min,'o-')
72 xlabel('Tension [N]')
73 ylabel('Probability')
74 title('CDF for Minimum Tension in Slings')
75 legend('Sling 1')
76
77 %           EMPIRICAL DISTRIBUTION FOR THE GUMBEL-PLOT
78 for k = 1:n
79     Empirical_S1(k) = -log(-log(1-(k/(n+1))));
80 end
81 lin_fit = polyfit(transpose(x1),Empirical_S1,1); % Fit linear line to data
82
83 figure(4); clf

```



```

84 % Plot estimated linear Gumbel-plot
85 plot(x1,G_S1_min,'Color',[0.5 0 0.5])
86 hold on
87 % Plot empirical distribution wiht fitted linear line
88 plot(x1,Empirical_S1,'*','Color',[1 0.5 0])
89 plot(x1,lin_fit(1)*x1 + lin_fit(2),'—')
90 % Plot slack requirements
91 line([0 30000],[-log(-log(0.9)) -log(-log(0.9))], 'LineStyle','—')
92 line([3680 3680],[min(G_S1_min) max(G_S1_min)], 'LineStyle','-.')
93 title('Gumbel Plot of Cumulative Probability, Hs = 3 m, Tp = 8 s')
94 xlabel('Tension [N]')
95 ylabel('-ln(-ln(F))')

```

## C.2 Season Segregation

```

1 % Season dependent duration of calms for various Hs criteria
2 A = importdata('Heidrun_Nora10_correct.txt');
3 L = length(A(:,2));
4 Hs = A(:,7);
5
6 % Counters
7 SpringT = 1;
8 SummerT = 1;
9 FallT = 1;
10 WinterT = 1;
11 for i = 1:L
12     if A(i,2) == 4 || A(i,2) == 5
13         spring_Heidrun(SpringT) = Hs(i);
14         SpringT = SpringT + 1;
15     elseif A(i,2) == 6 || A(i,2) == 7 || A(i,2) == 8
16         summer_Heidrun(SummerT) = Hs(i);
17         SummerT = SummerT + 1;
18     elseif A(i,2) == 9 || A(i,2) == 10
19         fall_Heidrun(FallT) = Hs(i);
20         FallT = FallT + 1;
21     else
22         winter_Heidrun(WinterT) = Hs(i);
23         WinterT = WinterT + 1;
24     end
25 end

```

### C.3 Season Dependent Duration of Calms

```

1 run('Seasons.m')
2 l = 3;           %time interval
3 Hs_start = 0.5;
4 Hs_max = 10;
5 step = 0.025;
6
7 %               SPRING
8 CalmS = 0;
9 StormS = 0;
10 dummyC = 0;
11 dummyS = 0;
12 for Hs = Hs_start:step:Hs_max
13     for i = 1:length(spring_Heidrun)
14         if spring_Heidrun(i) <= Hs
15             if StormS == 0;
16                 StormS = 0;
17             else
18                 dummyS = dummyS + 1;
19                 SpringStorm(dummyS) = StormS;
20                 StormS = 0;
21             end
22             CalmS = CalmS + l;
23         else
24             if CalmS == 0
25                 CalmS = 0;
26             else
27                 dummyC = dummyC + 1;
28                 SpringCalm(dummyC) = CalmS;
29                 CalmS = 0;
30             end
31             StormS = StormS + l;
32         end
33     end
34
35     if CalmS ~= 0
36         dummyC = dummyC + 1;
37         SpringCalm(dummyC) = CalmS;
38     end
39     if StormS ~= 0
40         dummyS = dummyS + 1;
41         SpringStorm(dummyS) = StormS;
42     end

```

```
43     Hsplot = Hs*ones(1,length(SpringCalm));
44     subplot(2,2,1)
45     plot(Hsplot, SpringCalm, '*','Color',[0 0.4 0.6])
46     hold on
47     axis([0 10 0 500])
48     xlabel('Significant Wave Height [m]')
49     ylabel('Duration of Calms, \tau_c [hours]')
50     title('Spring')
51     set(gca,'fontsize',28)
52     box on
53     set(gcf,'color','w');
54     CalmS = 0;
55     StormS = 0;
56     dummyC = 0;
57     dummyS = 0;
58     SpringCalm = [];
59     SpringStorm = [];
60 end
61 %                SUMMER
62 CalmSum = 0;
63 StormSum = 0;
64 SummerCalm = [];
65 SummerStorm = [];
66 for Hs = Hs_start:step:Hs_max
67     %SAME APPROACH AS FOR SPRING
68 end
69 %                AUTUMN
70 CalmF = 0;
71 StormF = 0;
72 FallCalm = [];
73 FallStorm = [];
74 for Hs = Hs_start:step:Hs_max
75     %SAME APPROACH AS FOR SPRING
76 end
77 %                OFF-SEASON
78 CalmW = 0;
79 StormW = 0;
80 WinterCalm = [];
81 WinterStorm = [];
82 for Hs = Hs_start:step:Hs_max
83     %SAME APPROACH AS FOR SPRING
84 end
```

## C.4 Operability

```

1 run('Seasons.m')
2 l = 3; %time interval
3 Tr = 2.5; %Reference Period
4 years = length(1958:2009); %years in data set
5 Hs_start = 0.5; %Not taken alpha factor into account
6 Hs_max = 4;
7 interval = 0.1;
8
9 % SPRING
10 CalmS = 0;
11 StormS = 0;
12 dummyC = 0;
13 dummyS = 0;
14 months = 2; %Spring = April and May
15 t = 1; %counter
16 hours = (30+31)*24/2; %hours each month
17
18 for Hs = Hs_start:interval:Hs_max
19     for i = 1:length(spring_Heidrun)
20         if spring_Heidrun(i) <= Hs
21             if StormS == 0;
22                 StormS = 0;
23             else
24                 dummyS = dummyS + 1;
25                 SpringStorm(dummyS) = StormS;
26                 StormS = 0;
27             end
28             CalmS = CalmS + l;
29         else
30             if CalmS == 0
31                 CalmS = 0;
32             else
33                 dummyC = dummyC + 1;
34                 SpringCalm(dummyC) = CalmS;
35                 CalmS = 0;
36             end
37             StormS = StormS + l;
38         end
39     end
40
41     if CalmS ~= 0
42         dummyC = dummyC + 1;

```

```

43     SpringCalm(dummyC) = CalmS;
44 end
45 if StormS ~= 0
46     dummyS = dummyS + 1;
47     SpringStorm(dummyS) = StormS;
48 end
49
50 CalmWait_S = [];
51 Calm_S = [];
52 a = 1; %counter in CalmWait vector
53 b = 1; %counter in Calm vector
54 for j = 1:length(SpringCalm)
55     if SpringCalm(j) < Tr
56         CalmWait_S(a) = SpringCalm(j);
57         a = a+1;
58     else
59         Calm_S(b) = SpringCalm(j);
60         b = b+1;
61     end
62 end
63
64 Operate_S(t) = sum(Calm_S)/years/months;
65 OperatePercent_S(t) = Operate_S(t)/hours*100;
66 Downtime_S(t) = (sum(SpringStorm) + sum(CalmWait_S))/years/months;
67 DowntimePercent_S(t) = Downtime_S(t)/hours*100;
68
69 t = t + 1;
70 CalmS = 0;
71 StormS = 0;
72 dummyC = 0;
73 dummyS = 0;
74 SpringCalm = [];
75 SpringStorm = [];
76 end
77 %                SUMMER
78 CalmSum = 0;
79 StormSum = 0;
80 months = 3;                %Summer = June, July and August
81 t = 1;
82 hours = (31+31+30)*24/3;    %hours each month
83 for Hs = Hs_start:interval:Hs_max
84     for i = 1:length(summer_Heidrun)
85         %SAME APPROACH AS FOR SPRING
86     end
87 end

```

```

88 % AUTUMN
89 CalmF = 0;
90 StormF = 0;
91 months = 2; %Fall = September and October
92 t = 1;
93 hours = (31+30)*24/2; %hours each month
94
95 for Hs = Hs_start:interval:Hs_max
96     for i = 1:length(fall_Heidrun)
97         %SAME APPROACH AS FOR SPRING
98     end
99 end
100 % OFF-SEASON
101 CalmW = 0;
102 StormW = 0;
103 months = 5; %Off-season = November, December, January, February, March
104 t = 1;
105 hours = (31+30+31+28+31)*24/months; %hours each month
106 for Hs = Hs_start:interval:Hs_max
107     for i = 1:length(winter_Heidrun)
108         %SAME APPROACH AS FOR SPRING
109     end
110 end
111
112 % PRINT AND PLOT
113 figure(1); clf
114 plot(Hs, OperatePercent_S, 'o-', 'linewidth', 4, 'MarkerSize', 10)
115 hold on
116 plot(Hs, OperatePercent_Sum, '-', 'linewidth', 4)
117 plot(Hs, OperatePercent_F, 'x-', 'linewidth', 4, 'MarkerSize', 20)
118 plot(Hs, OperatePercent_W, '-', 'linewidth', 4)
119 title('Operability per month during each season at Heidrun (1958–2009), T_R =
120         2.5 hours')
121 xlabel('Hs [m]')
122 ylabel('Operability [%]')
123 legend('Spring', 'Summer', 'Autumn', 'Off-season', 'Location', 'NorthWest')
124 axis([0 4 0 100])

```

## C.5 Distribution of Length of Calms

```

1 % Distribution of length of calms for SPRING only
2 run('Seasons.m')
3 HsLim = 2.5; %Design criterion
4 alphaS = 0.81; %alpha-factor

```

```
5 Tr = 2.5;           %Reference Period
6 l = 3;             %time interval
7 Hs = HsLim*alphaS; %Operational Criterion OPwf
8 years = length(1958:2009); %years in data set
9 hours = 30*24;     %hours each month
10
11 CalmS = 0;
12 StormS = 0;
13 dummyC = 0;
14 dummyS = 0;
15 months = 2;
16 SpringCalm = [];
17 SpringStorm = [];
18
19 for i = 1:length(spring_Heidrun)
20     if spring_Heidrun(i) <= Hs
21         CalmS = CalmS + l;
22     else
23         if CalmS == 0
24             CalmS = 0;
25             StormS = StormS + l;
26         else
27             if CalmS >= Tr
28                 dummyC = dummyC + 1;
29                 SpringCalm(dummyC) = CalmS;
30                 CalmS = 0;
31                 dummyS = dummyS + 1;
32                 SpringStorm(dummyS) = StormS;
33                 StormS = 0;
34                 StormS = StormS + l;
35             else
36                 StormS = CalmS + StormS + l;
37                 CalmS = 0;
38             end
39         end
40     end
41 end
42 end
43
44 if CalmS ~= 0
45     if CalmS >= Tr
46         dummyC = dummyC + 1;
47         SpringCalm(dummyC) = CalmS;
48     else
49         dummyS = dummyS + 1;
```

```

50         SpringStorm(dummyS) = StormS;
51     end
52 end
53
54 if StormS ~= 0
55     dummyS = dummyS + 1;
56     SpringStorm(dummyS) = StormS;
57 end
58 if SpringStorm(1) == 0
59     SpringStorm = SpringStorm(2:length(SpringStorm));
60 end
61
62 % Empirical Weibull-plot
63 for k = 1:length(SpringCalm)
64     F(k) = k/(length(SpringCalm)+1);
65 end
66 Weib = log(-log(1-F));
67 SpringCalms = log(sort(SpringCalm));
68
69 % Select max empirical value for each log(x)
70 k = 1;
71 d = 1;
72 for i = 1:(length(SpringCalms)-2)
73     if SpringCalms(i+1) == SpringCalms(i)
74         Max(k) = Weib(i);
75         k = k+1;
76         x(d) = SpringCalms(i);
77     else
78         if SpringCalm(i+2) ~= SpringCalm(i+1)
79             y(d) = Weib(i+1);
80             x(d) = SpringCalms(i);
81             d = d+1;
82         else
83             y(d) = max(Max);
84             x(d) = SpringCalms(i);
85             d = d+1;
86             k = 1;
87         end
88     end
89 end
90 %Create Weibull-plot from distribution
91 parameters = wblfit(SpringCalm);           %gives weibull parameters
92 alphaS = parameters(1);                   %scale parameter
93 betaS = parameters(2);                   %shape parameter
94 SpringCalms = sort(SpringCalm);

```



```

95 for i = 1:length(SpringCalm)
96     WeibDist(i) = betaS*log(SpringCalms(i)) - betaS*log(alphaS);
97 end
98
99 %Plot Weibull distribution to histogram of length of calms
100 figure(5); clf
101 subplot(1,2,1)
102 histfit(SpringCalm,30,'wbl')
103 xlabel('Length of calms [hours]')
104 ylabel('Number of periods with respective length')
105 title('Weibull Distribution of calms during Spring @ Heidrun')
106 legend('Spring Calms', 'Fitted Weibull PDF')
107
108 % Mean for weibull distribution
109 RealMeanS = mean(makedist('Weibull','a',alphaS,'b',betaS));
110 % Standard deviation for weibull distribution
111 RealStdS = std(makedist('Weibull','a',alphaS,'b',betaS));
112 % Plot both empirical Weibull-plot and Weibull-plot from distribution
113 subplot(1,2,2)
114 plot(x,y,'*','LineWidth',4)
115 hold on
116 plot(log(sort(SpringCalm)),WeibDist,'-','LineWidth',4)
117 xlabel('ln(calms)','Interpreter','Latex')
118 ylabel('ln(-ln(1- $\hat{F}$ ))','Interpreter','Latex')
119 legend('Empirical Weibull plot','Weibull plot from distribution')
120 title('Weibull Plot')

```

## C.6 Actual Duration of Operation with Random Start

```

1 run('Seasons.m')
2 l = 3;           %time interval
3 Tr = 2.5;       %Reference Period
4 HsWf = 2;       %Operational Criteria
5
6 %               SPRING
7 HsSpring = spring_Heidrun;
8 dummyS = 0;
9 dummyC = 0;
10 StormS = 0;
11 CalmS = 0;
12
13 % Make SpringCalm and SpringStorm Vectors
14 for i = 1:length(spring_Heidrun)
15     if spring_Heidrun(i) <= HsWf

```

```

16         if StormS == 0
17             StormS = 0;
18         else
19             dummyS = dummyS + 1;
20             SpringStorm(dummyS) = StormS;
21             StormS = 0;
22         end
23         CalmS = CalmS + 1;
24     else
25         if CalmS == 0
26             CalmS = 0;
27         else
28             dummyC = dummyC + 1;
29             SpringCalm(dummyC) = CalmS;
30             CalmS = 0;
31         end
32         StormS = StormS + 1;
33     end
34 end
35
36 if CalmS ~= 0
37     dummyC = dummyC + 1;
38     SpringCalm(dummyC) = CalmS;
39 end
40 if StormS ~= 0
41     dummyS = dummyS + 1;
42     SpringStorm(dummyS) = StormS;
43 end
44
45 % Duration of Operation
46 C_S = 0;
47 S_S = 0;
48 s = 0;
49 countS = 1;
50
51 if HsSpring(1) <= HsWf
52     for i = 1:length(Spring_Heidrun)
53         if HsSpring(i) <= HsWf
54             if s == 1
55                 countS = countS+1;
56                 s = 0;
57             end
58             j = i;
59             while HsSpring(j) <= HsWf
60                 C_S = C_S + 1;

```

```

61         if j == length(spring_Heidrun)
62             break
63         end
64         j = j+1;
65     end
66     if C_S >= Tr
67         T_opS(i) = Tr;
68     else
69         q_find = find(SpringCalm((countS+1):end) >= Tr);
70         q = min(q_find);
71         if q == 1
72             T_opS(i) = SpringStorm(countS) + Tr + C_S;
73         else
74             T_opS(i) = sum(SpringStorm(countS:(countS+q-1))) + sum(
                SpringCalm(countS+1:(countS+q-1))) + Tr + C_S;
75         end
76     end
77     else
78         s = 1;
79         k = i;
80         while HsSpring(k) > HsWf
81             S_S = S_S + 1;
82             if k == length(spring_Heidrun)
83                 break
84             end
85             k = k+1;
86         end
87         q_find = find(SpringCalm(countS:end) >= Tr);
88         q = min(q_find);
89         if q == 1
90             T_opS(i) = Tr + S_S;
91         else
92             T_opS(i) = sum(SpringStorm(countS+1:(countS+q-1))) + sum(
                SpringCalm(countS+1:(countS+q-1))) + Tr + S_S;
93         end
94     end
95     C_S = 0;
96     S_S = 0;
97 end
98 else
99     for i = 1:length(spring_Heidrun)
100         if HsSpring(i) <= HsWf
101             s = 1;
102             j = i;
103             while HsSpring(j) <= HsWf

```

```

104         C_S = C_S + 1;
105         if j == length(spring_Heidrun)
106             break
107         end
108         j = j+1;
109     end
110     if C_S >= Tr
111         T_opS(i) = Tr;
112     else
113         q_find = find(SpringCalm((countS+1):end) >= Tr);
114         q = min(q_find);
115         if q == 1
116             T_opS(i) = SpringStorm(countS+1) + Tr + C_S;
117         else
118             T_opS(i) = sum(SpringStorm(countS+1:(countS+q))) + sum(
                SpringCalm(countS+1:(countS+q-1))) + Tr + C_S;
119         end
120     end
121     else
122         if s == 1
123             countS = countS+1;
124             s = 0;
125         end
126         k = i;
127         while HsSpring(k) > HsWf
128             S_S = S_S + 1;
129             if k == length(spring_Heidrun)
130                 break
131             end
132             k = k+1;
133         end
134         q_find = find(SpringCalm(countS:end) >= Tr);
135         q = min(q_find);
136         if q == 1
137             T_opS(i) = Tr + S_S;
138         else
139             T_opS(i) = sum(SpringStorm(countS+1:(countS+q-1))) + sum(
                SpringCalm(countS:(countS+q-2))) + Tr + S_S;
140         end
141     end
142     C_S = 0;
143     S_S = 0;
144 end
145 end
146

```

```
147 %                               SUMMER
148 HsSummer = summer_Heidrun;
149 StormSum = 0;
150 CalmSum = 0;
151 for i = 1:length(summer_Heidrun)
152     %SAME APPROACH AS FOR SPRING
153 end
154 %                               AUTUMN
155 HsFall = fall_Heidrun;
156 StormF = 0;
157 CalmF = 0;
158 for i = 1:length(fall_Heidrun)
159     %SAME APPROACH AS FOR SPRING
160 end
161 %                               WINTER/OFF-SEASON
162 HsW = winter_Heidrun;
163 StormW = 0;
164 CalmW = 0;
165 for i = 1:length(winter_Heidrun)
166     %SAME APPROACH AS FOR SPRING
167 end
168
169 %                               SUMMARY
170 T_op(1,:) = [mean(T_opS) mean(T_opSum) mean(T_opF) mean(T_opW)];
171 %Weibull Fit
172 WeiPar_S = wblfit(T_opS);
173 WeiPar_Sum = wblfit(T_opSum);
174 WeiPar_F = wblfit(T_opF);
175 WeiPar_W = wblfit(T_opW);
176
177 S_90 = wblinv(0.9,WeiPar_S(1),WeiPar_S(2));
178 Sum_90 = wblinv(0.9,WeiPar_Sum(1),WeiPar_Sum(2));
179 F_90 = wblinv(0.9,WeiPar_F(1),WeiPar_F(2));
180 W_90 = wblinv(0.9,WeiPar_W(1),WeiPar_W(2));
181 Q_90 = [S_90 Sum_90 F_90 W_90];
182
183 S_50 = wblinv(0.5,WeiPar_S(1),WeiPar_S(2));
184 Sum_50 = wblinv(0.5,WeiPar_Sum(1),WeiPar_Sum(2));
185 F_50 = wblinv(0.5,WeiPar_F(1),WeiPar_F(2));
186 W_50 = wblinv(0.5,WeiPar_W(1),WeiPar_W(2));
187 Q_50 = [S_50 Sum_50 F_50 W_50];
188
189 S_10 = wblinv(0.1,WeiPar_S(1),WeiPar_S(2));
190 Sum_10 = wblinv(0.1,WeiPar_Sum(1),WeiPar_Sum(2));
191 F_10 = wblinv(0.1,WeiPar_F(1),WeiPar_F(2));
```

```

192 W_10 = wblinv(0.1,WeiPar_W(1),WeiPar_W(2));
193 Q_10 = [S_10 Sum_10 F_10 W_10];
194
195 for i = 1:4
196     if Q_10(i) < Tr
197         Q_10(i) = Tr;
198     end
199 end
200
201 figure(1); clf
202 x = 1:4;
203 plot(x,Q_90,'o-', 'linewidth',4, 'MarkerSize',10)
204 hold on
205 plot(x,Q_50,'x-', 'linewidth',4, 'MarkerSize',20)
206 plot(x,Q_10,'-', 'linewidth',4)
207 plot(x,T_op(1,:), '—', 'linewidth',4)
208 axis([1 4 0 150])
209 set(gca, 'XTick',1:4, 'XTickLabel',{'Spring' 'Summer' 'Autumn' 'Off-Season'})
210 xlabel('Seasons')
211 ylabel('Duration [hours]')
212 title(['Hs_{WF} <= ' num2str(HsWf) ' m for ' num2str(Tr) ' hours'])
213 legend('P90', 'P50', 'P10', 'Mean', 'Location', 'NorthWest')

```